RESULTS

The results of the gross, subgross, and microscopic studies of the Lung/Skin Research Unit were as varied as the methods utilized and the diversity of tissues and organs available for collection by RU 180. The number and type of samples made available has had a direct effect on results. The extreme weather and other collection conditions imposed on RU 180 personnel prevented some samples from being as well or as quickly preserved as is usually required for most types of anatomical study. Organ and medium sized sample quality overall was good to excellent with only a small proportion exhibiting some internal deterioration. Samples for electron microscopy, however, were not as well preserved: their condition ranged from adequate to poor apparently owing to autolysis and temperature constraints. Results are presented from all samples studied since they represent in some cases the first and in other cases the best samples of bowhead whale tissues and organs available for anatomical analysis to date. Standard anatomical terminology based on that prescribed in the Nomina Anatomica Veterinarian (Schaller et al 1973) is used.

1. Lung

The respiratory system was studied from the external nares (blowholes) to the alveoli within the lung where actual gaseous exchange occurs (with the exception of the nasal passages which were not available). The total amount of pulmonary tissue viewed grossly was lower in proportion to the conducting airways than we expected from 10.32 m (average) animals.

The external nares, commonly referred to as the blowholes, have a cutaneous covering. They are situated on the dorsum of the skull in a recessed area in the maxillae. The external nares of 79KK1 were symmetrical, 20 cm in length and separated 3 cm rostrally. They curved caudolaterally in a semicircular fashion and were separated 18 cm at their caudal extent (Fig 13-1). Eight tactile hairs, 9-12 mm long and arranged in a V-shaped configuration were located between the caudal extremities of the right and left nares (Fig 13-2). The nares led into paired right and left vestibuli and on into right and left nasal cavities which were divided by paired cartilages surrounded by dense vascular connective tissue (Fig 13-3). Rostrally the cartilages were 15 cm below the dorsal surface (Fig 13-4A) and then inclined caudally to lie only 2 cm below the dorsum in the midportion of the external

nares (Fig 13-4E). The cartilages then declined caudally to lie 6 cm below the dorsal surface (Fig 13-4 F). The cartilages were surrounded by vascular tissue, became pleated caudally and curved laterally to partially surround the meati (Fig 13-4G).

The vestibular epitheliums was 2 mm thick overlying a very tendinous lamina propria that was 10 mm thick. The stratified squamous epitheliums was keratinized with a 15 µm thick stratum corneum (Figs 13-5, 13-6). Connective tissue papillae averaging 800 µm long i,nterdigitated with the epitheliums. The stratum basale and stratum spinosum appeared typical with the outer layers of the spinosum becoming flattened gradually toward the stratum corneum. No sensory nerve endings were noted in the lamina propria of this region.

Between the nasal septa, the tissue was histologically dense irregular connective tissue sheets (Fig. 13-7) interlaced with some adipose tissue and longitudinally arranged tendinous tissue. The region-was heavily vascularized.

The rostral and lateral walls of the vestibuli and the nasal cavities contained an anatomical sphincter which appeared to passively push the vestibular walls medially to close the nares. This narial sphincter was made of specialized blubber laced with radially oriented 2-4 mm diameter skeletal muscle bundles (Figs 13-4, 13-8, 13-9). The orientation of the muscle fibers appeared to be directed to the medial surfaces of the recessed areas in the maxillae.

The depths of the cartilages (Fig 13-10) led to an osseous midline septum thus completing the division into totally separate right and left nearly vertical nasal cavities. The internal nares lead into the vertically elongated nasopharynx which lies dorsal to the soft palate, but was not available for study. The nasopharynx communicated with the laryngopharynx via a circular opening in the soft palate (79B1) which was surrounded by skeletal muscle commonly referred to as the palatopharyngeal sphincter (Fig 13-10).

The larynx (79B1 and 80B1) was composed of the four classical cartilages which differed in arrangement and structure from those of terrestrial mammals (Figs 13-11, 13-12, 13-13). The rostral extension was typically cetacean, but blunter. The rostral free end of the epiglottis cartilage did not extend beyond the arytenoid cartilages. The epiglottis cartilage had a longitudinal median pyramidal eminence which fit between the rounded ventral surfaces of the arytenoid cartilages (Fig 13-10). The caudal end of the epiglot-

tic cartilage was assumed to be continuous with the cranioventral aspect of the thyroid cartilages (Fig 13-11) .

The rostral most portions of the arytenoid cartilages displayed corniculate processes which lay rostral to the cricoid cartilages (Figs 13-11, 13-14). The arytenoid cartilages extended the entire length of the larynx and laid ventral to the cricoid cartilage, but dorsal to the thyroid cartilages. Their caudal tips were connected by dense connective tissue and were not fused (Figs 13-126, 13-13 B).

The cricoid cartilage was a flattened plate rostrally which became trough shaped caudally (Figs 13-12B, 13-13B, 13-15A, 13-16A) and was partially fused to the first tracheal ring. The thyroid cartilages were paired and formed a shallow wedge as they fused in the midline (Figs 13-15A, 13-1A). Caudal cornua extended caudad beyond the larynx proper, lay next to and attached to the laryngeal sac muscle via dense connective tissue near the second tracheal ring (Fig 13-17). The cranial cornua inclined craniodorsally and then curved caudally to lay along the dorsolateral aspect of the cricoid cartilages (Fig 13-12). The cricothyroid muscle was well developed arising from the dorsum of the thyroid cartilage near the midline (Fig 13- 165).

Measurements of the caudal portion of the larynx of 8061 were: cricoid cartilage was 24 cm long, 19 cm wide and 13 cm deep; thyroid cartilage was 30 cm long by 17 cm wide; the cranial cornua of the thyroid cartilage were 22 cm long; and the arytenoid cartilages of 7961 measured 14 cm and 13 cm respectively in length. The corniculate process was 5 cm long.

The dorsal (inner) epiglottis epitheliums (Fig 13-18) was 875 µm thick, keratinized, stratified squamous with a 50 µm thick stratum corneum. Sensory papillae up to 700 µm long occured from 0.25-0.4 mm apart with smaller nonsensory papillae in between (Fig 13-19). The lamina propria was 5500 µm thick and consisted of dense irregular connective tissue overlying hyaline cartilage. The ventral (outer) epiglottis surface was 550-1000 µm thick keratinized stratified squamous epitheliums with a 40 µm stratum corneum and 350-800 µm long sensory papillae (Fig 13- 20A). The 875 µm thick lamina propria contained numerous blood vessels, nerves, Herbsti-like encapsulated sensory nerve endings and dense irregular connective tissue. The submucosa contained compound tubuloalveolar mucoserous glands with serous demilunes (Fig 13-206). The gland excretory ducts were 450 µm in diameter with stratified cuboidal to stratified columnar epitheliums up to 110 µm thick. The median ridge of the epiglottis epitheliums was 925 µm thick stratified squamous with a 62.5 µm

stratum corneum. No sensory nerve endings were seen, although small nerve tracts were present. The papillae of the lamina propria were 750 μm high.

The inner surface of the arytenoid cartilages (Fig 13-21) was 750 μm thick keratinized stratified squamous epitheliums with a 50 μm stratum corneum. Sensory papillae up to 625 μm long occurred from 0.4-0.6 mm apart with smaller nonsensory papillae in between (Fig 13-22). The lamina propria was dense irregular connective tissue 1875 μm thick and overlaying vascularized hyaline cartilage. The lamina propria of the outer epitheliums of the arytenoid consisted of a superficial layer of dense irregular connective tissue 150 μm thick and a deeper layer 5.75 mm thick of adipose connective tissue over the hyaline cartilage.

Near the caudal end of the arytenoid cartilages, the covering was 250 μm thick stratified squamous epithelium with a 12.5 μm thick stratum corneum that was parakeratotic. Some areas, however, appeared to change to a thick pseudostratified columnar type. The connective tissue papillae were up to 150 μm high. The lamina propria was heavily infiltrated with plasma cells and the deeper parts of the lamina had elastic fibers. The caudalmost aspects of the arytenoid cartilages were covered with 20 μm ciliated pseudostratified columnar epitheliums whose surface cells produced mucus. The lamina propria contained dense irregular connective tissue with simple tubuloalveolar mucous glands and a 750 μm thick elastic lamina with longitudinally oriented fibers in lieu of a muscularis mucosae.

Rostrally, the laryngeal cavity lies between the arytenoid and epiglottis cartilages. Caudally it divided into a ventral portion which had a caudal diverticulum (the laryngeal sac), and a dorsal portion which led into the trachea. The ventral portion lays between the arytenoid and thyroid cartilages. The laryngeal sac was a mucous membrane lined diverticulum from the caudalmost area of the ventral laryngeal cavity. It was surrounded by circularly arranged skeletal muscle (Fig 13-23) which formed the floor of the tracheal airway between the open tips of the C-shaped cartilages (Fig 13-23B). The laryngeal sac was 10 cm long and from 3.5 to 5.5 cm wide. It had stratified squamous epitheliums which was 500 μm thick with connective tissue papillae up to 350 μm high. The parakeratotic stratum corneum was 25 μm thick. Sensory nerve tracts were seen in the lamina propria, but no sensory nerve endings were noted. The lamina propria was deep with small skeletal muscle bundles, adipose cells (Fig' 13-24), and nerve tracts throughout. The dorsal portion of the laryngeal cavity was inclined dorsocaudally between the aryten-

oid cartilages passing over their caudal aspects and ventral to the cricoid cartilage to communicate directly with the tracheal airway.

The trachea (80B1) was composed of ten white tracheal cartilages which were C-shaped with distinct yellow elastic connective tissue surrounding them. The ventral aspect of the trachea contained the open portion of the C-shaped cartilages. The space between their free ends was closed by the circularly arranged laryngeal sac muscle which surrounded the sac (Fig 13-23). The first tracheal cartilage was partially fused with the caudal aspect of the cricoid cartilage. The caudal four tracheal cartilages were closed by a cartilaginous plate, dense connective tissue and muscle (Fig 13-25). The tracheal cartilages were not symmetrical but often overlapped the preceding tracheal cartilage. The trachea was dorsoventrally flattened with inside vertical height of 7-9 cm and horizontal width of 16-16.5 cm. The tracheal length was 19 cm. The laryngeal sac muscle mass was V-shaped and served as part of the ventral tracheal floor. It extended throughout the tracheal length tapering to a fine point near the tracheal bifurcation. Cranially it encompassed the laryngeal sac and caudally held the tracheal plate. The tracheal plate was hyaline cartilage 6 cm long X 2-5 cm wide and up to 1 cm thick (Fig 13-25). It served, along with the laryngeal sac muscle, as the tracheal floor. The dorsal surface of the trachea was slightly concave and was overlain by the esophagus.

The epitheliums changed abruptly on the dorsal wall of the laryngotracheal junction from 100 µm nonkeratinized stratified squamous with 1-2 mm diameter lymphatic nodules in the lamina propria (Fig 13-26) to 50 µm ciliated pseudostratified columnar with diffuse lymphatic tissue underneath (Fig 13-27). The propria consisted of dense irregular elastic connective tissue and adipose cells. Midway in the tracheal length the ciliated pseudostratified columnar epitheliums was 32.5 µm thick. The dense irregular connective tissue of the lamina propria contained a 400 µm layer of mucous glands and an elastic lamina 150 µm thick. The vascularized hyaline tracheal cartilages were 8 mm thick (Fig 13-28).

The tracheal bifurcation (80B1) was 19 cm caudal to the cricoid cartilage (Fig 13-29A). The right primary bronchus (8061) came off at a 130° angle while the left one arose at a 120° angle. The primary bronchi were yellow except for the cartilage and 13 cm long. At their bifurcation they were dorsoventrally compressed with inner dimensions of 11 x 7 cm for the left and 13 x 7 cm for the right (Fig 13-29C). Primary bronchi measurements for 80B2

were 11 x 6.5 cm and 12 x 7 cm for 80B7. The bronchi contained complete rings of hyaline cartilage which branched and anastomosed. The histological specimens were taken from gross specimens and not all areas sampled had cilia. This may have been due to poor preservation. The epitheliums was pseudostratified columnar (Fig 13-30, 13-31, 13-32) 45 µm in height. The lamina propria contained simple branched alveolar mucous glands interdigitated into 1.9 mm thick elastic laminae which had predominately longitudinally oriented fibers. No nerve fibers were noted. Complete 9.8 mm thick hyaline cartilage rings were permeated with connective tissue channels containing blood vessels. The tunics adventitia was typical dense irregular connective tissue with no smooth muscle.

The surface epitheliums of the 80B8 main bronchus was composed of both ci 1 iated and noncil iated cel 1s (Fig 13-33). The noncil iated cel 1s bulged from the surface and possessed numerous microvil 1 i (Fig 13-34). The ciliated cells also possessed microvilli positioned among the cilia but these were more slender than the microvilli of conciliated cells (Fig 13-35). Observation of the main bronchus of 80B1 revealed a poorly preserved surface covered with debris. Ciliated cells were visible in distinct rows but cells containing microvilli were not observed (Fig 13-36). Poor preservation renders these observations suspect.

Tissue from the main bronchus of 80B8 was examined with a transmission electron microscope and contained conciliated mucus producing cells with microvilli on their surfaces (Fig 13-37). The columnar cells of this epithelium were of two types based on staining characteristics and morphology. One cell type possessed a highly vesicular cytoplasm which stained heavily. The other type stained less densely and contained fewer vesicles. Both types contained numerous secretory vesicles (Figs 13-37, 13-38). Since preservation was not optimal, these morphological and staining differences could simply have been due to poor preservation with vesiculation due to post mortem disintegration. Near the base of these columnar epithelial cells was one or more strata of basal cells. The basal portions of the columnar cells consisted of a complex of numerous fine fingerlike processes which wound among the processes of basal cells to ultimately rest on the basal lamina which separated the epithel ium from the underlying connective tissue (Figs 13-37, 13-38). The dense staining cells were particularly useful in following these processes (Figs 13-37, 13-38).

The basal cells were shorter than the columnar cells with numerous surface processes which interdigitated with processes of adjacent basal cells and with those of columnar cells (Figs 13-37, 13-38, 13-39). Desmosomes were seen along many of these processes (Figs 13-39, 13-40). Whether these desmosomes joined only basal cell processes or also joined columnar cells processes could not be determined. Hemidesmosomes joined basal cells to the basal 1 amina (Fig 13-40). The basal lamina measured approximately 100 nm in thickness. Beneath the basal lamina, fibroblasts and numerous fine collagen fibers were seen (Figs 13-33, 13-34) as well as a large number of plasma cells identified by a distinctive pattern of heterochromatin distribution and the expanded cisternae of rough endoplasmic reticulum (Figs 13-41, 13-42).

Mucous glands were found deep in the connective tissue (Figs 13-43, 13-44) . Their secretory cells rested on a basal lamina and secretory granules were accumulated in the apical regions. The apical region of these cells contained numerous microvilli and the cytoplasm was rich with endoplasmic reticulum (Figs 13-43, 13-44). Junctions were seen on the lateral surfaces of adjoining cells and canaliculi appeared to be present between some cells (Fig 13-44) .

The principal bronchi (8051, 80B2, 80B7 and 8068) divided into cranial and caudal lobar bronchi (Fig 13-45) 13 cm caudal to the tracheal bifurcation. The cranial lobar bronchus (80B1) of the left lung arose at a less obtuse angle (145°) than did the cranial lobar bronchus of the right lung (1600). The cartilaginous rings were white in color and complete, but branched and anastomosed. Bronchial lymph nodes (80B7) were present. The epitheliums was ciliated pseudostratified columnar. The pulmonary artery coursed dorsolaterally between the bifurcation of the principal bronchi (Figs 13-46, 13-47) the arterial branches followed the branching of the bronchial tree along its dorsolateral aspects. The major pulmonary vein lay just caudomedial to the artery. Its branches did not follow the bronchi deeply, however, but lay just beneath the pleura on the ventromedial surface of the lung (Fig 13- 46). The lobar bronchi branched dichotomously into smaller dissectable segmental branches ranging from 1-5 cm in external diameter. Relatively large segmental bronchi were routinely found lying near the lung surface (Fig 13- 45).

Mid sized (19 x 31 mm) segmental bronchi (80B1) of the ordinary bowhead (Fig 13-48) had 68 µm thick ciliated pseudostratified columnar epithelium with mucus producing pockets. The loose connective tissue lamina propria

had abundant longitudinally oriented, 150 µm thick laminae of elastic fihers and abundant plasma ells, but no mucous glands. Cartilage rings were 3.8 mm thick. The Ingutuk variant (80B8) had the same type of epitheliums (Figs 13-49, 13-50), but it was only 30 µm thick. The loose connective tissue lamina propria had 98 µm thick elastic laminae and cartilage rings, which were 3.6 mm thick.

Smaller segmental bronchi (15 mm) of the ordi nary bowhead (80B7) had ciliated pseudostratified columnar epithel ium 96 µm thick (Fig 13-51). The lamina propria was of loose, connective tissue with 75 µm thick elastic laminae and mucous glands. . The cartilage rings were 2.47 mm thick surrounded by dense irregular connective tissue. The Ingutuk variant (80B8) was similar with 41.8 µm epitheliums (Fig 13-52) and elastic lamina 450 µm thick in the loose connective tissue lamina propria which also contained mucous glands. The cartilaginous rings measured 1.5 mm thick and were surrounded by dense irregular connective tissue.

A 1 cm bronchus from 80B8 was examined with the scanning electron microscope. The surface epitheliums resting on the connective tissue which overlay cartilage bands was composed of both ciliated and conciliated cells which were similar to those seen in the main bronchus (Figs 13-53, 13-54, 13-55). The number of ciliated cells was greatly increased with some areas completely covered by cilia (Fig 13-54).

Smaller segmental bronchi (1.5-3 mm) from 80B1 and 80B8 had 30 µm thick ciliated pseudostratified columnar epitheliums. The loose connective tissue lamina propria had mucous glands. The cartilage rings were 0.75 mm thick (Figs. 13-56, 13-57). Two mm bronchi from 8068 and 80B1 were examined with SEM. In both cases the epitheliums rested on connective tissue which overlays cartilage bands (Fig 13-58). The epithelium was largely covered by a mucous coating in which debris was embedded (Figs 13-59, 13-62). Beneath the mucus, the cell surfaces appeared to be uniformly ciliated (Figs 13-60, 13-61, 13-63, 13-64). Cilia could be seen to be the surface modifications of columnar epithelial cells (Figs 13-62, 13-63).

Bronchioles 1.5 to 0.3 mm in diameter (80B1 and 80B8) had 30 µm high ciliated pseudostratified columnar epitheliums. The presence of a circularly arranged muscularis mucosae (smooth muscle) caused the tunics muscularis to be thrown into folds (Figs 13-65, 13-66). Myoelastic sphincters were not present. No mucous glands occurred in the lamina propria and the cartilage became plaques instead of rings.

Respiratory bronchioles 0.68 to 0.36 mm in diameter (79B1 and 80B2) had respiratory (simple squamous) epitheliums closely covering a capillary network (Figs 13-67, 13-68). The lamina propria was loose connective tissue in the larger respiratory bronchioles, but became dense irregular connective tissue in the smaller ones. No glands were present. A muscularis mucosae of smooth muscle with elastic fibers occurred in bronchioles of 0.5-0.68 mm diameter. In smaller respiratory bronchioles the muscularis mucosae position was occupied only by elastic fibers. Individual alveoli and alveolar ducts penetrated the mucosa between the cartilaginous plaques with their orifices surrounded by exclusively elastic fiber sphincters.

Examination of respiratory bronchioles with a transmission electron microscope revealed a surface epitheliums composed of type I and type II pneumocytes resting on a basal lamina (Figs 13-69, 13-70). Thin cytoplasmic processes of type I pneumocytes extended over capillaries and in places shared a common basal lamina with the capillary endothelial cells (Fig 13-69). Type II pneumocytes were found between capillaries and were identified by their numerous microvilli and the presence of multilamellar bodies in their cytoplasm (Fig 13-69, 13-70) . Occasionally, type 11 pneumocytes extended over capillaries greatly increasing the blood-air barrier (Fig 13-70). The lateral surfaces of adjacent pneumocytes showed complex interdigitations and cell junctions including desmosomes (Fig 13-70). Beneath the basal lamina, the connective tissue was composed of collagen fibers among which numerous fibroblasts and their processes could be seen (Figs 13-69, 13-70). Beneath this fibrous layer, typical hyaline cartilage could be seen (Fig 13-71) in which chondrocytes of varying structure were evident (Figs 13-71, 13-72). See Tables 13-1 and 13-2 for a comparison of bronchial and bronchiolar structures.

Alveolar ducts measured 0.46-0.6 mm (80B2) with the tunics mucosa (Fig 13-73) lined exclusively with respiratory epithel ium (simple squamous covering capillaries) and alveolar sacs protruding peripherally. Cartilage plaques and mucous glands were absent. An undetermined number of alveoli were connected to the alveolar sacs. Orifices to alveolar sacs and to individual alveoli were surrounded by exclusively elastic fiber sphincters (Figs 13-74, 13-75) . Frequently with light microscopy, the sphincter areas appeared not to have an epithelial covering. Semi-thin sections cut from Epon embedded material (Figs 13-76, 13-77) showed clearly that type I pneumocytes of the respiratory epitheliums always covered such areas as well as the capillaries. Ultrastructurally the epitheliums covering the elastic sphincters (80B8) was

TABLE 13-1. COMPARISON OF THE MICROSCOPIC STRUCTURE OF AIRWAYS IN ORDINARY BOWHEAD WHALE LUNGS

Structure	Inside Diameter" (mm)	Epithelial Height (μm)	Elastic Lamina Thickness (mm)	G1 and Occurrence	Cartilage Thickness (mm)	Smooth Muscle Occurrence
Lobar Bronchus	19 x 31	69*	0.15	+	3.8	
Segmental Bronchus	16	96*	0.75	+	2.47	
Segmental Bronchus	6	34.2*	no.		no.	
Segmental Bronchus	1.37	34.2*	no.	-	0.13	
Bronchiole	0.75	30.0*	-		n.o.	+
Respiratory Bronchiole	0.64	Resp**	-		no.	+
Respiratory Bronchiole	0.48	Resp			0.01	+
Respiratory Bronchiole	0.45	Resp				

* Ciliated pseudostratified columnar epitheliums

** Respiratory epitheliums

no. Not observed"

TABLE 13-2. COMPARISON OF THE MICROSCOPIC STRUCTURE OF AIRWAYS IN INGUTUK VARIANTS

Structure	Inside Diameter (mm)	Epithelial Height (µm)	Elastic Lami na Thickness (mm)	Gl and Occurrence	Cartilage Thickness (mm)	Smooth Muscle Occurrence
Primary Bronchus	38 X 95	45.0*	1.9	+	9.8	
Segmental Bronchus	19.8 X 33.2	30.0*	0.98	+	3.6	
Segmental Bronchus	8.2 X 14.8	41.8*	0.45	+	1.5	
Segmental Bronchus	3.7	38. 0*	1.06	no.	3.42	
Segmental Bronchus	3.4	30 .o*	0.7	+	006	
Segmental Bronchus	3.3	30. o*	nom.	no.	0.75	
Segmental Bronchus	2.89	22.8*	n.m.	no.	1.36	
Segmental Bronchus	2.24	30. o*	n.m.	+	0.56	
Bronchiole	0.59	30. o*				
Bronchiole	0.36	30. o*				+
Bronchiole	0.3	30. o*				+
Respiratory Bronchiole	0.24	Resp**	-			

* Ciliated pseudostratified columnar epitheliums

** Respiratory epitheliums

n.m. Not measured

no. Not observed

similar to that of the respiratory bronchioles (Fig 13-78). A number of fibroblast like cells were seen beneath the epitheliums while below them were numerous elastic fibers (Fig 13-78) composed of amorphous substance and microfibrils (Fig 13-79). Among these elastic fibers were delicate collagen fibers and fibroblasts (Figs 13-79, 13-80)." The fibroblasts possessed many fine processes which extended outward in all directions and were visible in virtually any section through the sphincter (Figs 13-79, 13-80, 13-81). Similar structures with somewhat poorer preservation were seen in 80B2 (Fig 13- 81).

Each alveolus was also lined with respiratory epitheliums covering individual capillary beds of the cetacean type. The interalveolar septa (Fig 13-82) were composed of loose connective tissue with a capillary bed as well as covering respiratory epitheliums on each side. TEM photomicrographs clearly demonstrated the same arrangement (Fig 13-87). A very dense staining material was observable just outside the plasma membranes of respiratory epithelial cells. Within the lumen of all cavities lined by respiratory epitheliums, multilamellar bodies could be seen in various stages of disintegration (Figs 13-78, 13-88) . They appeared to be composed of membranous material arranged in concentric swirls (Fig 13-83) and may have contained tubular myelin (Fig 13-84) . Scanning electron photomicrographs revealed an alveolar wall consisting of two capillary networks separated by an alveolar septum (Fig 13-85). Red blood cells could be seen within the capillaries (Fig 13-86). With TEM, typical type I and type 11 pneumocytes became evident making up the respiratory epitheliums. The septal thickness, while quite variable, appeared to be about 6 µm from basal lamina to basal lamina in the relatively expanded condition. The septum appeared to consist of loose connective tissue in which relatively few collagen fibrils occurred. Fibroblasts were evident within this matrix (Fig 13-87). Monocyte-like cells were occasionally seen in the capillaries beneath the respiratory epitheliums (Figs 13-88, 13-89). In addition to the usual complement of organelles and multilamellar bodies, one type II pneumocyte displayed an inclusion resembling a thumb print (Fig 13-89) which is still unidentified.

The pleura was thick, fibrous and had abundant elastic fibers (Figs 13-91. 13-92). No lobulation was evident either in the pleura or in the parenchyma of the lung to divide it into cranial and caudal lobes. The gross measurements of the preserved lungs are listed in Table 13-3. The lungs were roughly rectangular with nearly uniform thickness. The hilus area was large measuring 26-29 cm mediolaterally and 30-47 cm craniocaudally (Figs 13-93, 13-94) .

TABLE 13-3. GROSS MEASUREMENTS OF INDIVIDUAL LUNGS OF BOWHEADS AND INGUTUK VARIANTS

Whale Number	Whale Length (m)	Lung Thickness (cm)	Lung Length			Lung Width			Lung
			Dorsal (cm)	Middle (cm)	Ventral (cm)	Cranial (cm)	Middle (cm)	Caudal (cm)	
80B8*	8.7	12	71	72	72	41	38	30	Right
79B1*	8.7	11	90	87	85	37	44	44	Right
Average		11.5	80.5	79.5	78.5	39	41	37	
80B1	10.9	12	72	71	73	38	42	46	Left
80B2	10.8	13	79	77	76	52	50	48	Right
80B7	10.0	13	75	77	80	37	42	45	Left
Average		12.6	75.3	75	76.3	42.3	44.6	46.3	

* Ingutuk

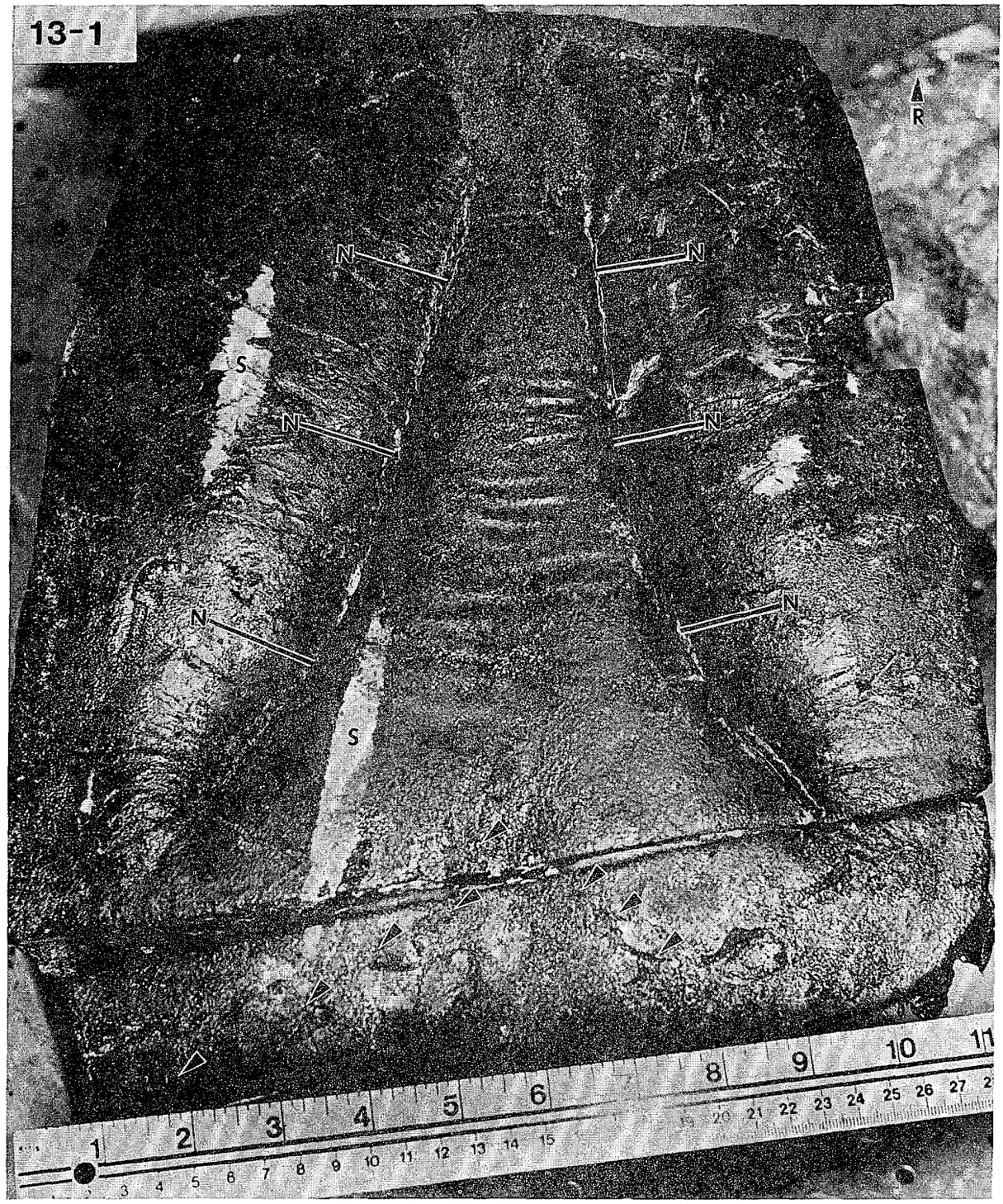

Figure 13-1. Photograph of the external nares (blowholes), dorsal view, 79KK1. The paired external nares (N) lie close together rostrally and curve caudolaterally to lie 18 cm apart. Tact i 1 e hairs (arrowheads) 'lie just caudal "to the nares. Rostral (R). Apparent scars (S) are also visible.

Figure 13-2. Photograph, dorsal view of tactile hairs, 79KK1. Eight tactile hairs (arrowheads) are visible just caudomedial to the external nares. Rostral (R). XO.9

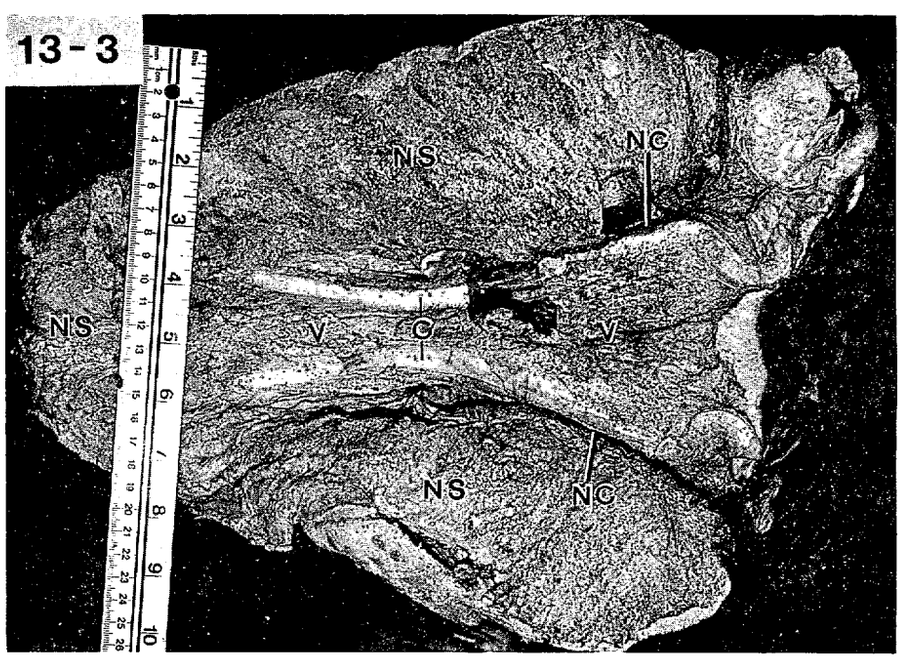

Figure 13-3. Photograph, ventral view of the paired nasal cartilages, 79KK1. Right and left vestibuli and nasal cavities (NC) are separated by the paired nasal cartilages (C). The marial sphincter (NS) lies lateral and rostral to each cavity. Note the dense vascular connective tissue (V) between the nasal cartilages.

Figure 13-4. Photographs of serial transverse sections through the external nares, vestibule and nasal cavity, 79KK1. XO.22

A. The rostralmost serial section of the series. Note the cutaneous (E) covering. The paired nasal cartilages (C)"are just becoming evident in the ventral aspect of the section. Note the narial sphincter (NS) of specialized blubber with cut bundles of skeletal muscle (arrows). Only the rostrodorsal portions of the vestibule (V) are evident.

B. The second serial section moving caudally. Note the increased depth of the vestibule and nasal cavity (CV). The narial sphincter (NS) tissue is seen with its muscle fibers. The nasal cartilages (C) are increased in height.

C. and D. The third (C) and fourth (D) serial sections moving caudally. The nasal cartilages (C) are increased in height as the vestibule and nasal cavities (CV) extend through the entire depth of the sections. Narial sphincter (NS).

E. The fifth section. Note the cartilages (C) are now inclined near the epidermis and are pleated. The narial sphincter (NS) is more circular in appearance.

F. The sixth section. The nasal cartilages (C) are more pleated, curve laterally and decline in height.

G. The caudalmost aspect of the external nares which we examined. Note the extensive pleating (C) of the nasal cartilages which nearly surround the nasal cavities (arrowheads) emerging ventrally.

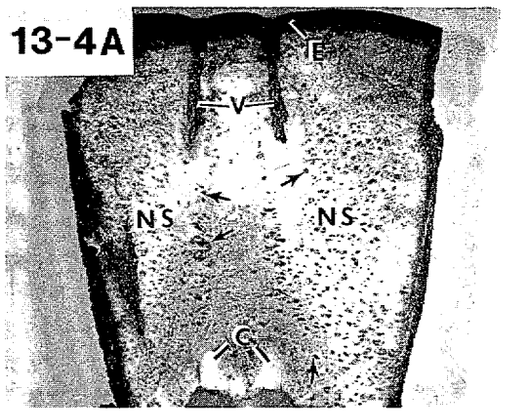
13-4A
E
V
NS
NS
C

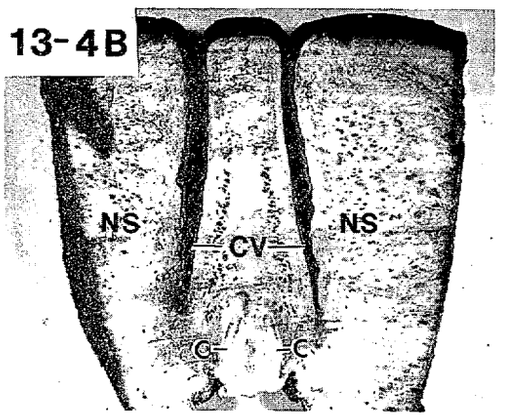
13-4B
NS
CV
NS
C
C

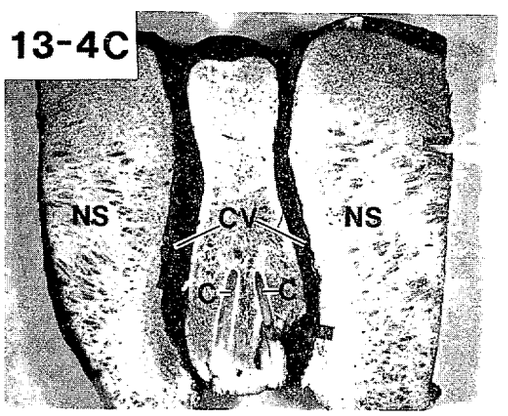
13-4C
NS
CV
NS
C
C

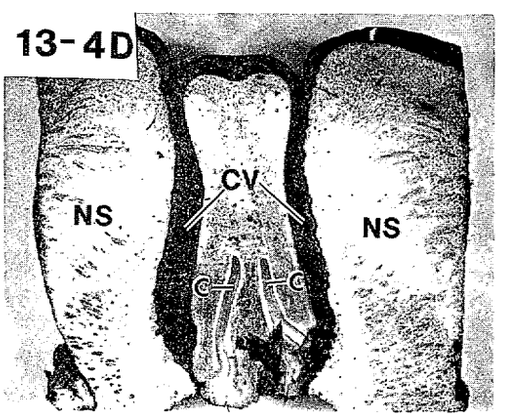
13-4D
CV
NS
NS
C
C

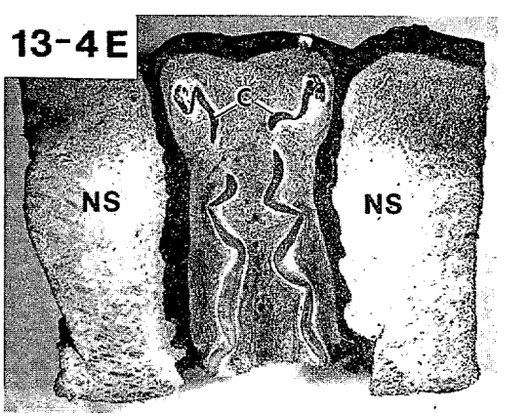
13-4E
C
NS
NS

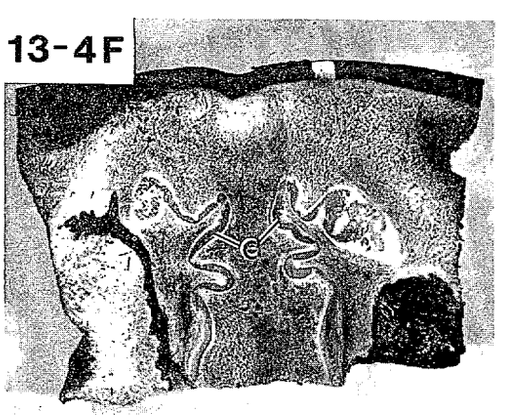
13-4F
C

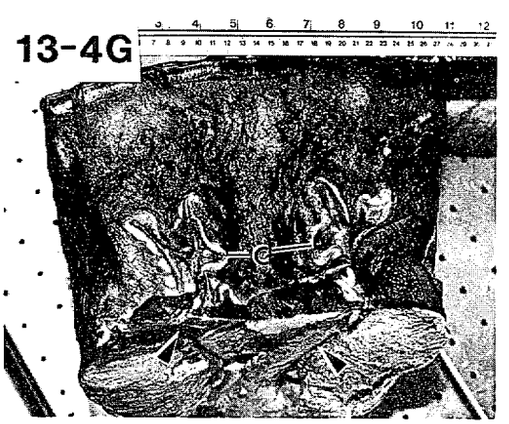
13-4G
C

Figure 13-5. Photomicrograph of the nasal mucosa of 79KK1 at 20 cm into the vestibule from the body surface. The mucosal epitheliums (E) is keratinized stratified squamous covering dense irregular connective tissue of the lamina propria (LP). Vascularized connective tissue papillae (P) interdigitate with the epitheliums. L.S.*, H and E, X50

Figure 13-6. Higher magnification photomicrograph of the stratum corneum of Fig 13-5. The surface cell layers (stratum corneum) are of the typical flattened keratinized squamous type, the same as occurs in any moist keratinized stratified squamous epitheliums in terrestrial mammals. Cell junctions (arrows) are barely discernible and the pyknotic nuclei (Nu) have not disappeared completely in the lower layers. X.S.*, H and E, X320

Figure 13-7. Photomicrograph of the interseptal tissue of 79KK1 taken 18 cm below the body surface. Dense irregular connective tissue (DCT) contains aggregations of adipose cells (AC) in a lower proportion than seen in blubber (see Fig 13-9A). Several fascicles of tendinous connective tissue (T), arteries (A), veins (V) and nerve tracts (N) are also present. X.S., H and E. X130

*L.S. = longitudinal section, X.S. = transverse section

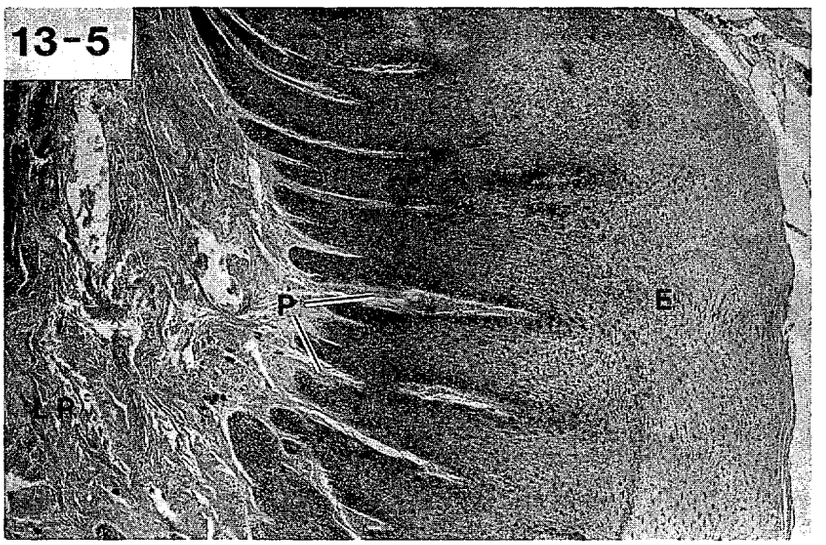
13-5
P
E
LP

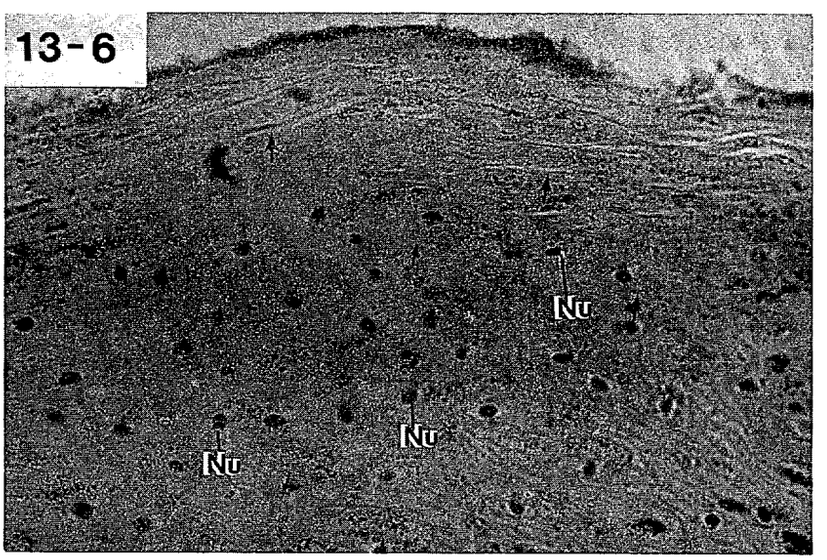
13-6
Nu
Nu
Nu

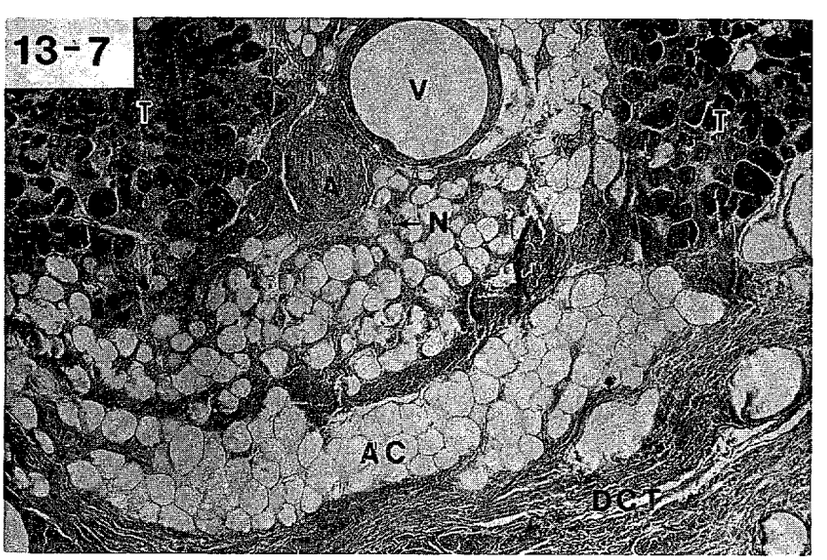
13-7
V
T
T
N
AC
DCT

Figure 13-8. Photograph of a lateral view of the narial sphincter, 79KK1. Note the circular arrangement of the mass of blubber (B) extending nearly to the epidermis (E). The skeletal muscle fibers (arrows) have been cut from their attachment to the maxillae. Rostral (R).

Figure 13-9. Photomicrographs of the narial sphincter, 79KK1.

A. Low magnification of a transverse section of the narial sphincter at 6.5 cm below the body surface and 9.5 cm lateral to the vestibule. The sphincter is specialized blubber with abundant adipose connective tissue (AC) laced with dense irregular connective tissue (DCT). Numerous 2-4 mm diameter fascicles of skeletal muscle (SK) permeate the entire mass apparently pulling the lateral wall of the vestibule laterad when contracted to open the nostril. L.S., H and E, X21

B. Higher magnification of one skeletal muscle fascicle from Fig 13-9A. Individual skeletal muscle fibers (SKF) are of the light muscle type with myofibrils and peripherally located nuclei (Nu). L.S., H and E, X130

C. High magnification of a longitudinal section through a muscle bundle of the narial sphincter of 79KK1. The striations (arrows) verify that the fibers are skeletal in type. L.S., H and E, X260

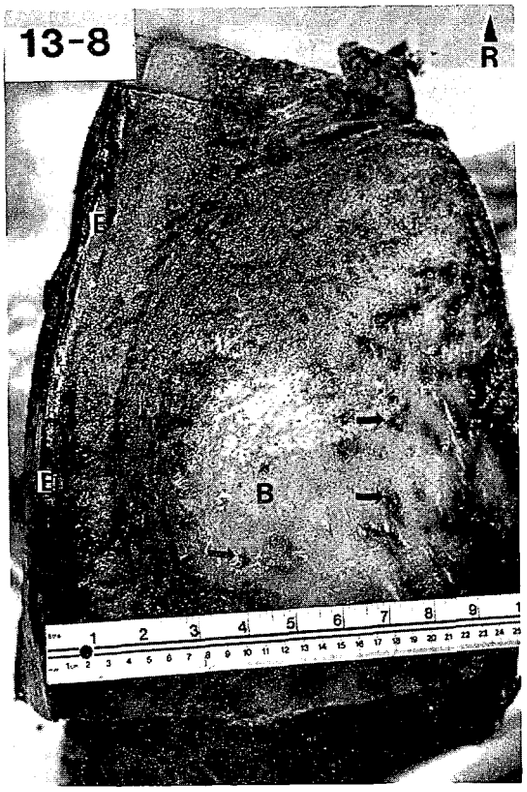
13-8
R
F
B

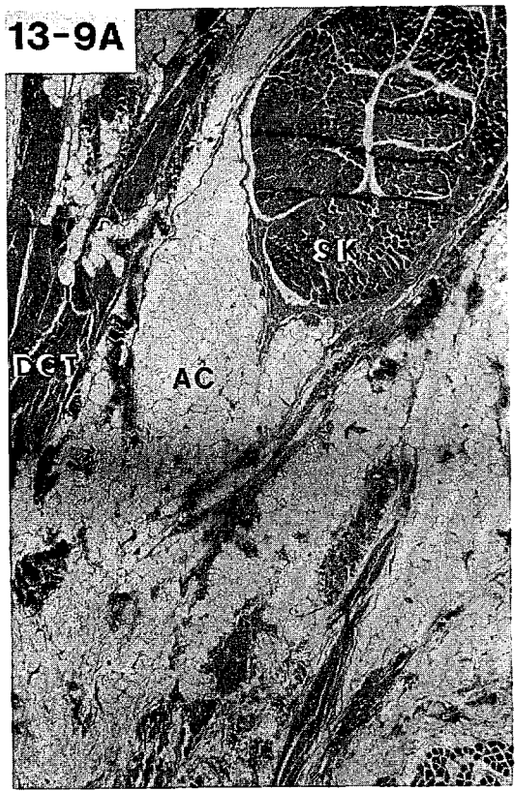
13-9A
SK
DCT
AC

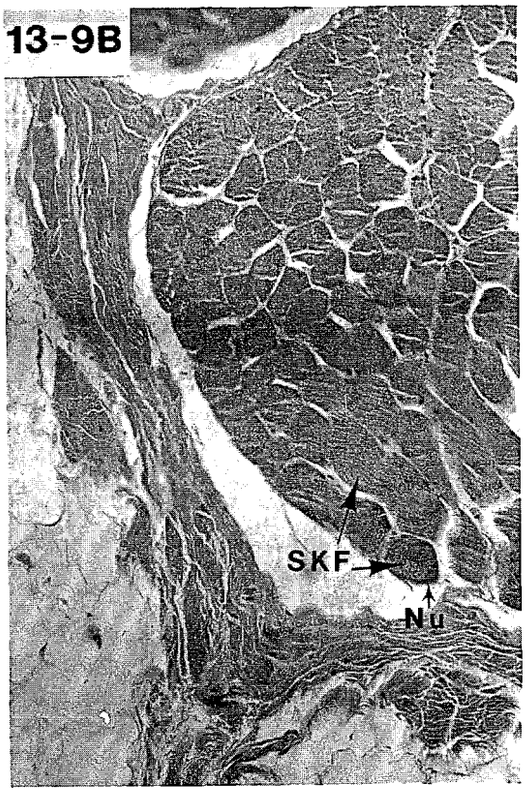
13-9B
SKF
Nu

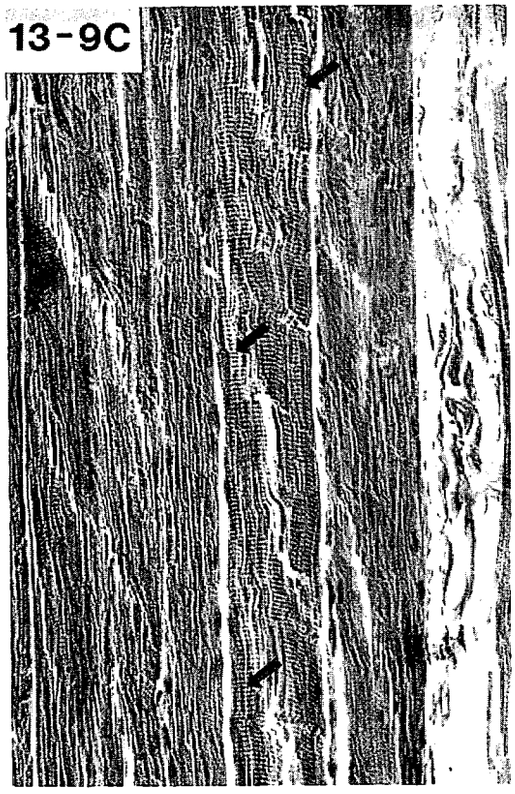
13-9C

Figure 13-10. Photographs of the rostral end of the larynx, caudal portion of the palatopharyngeal sphincter and the pharyngeal wall, 79B1.

A. Partial view of the pharynx and rostral larynx. The epiglottic cartilage (E) with its median pyramidal eminence (M) is seen fitting tightly up between the arytenoid cartilages (A) effecting a sealing anatomical closure. The cut palatopharyngeal sphincter (S) partially obscures the pharyngeal opening (arrowhead) of the esophagus. The short aryepiglottic fold (Ae) attaches the arytenoid cartilage to the epiglottis cartilage. X0.85

B. Drawing of the rostral larynx. The median pyramidal eminence (M) of the. epiglottis cartilage (E) serves as a sealing device when the whale swallows. The muscular palatopharyngeal sphincter (S) in the caudal soft palate 1 ies rostrodorsal to the esophageal opening (arrowhead). Aryepiglottic fold (Ae), corniculate processes (C) of the arytenoid cartilages, caudal pharyngeal all (W).

c. Oblique view of the rostral larynx. The corniculate processes (C) of the arytenoid cartilages (A) curve dorsally forming the dorsolateral rim of the laryngeal opening. Soft palate (P), epiglottis cartilage (E). Note raised areas on pharyngeal surface ventral to the epiglottis cartilage which are openings of glands (G). X0.9

13-10A
S
Ae
Ae
A
A
M
E
E

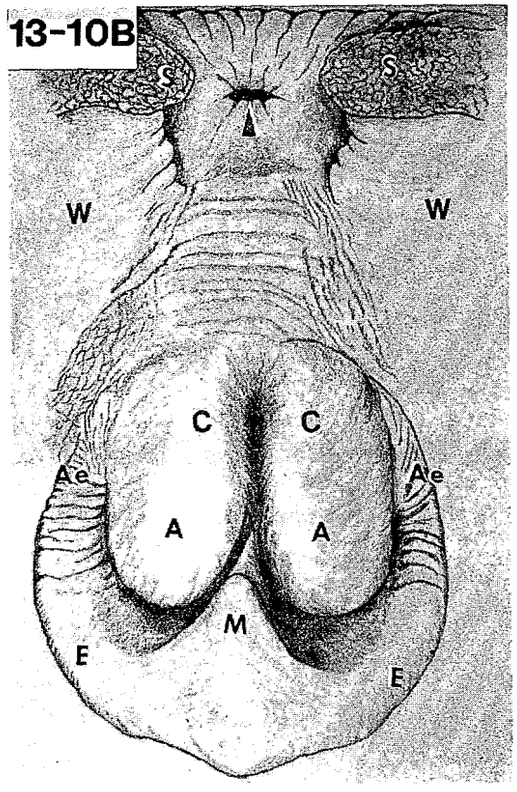
13-10B
S
S
W
W
C
C
Ae
Ae
A
A
M
E
E

13-10C
P
C
C
A
E
G
G
G

Figure 13-11. Composite drawing of the laryngeal cartilages using parts from 80B1 and 79B1. The lightly stippled area(S) represents parts 'which we did not have. The arytenoid cartilages (A) extend the complete length of the larynx. Corniculate process (Cp) of the arytenoid cartilage, epiglottis cartilage (E), cricoid cartilage (C), thyroid cartilage (T), caudal cornu (CC) and cranial cornu (Cr) of the thyroid cartilage. Rostral (R).

13-11

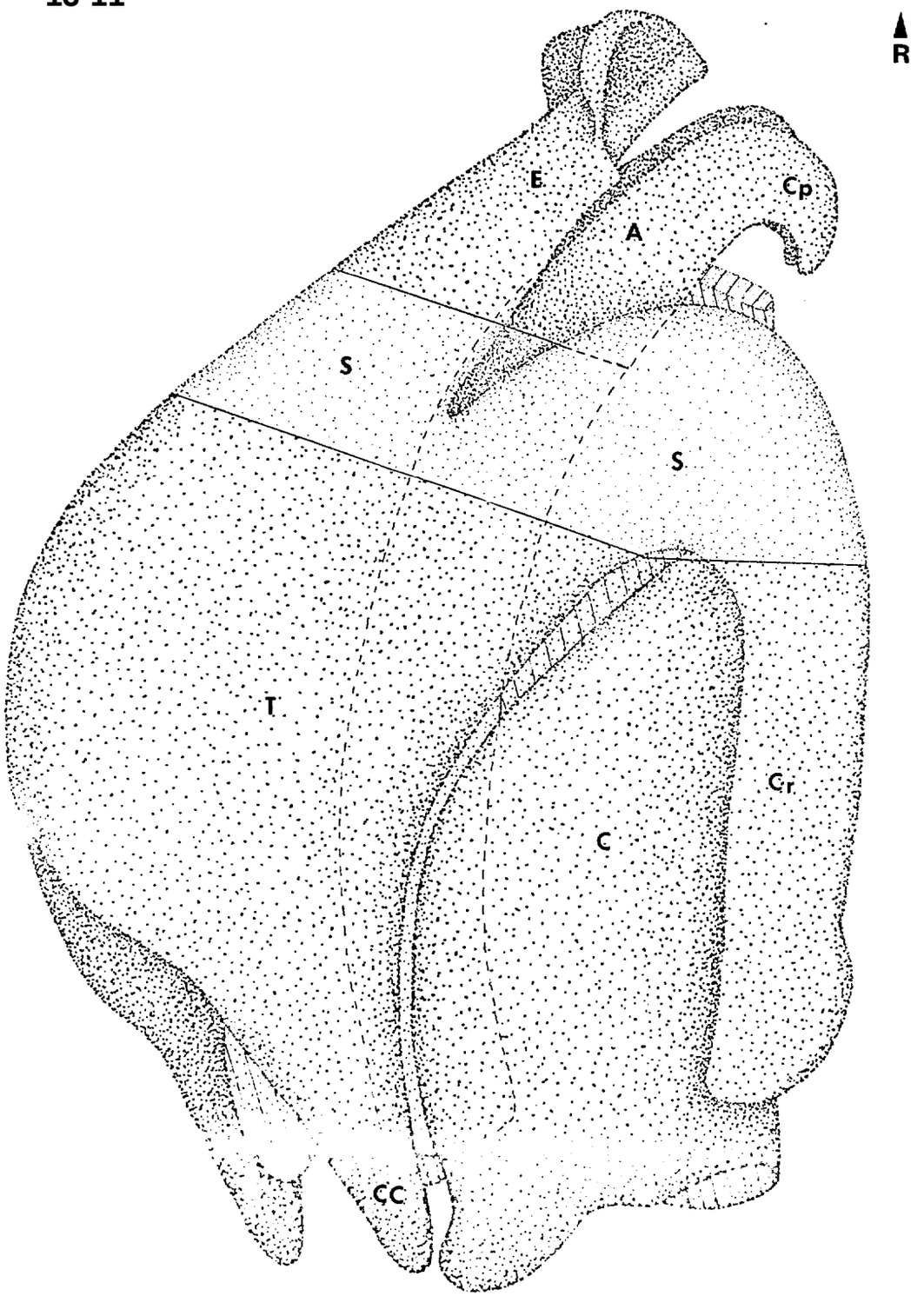

Figure 13-12". Composite drawings of, the arytenoid, cricoid and thyroid cartilages of 80B1.

A. Ventrolateral view showing the position of the arytenoid cartilages (A) in relationship to the cricoids (C) and the cranial cornu (Cr) of the thyroid cartilage. Rostral (R).

B. Cranioventral view showing the cricoid (C) cartilage is trough-shaped and not signet ring shaped. The rostral portion of the cricoid cartilage is a flattened plate. The thyroid cartilage (T) serves as a ventral floor of the larynx. Cranial cornu (Cr), of the thyroid cartilage arytenoid cartilage (A).

13-12A

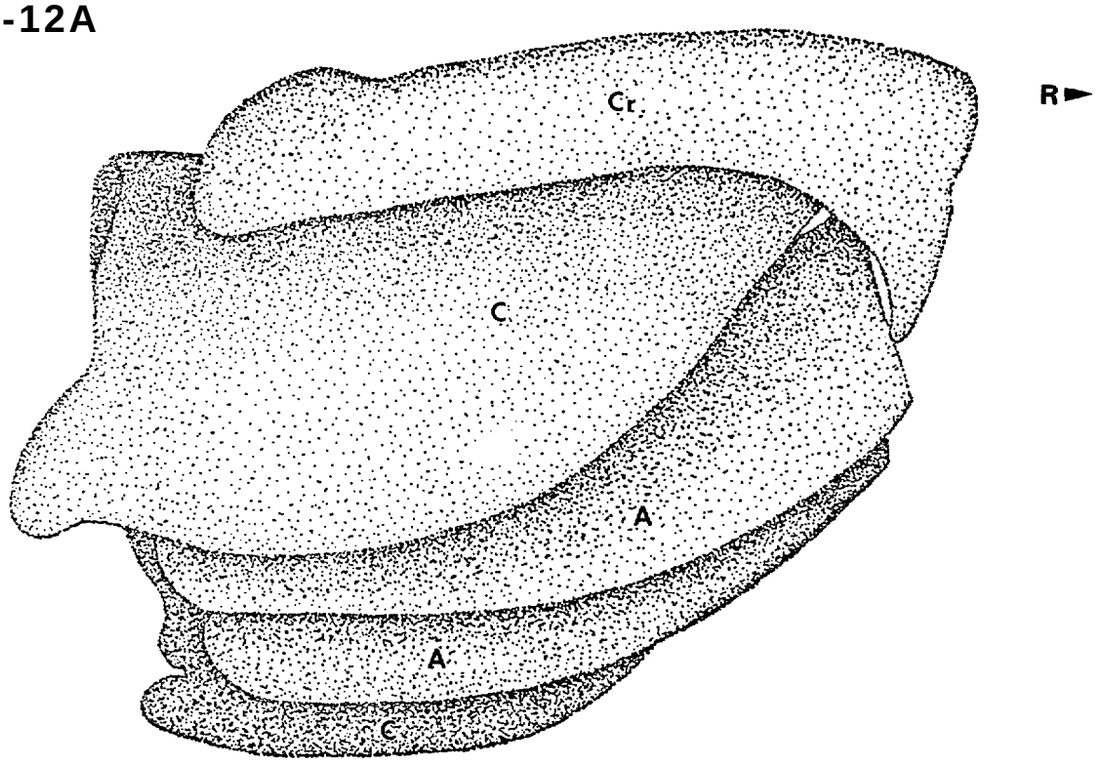

13-12B

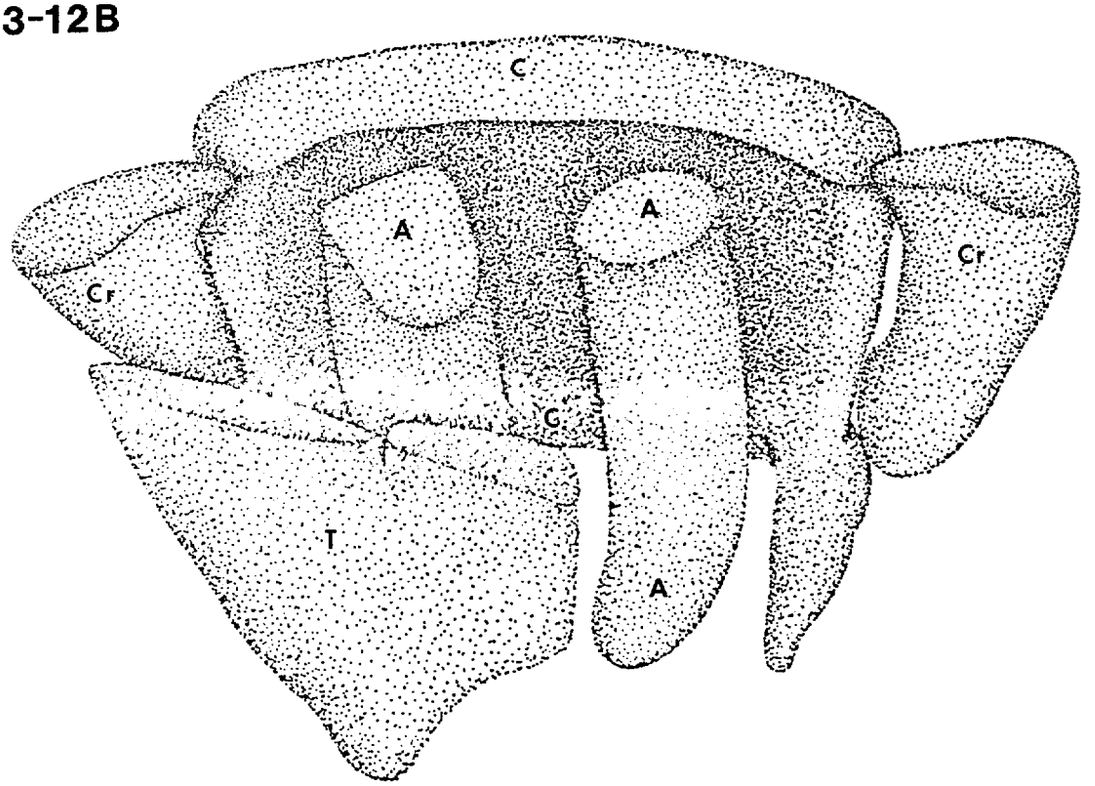

Figure 13-13. Photographs of the reconstruction of the serially sectioned cricoid, arytenoid and the thyroid cartilages.

A. Right ventral, lateral view showing the relationship of the cricoid (C), arytenoid (A) and cranial cornu (Cr) of the thyroid cartilage. X0.5

B. Cranioventral view. Note the arytenoid cartilages (A) are not fused caudally (N). The thyroid cartilage (T) forms the floor of the larynx. C - cricoid; Cr - cranial cornua of the thyroid cartilage. X0.5

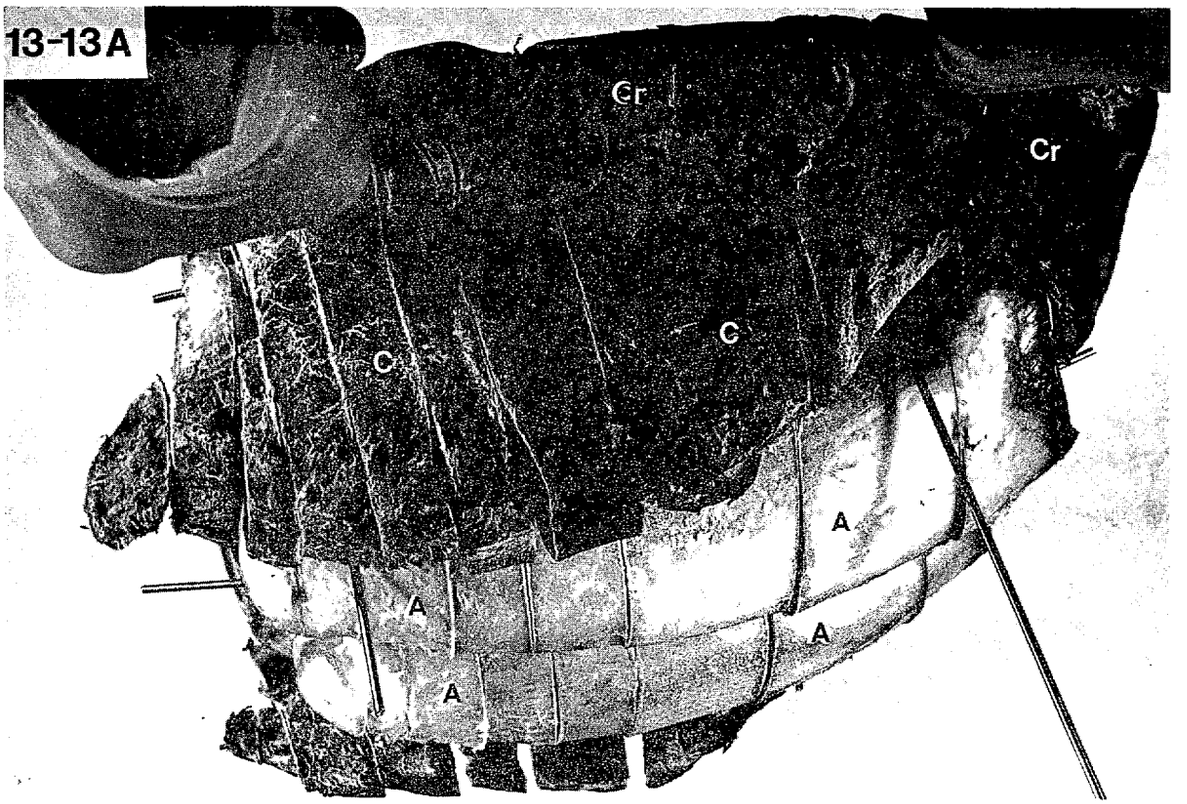
13-13A
Cr
Cr
C
C
A
A
A
A

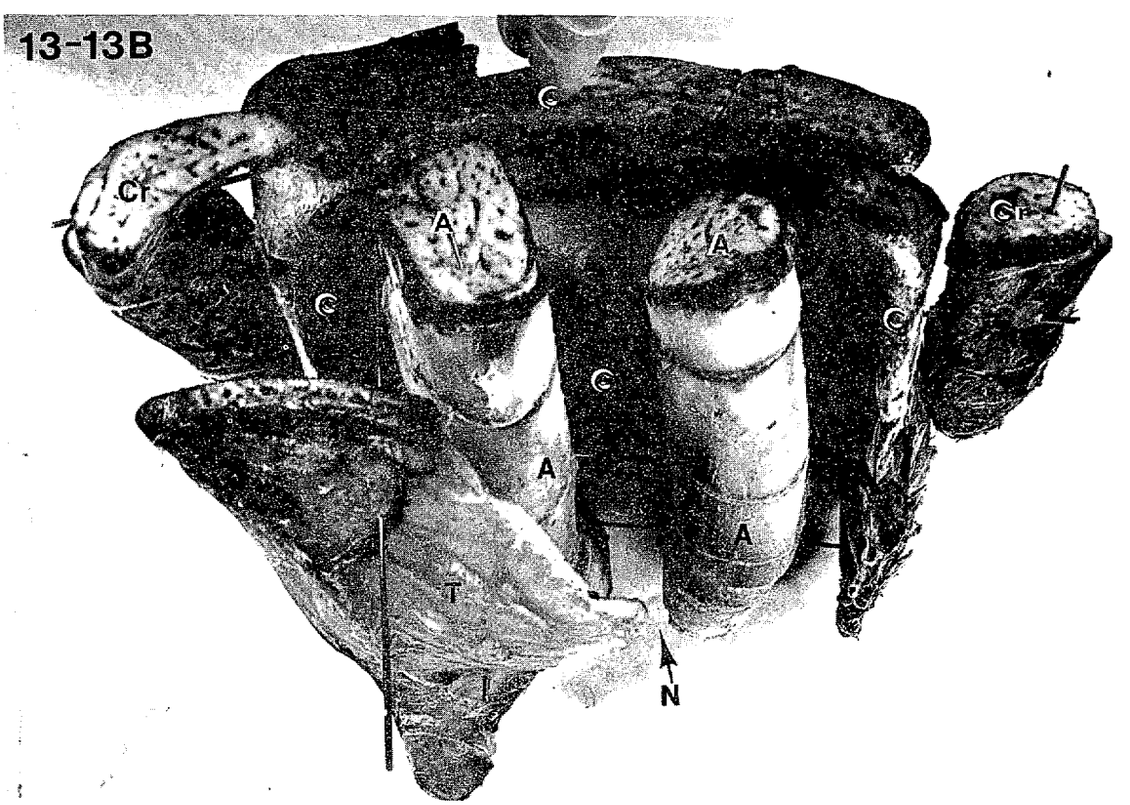
13-13B
C
Cr
A
A
Cr
C
C
C
A
A
T
N

Figure 13-14. Photographs of the corniculate process of the right arytenoid cartilage, 79B1.

A. Lateral view. The corniculate process (Cp) curves dorsomedially as the rostrodorsal end of the right arytenoid cartilage (A). R - rostral Xl

B. Drawing of the corniculate process (Cp) of the right arytenoid cartilage (A).

c. Dorsal view. The corniculate process (Cp) of the arytenoid cartilage extends rostral to the cricoid cartilage (C). Caudal extensions of cranial cornua of the thyroid cartilage (Cr). X0.35

13-14A
R
Cp
A

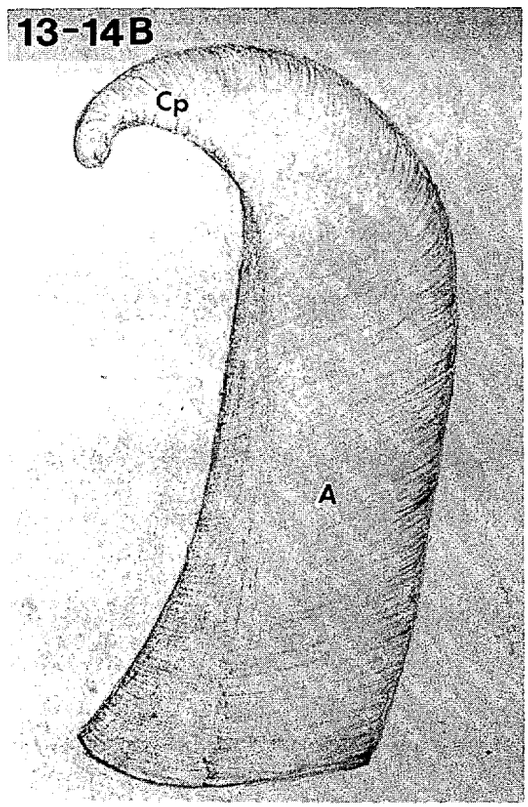
13-14B
Cp
A

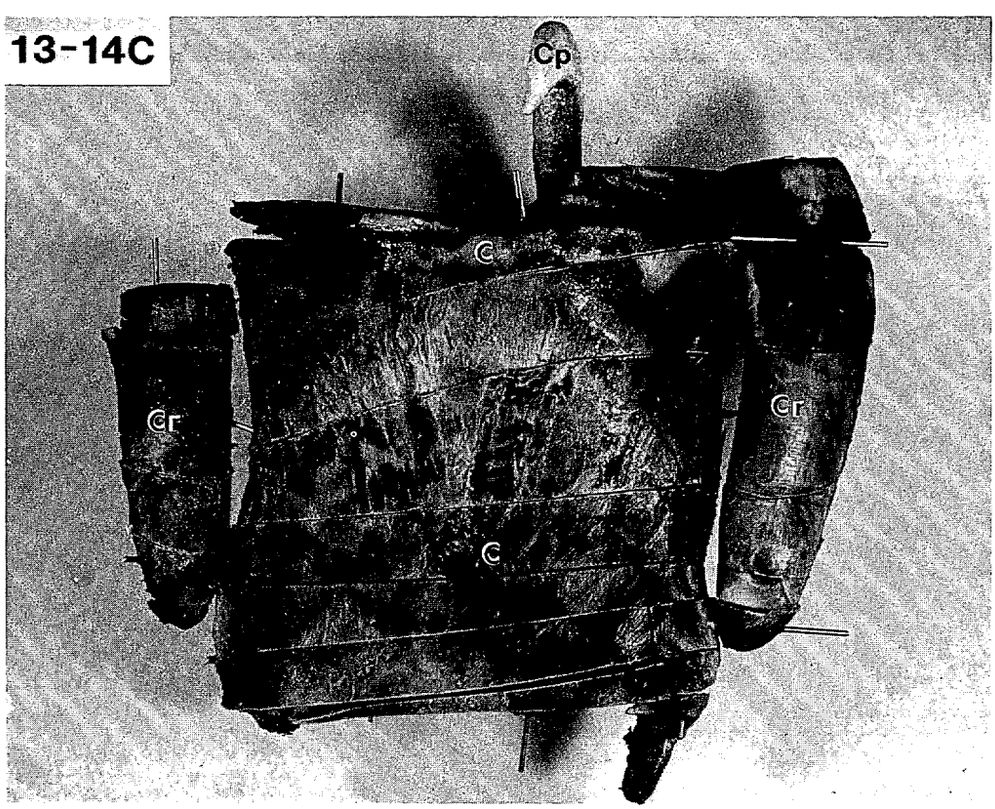
13-14C
Cp
C
Cr
Cr
C

Figure 13-15. Drawings of reconstructions of serially sectioned cricoid and thyroid cartilages, 80B1.

A. Right lateral view. The cricoid cartilage is trough shaped with the ventral aspect open. Note the ligament (L) for the attachment of the caudal end of the right cranial cornua of the thyroid cartilage. Rostral (R)

B. Left lateral view. Thyroid cartilages form a shallow wedge as the right (R) and left (L) cartilages fuse on the midline (arrowheads). Prominent caudal cornua (Cc) attach to the connective tissue covering the laryngeal sac muscle. Rostral (R)

13-15A

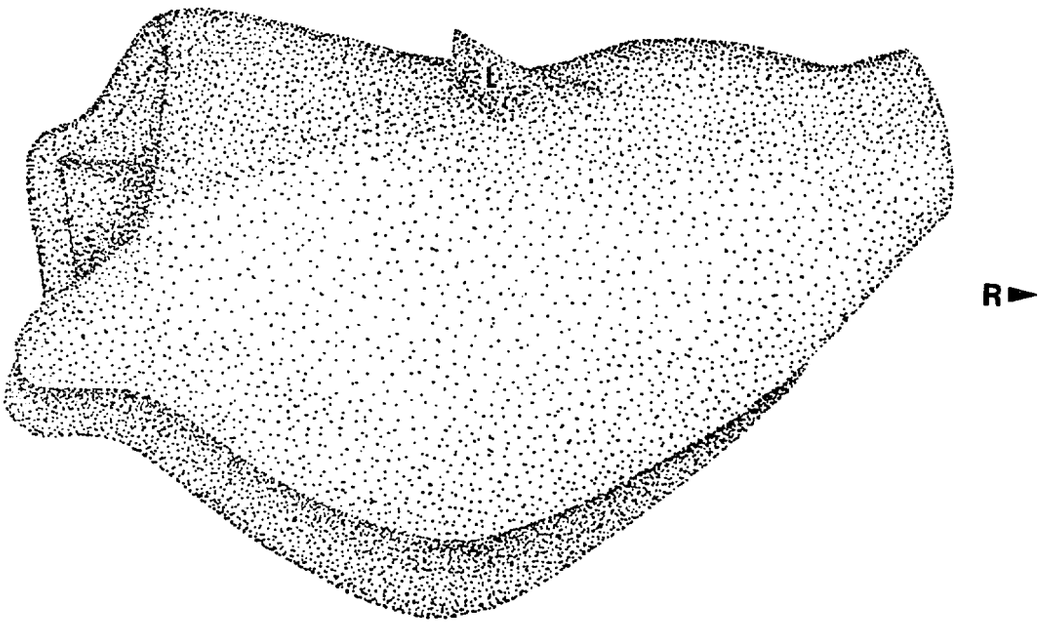

13-15B

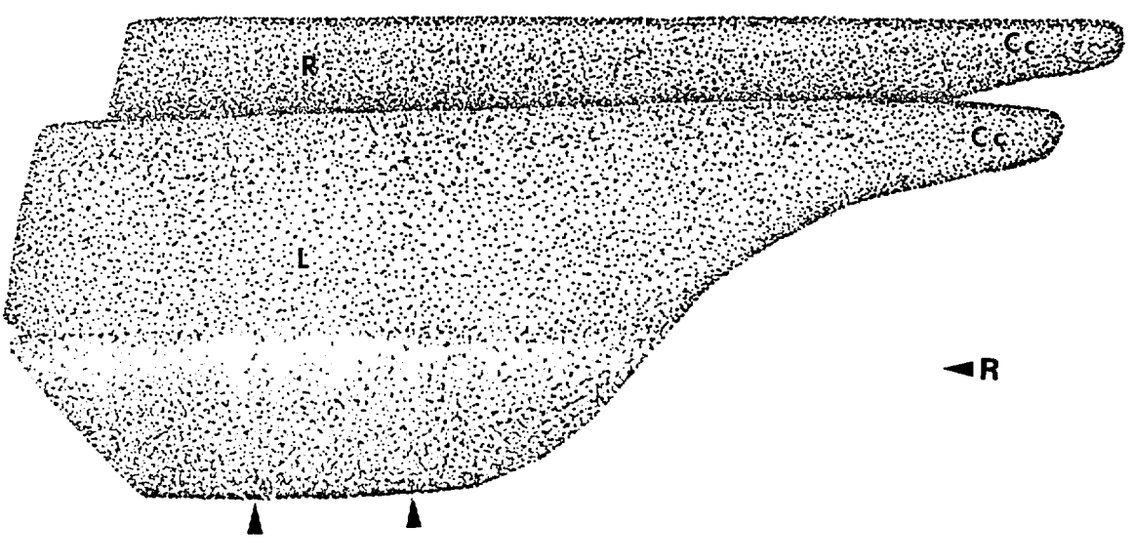

Figure 13-16. Photographs of a drawing of the cricoid and of the thyroid cartilages.

A. The conception of the entire cricoid cartilage (79B1). Note it begins rostrally (R) as a flattened plate and becomes trough shaped caudally. Note the cut ligament (L) which serves for attachment of the caudal ends of the cranial cornu of the thyroid cartilage.

B. Thyroid cartilages, dorsal view 80B1. Note the caudal cornua (Cc) and the transected skeletal muscle (S) (crico-thyroid muscle) on each side of the midline (arrowheads). The left caudal cornu is incomplete. X0.14

c. Thyroid cartilages, ventral view (80B1). Caudal cornua (Cc) , ventral midline (arrowheads). X0.16.

13-16A

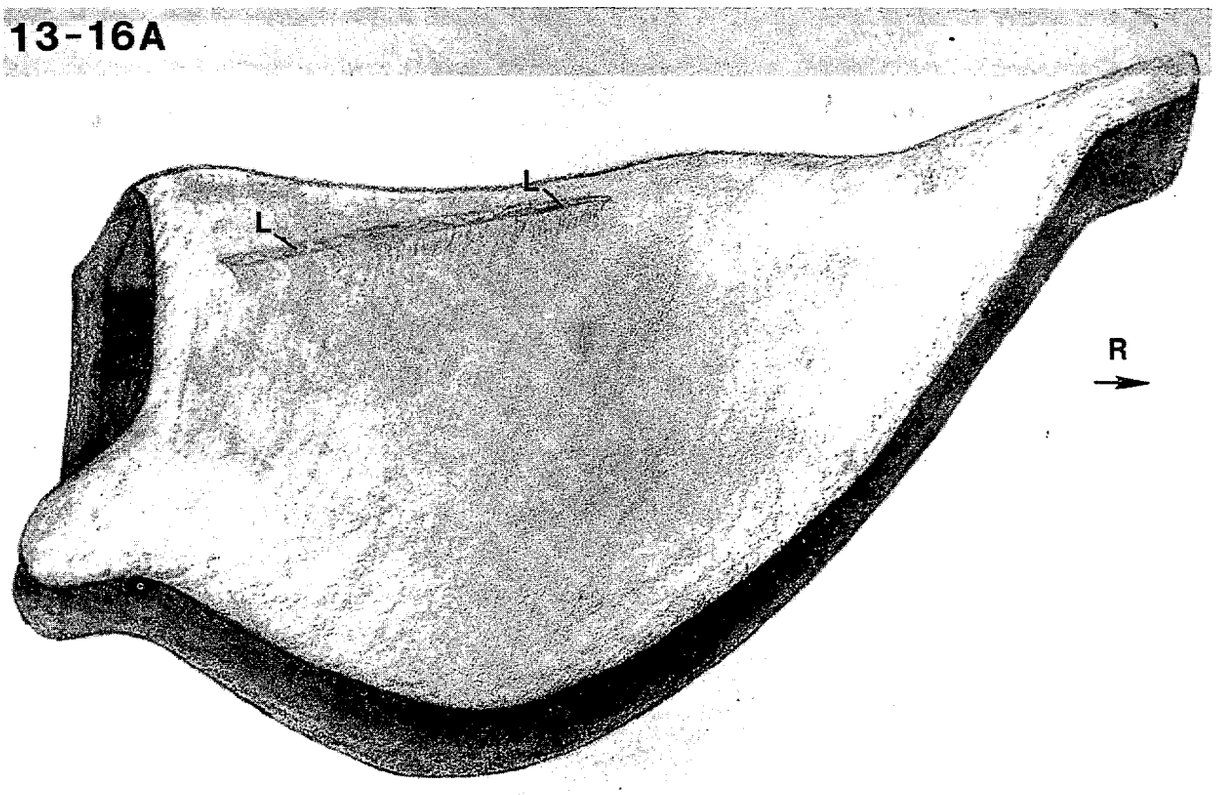

13-16B

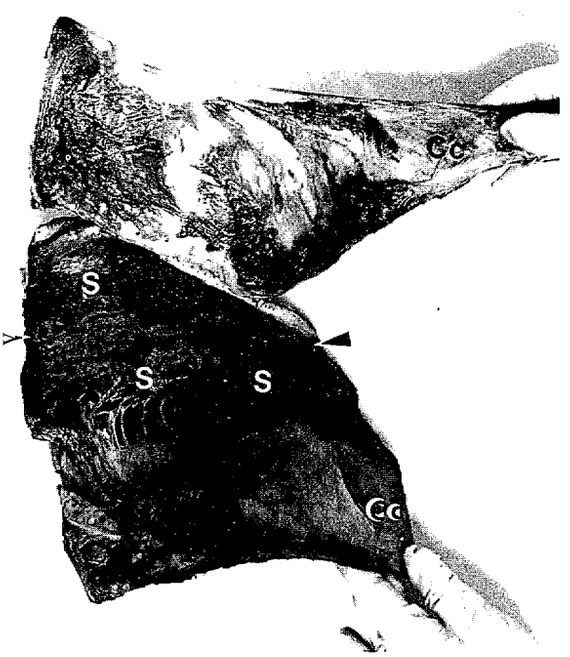

13-16C

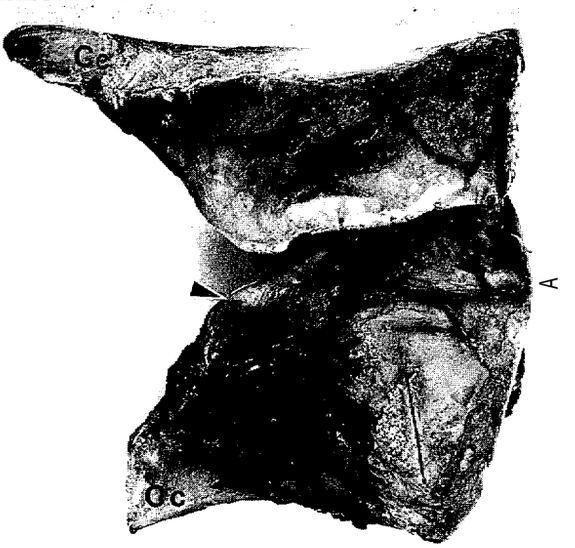

Figure 13-17. Photograph showing that the caudal cornua of the thyroid cartilages attach (arrowheads) via tough connective tissue sheets to the laryngeal sac muscle (M) at the level of the second tracheal ring, 80B1. The arytenoid cartilages (A) are connected caudally by dense connective tissue (Ct). Primary Bronchi (P). XO.4

13-17
A
A
Gt
M
P
P

Figure 13-18. Photomicrograph of the mucosal layer of the rostral extension of the epiglottis, 79B1. The epitheliums (E) is pigmented, keratinized, stratified squamous with vascularized connective tissue papillae (P) and periodic sensory papillae (SP). The lamina propria (LP) is typical dense irregular connective tissue with elastic fibers, blood vessels, nerve tracts, and adipose cells. L.S., H and"E, X50

Figure 13-19. Higher magnification photomicrograph of the sensory papilla of Fig 13-18. The normal layers of the keratinized stratified squamous epitheliums show well as stratum basale (B), stratum spinosum (S), and the keratinized stratum corneum (C). The sensory papilla is composed of one or more convoluted and elongated Herbsti-like encapsulated nerve end organs (arrows) surrounded by dense irregular connective tissue. L.S., H and E, X130

Figure 13-20. Photomicrograph of the ventral (outer) mucosa of the epiglottis, 79B1.

A. The deep propria submucosa (PS) contains mucoserous glands (arrowheads). A large excretory duct (D) is seen near the epidermis (E). X.S., Masson's stain, X50

B. Serous demilunes (arrowheads) are seen on the periphery of mucous acini (A) in the glands from Figure 13-20A. X.S. Masson's stain, X320

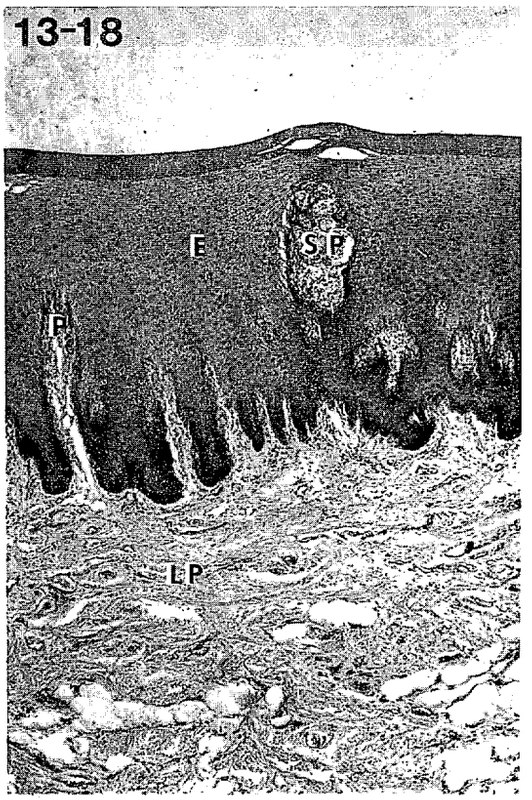
13-18
E
SP
P
LP

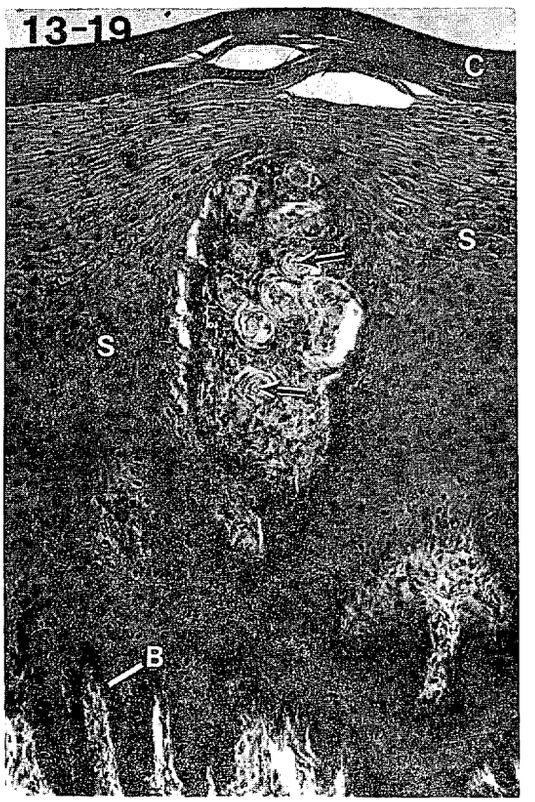
13-19
C
S
S
B

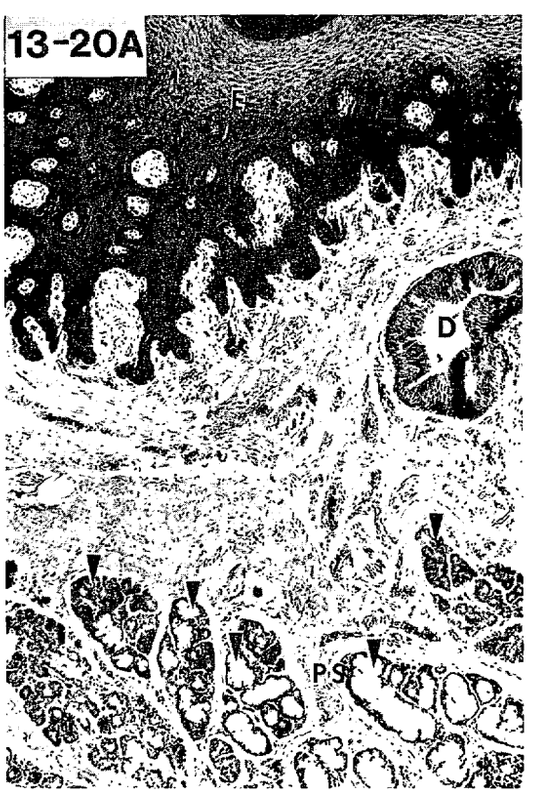
13-20A
E
D
PS

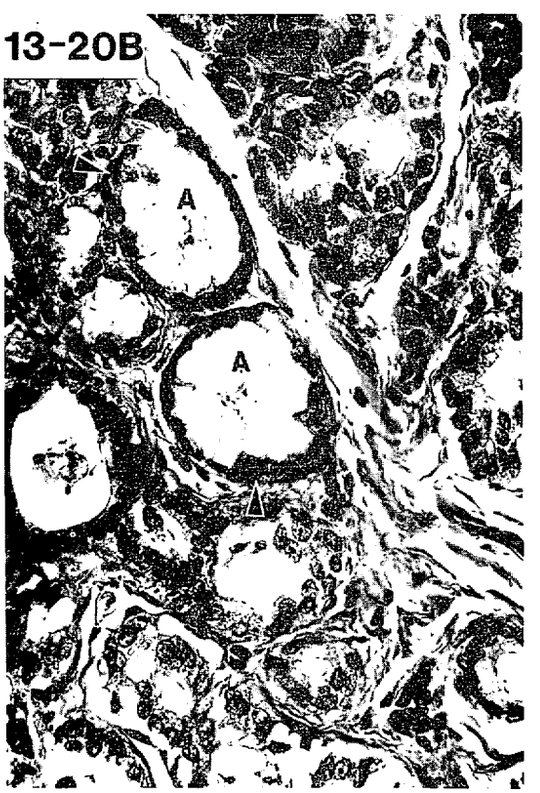
13-20B
A
A

Figure 13-21. Photomicrograph of the mucosal layer and hyaline cartilage of the mediorostral surface of the left arytenoid of 79B1. The mucosa is typical dense irregular connective tissue (CT) with elastic fibers, blood vessels, and nerve tracts covered by a pigmented, keratinized, stratified squamous epitheliums (E) as on the epiglottis (Fig 13-18). Enlarged sensory papillae (SP) are interspersed with connective tissue papillae (P). The arytenoid cartilage (HC) is of the hyaline type with vascular channels (VC) filled with blood vessels and loose connective tissue. L.S., Hand E, X21

Figure 13-22. Higher magnification photomicrograph of the sensory papilla (SP) in Fig 13-21. The elongated and convoluted nature of the Herbsti-like sensory, encapsulated, nerve end organ (arrow) shows well. The layers of the epitheliums can be seen: stratum corneum (C), stratum spinosum (S) and stratum basale (B).

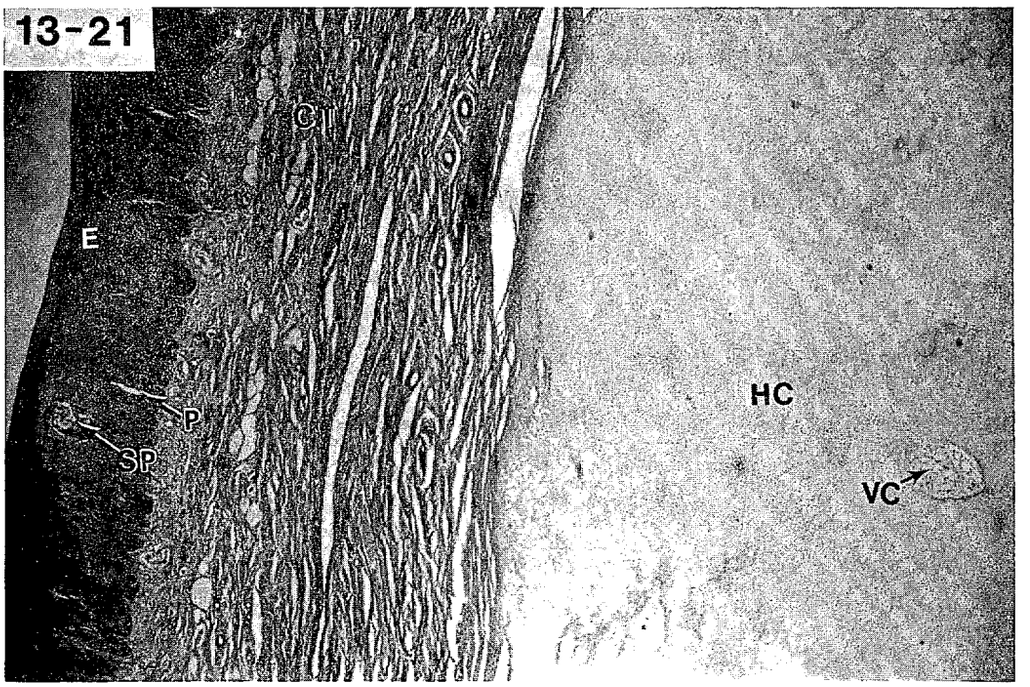
13-21
CI
E
P
SP
HC
VC

13-22
SP
C
S
B

Figure 13-23. Photographs of the trachea and laryngeal sac, 8061.

A. Cranial view. This reconstruction of serial sections shows the laryngeal sac (S) to be a caudal diverticulum of the caudal portion of the laryngeal cavity. It has a heavy muscular wall (M) which serves to close the ventral open portions of the "C" shaped tracheal cartilages (T). Caudal (c). X0.04

B. This section is through the midportion of the laryngeal sac (S) which is surrounded by the laryngeal sac muscle (M). The "C" shaped tracheal cartilages (T) are seen. X0.5

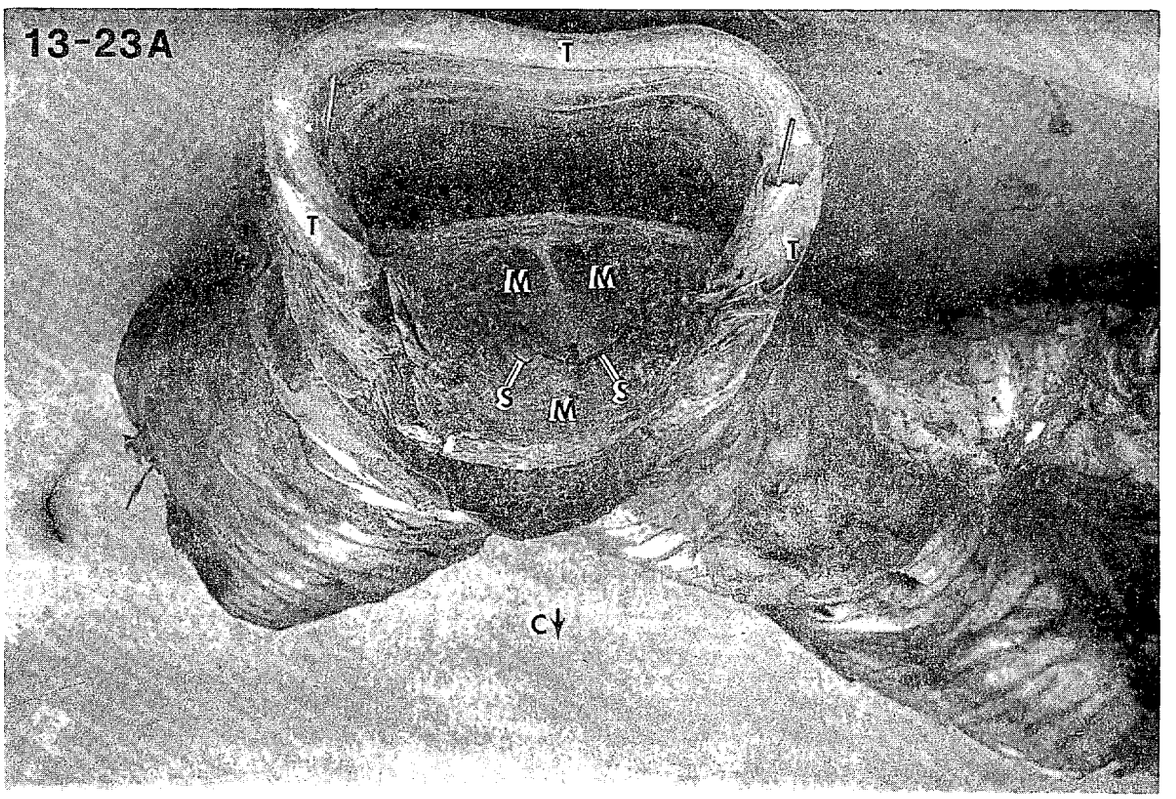
13-23A
T
T
T
M
M
S
M
S
C

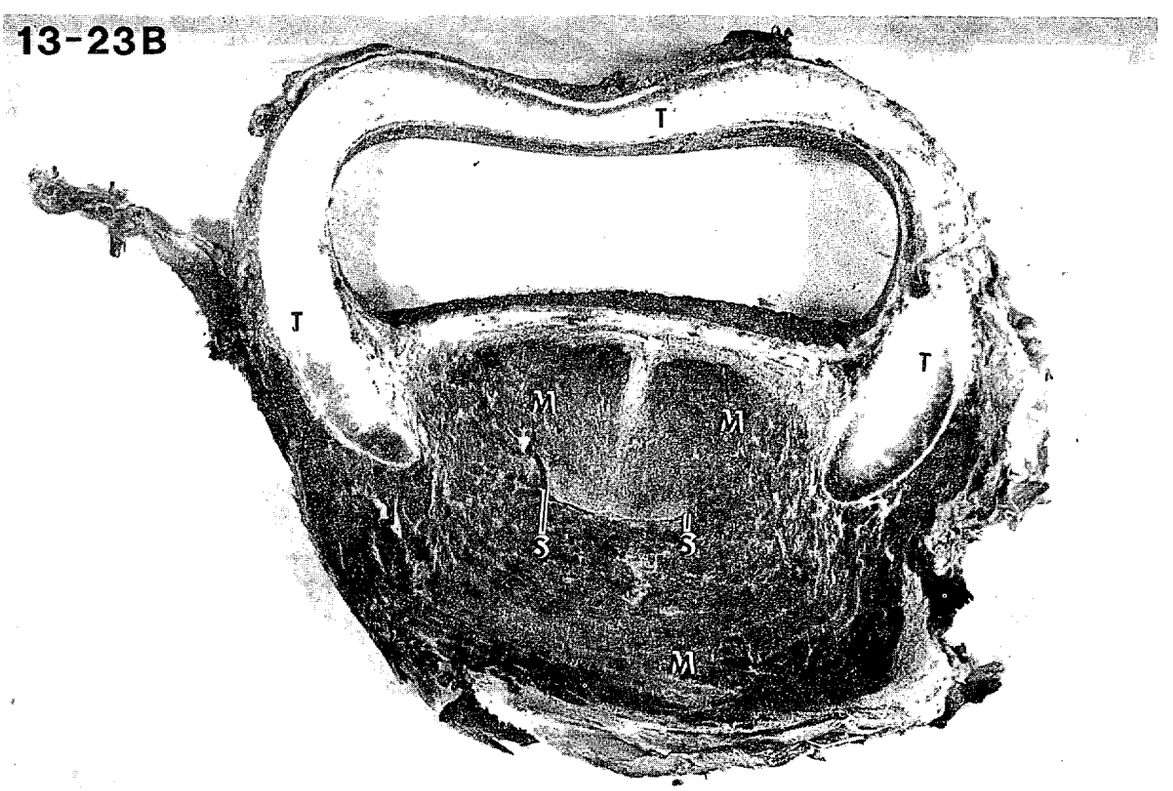
13-23B
T
T
T
M
M
S
S
M

Figure 13-24. Photomicrographs of the laryngeal sac microanatomy, 80B1.

A. The laryngeal sac is a mucous membrane lined diverticulum. The epitheliums (E) is stratified squamous. The lamina propria (LP) is dense irregular connective tissue with increased amounts of elastic fibers which overlays the laryngeal sac muscle. (not shown) X.S, Masson's stain. X50

B. The wal 1 of the sac has skeletal muscle bundles (arrows). Adipose cells (A). X. S., Masson's stain. X530

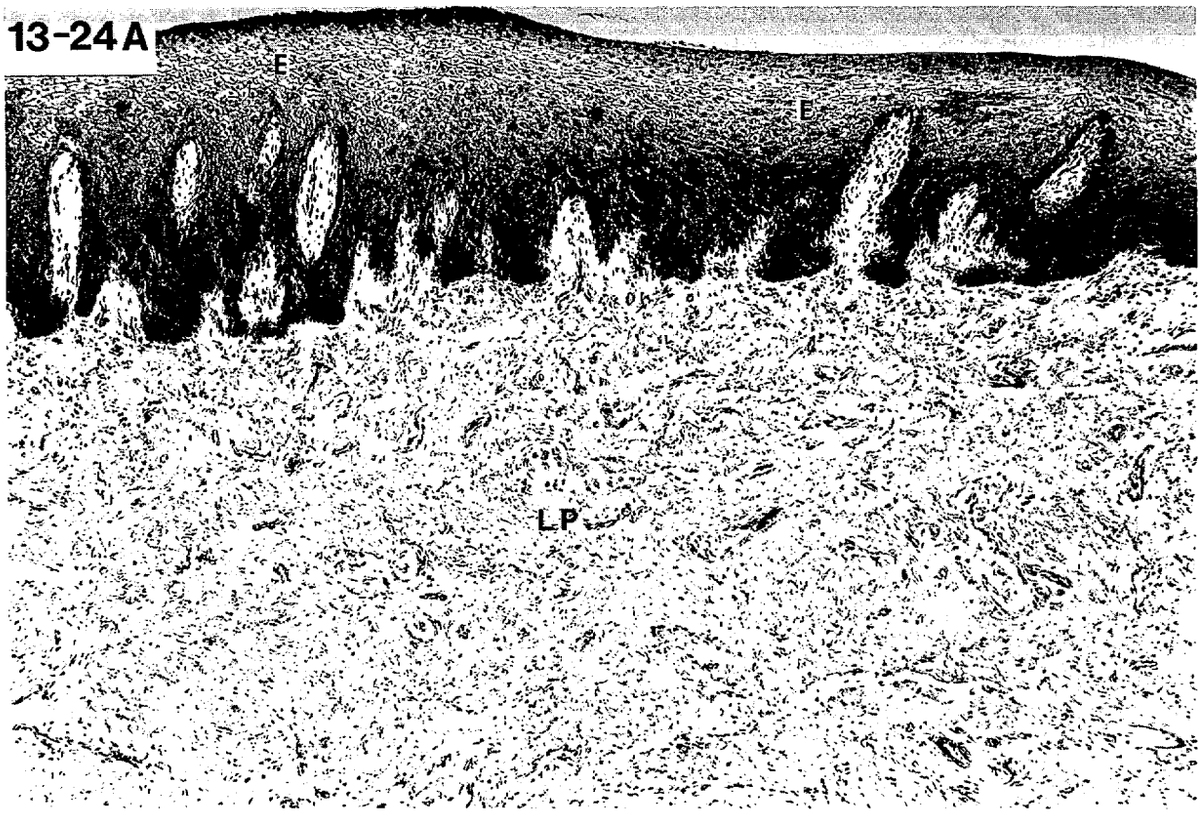
13-24A
E
E
LP

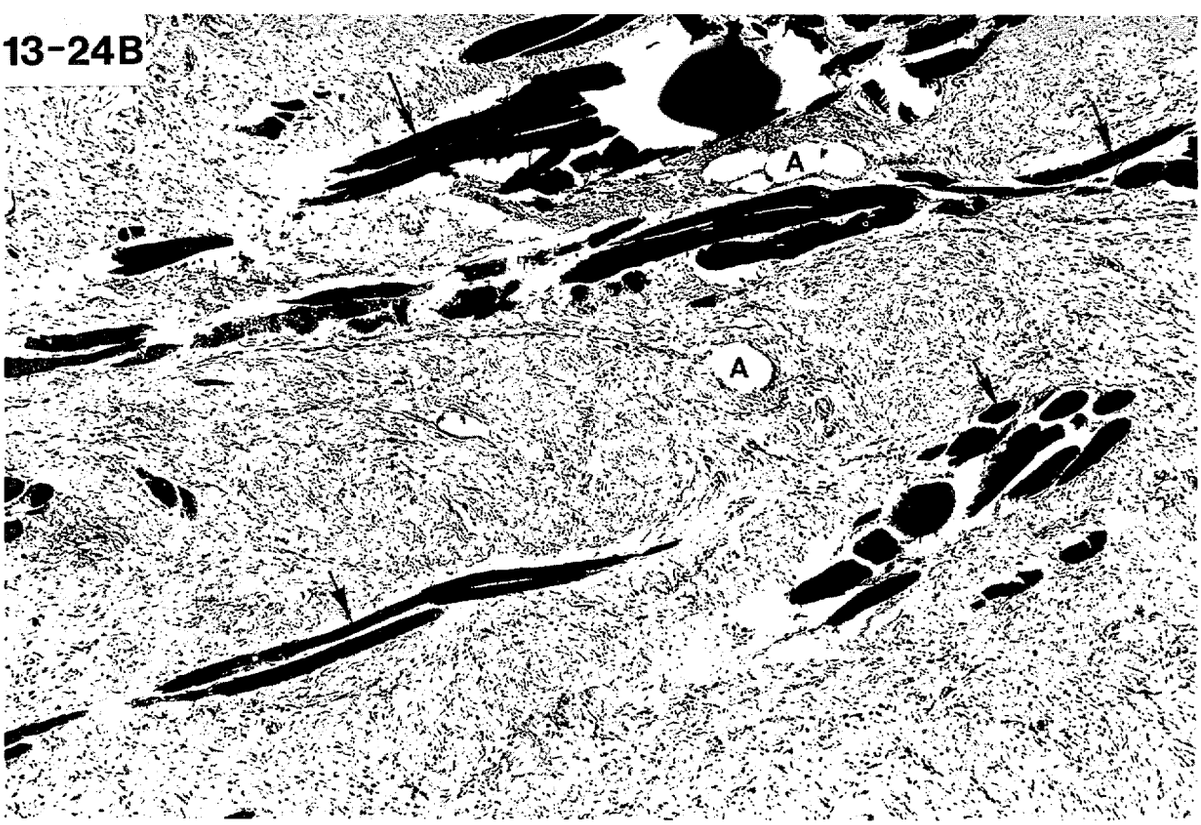
13-24B
A
A

Figure 13-25. Photographs showing the caudal one-third of the ventral trachea is closed by a cartilaginous plate, dense connective tissue and muscle, 80B1.

A. The rostralmost tip of the cartilaginous plate (CP) is surrounded by laryngeal sac muscle (M). Tracheal cartilages (T). X0.35

B. The middle portion of cartilaginous plate (CP) surrounded by laryngeal sac muscle (M). Tracheal cartilages (T). X0.4

CO The caudal portion of cartilaginous plate CP). Laryngeal sac muscle (M), overlapping tracheal carti ages (T), lumen of right principal bronchus (P). X0.4

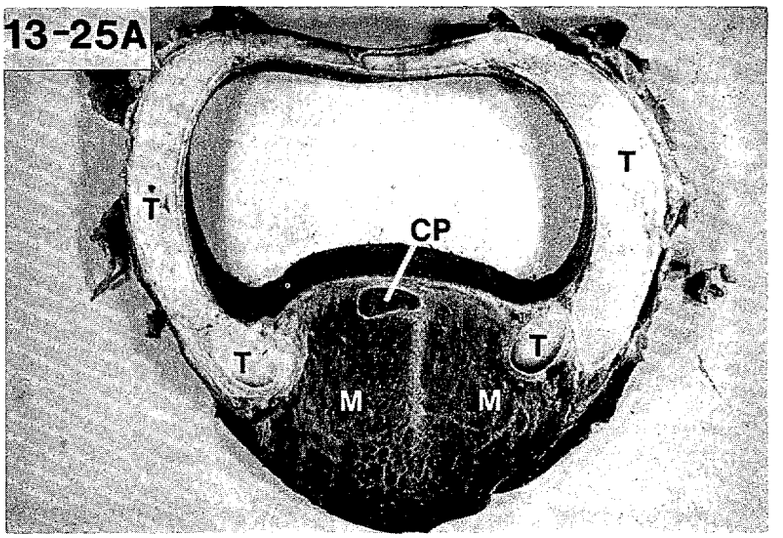
13-25A
T
T
CP
T
T
M
M

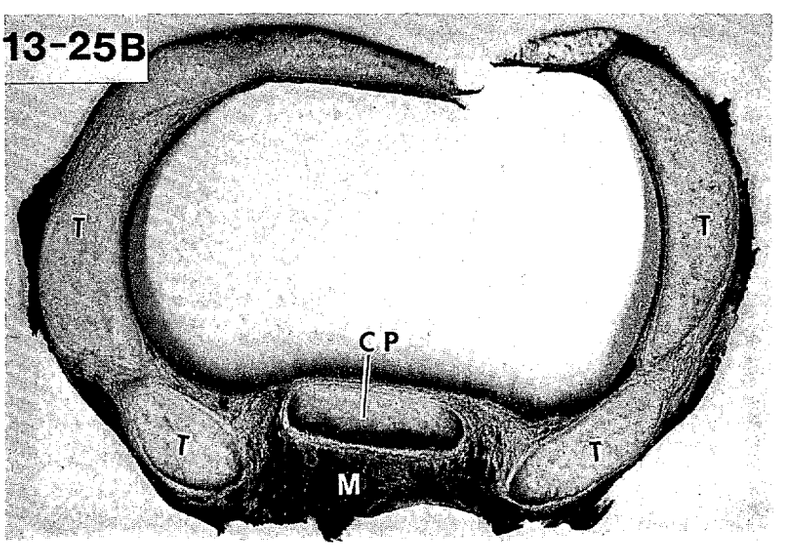
13-25B
T
T
CP
T
T
M

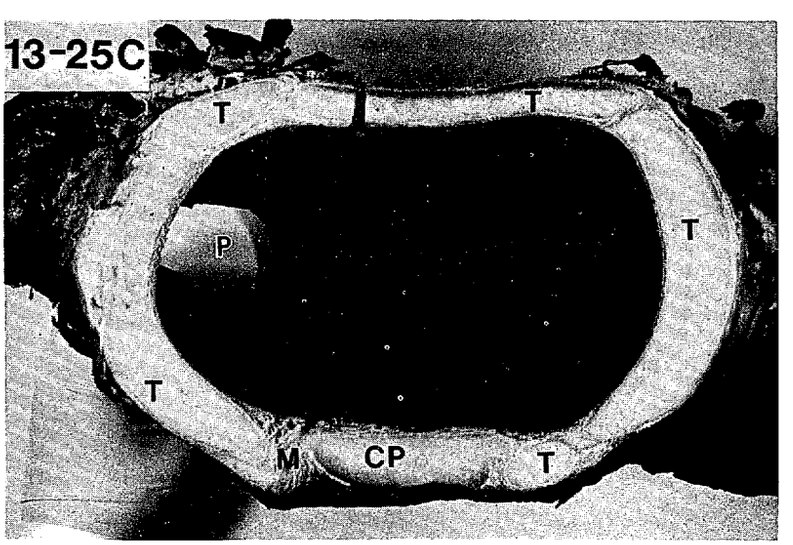
13-25C
T
T
P
T
T
M
CP
T

Figure 13-26. Photomicrographs of a longitudinal section of the larynx near the laryngotracheal junction, 80B1.

A. The laryngeal epitheliums (E) is nonkeratinized stratified squamous changing to ciliated pseudostratified columnar epitheliums of the laryngotracheal junction. The lamina propria (LP) has lymphatic nodules (N) just deep to the epitheliums which is underlain by a dense irregular connective tissue. The connective tissue has abundant elastic and collagen fibers and some adipose cells (A). L.S., H and E, X50

B. Higher magnification of the lymph nodule (N) in Figure 13-26A. Labels as above. L.S., H and E, X130

Figure 13-27. Photomicrographs of a longitudinal section of the trachea at the laryngotracheal junction, 80B1.

A. The tracheal epitheliums at the laryngotracheal junction is primarily ciliated pseudostratified columnar epitheliums (E), however, it is a transitional area from the stratified squamous epitheliums of the larynx. The lymphatic (L) infiltration of the lamina propria (LP) is diffuse with only occasional nodular formation. The connective tissue is highly elastic. L.S., H and E, X50

B. This is a higher magnification of Fig 13-27A illustrating the more diffuse nature of the lymphatic tissue (L) underlying the epitheliums (E). LP - lamina propria. L.S., H and E, X130

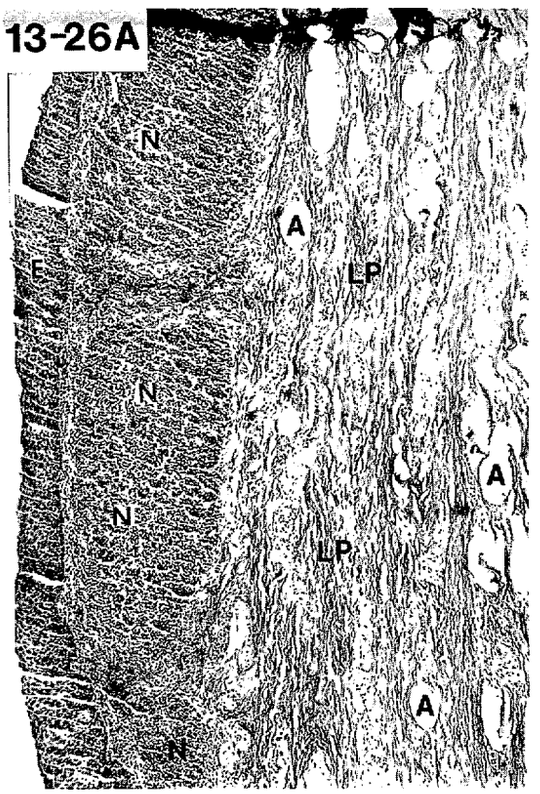
13-26A
N
E
A
LP
N
N
A
LP
A
N

13-26B
E
A
N
LP

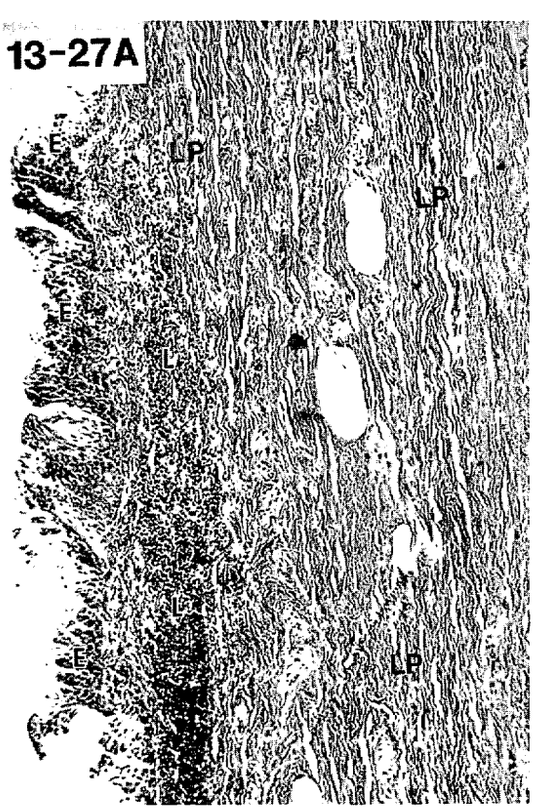
13-27A
E
LP
LP
E
L
L
E
LP

13-27B
E
E
L
L
LP

Figure 13-28. Photomicrographs of a longitudinal section of the mid-trachea, 80B1 .

A. The tracheal epitheliums (E) at this level is ciliated pseudostratified columnar. The lamina propria has dense irregular elastic fibers (EF) and contains a 400 μm layer of mucous glands (G). L.S., H and E. X50.

B. Higher magnification of Fig 13-28A. Bundles of elastic fibers (EF) course through the mucous glands (G) which are just below the ciliated pseudostratified columnar epithelium (E). L. S., H and E. X130.

C. Section through the junction of two tracheal cartilages (TC). Note the high percentage of elastic fibers (EF). L. S., Verhoeff stain. X50

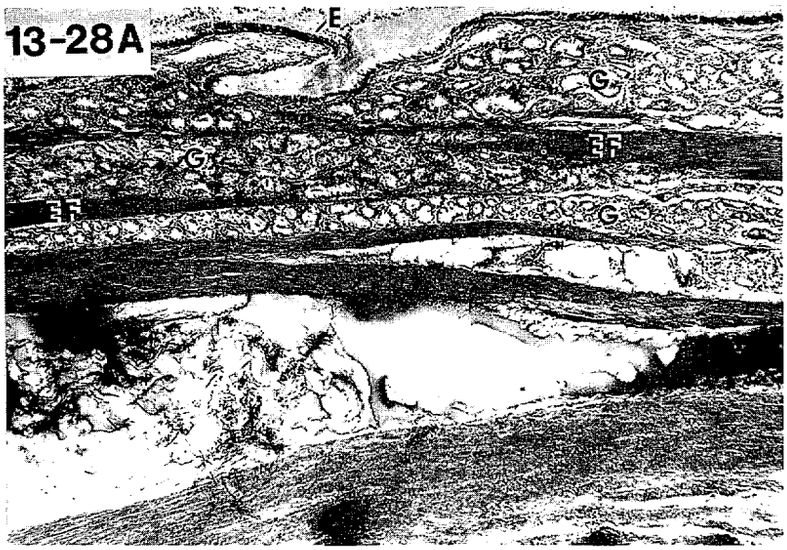
13-28A
E
G
G
EF
EF
G

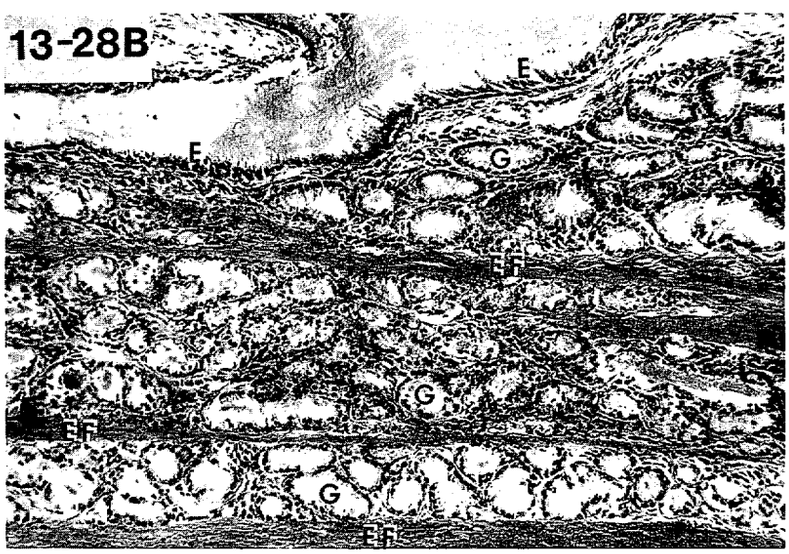
13-28B
E
E
G
EF
G
EF
G
EF

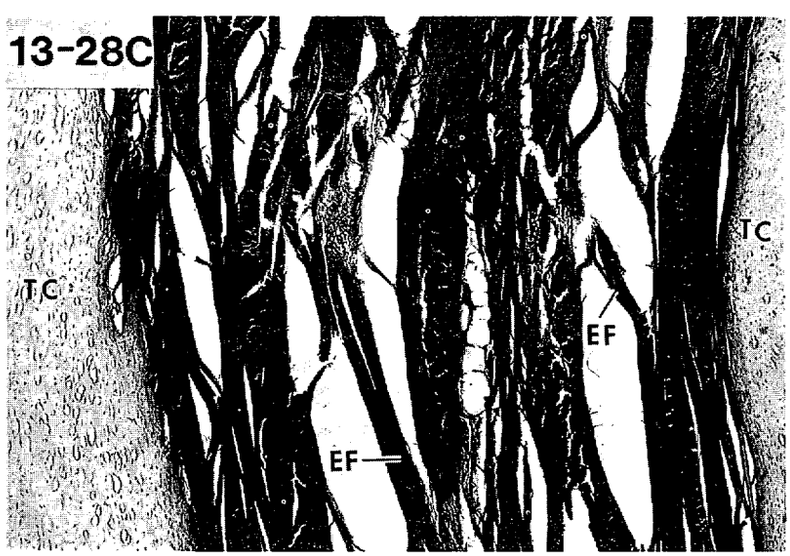
13-28C
TC
TC
EF
EF

Figure 13-29. Photographs of the tracheal bifurcation, 80B1.

A. A cranial view showing the lumina (L) of the principal bronchi (B). Trachea (T). XO.4

B. A dorsal view of the slight depression (D) formed by the esophagus as it lies on the dorsal surface of the trachea. The tracheal cartilages (R) are open ventrally. Bronchi (B). XO.25

C. A ventral view as the trachea (T) bifurcates 19 cm caudal to the cricoid cartilage. The principal bronchi (B) which result from the tracheal division have complete cartilaginous rings (R) which branch and anastomose. Laryngeal sac muscle (M). XO.75

D. A ventral view demonstrating the ventrally open tracheal cartilages (C) but the complete principal bronchial rings (R). The open cartilages are closed by the laryngeal sac muscle (M) except where it has been removed. XO.25

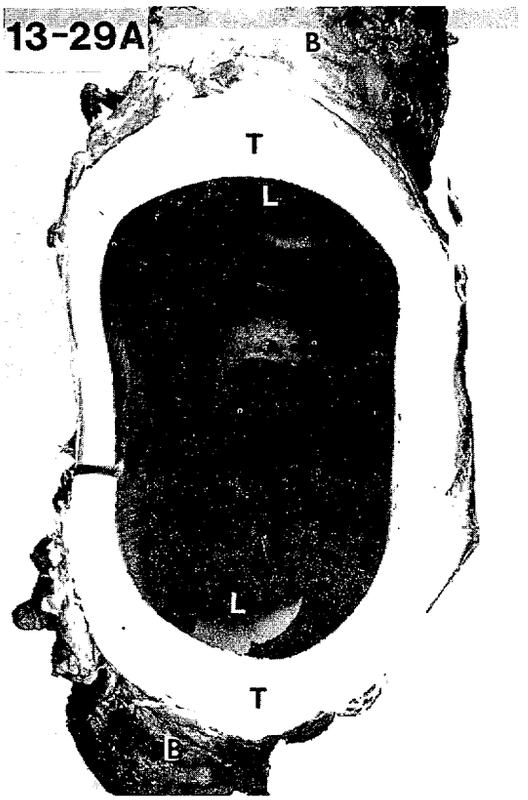
13-29A
B
T
L
L
T
B

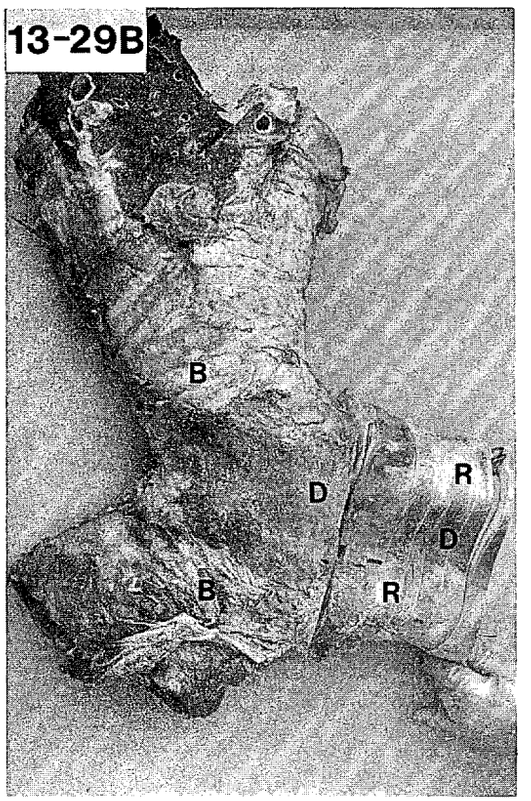
13-29B
B
D
R
D
B
R

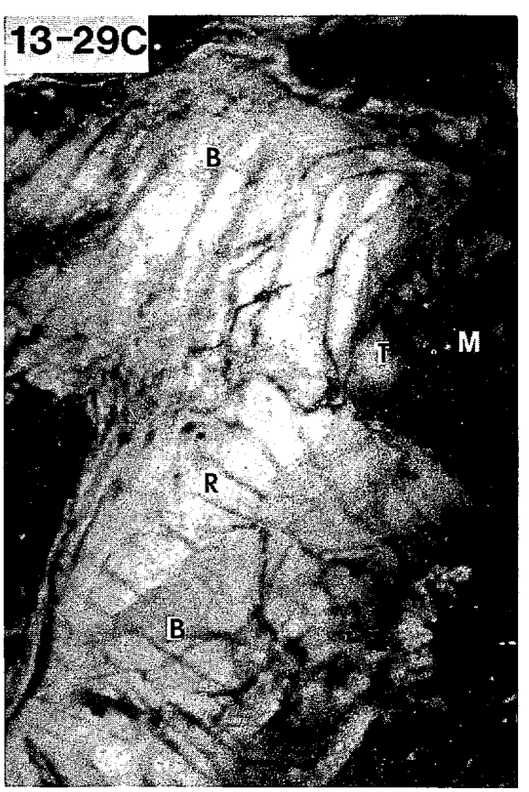
13-29C
B
T
M
R
B

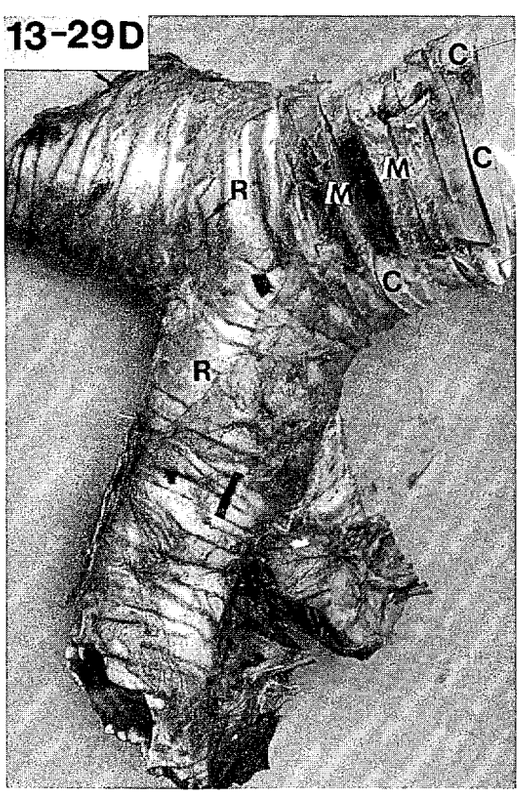
13-29D
C
C
M
R
M
C
R

Figure 13-30. Photomicrograph of the mucosal lining of a primary bronchus of 38 x 95 mm size from 80B8 Tag 3. Ciliated pseudostratified columnar epitheliums (Ep) lines the bronchus covering a dense irregular connective tissue lamina propria with mucosal mucous glands (G). Thick laminae of longitudinally oriented dense elastic fibers (E) are located between the lamina propria and the dense irregular connective tissue surrounded hyaline cartilage ring (not in picture). X.S., H and E, X130

Figure 13-31. Higher magnification photomicrograph of the mucosa in Fig 13-30. The mucus producing cells (arrows) of the pseudostratified columnar epitheliums (Ep) and mucosal mucous glands (G) are well illustrated. The elastic lamina (E) is also illustrated. X.S., H and E, X320

Figure 13-32. Photomicrograph of a semi-thin section of the mucosa of the primary bronchus of 80B8 Tag 3. The mucous nature of the tall cells (M) is more visible. Tall surface cells reach the basement membrane (arrow). TEM (see Fig 13-33) provides the verification. The vascularity (V) of the dense irregular connective tissue (D) of the lamina propria is also visible. Epon, X.S., Toluidine blue stain, X160

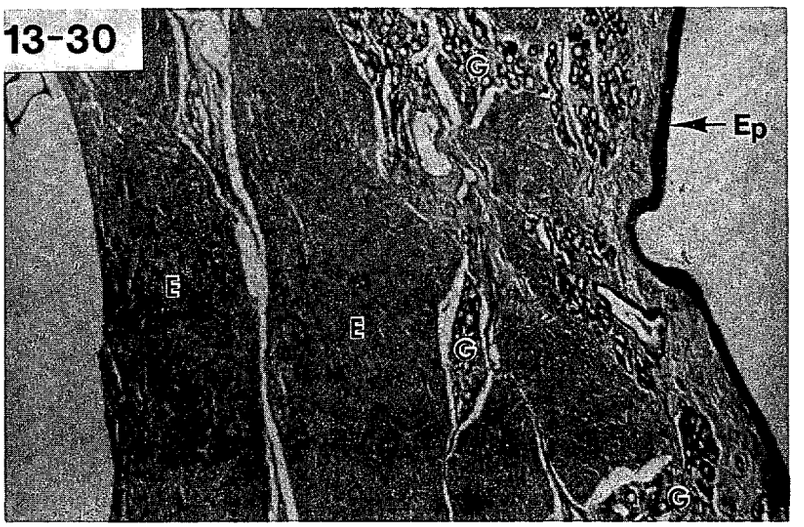
13-30
Ep
E
E
G
G
G

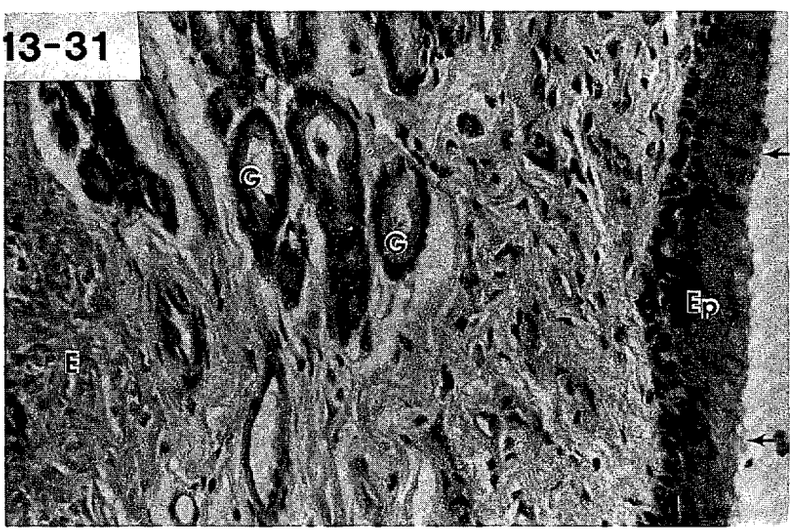
13-31
G
G
Ep
E

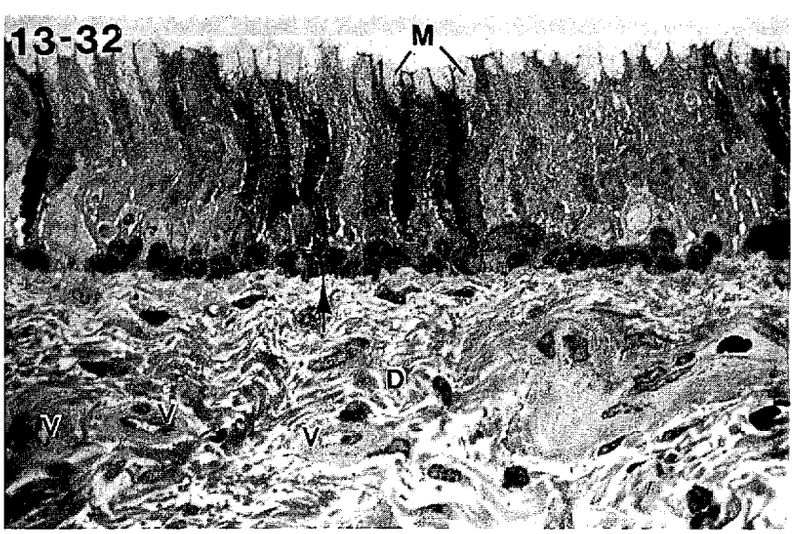
13-32
M
D
V
V
V

Figure 13-33. Scanning electron photomicrograph of a representative area of the surface of the primary bronchus of whale 80B8. Numerous ciliated cells (C) and conciliated cells containing microvilli (NC) may be seen. The number of ciliated and conciliated cells appear to be about equal . X3 ,800

Figure 13-34. Higher magnification scanning electron photomicrograph of a region similar to that seen in Fig 13-33. Conciliated cells may be seen bulging from the surface with numerous microvilli (MV). x7 ,500

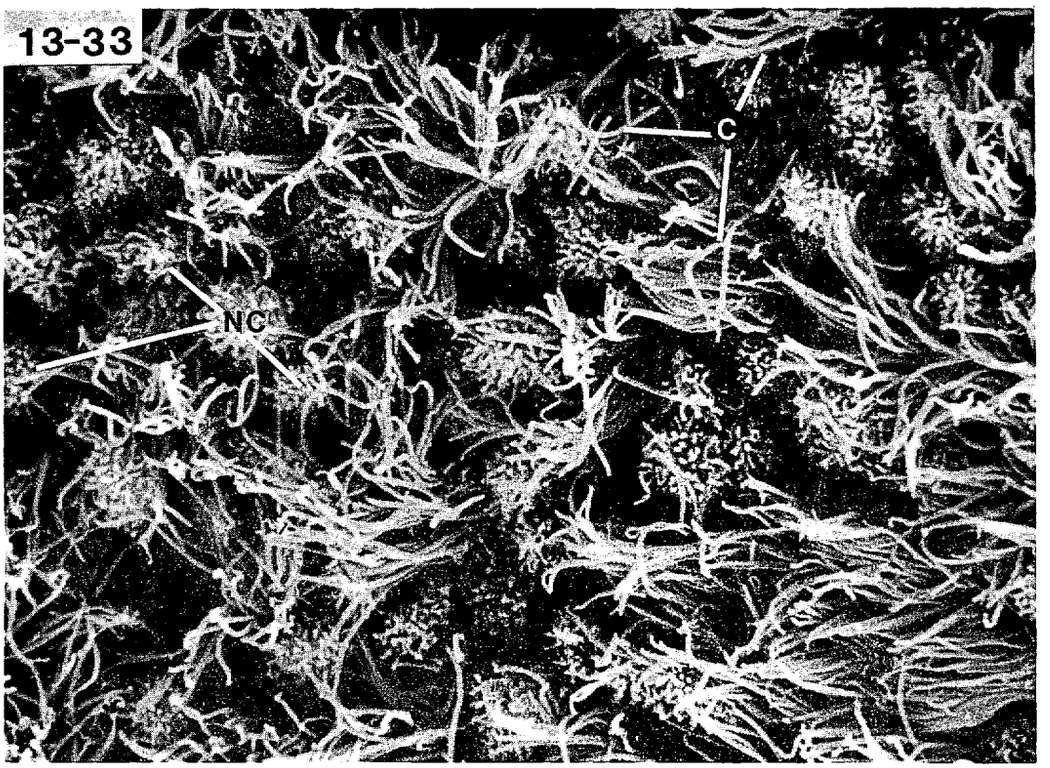
13-33
C
NC

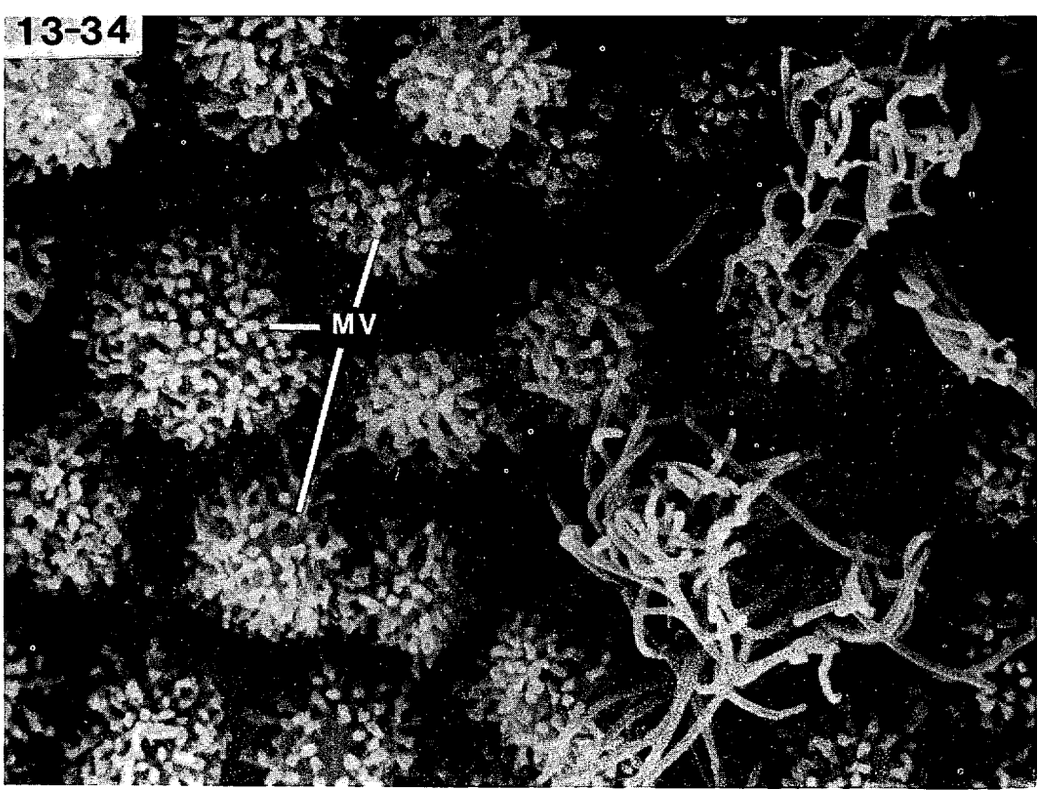
13-34
MV

Figure 13-35. Higher magnification scanning electron photomicrograph of a region similar to that seen in Fig 13-33. The ciliated cells are seen to have microvilli (MV) interspersed among the cilia (c). The microvilli of ciliated cells are more slender than those seen on the surface of noncil iated cel 1s (NC). X22,400.

Figure 13-36. Scanning electron photomicrograph of a representative area of the surface of the primary bronchus of whale 80B1. Rows of ciliated cells (C) are seen to alternate with conciliated regions. The conciliated region shows no evidence of cells possessing only microvilli on their surfaces. Debris (D) may be seen in the conciliated regions. The lack of cells possessing only microvilli and the presence of debris may indicate poor tissue preservation. X5,300

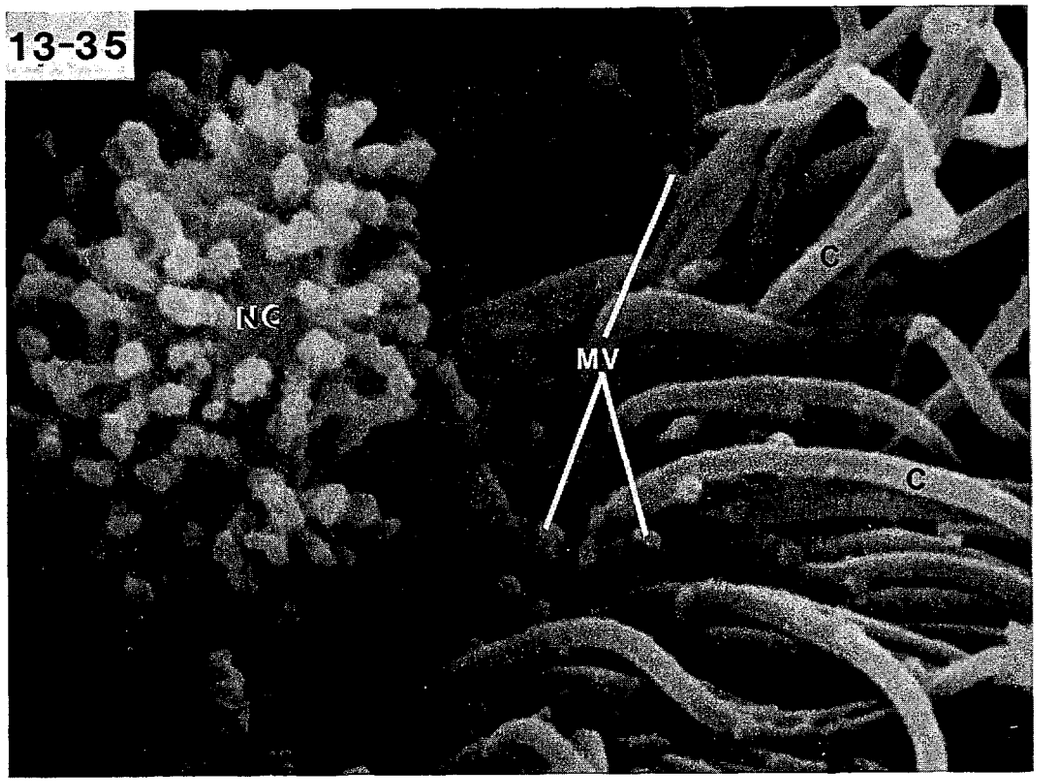
13-35
NC
MV
C
C

13-36
D
D
C

Figure 13-37. Transmission electron photomicrographic montage illustrating a portion of the primary bronchus of whale 80B8. In this region only mucus producing cells are seen at the luminal surface. Microvilli (MV) protrude from their surfaces. Cells with two different staining characteristics (light and dark) may be seen. Both cel 1 types contain mucus granules (MG). The 1 ateral surfaces of these columnar cells show complex interdigitations and near the base possess extremely delicate and tortuous cytoplasmic projections. Intermediate cel 1s (IM) and basal cells (BC) are also evident in this micrograph. A thin basal lamina (BL) may be seen beneath the basal cells and below it collagen of the underlying connective tissue. The extension of columnar mucous cell processes to the basal lamina may best be seen by following the fine processes of a densely stained cell (arrow). X4,100

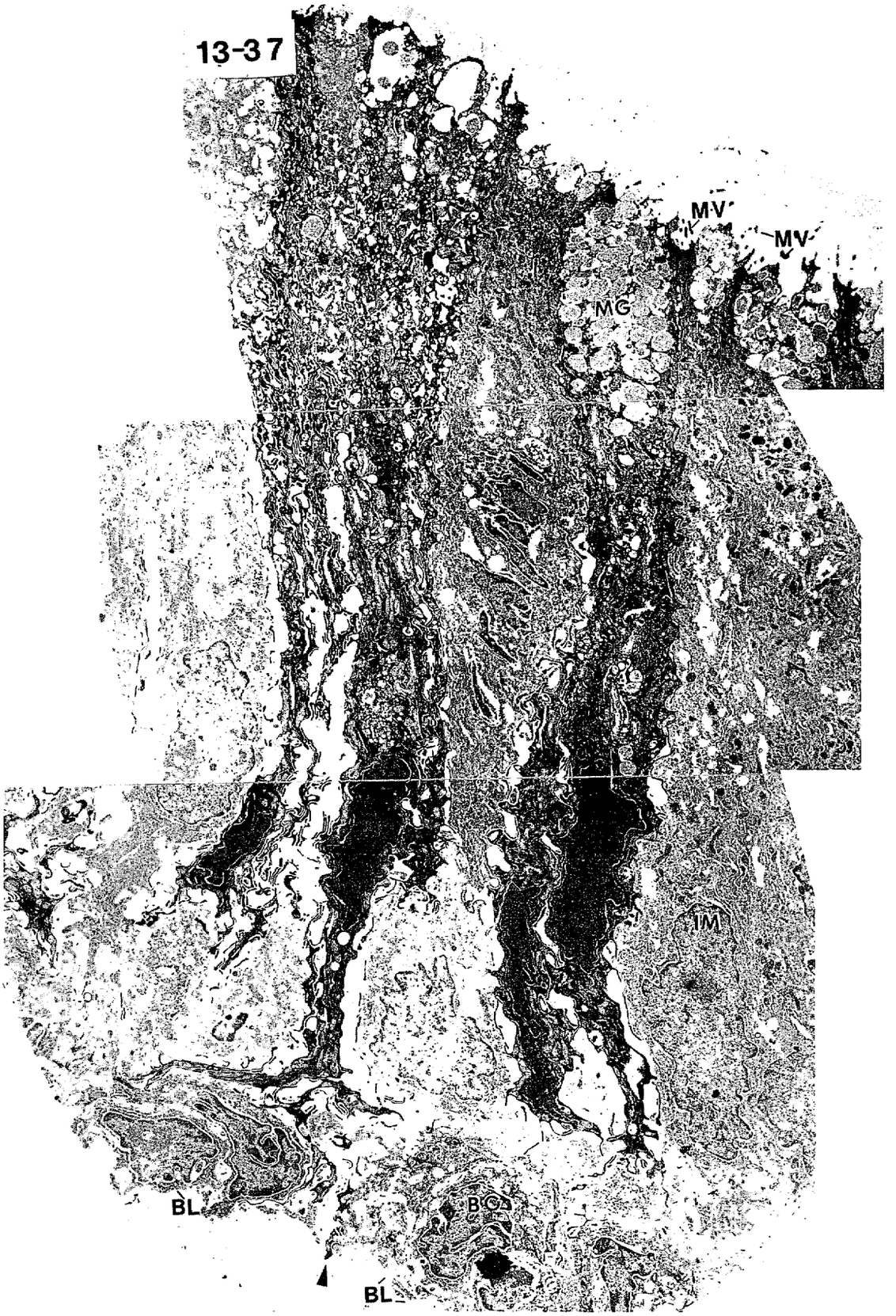
13-37
MV
MV
MG
IM
BL
BG
BL

Figure 13-38. Transmission electron photomicrographic montage illustrating a portion of a primary bronchus of whale 80B8. Microvilli (MV) may be seen protruding from the luminal surface of the columnar mucous cells whose basic morphology is similar to that described in Fig 13-37. The basal portion of a densely staining cell may be clearly seen to contact the basal lamina (BL) at the arrow. Intermediate (IM) and basal (BC) cel 1s may be seen. Certain regions appear to contain two layers of basal cells (arrowheads). A mononuclear cell, (+) possibly a lymphocyte, may be seen infiltrating the epitheliums. Beneath the basal lamina (BL) collagen and fibroblast nuclei (FB) are evident. An endothelial cell (EC) may be seen lining a small vessel in the connective tissue. x4 ,100

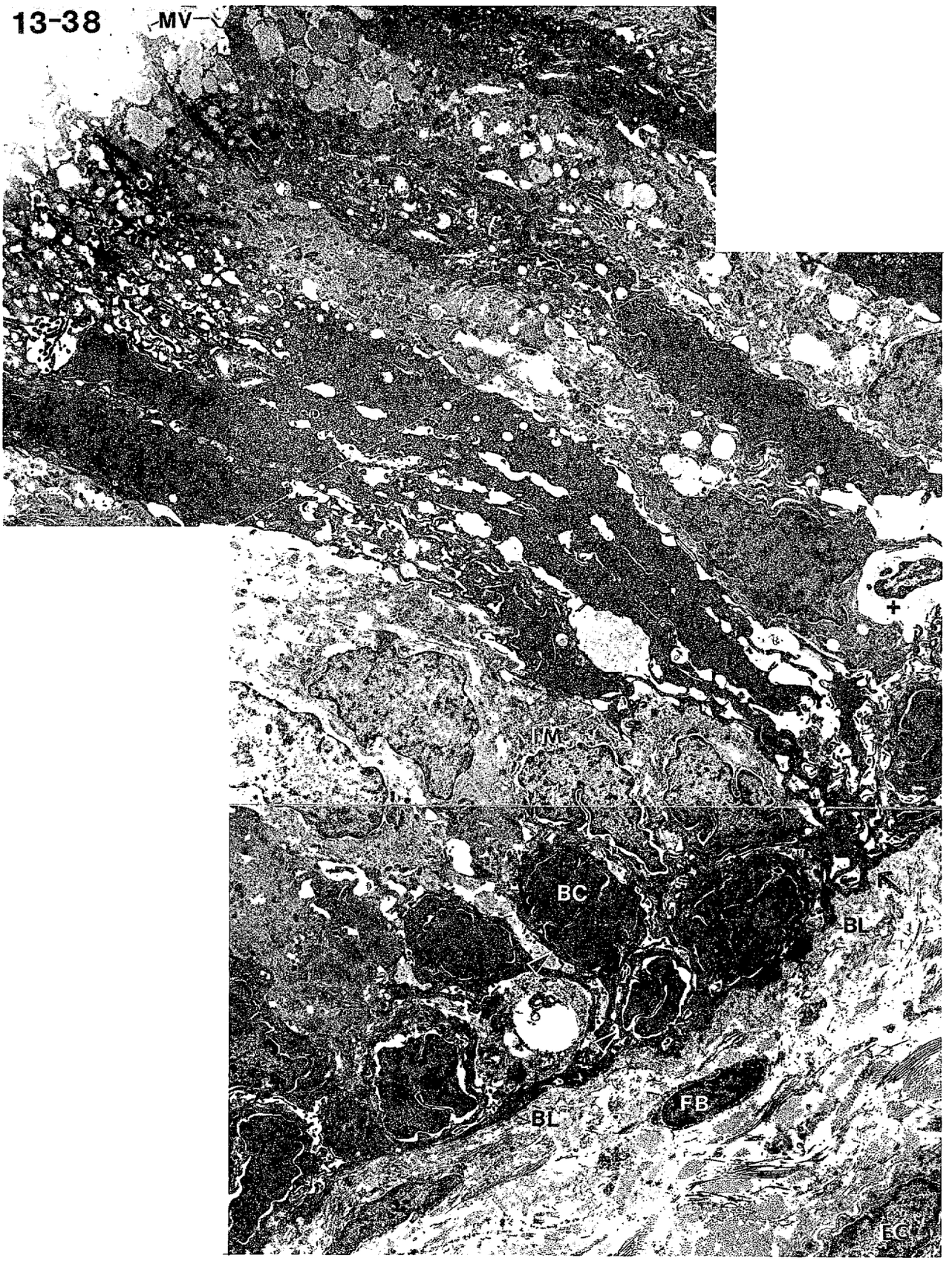
13-38
MV
IM
BC
BL
BL
FB
EC

Figure 13-39. Transmission electron photomicrograph of the basal region of the lining epitheliums from the primary bronchus of whale 80B8. Complex interdigitations of the cytoplasmic processes of cells in the basal region may be seen. Desmosomes (D) forming junctions between adjacent processes are evident. The nuclei (N) of basal cells are also evident exhibiting deep invaginations and occasional nucleoli (NI). X14,600

Figure 13-40. Higher magnification transmission electron photomicrograph of a region similar to that seen in Fig 13-39. The basal cells rest on the basal lamina (BL) and are anchored to it by hemidesmosomes (HD). A desmosome (D) can also be seen forming a junction between cytoplasmic extensions of cells in the basal region. X30,000

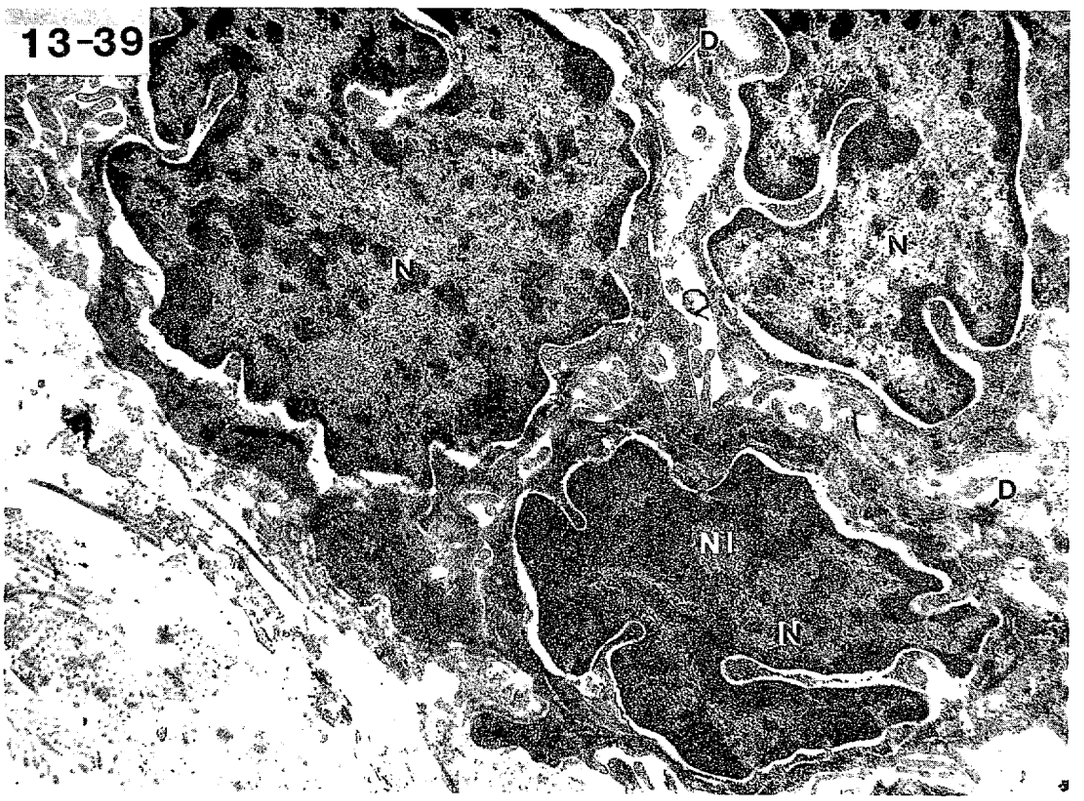
13-39
D
N
N
D
NI
N

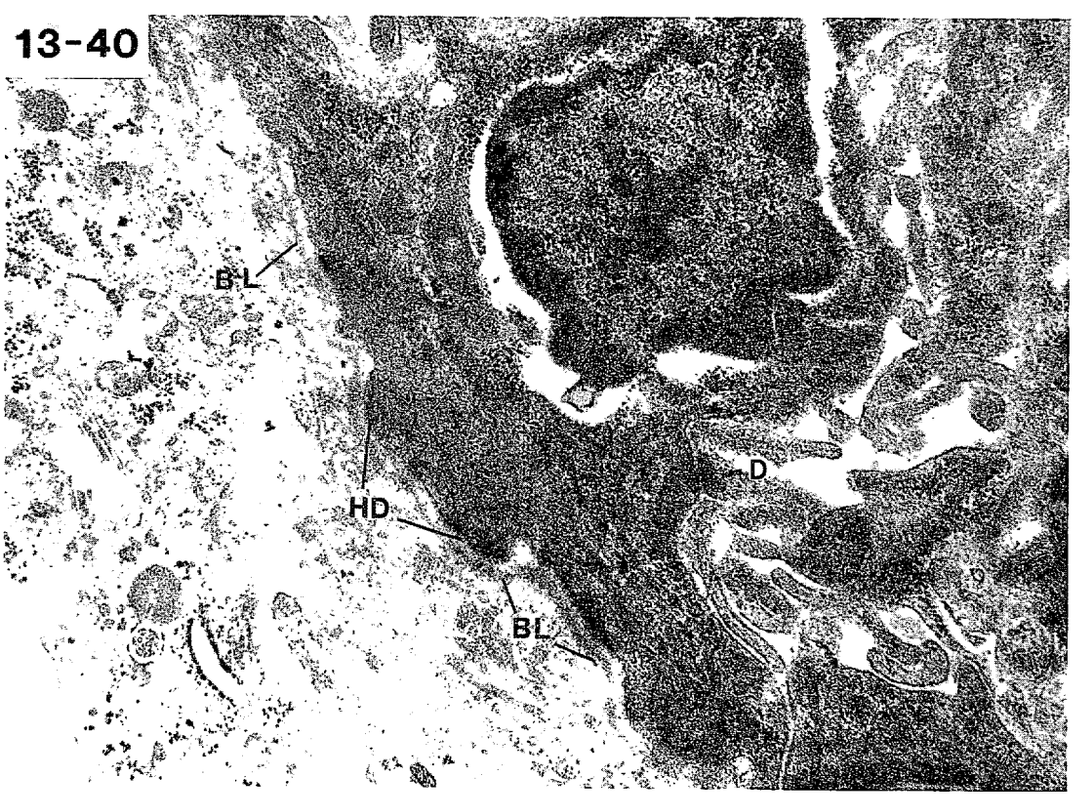
13-40
BL
D
HD
BL

Figure 13-41. Transmission electron photomicrograph of a plasma cell in loose connective tissue beneath the epitheliums of a primary bronchus of whale 80B8. This cell displays typical plasma cell morphology with highly expanded cisternae of rough endoplasmic reticulum evident (arrows). X14,500

Figure 13-42. Transmission electron photomicrograph of a plasma cell similar to that shown in Fig 13-41 but displaying the characteristic cartwheel distribution of heterochromatin within the nucleus. A number of electron dense inclusions (I) are evident in a region of cytoplasm devoid of rough endoplasmic reticulum. X10 ,300

13-41

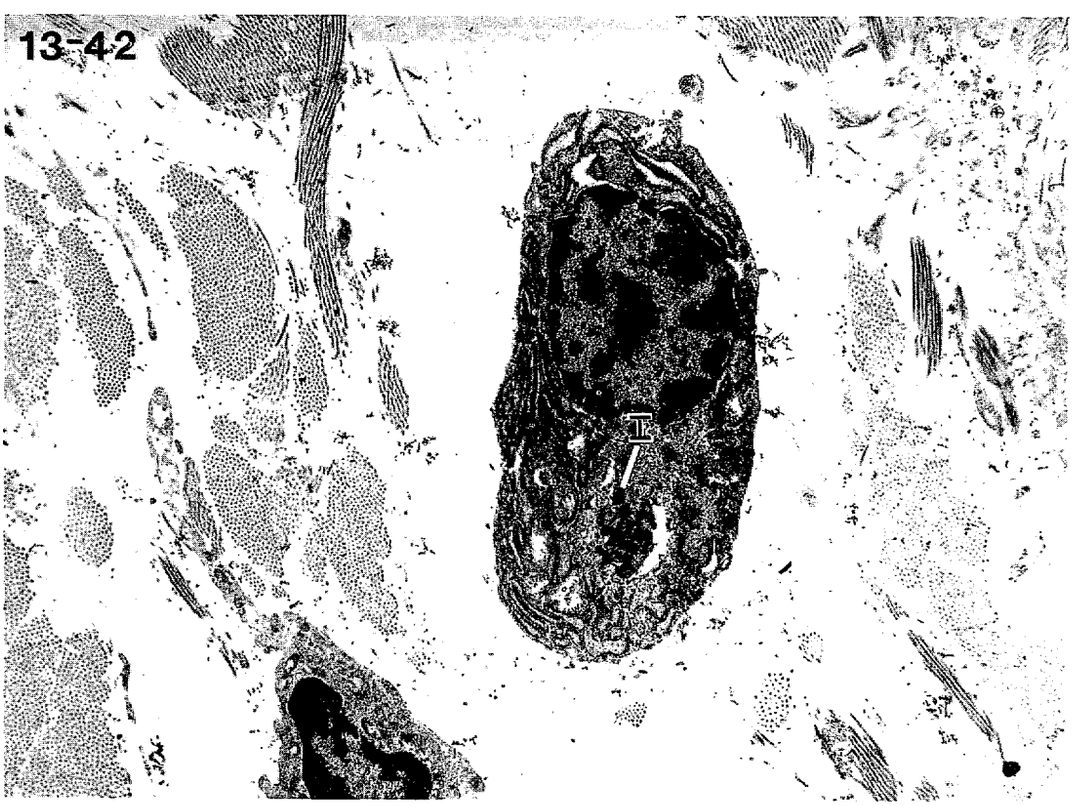
13-42

Figure 13-43. Transmission electron photomicrograph of cells of a submucosal mucous gland in the primary bronchus of whale 80B8. The apical surface of these cells display microvilli (MV) which extend into the lumen filled with secretory product (SP). Numerous mucous granules (MG) may be seen near the cell apex. Rough endoplasmic reticulum (RER) is evident in the cytoplasm. The cells rest on a basal lamina (BL) which separates them from the underlying connective tissue. X7,100

Figure 13-44. Transmission electron photomicrograph of cells similar to those shown in Fig 13-43. Apical microvilli (MV) are visible as are many junctional regions (J) between adjoining cells. An intercellular canaliculus (IC) may also" be seen. X9,800

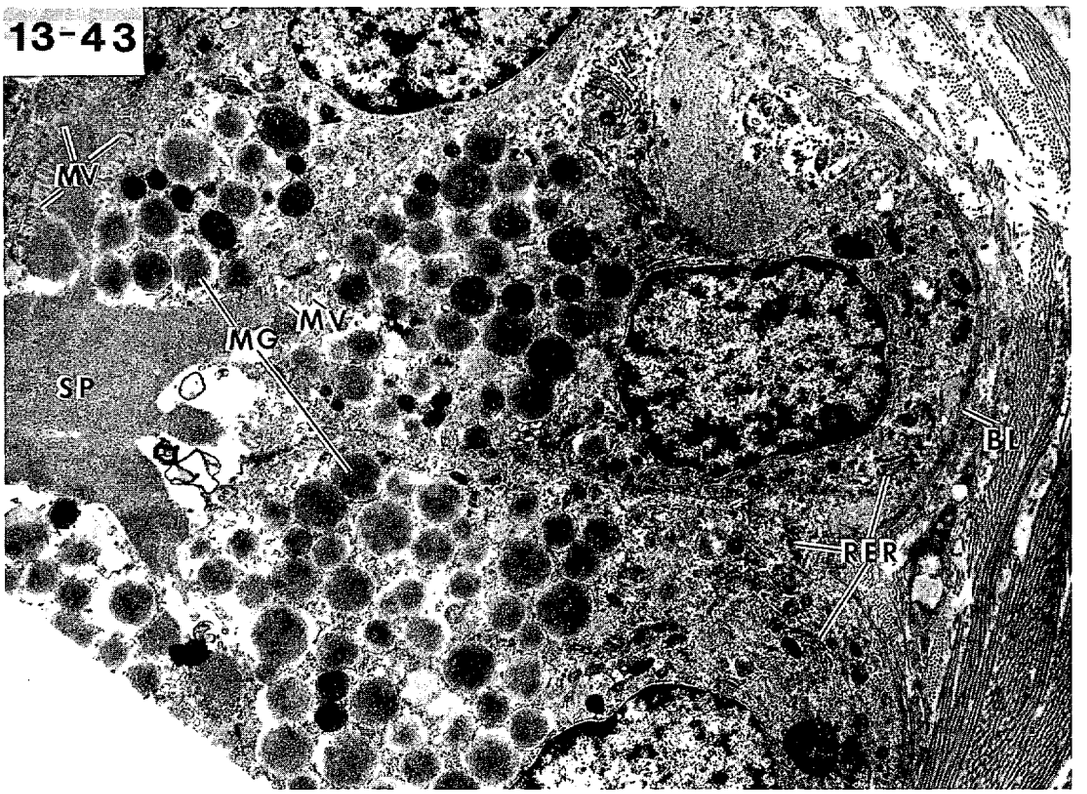
13-43
MV
MG
MV
SP
BL
RER

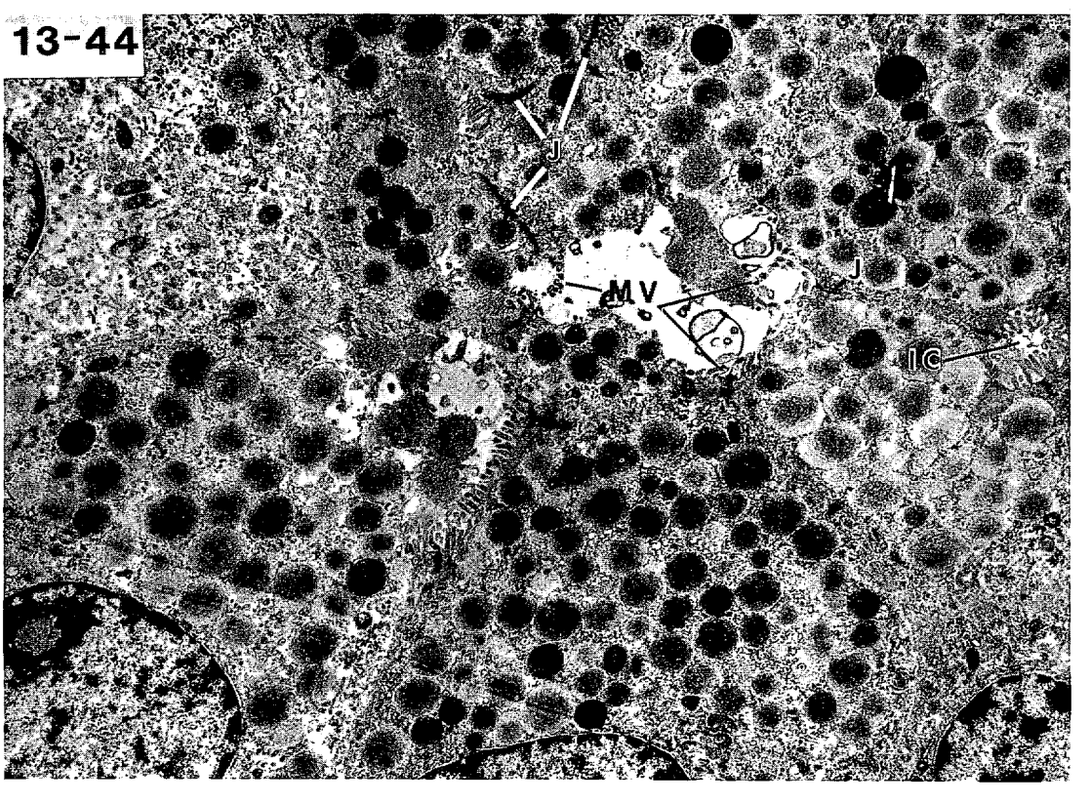
13-44
J
MV
J
IC

Figure 13-45. Photographs of the principal bronchial bifurcation into lobar bronchi.

A. Dorsal view (80B1). The principal bronchi (P) bifurcate into cranial (Cr) and caudal (C) lobar bronchi 13 cm caudo-1 ateral to the tracheal bifurcation (T). The left cranial lobar (LCr) bronchus leaves at a less obtuse angle (145°) than does the right cranial lobar bronchus (160°). XO.23

B. Ventral (medial) view (80B1). This vinyl acetate cast of the bronchial tree shows the lobar bronchi (L) of the left 1 ung. The dichotomous branching of the principal bronchi into segmental bronchi (S) is seen. XO.16

c* Ventral (medial) view (80B7). The principal bronchus (P) divides into cranial (Cr) and caudal (C) lobar bronchi in this left lung. The left pulmonary artery (A) and vein (V) are seen just caudal to the bifurcation. XO.13

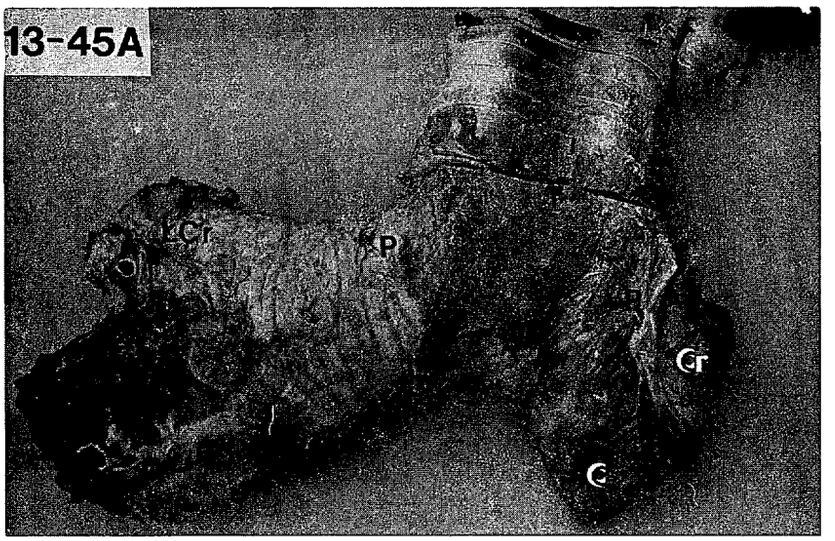
13-45A
Cr
P
Gr
C

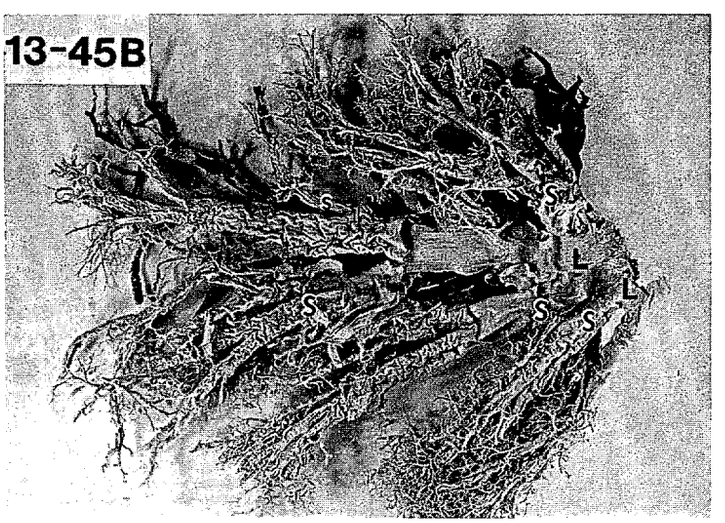
13-45B
S
S
S
S
S
S
L
L

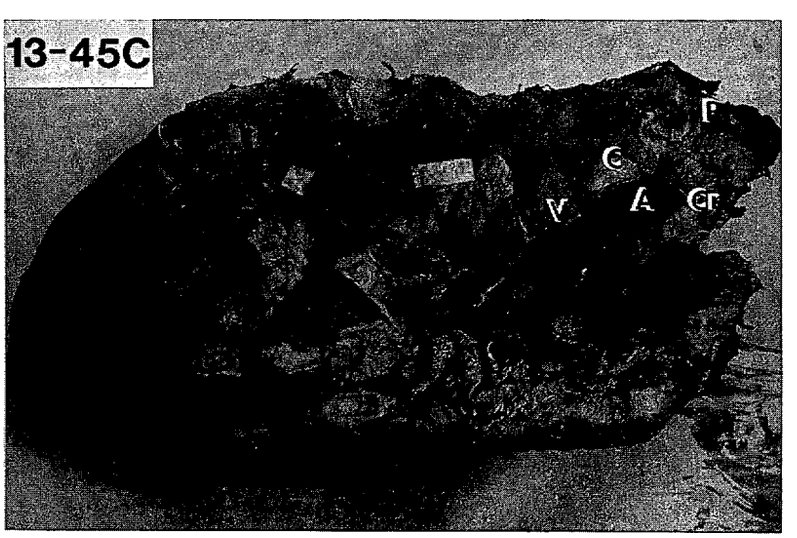
13-45C
P
C
V
A
Cr

Figure 13-46. Photographs of the principal bronchus bifurcation, pulmonary artery and vein.

A. The pulmonary artery (A) and vein (V) (8087) are found just caudal to the bifurcation of the principal bronchus (P). The branching of the pulmonary artery is deep and follows the bronchial tree (Fig B). The venous branching (arrow-heads) is superficial lying just below the pleura. Bronchial lymph nodes (N) are seen among the veins on the ventral (medial) surface of the left lung. X0.2

B. The pulmonary artery (A) (8051) and its branches can be seen lying next to and following the bronchial tree in this vinyl acetate cast. The arteries lie on the dorsal aspect of this cast of the left bronchial tree. X0.25

13-46A
P
A
N
V
N

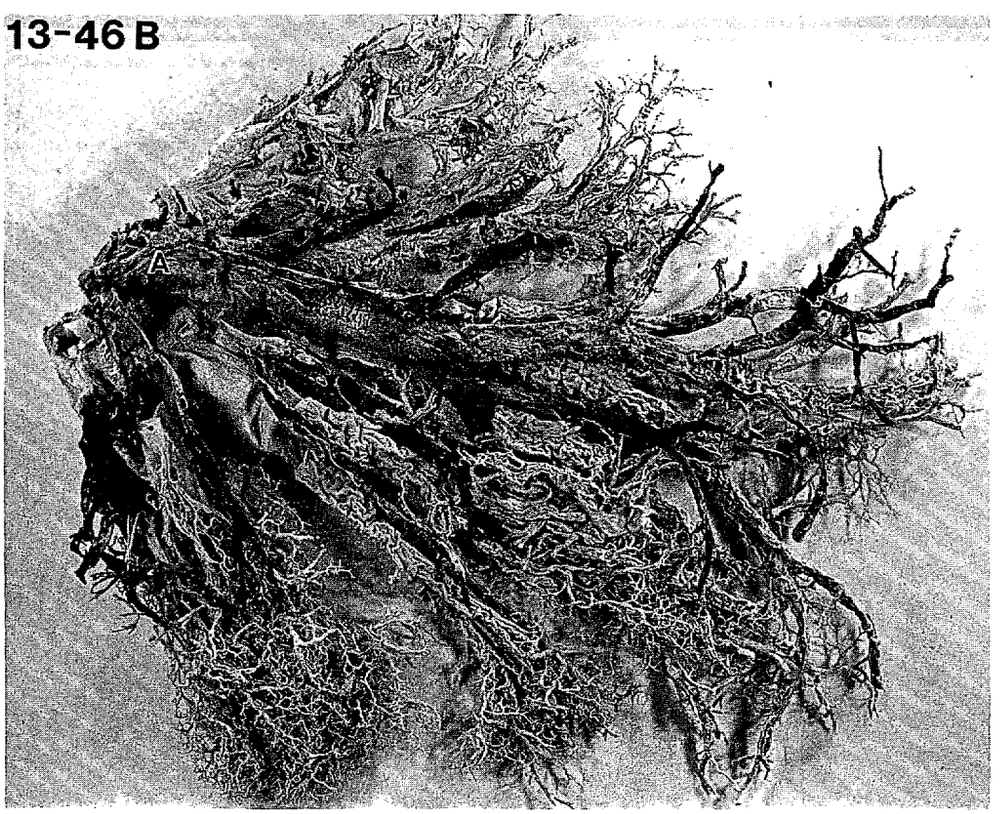
13-46 B
A

Figure 13-47. Photographs of the principal bronchus bifurcation, pulmonary artery and vein.

A. The right pulmonary artery (A) (80B2) is seen lying caudal to the bifurcation of the principal bronchus (P). The cranial lobar bronchus (Cr) is torn away from the bifurcation. Note the dichotomous branching of the caudal lobar bronchus (C) into numerous segmental bronchi (S) which course near the surface beneath the pleura (PL). Ventral (medial) view. X0.18

B. The pulmonary artery (A) (80B8) is seen lying just caudal to the bifurcation of the principal bronchus (P). Right cranial (Cr) and caudal (C) lobar bronchi can be seen as well as segmental bronchi (S) on this dissected lung. The thick pleura (PL) can be seen, but there is no evidence of the parenchyma being divided into lobes. Ventral (medial) view. X0.21

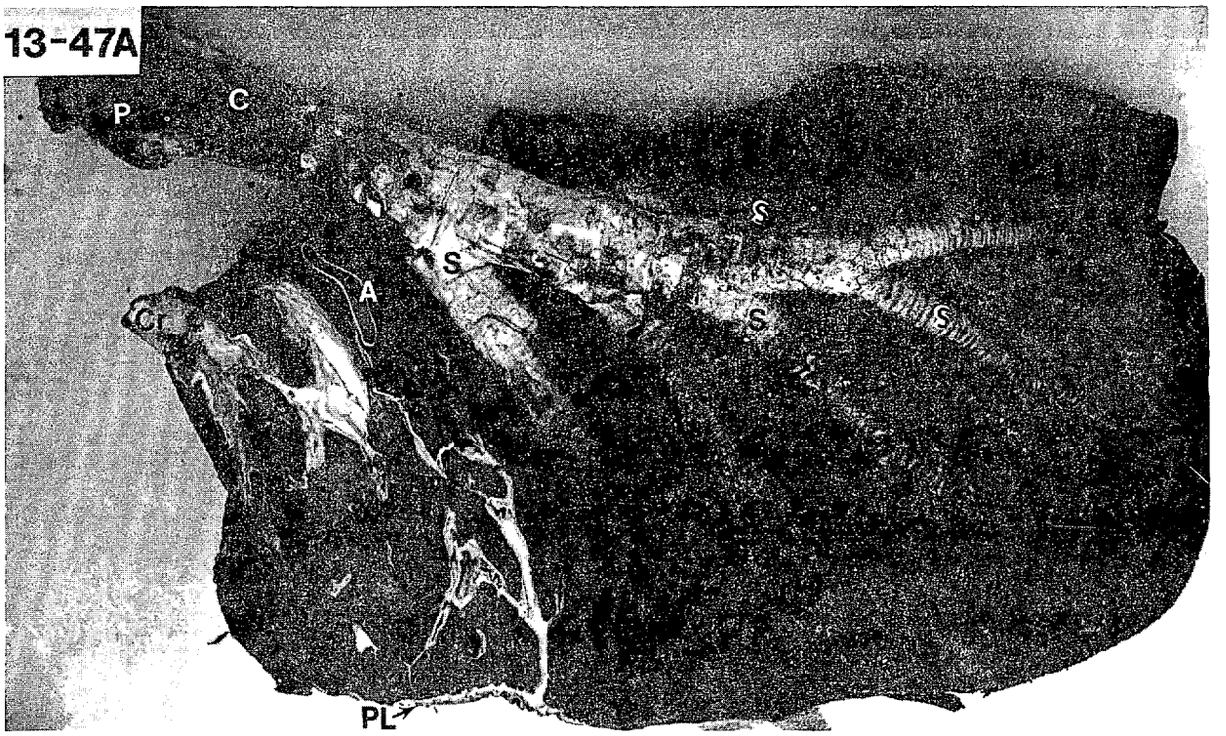
13-47A
P
C
S
S
A
Cr
S
S
PL

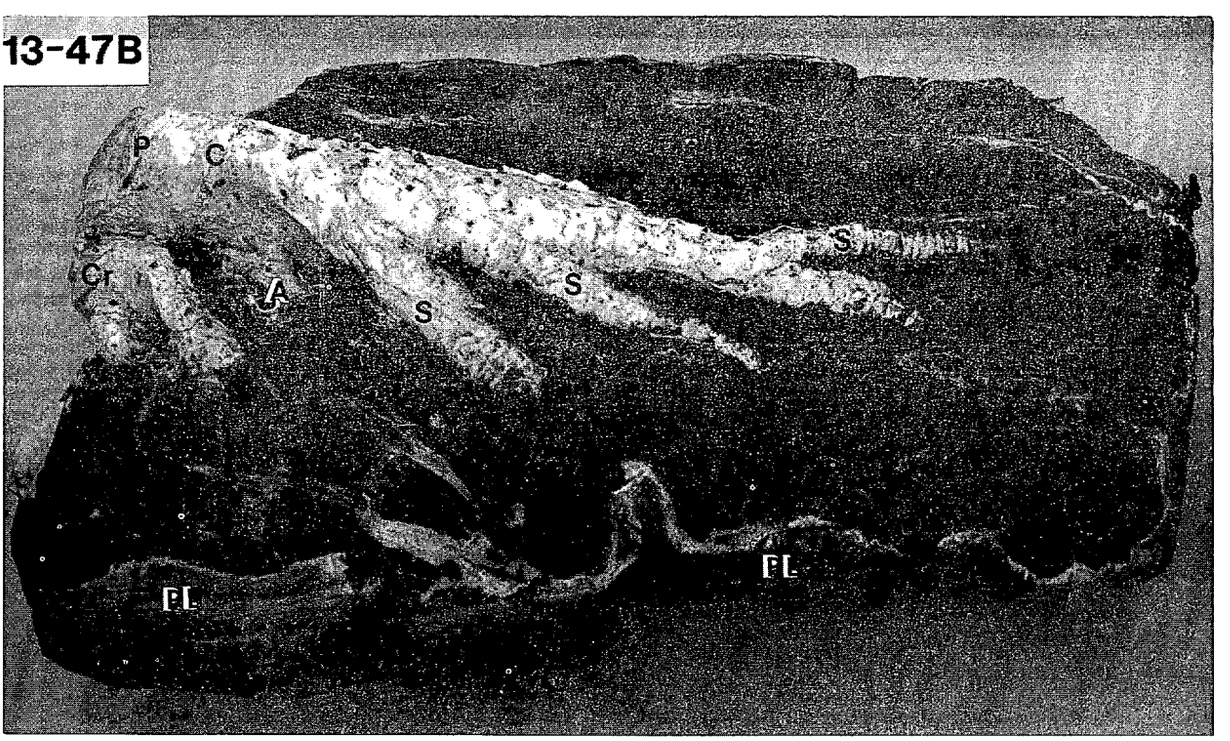
13-47B
P
C
S
Cr
A
S
S
PL
PL

Figure 13-48. Photomicrograph of the mucosal lining of the 19 x 31 mm bronchus from 80B1 taken near the center of the cartilaginous ring. The lamina propria (LP) consists of vascularized dense irregular connective tissue without mucous glands and is covered with a ciliated pseudostratified columnar epitheliums (EP). Instead of a muscularis mucosae, longitudinally oriented laminae of dense elastic fibers (F) only are present. The hyaline cartilage. ring (HC) is covered by a dense irregular connective tissue perichondrium. X.S., H and E, X50

Figure 13-49. Photomicrograph of a similar sized bronchus (19 x 33 mm) from 80B8 taken near the junction between cartilage rings. The mucosa has mucous glands (G) in addition to the layers visible in Fig 13-48 which interdigitate with the longitudinal elastic laminae (E). X. S., H and E, X50

Figure 13-50. Higher magnification photomicrograph of the mucosa in Fig. 13-49. Cilia (arrow) are visible as well as the pseudostratified columnar nature of the epitheliums (Ep) and the mucous glands (G). X. S., H and E, X120

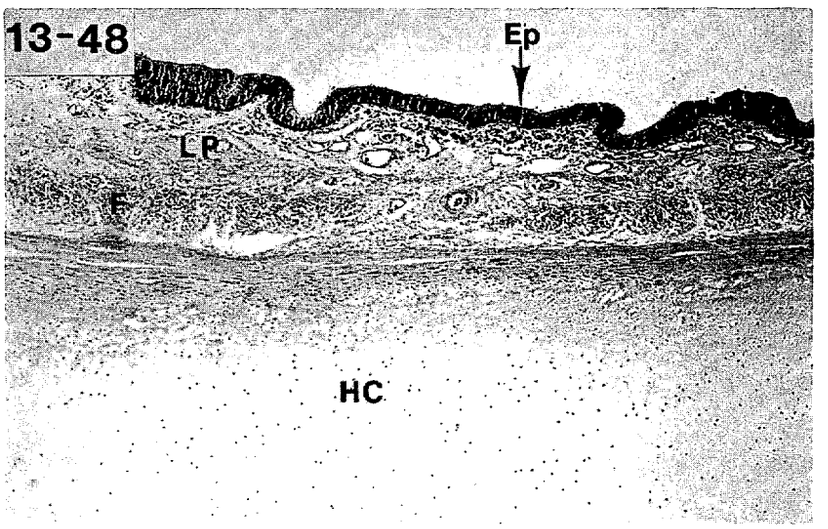
13-48
Ep
LP
E
HC

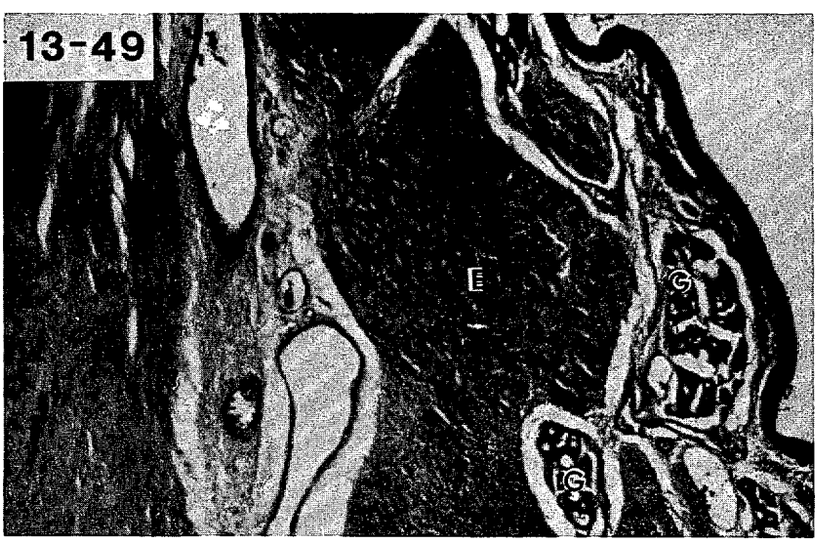
13-49
E
G
G

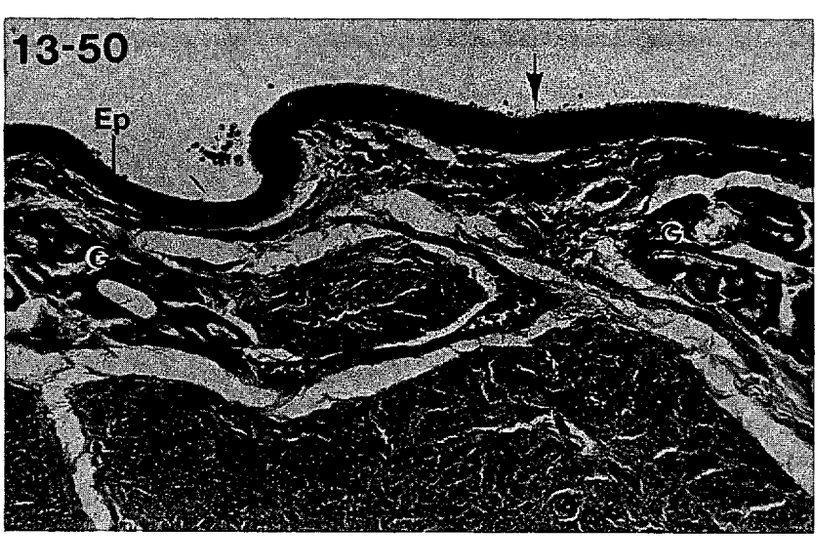
13-50
Ep
G
G

Figure 13-51. Photomicrograph of the mucosa and cartilage of a 16 mm bronchus from 80B7. The basic structure is the same as in large bronchi (Figs 13-48, 13-49). Mucus and debris (D) are present on the epithelial surface. The longitudinal elastic lamina (E) is thinner representing the only significant changes other than size. X.S., H and E, X130

Figure 13-52. Photomicrograph of a semi-thin section of the mucosa of a 10 mm bronchus of 8068. The epitheliums is ciliated pseudostratified columnar (Ep). The tall columnar cells (arrow) penetrate between the basal cell layer (arrowhead) to the basement membrane. Epon, X.S., Toluidine blue stain, X160

Figure 13-53. Scanning electron photomicrograph of a portion of a 10 mm bronchus from whale 80B8. Both the ciliated surface epitheliums (SE) and the underlying cartilage (C) and associated connective tissue may be seen. X47

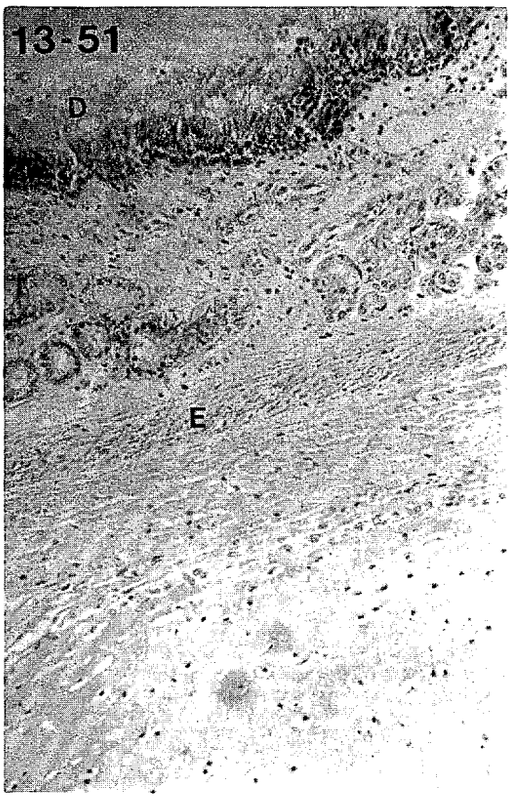
13-51
D
E

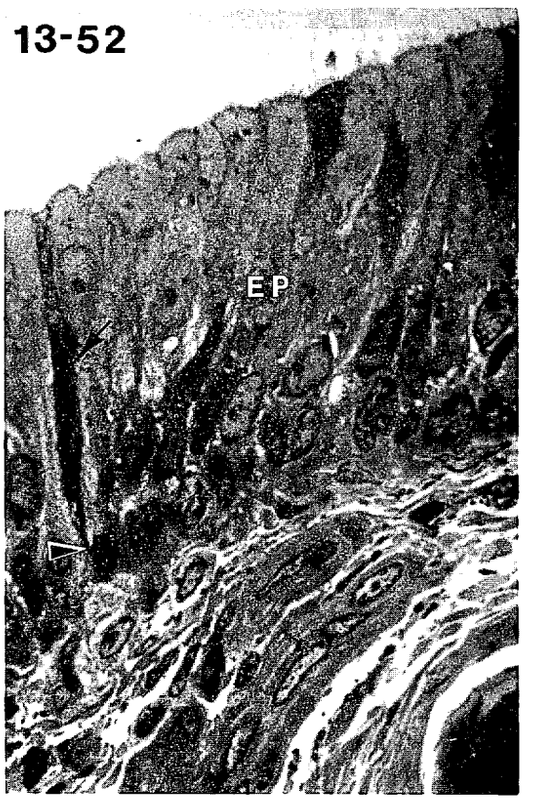
13-52
EP

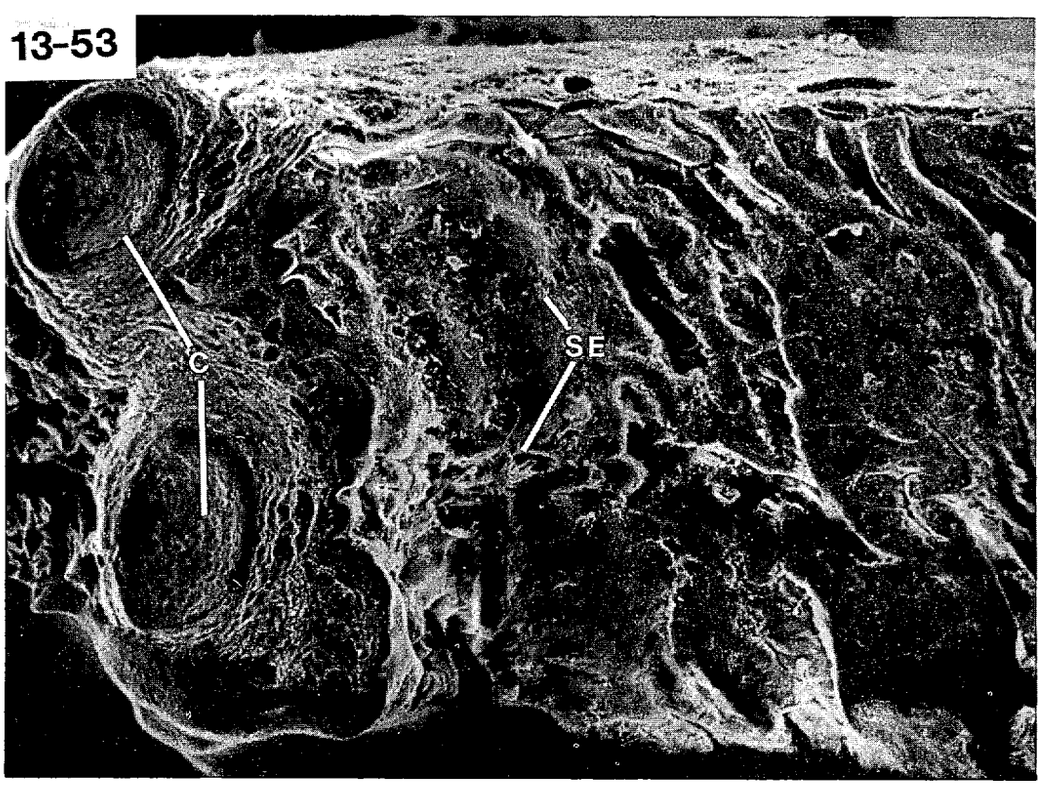
13-53
C
SE

Figure 13-54. Higher magnification scanning electron photomicrograph of a portion of the bronchus shown in Fig 13-53. Both ciliated and conciliated epithelial cells are seen. The number of ciliated cells (C) appears to be much greater than conciliated cells (NC). X1,300

Figure 13-55. Higher magnification scanning electron photomicrograph of a portion of the bronchus shown in Figure 13-53. Individual ciliated and conciliated cells may be seen. Conciliated cells possess numbers of microvilli (MV). Ciliated cells also appear to possess thin microvilli (arrows). X7,500

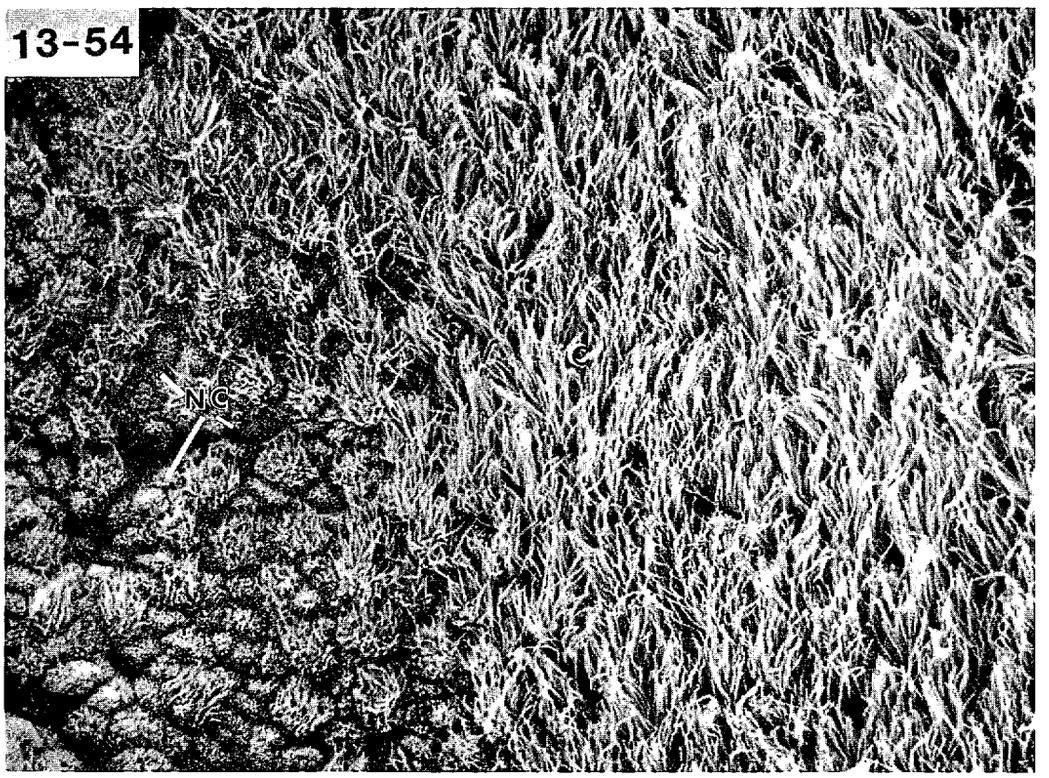
13-54
NC
C

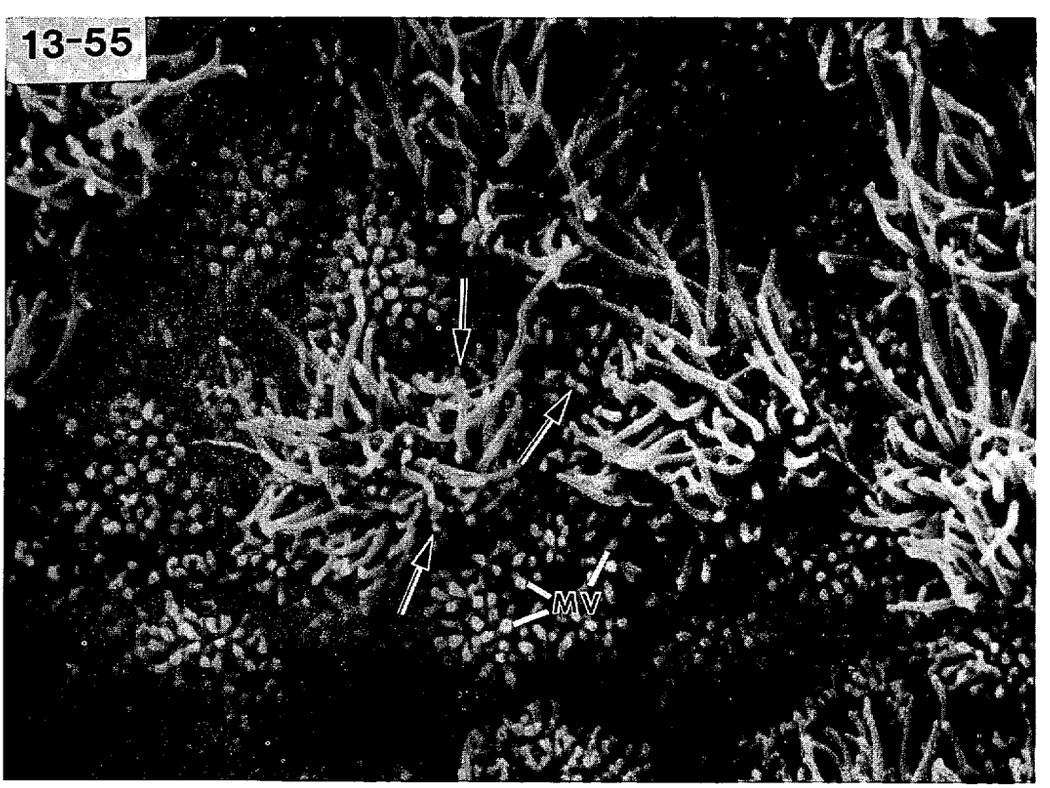
13-55
MV

Figure 13-56. Photomicrograph of a small bronchus (3.7 mm) from 80B8. The entire bronchial wall is visible surrounded by pulmonary tissue (P). Mucous glands (G) are still present tending to be less abundant at the level of the cartilaginous rings (R). The elastic lamina is no longer present. A nerve trunk (N) runs just outside the rings. L.S., H and E, X50

Figure 13-57. Photomicrograph of a slightly smaller bronchus (3.2 mm) from 80B8. The bronchial wall is even thinner with the mucous glands (G) occurring only between the cartilage rings (R). The surrounding pulmonary tissue (P) intrudes (arrow) between rings. L.S., H and E. X50.

Figure 13-58. Scanning electron photomicrograph of an excised portion of a 2 mm bronchus from whale 80B8. The ciliated epitheliums (CE) is evident as is the hyaline cartilage (HC) which underlies it. Exposed lung parenchyma (P) can be seen beneath the bronchus. X40

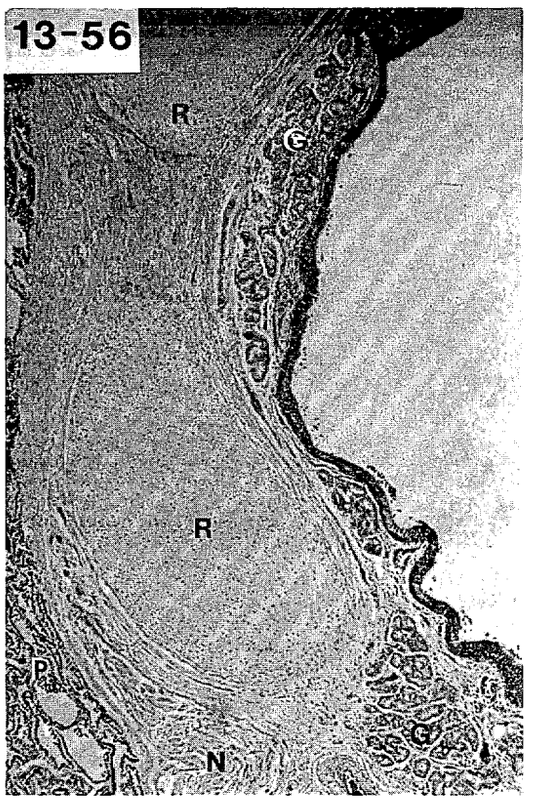
13-56
R
G
R
P
N
G

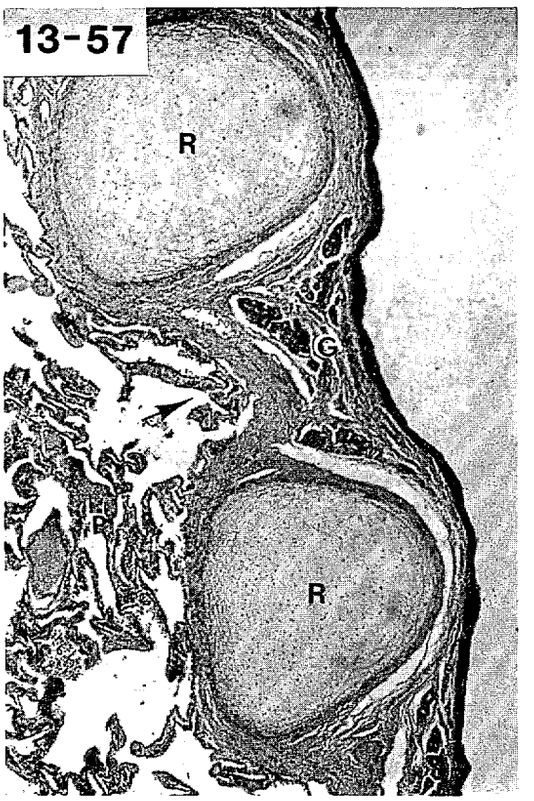
13-57
R
G
P
R

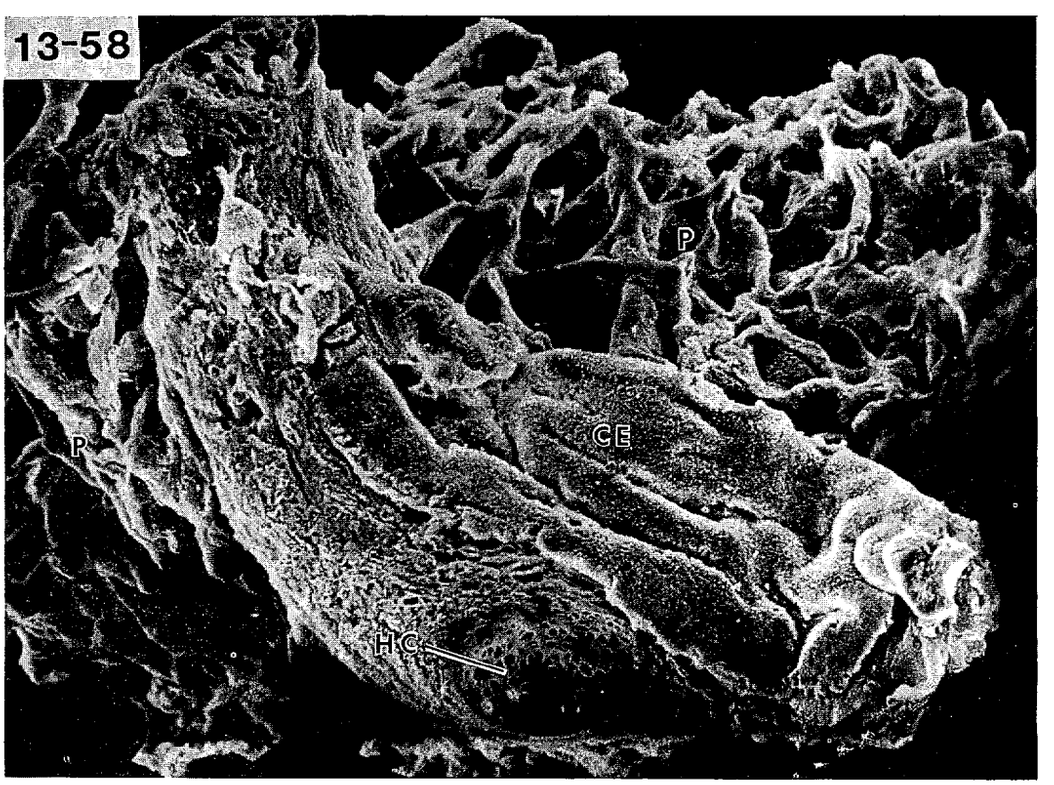
13-58
P
P
CE
HC

Figure 13-59. Higher magnification scanning electron photomicrograph of the surface and cut edge of the bronchus shown in Fig 13-58. Debris (D) can be seen covering the surface except in an exposed area (EA) where the debris is lifted from the surface revealing the ciliated surface below. Connective tissue (CT) can be seen beneath the epitheliums. X250

Figure 13-60. Higher magnification scanning electron photomicrograph of the surface of the bronchus shown in Fig 13-58. The uniformly ciliated epitheliums is thrown into folds. Red blood cell (R). X640

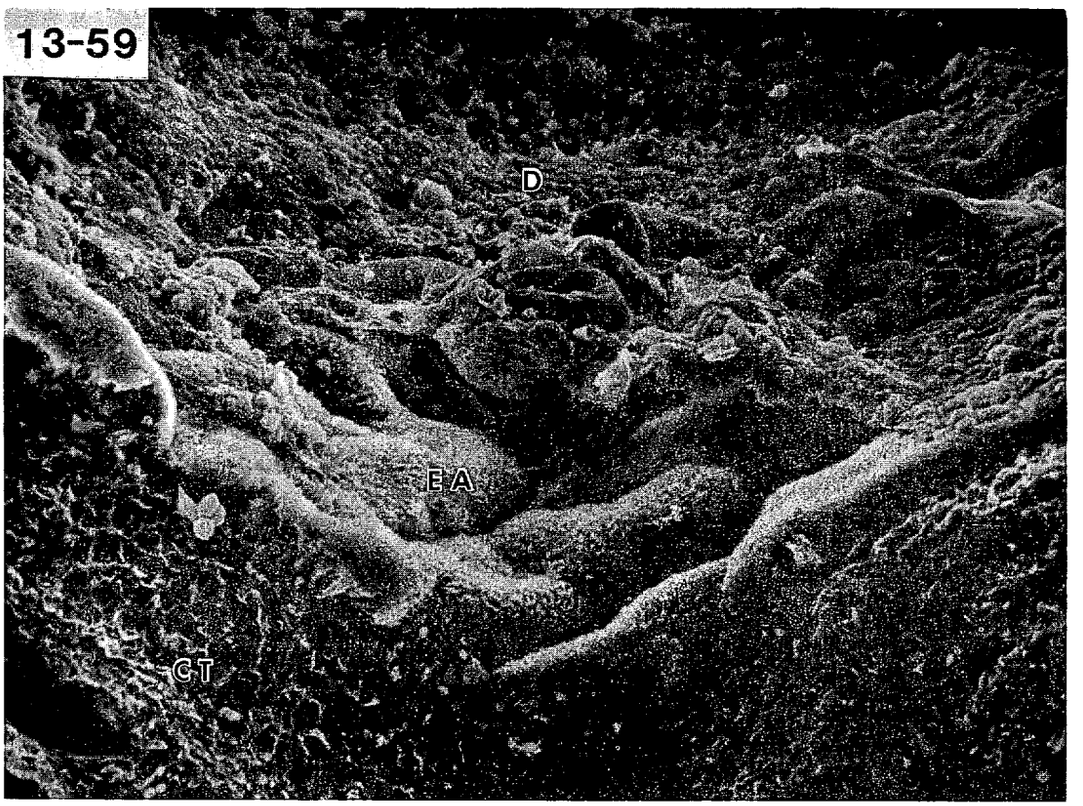
13-59
D
EA
CT

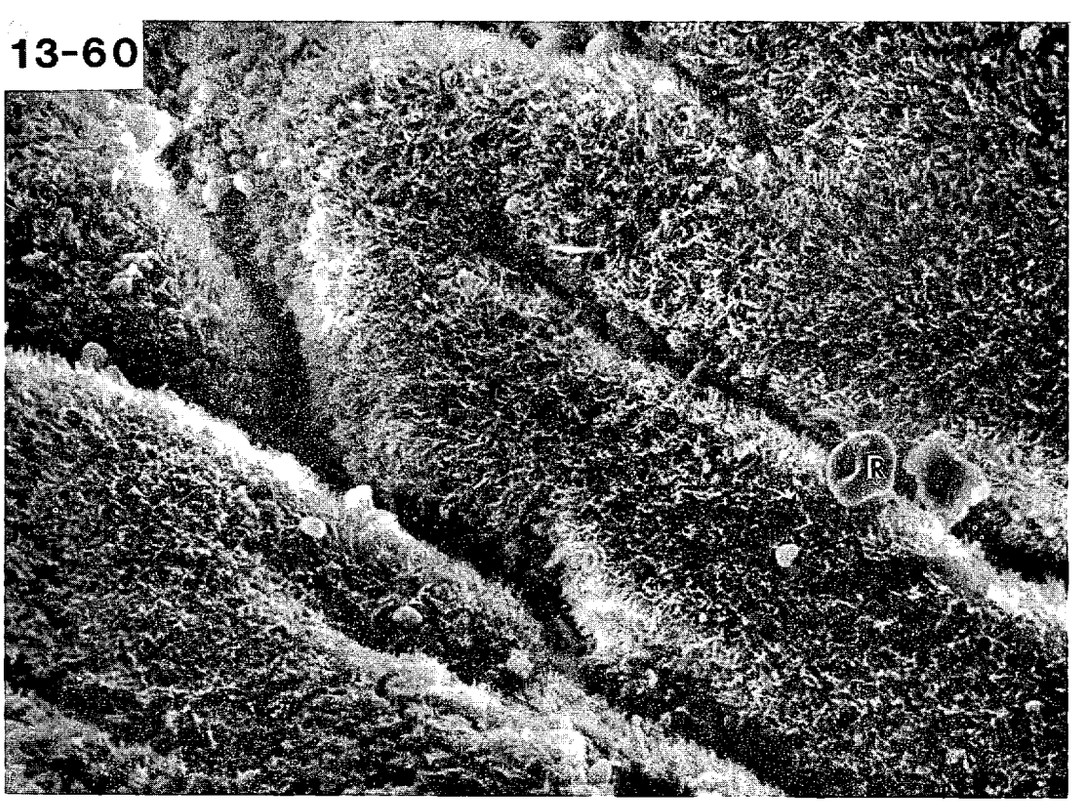
13-60
R

Figure 13-61. Higher magnification scanning electron photomicrograph of the surface of the bronchus shown in Fig 13-58. Cilia (C) are clearly evident but the borders of ciliated cells are difficult to see due to the large number of cilia and their uniform distribution. X4,200

Figure 13-62. Scanning electron photomicrograph of a portion of a 2 mm bronchus taken from whale 80B1. Debris (D) covers a portion of the surface. A portion of the surface is relatively free (F) of debris. The columnar nature of the epitheliums is evident (arrows) as is the connective tissue (CT) beneath the epithelium. X270

13-61
C

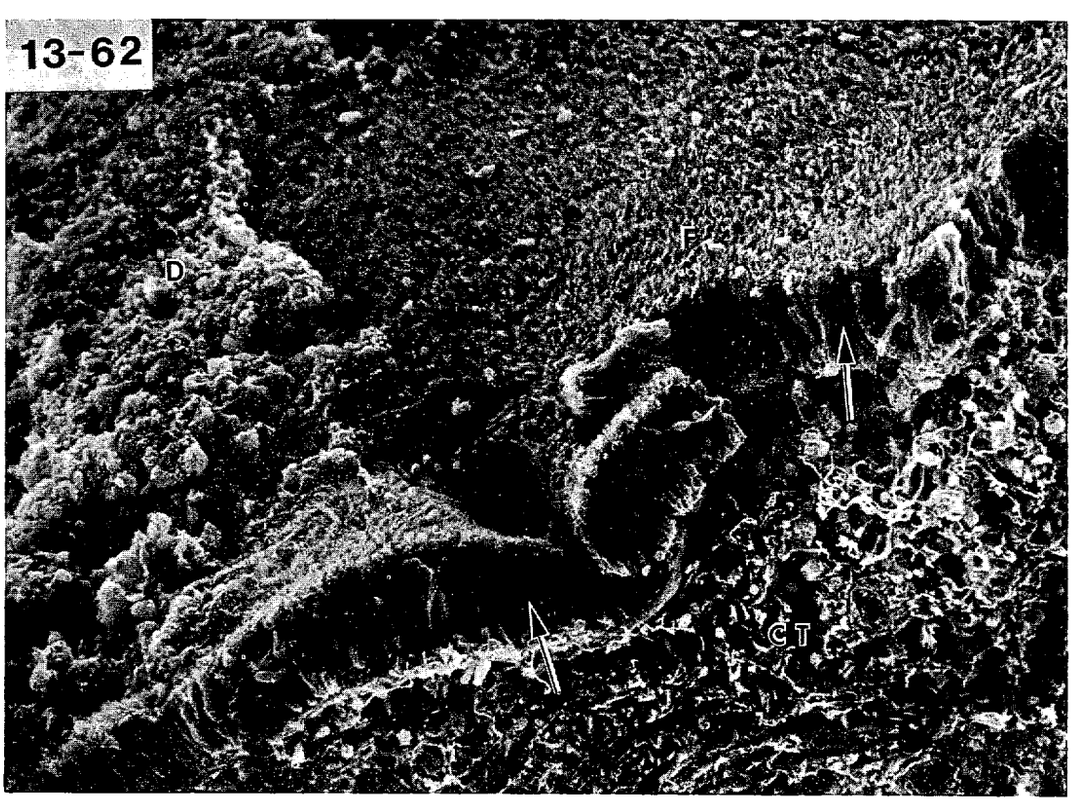
13-62
D
F
CT

Figure 13-63. Higher magnification scanning electron photomicrograph of a portion of the bronchus shown in Fig 13-62. The columnar cell bodies (CB) of the ciliated epithelial cells can be seen in this area where the epitheliums has been broken perpendicular to the surface of the bronchus. Fibers of the underlying connective tissue (CT) are also evident. X890

Figure 13-64. Higher magnification scanning electron photomicrograph of the surface of the bronchus shown in Fig 13-62. The uniform character of the ciliated epitheliums is evident. x2 ,400

13-65

13-66A

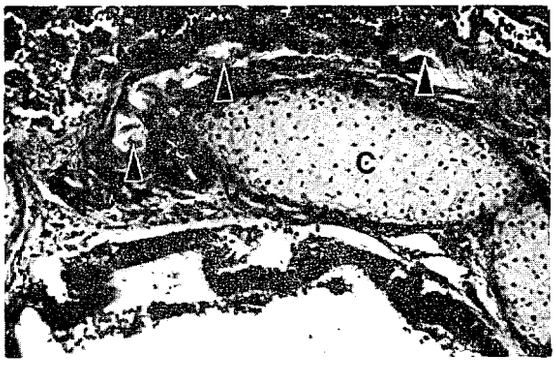

13-66B

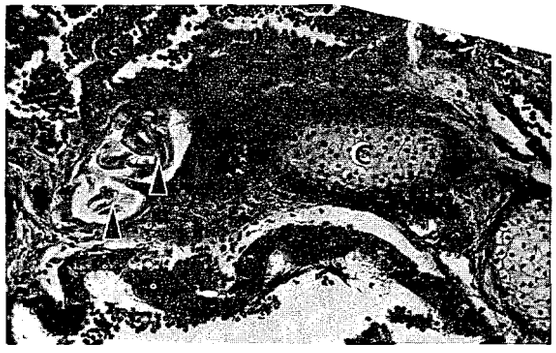

13-66C

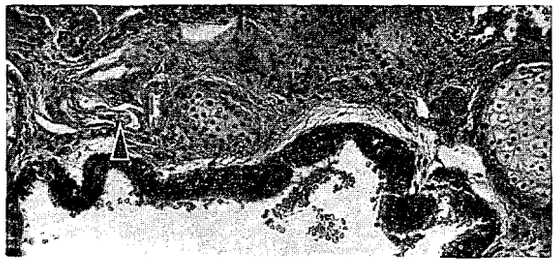

Figure 13-65. Photomicrograph of a bronchiole (1.9 mm) from 8068 illustrates the typical mammalian characteristic of a folded lining with ciliated pseudostratified columnar epitheliums (Ep) owing to the contraction of the circular smooth muscle (M) layer present within the mucosa for the first time. The cetacean modification of cartilage plaques (C) within the bronchiolar wall is well demonstrated. Note the Herbsti-like elongated and convoluted sensory end organ (S) within the bronchiolar wall. D - debris. X.S., Verhoeff stain, X130

Figure 13-66. Photomicrographs of a nerve tract and Herbsti-like encapsulated sensory nerve ending in a bronchiole of 80B8. Serial sections permit one to follow the connection of the nerve end organ to its afferent nerve tract. Follow illustration top to bottom (A-C) for nerve tract to end organ. The sensory nerve impulse actually originates and proceeds from illustration C to A. Sections cut at 5 µm. X130

A. The nerve tract (arrowheads) connects to a larger tract adjacent to a small bronchus (out of the picture to right). Cartilage (C). Section is 20 sections above B. Masson's stain.

B. The Herbsti-like end organ (arrowheads) expands and becomes convoluted within the bronchiolar wall between cartilage plaques (C). Section is 18 sections above C. Masson's stain.

c. The Herbsti-like end organ (arrowhead) continues down the bronchiolar wall. H and E stain.

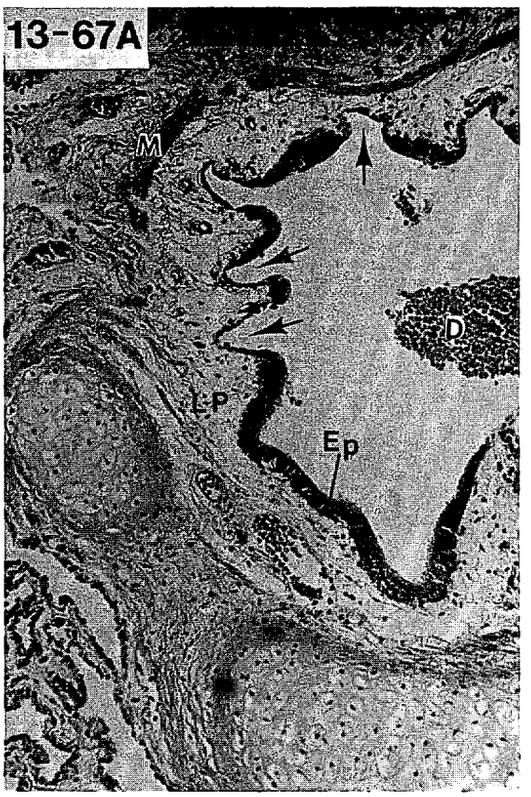
13-67A
M
D
LP
Ep

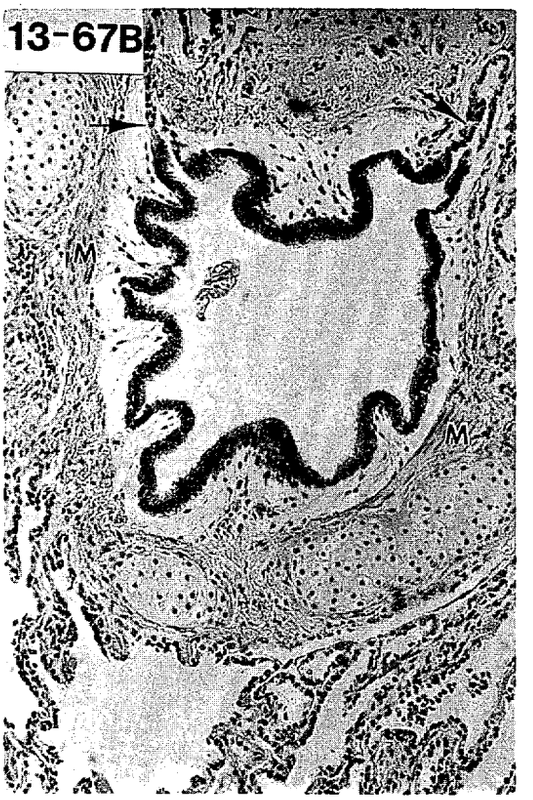
13-67B
M
M

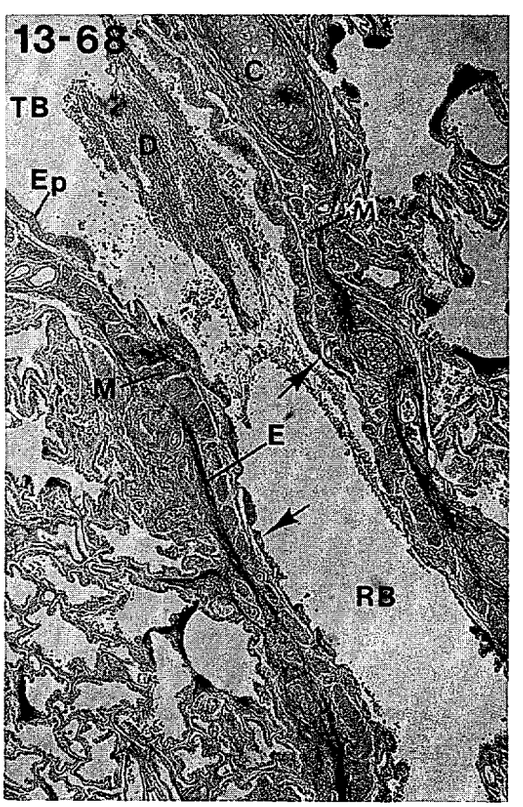
13-68
C
TB
D
Ep
M
M
E
RB

Figure 13-69. Transmission electron photomicrograph of a portion of a respiratory bronchus, from whale 80B8. A thin cytoplasmic process of a type I pneumocyte may be seen extending over a capillary (1). A shared basal lamina separates the type I cell from the endothelial cell (EC) lining the capillary. A type II pneumocyte (II) with surface microvilli (MV) and multi lamellar bodies (MB) is also evident. Dense irregular connective tissue (CT) with processes from fibroblasts (F) is seen beneath the epitheliums. Collagen fibers (CF) are also visible. 'X7,000

Figure 13-70. Transmission electron photomicrograph of a bronchus similar to that shown in Fig 13-69. A type II pneumocyte (11) covers the capillary (C) seen here. Junctional regions may be seen between adjacent pneumocytes (arrows). Complex lateral extensions are seen between two type II pneumocytes (arrowhead). Collagen (CF) and fibroblasts (F) may also be seen beneath the epitheliums. X8 ,800

13-69

13-70

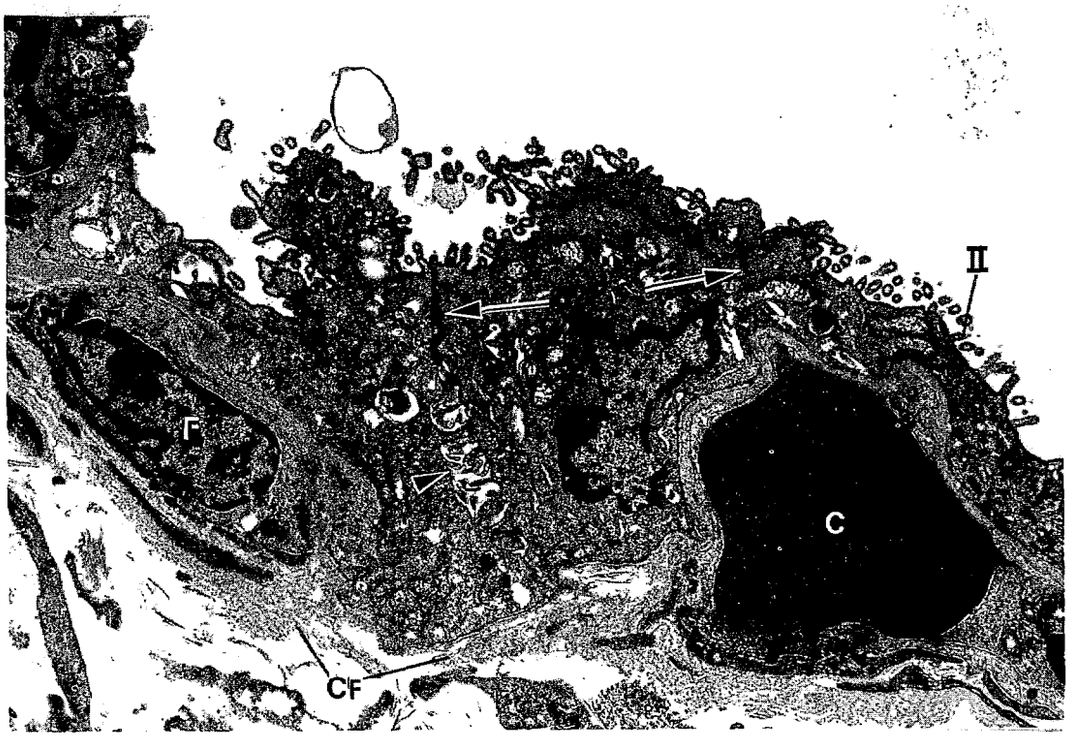

Figure 13-71. Transmission electron photomicrograph of hyaline cartilage from a respiratory bronchiole taken from whale 80B8. The densely p-acked collagen (CF) is evident as are several chondrocytes (CH) . X5,700

Figure 13-72. Transmission electron photomicrograph of a chondrocyte from a region of hyaline cartilage in a respiratory bronchiole from whale 80B8. The nucleus (N), lipid inclusions (L), mitochondria (M), as well as other cytoplasmic structures may be seen. Many thin cytoplasmic extensions (CX) may be seen radiating from the cell body. X10,700

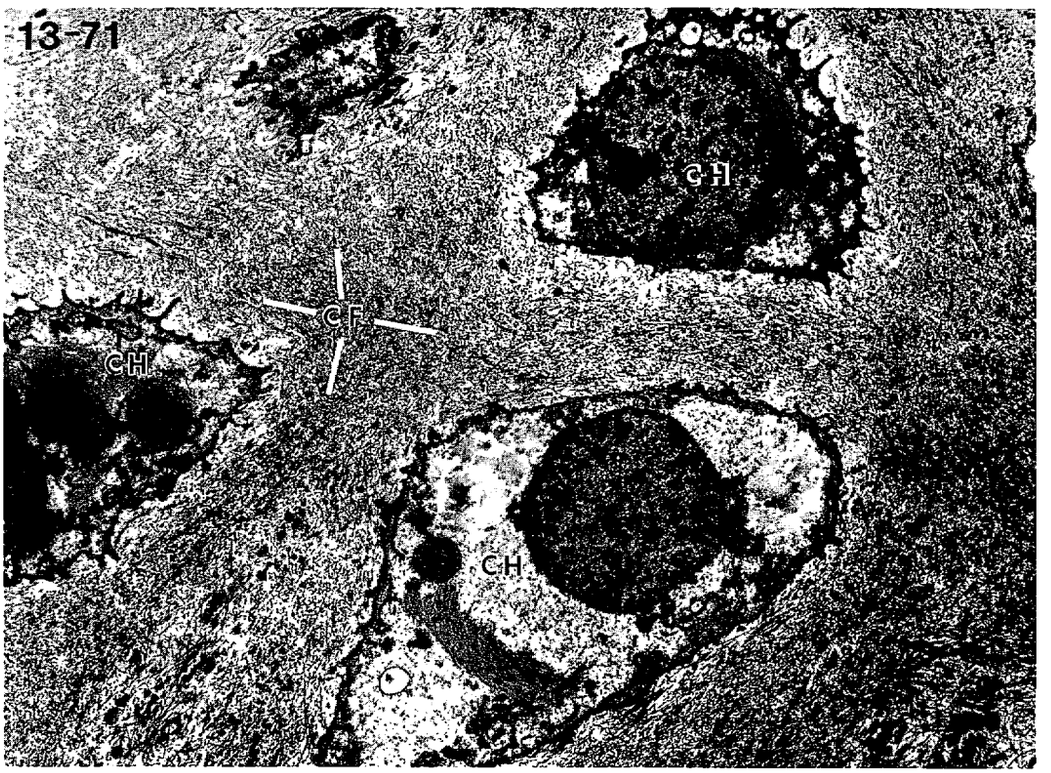
13-71
CH
CF
CH
CH

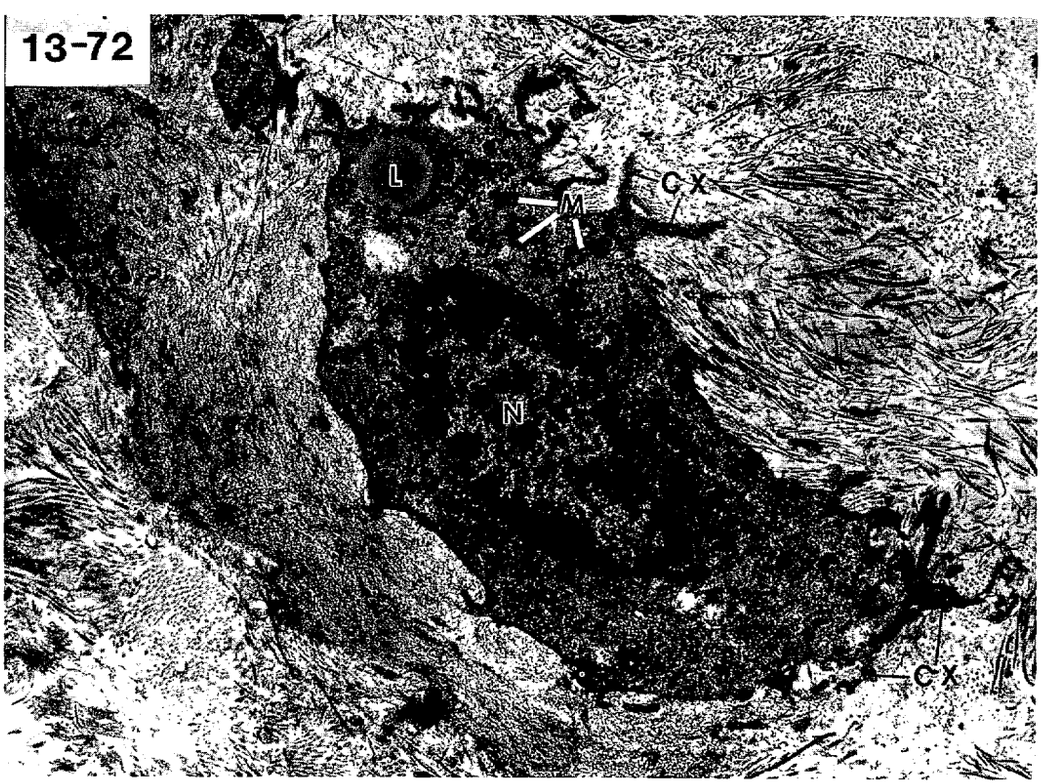
13-72
L
M
CX
N
CX

Figure 13-73. Photomicrographic montage of a terminal bronchiole, respiratory bronchioles, alveolar duct, alveolar sacs, and alveoli of 80B8. The entire final pathway from the termination of the airway (terminal bronchi ole-TB) to the ultimate sites of gaseous exchange (alveoli) show well in this composite. Gaseous exchange occurs from the first alveoli arising directly from the terminal bronchioles (none visible, see Fig 13-67B), the small alveolar sacs (SAS) and alveoli (A2) arising from the respiratory bronchioles, as well as the respiratory epitheliums (arrows) 1 i ni ng the respiratory bronchioles (RB), the alveolar ducts (AD), the large alveolar sacs (LAS), and the terminal alveoli (TA). Cartilage plaques (C) extend throughout the respiratory bronchioles. The walls of alveolar ducts are highly fenestrated by the orifices of almost continuous eruptions of alveoli and small and large alveolar 'sacs. About all that remains are widely spaced pillars and plaques of loose connective tissue containing spirally and circularly arranged concentrations of elastic fibers (E). X.S., H and E, X50

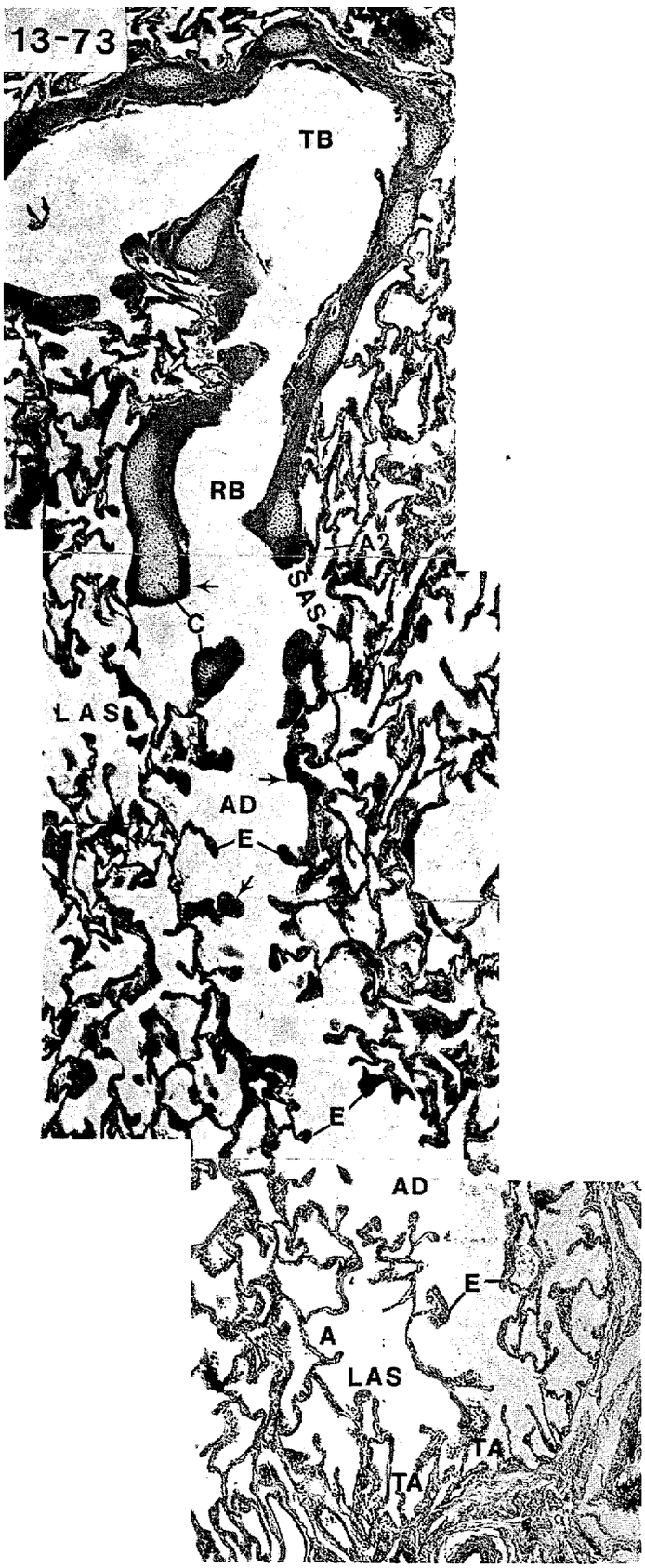
13-73
TB
RB
A2
SAS
C
LAS
AD
E
E
AD
E
A
LAS
TA
TA

Figure 13-74. Photomicrograph of an alveolar duct and alveolar sac from 80B2. The wall of the alveolar duct (AD) is penetrated by the orifices of individual alveoli (A) and is composed of spirally arranged elastic fibers (arrows) that encircle the duct and, particularly, the orifices forming sphincters. The surface is covered by respiratory epitheliums. Alveolar sacs (AS) are likewise constructed with the elastic fibers confined mostly in the sphincters leading to their alveoli (A2). Smal l pulmonary arteries (PA) are encased in minimal amounts of dense irregular connective tissue and give rise abruptly to thin walled arterioles (Ar). Thin walled veins (V) are also located in the connective tissue. X. S., Verhoeff stain, X50

Figure 13-75. Higher magnification photomicrograph of an alveolar duct wall from 80B2. The alveolar duct wall (W) consists predominantly of dense elastic tissue (E) composed of fibroblasts, elastic fibers, and occasional arterioles (Ar). The surface is covered by a respiratory epitheliums (simple squamous cells closely covering capillaries). The arrows indicate the epitheliums and erythrocytes in the capillaries. Debris (D) is primarily blood cells from collection and some mucus. L.S., H and E, X130

Figure 13-76. Photomicrograph of a semi-thin section of the alveolar duct wall from 80B8. The mucosa is lined with respiratory (simple squamous) epitheliums covering erythrocytes (RBC) in capillaries. The wall contains numerous spirally arranged elastic fibers (arrows). The only cells present within the wall are f ibrobl asts (F). No smooth muscle cells occur. The interalveolar septa (S) are generally devoid of elastic fibers. Epon, L.S., Toluidine blue stain, X160

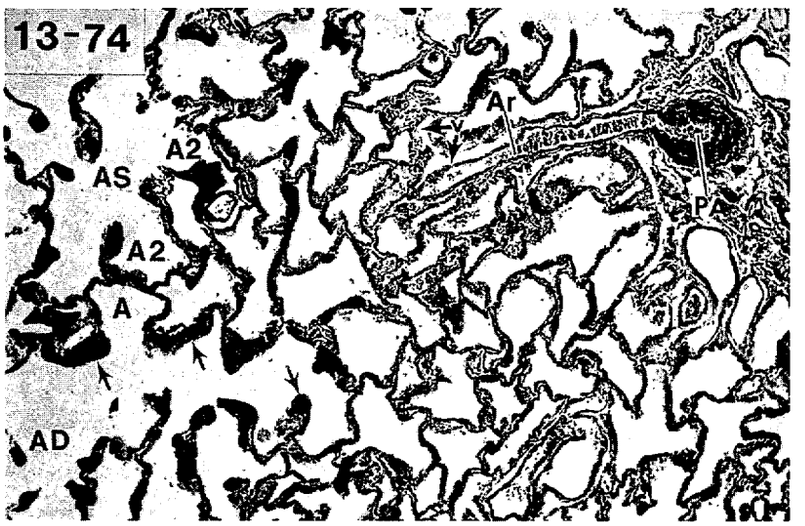
13-74
Ar
A2
AS
PA
A2
A
AD

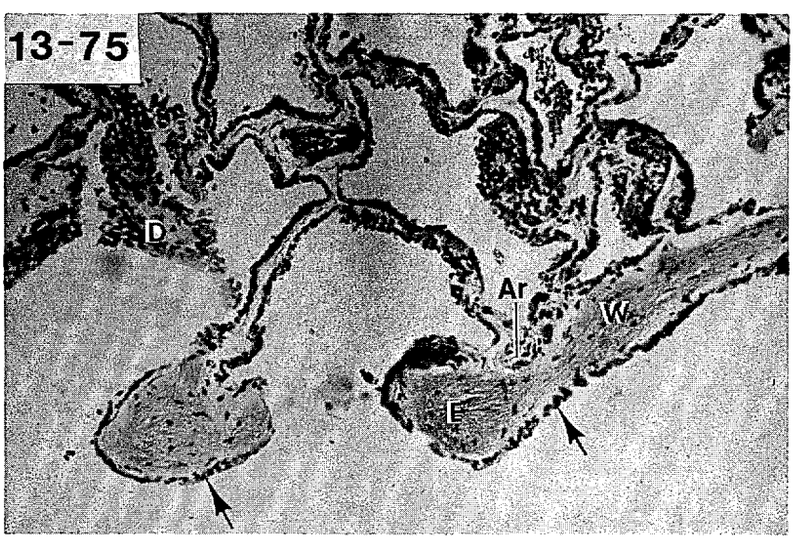
13-75
D
Ar
W
F

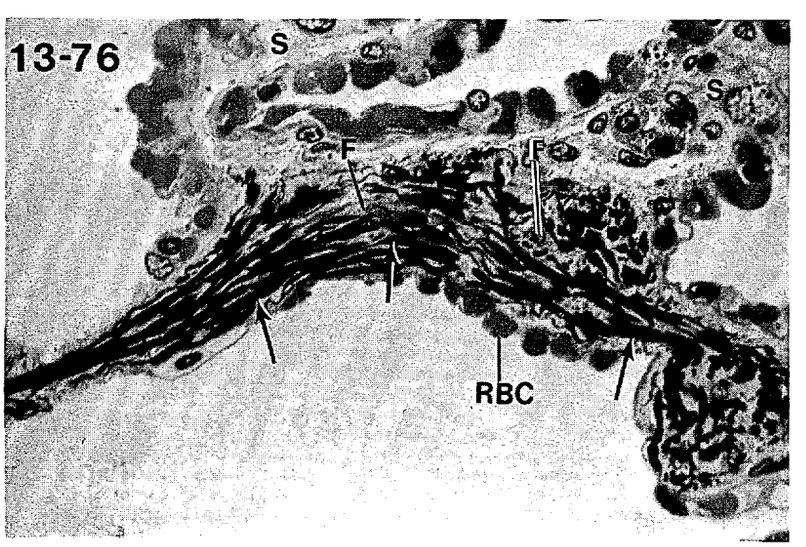
13-76
S
S
F
F
RBC

Figure 13-77. Photomicrograph of a semi-thin. section of an alveolar sac orifice from 80B8. The margins of the alveolar sacs (AS) contain fibroblasts (nucleus - arrow) and elastic fibers (black) without smooth muscle cells. An apparent microphage (M) was caught within the lumen. Epon, X.S., Toluidine blue stain X160

Figure 13-78. Transmission electron photomicrograph of the epitheliums over an elastic sphincter from the lung of whale 80B8. Both type I (I) and type II (II) pneumocytes are seen. The nucleus of a type I pneumocyte (N) is also seen in this micrograph. Fibroblasts (F) i n the connective tissue beneath the basal lamina may be seen. Elastic fibers (EF) are the prominent feature of this subepithelial connective tissue. x4 ,700

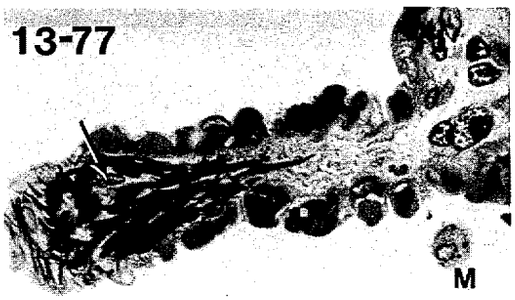

AS

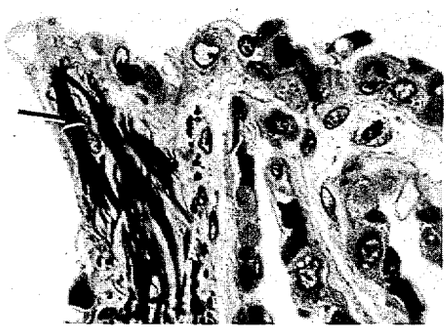

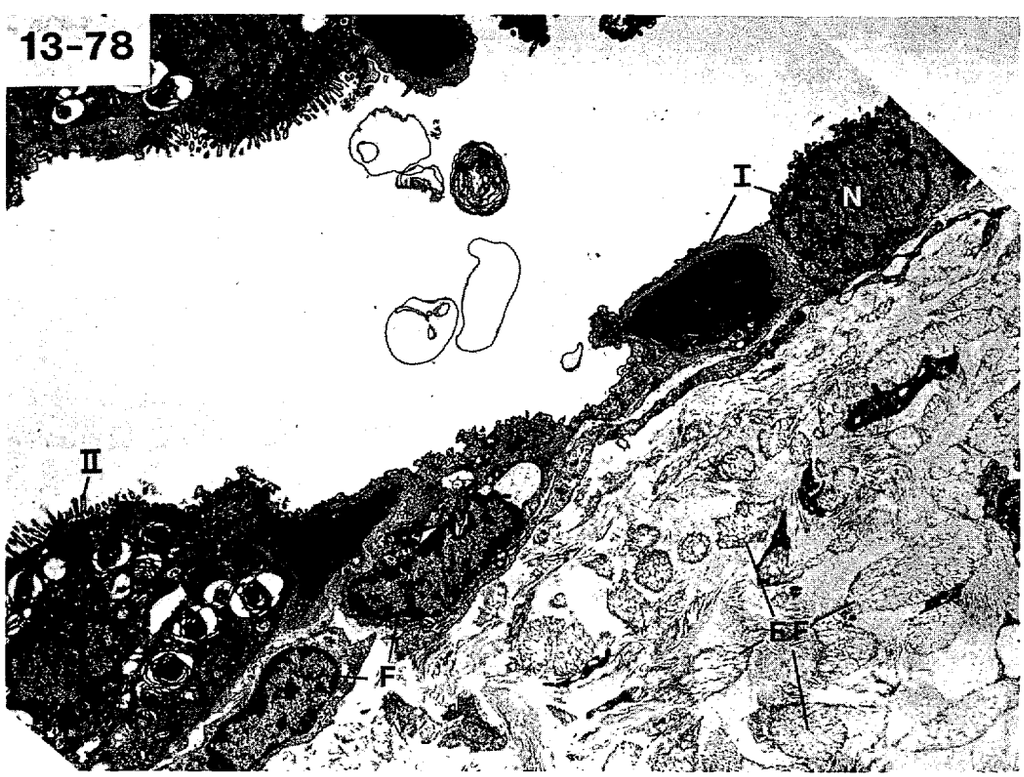

Figure 13-79. Higher magnification transmission electron photomicrograph of a region of the connective tissue shown in Fig 13-78. Elastic fibers are evident. The elastic fibers are composed of microfibrils (MF) and amorphous substance (AS). Mixed among the elastic fibers are delicate collagen fibers (CF). X8,900

Figure 13-80. Transmission electron photomicrograph through a more 'cellular region of an elastic sphincter from whale 80B8. Both collagen (CF) and elastic fibers (EF) are evident Fibroblast-like cells are seen. These cells display narrow, irregular, cell processes' (P) extending away from the cell body. A pair of centrioles (CL) are evident in one fibroblast. No evidence of smooth muscle is seen. X8 ,900

13-79
CF
AS
CF
MT

13-80
P
EF
EF
CF
P
CL
CF
EF
P

Figure 13-81. Transmission electron photomicrograph of a portion of an elastic sphincter from the lung of whale 80B2. The preservation is not as good as shown for whale 80B8 in Figs 13-78 and 13-79. Many open spaces are seen in the fibroblasts (F). Many cells are seen in the micrographs but no smooth muscle is evident. X5,600

Figure 13-82. Photomicrograph of a semi-thin section of an interalveolar septum from 80B8. The septum between adjacent alveoli is typically cetacean consisting of loose connective tissue with fine collagen fibers (C) and fibroblasts (F). Each alveolar lumen is not only lined with its own simple squamous epitheliums, but each has its own capillary network filled here with erythrocytes (RBC). The entrance to each alveolus is controlled by an elastic sphincter (arrow). Epon, X.S., Toluidine blue stain, X160

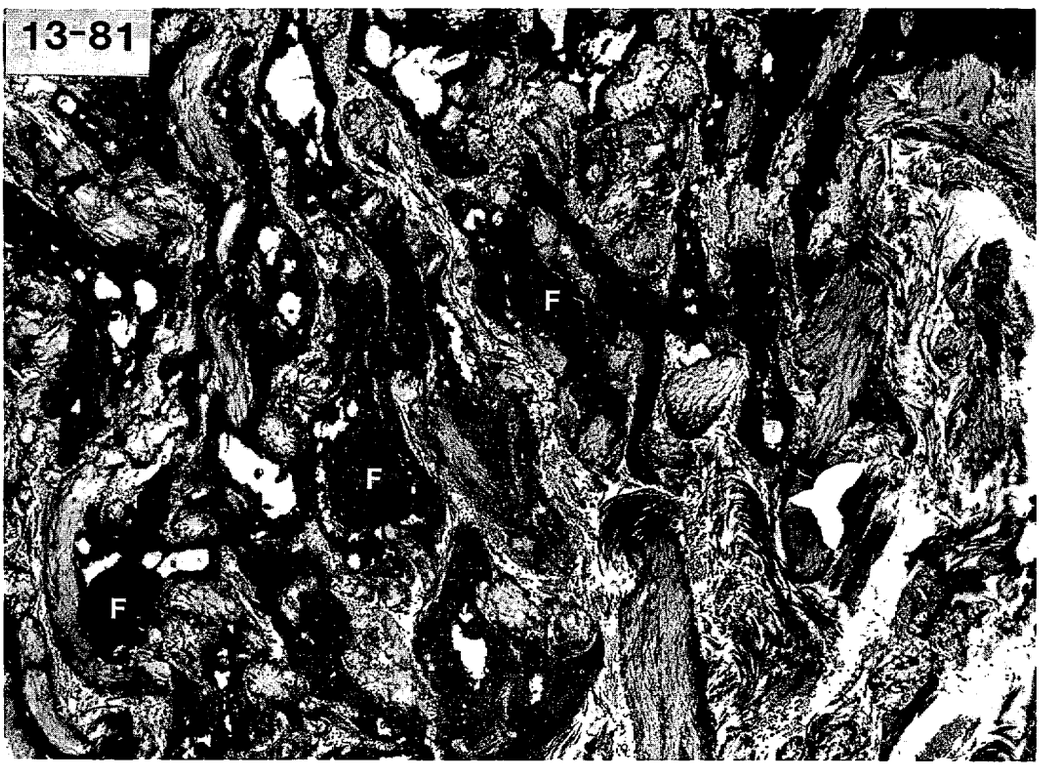
13-81
F
F
F

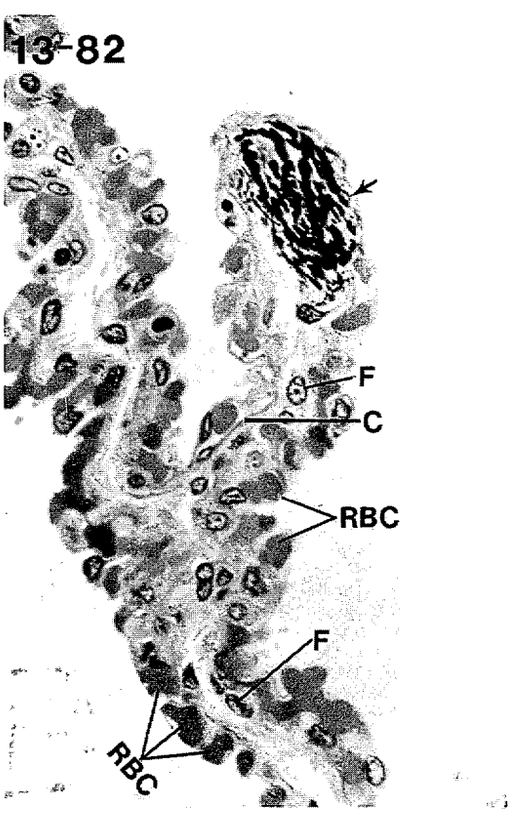
13-82
F
C
RBC
F
RBC

Figure 13-83. Transmission electron photomicrograph of a multilamellar body extruded by a type II pneumocyte into the lumen of an airway 1 ined by respiratory epithel ium from whale 80B8. Concentric rings of membranous material may be seen. This probably represents material destined to form the surfactant coating over the respiratory epitheliums. X27 ,500

Figure 13-84. Transmission electron photomicrograph of a multilamellar body similar to that. shown in Fig 13-83. Tubular myelin (TM) often seen in mammalian lungs is evident. X16,500

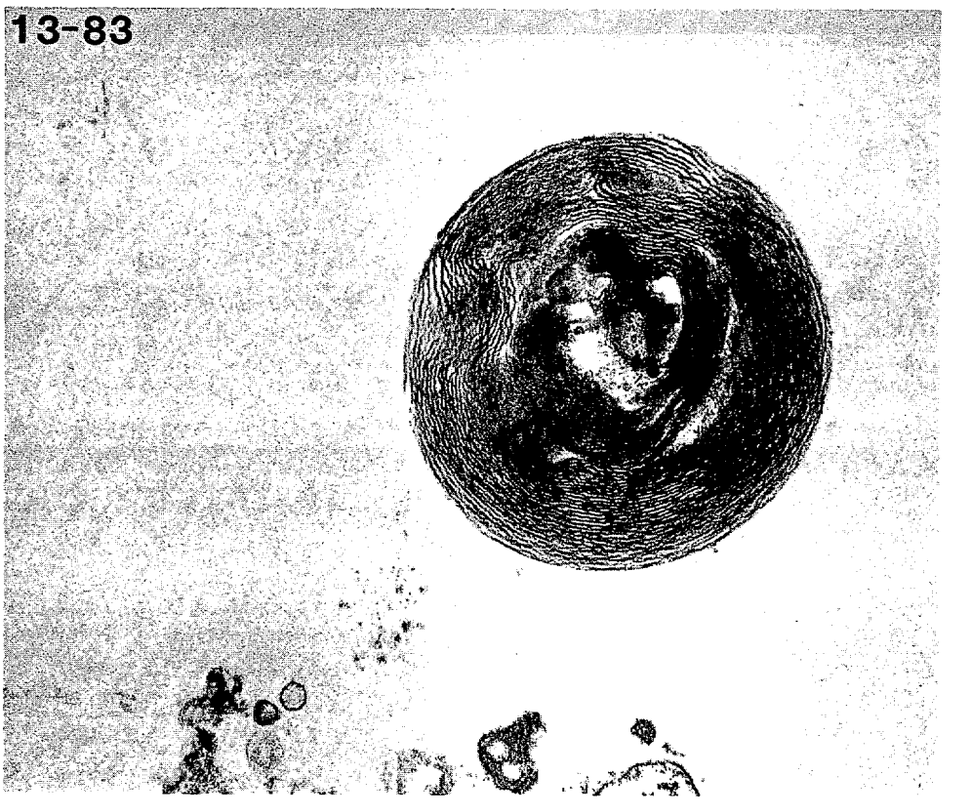
13-83

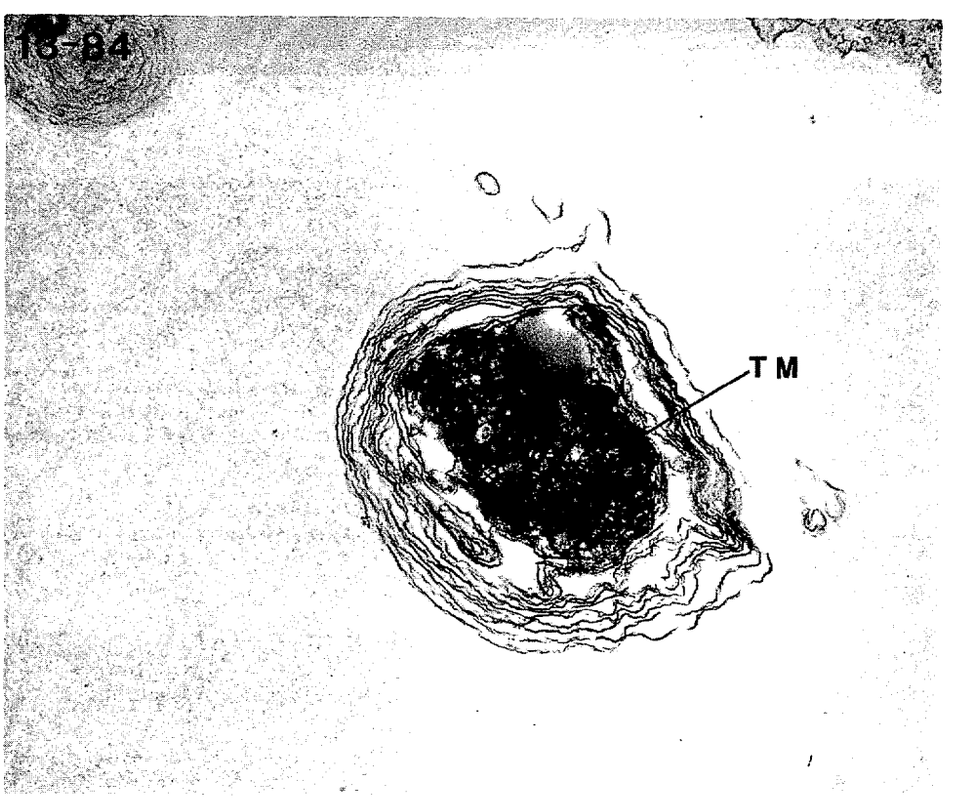
16-84
T M

Figure 13-85. Scanning electron photomicrograph of alveoli from the lung of whale 80B1. The alveolar septum (S) and alveolar epitheliums (AE) are evident. X1 ,400

Figure 13-86. Higher magnification scanning electron photomicrograph of a region of an alveolus shown in Fig 13-85. Red blood cells (RBC) are evident within the capillaries while collagen fibers (CF) are seen in the connective tissue. X6 ,700

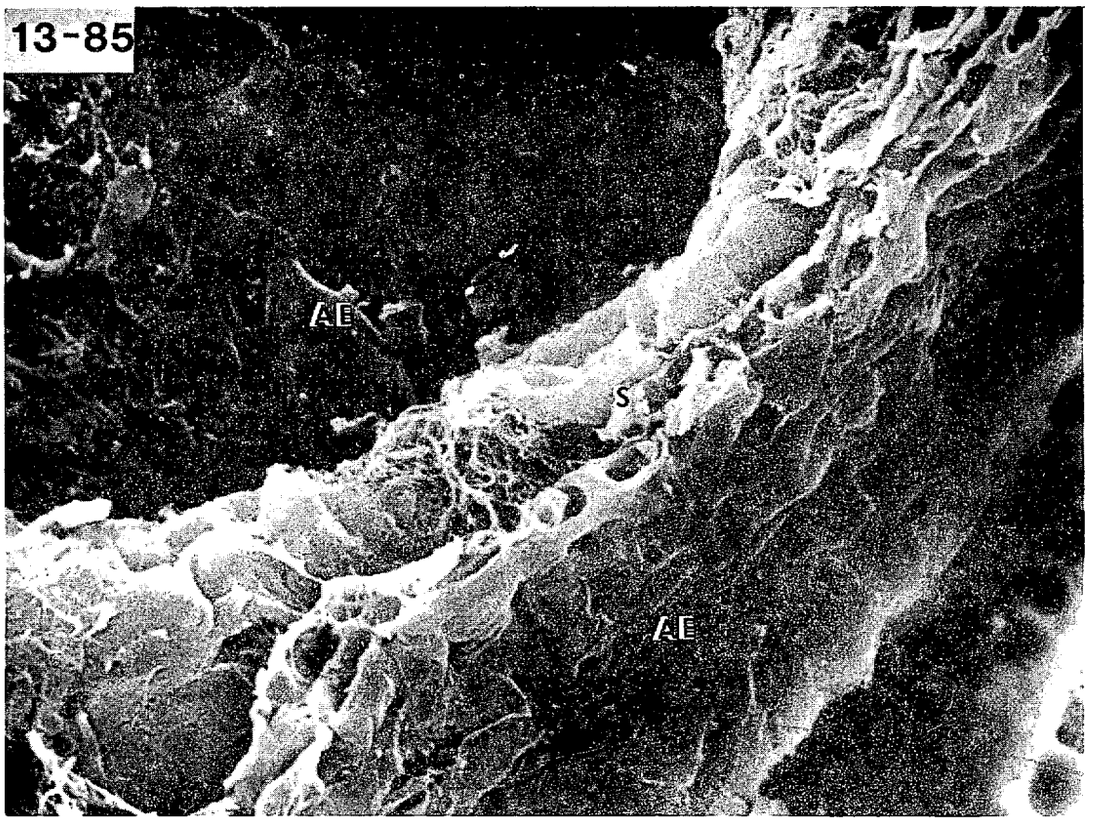
13-85
AE
S
AE

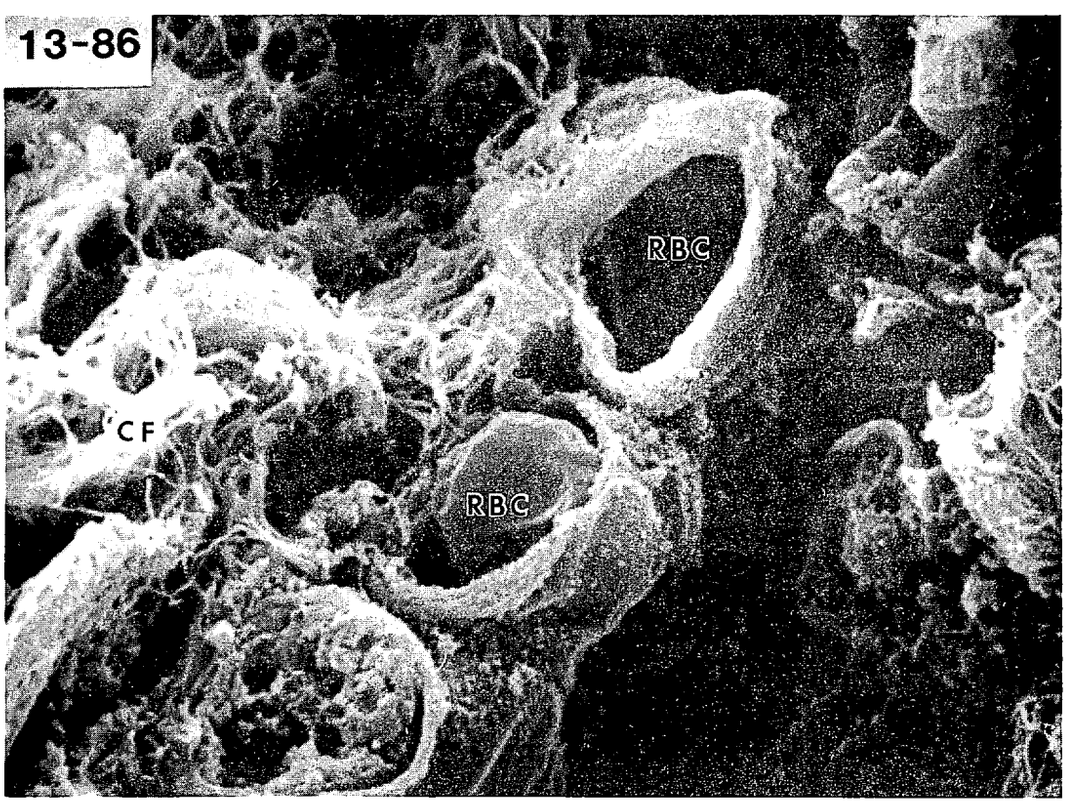
13-86
RBC
CF
RBC

Figure 13-87. Transmission electron photomicrograph of a portion of an alveo-1 ar wal 1 from the lung of whale 80B8. Capillaries (CV) line both sides of the alveolar septum (S) and are covered with respiratory epitheliums similar to that seen elsewhere. Fibroblasts (F) and collagen (C) are evident within the septum. x7 ,200

Figure 13-88. Transmission electron photomicrograph of a portion of the respiratory epitheliums from the lung of whale 80B8. Two mononuclear cells (MNA and MNB) are evident. These probably represent phagocytic cells (possibly a monocyte) in the capillary (MNA) and a connective tissue microphage (MNB). Free multilamellar bodies (ML) are also seen. X9,000

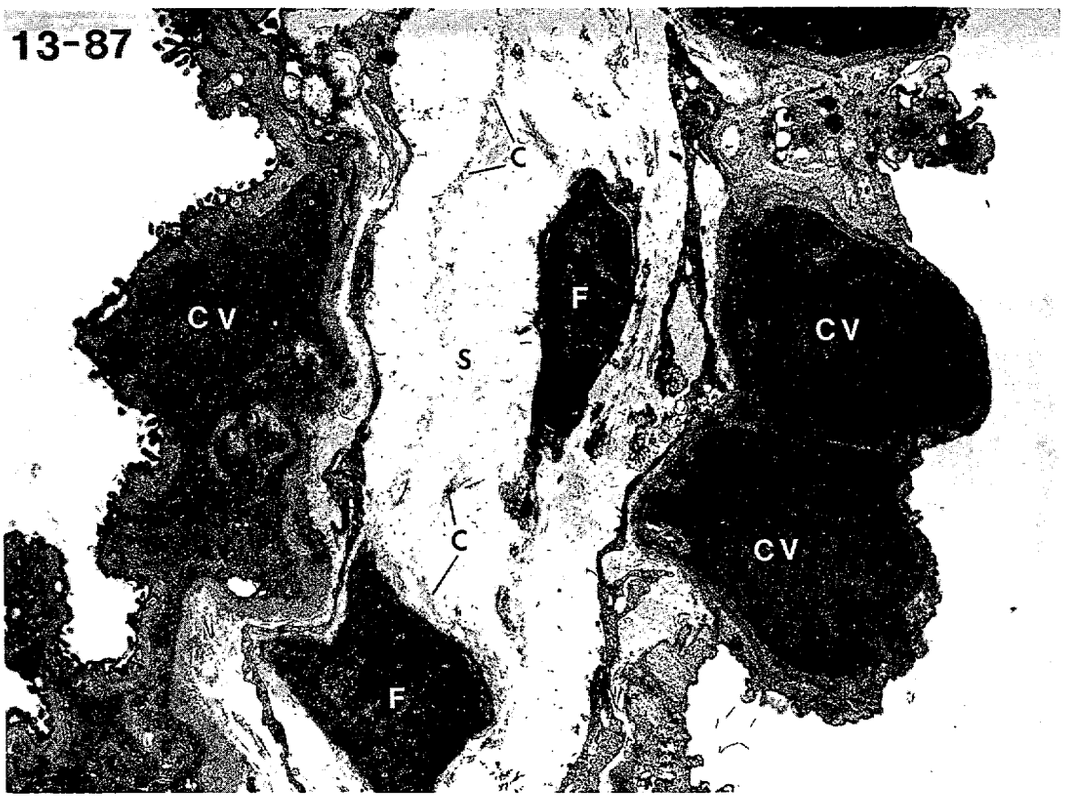
13-87
C
CV
F
S
CV
C
CV
F

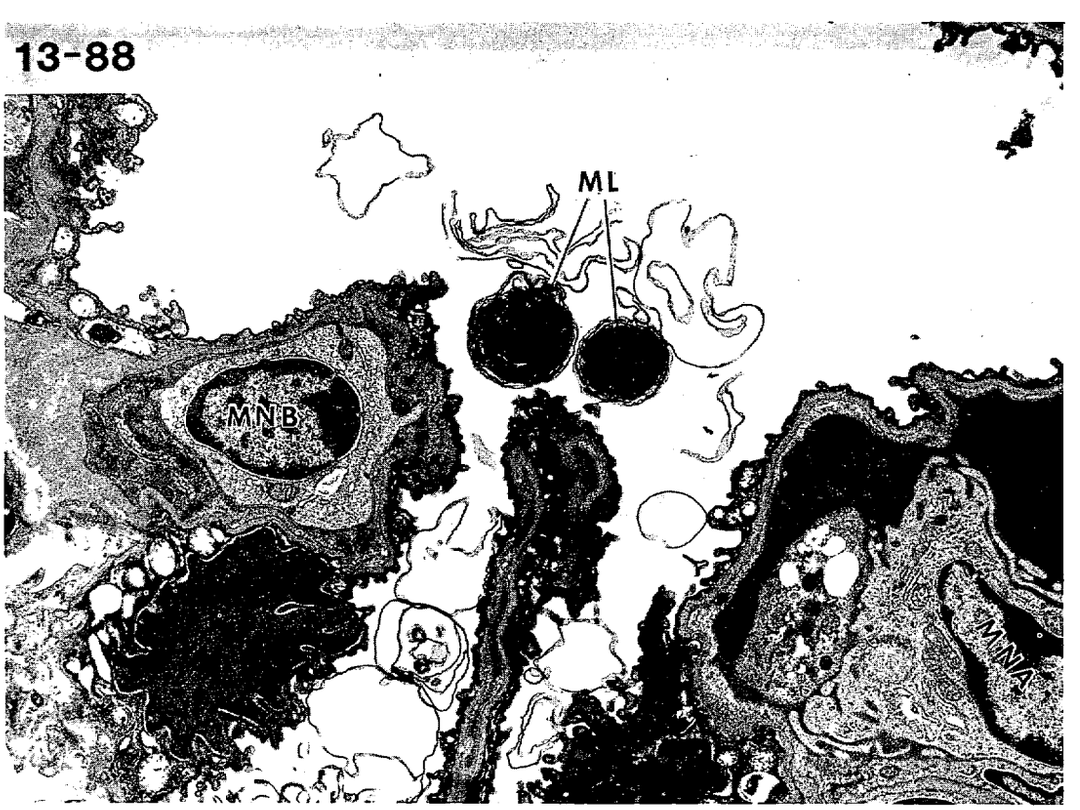
13-88
ML
MNB
MNA

Figure 13-89. Higher magnification transmission electron photomicrograph of a mononuclear cell similar to that shown in Fig 13-88. Complex cytoplasmic extensions (CE) are seen as are numerous organelles within the cytoplasm. This is probably a monocytic cell. X10,400

Figure 13-90. Transmission electron photomicrograph of a type II pneumocyte from the lung of whale 80B8. Along with the usual intracellular organelles, an inclusion showing a fingerprint-like structure is seen (FP). X15,300

13-89

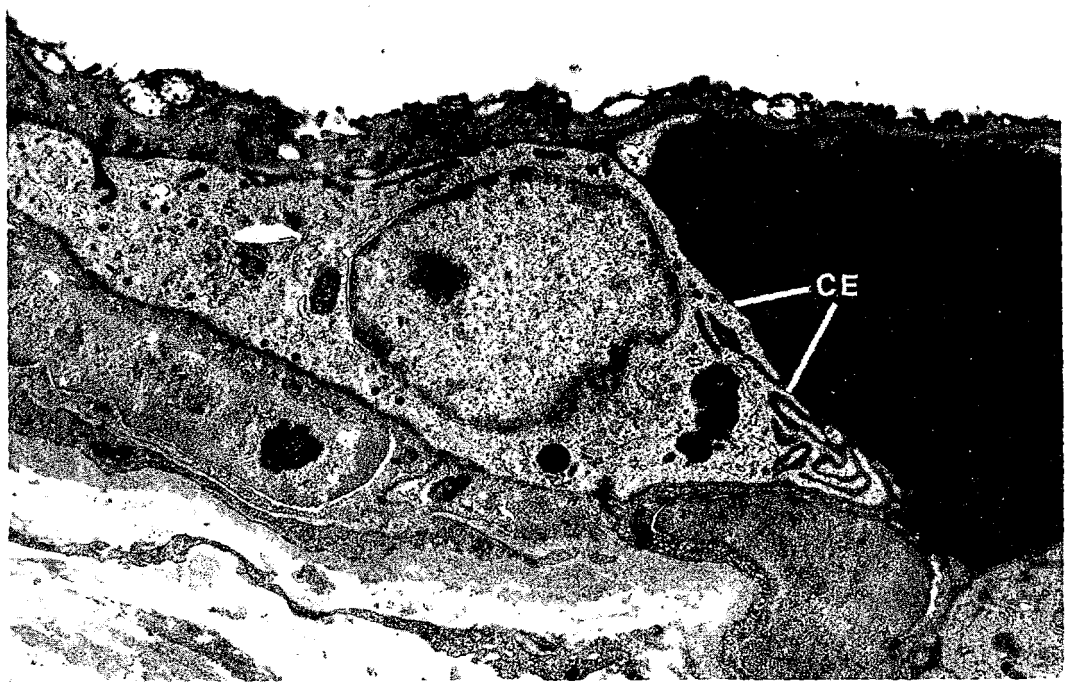

13-90

Figure 13-91. Photomicrograph, lung with pleura, 80B1. The 1.2-2.4 mm thick elasticized pleura is predominantly dense irregular connective tissue (Ct) throughout with the outermost region highly elasticized (E). Variously sized arteries (A) and veins (V) occur randomly. The only "septa" (S) within the lung tissue are typical as illustrated and seem to be confined to the coursing of the pulmonary vessels. Large continuations of pulmonary tissue (P) are the rule. Note the numerous alveolar sacs (AS) surrounded by their connecting alveoli. X.S, Verhoeff stain, X50

Figure 13-92. Higher magnification photomicrograph of the pleural wall in Fig 13-91. The outer surface is covered with typical mesothelium (arrow) and a thin region of dense irregular connective tissue followed by a variably thick concentration of elastic fibers (black wavy lines) and then dense irregular connective tissue continues inwardly with the more usual quantity of elastic fibers. Large thin walled arteries (A) and veins (V) course randomly. X.S., Verhoeff stain, X160

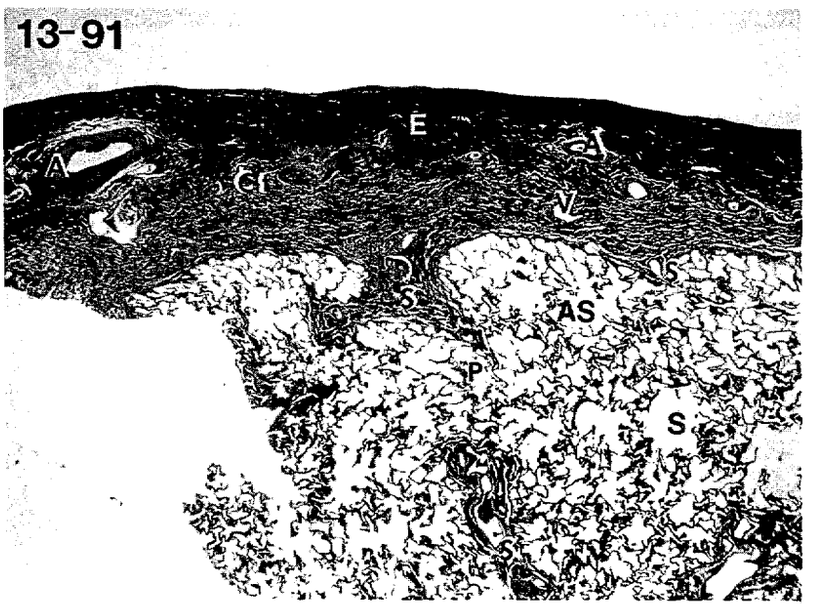
13-91
E
A
A
Cr
V
D
S
AS
P
S
S

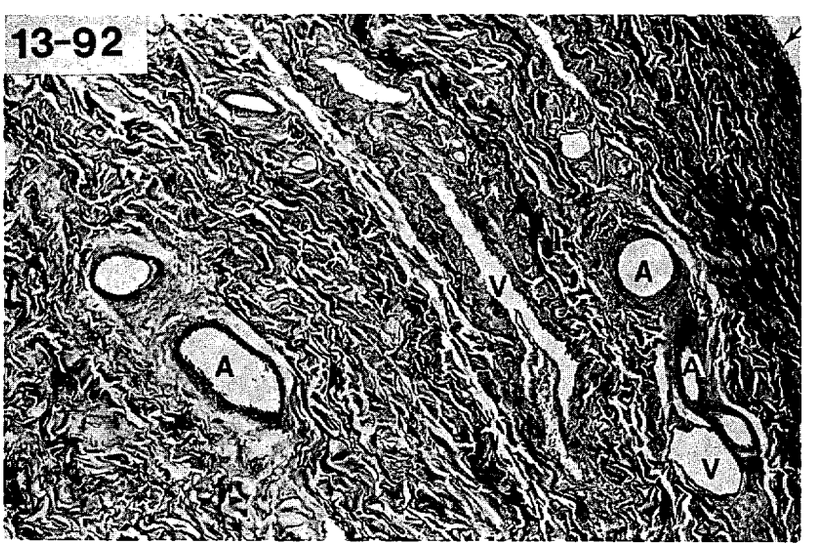
13-92
A
V
A
A
V

Figure 13-93. Photographs of the lungs of 7961 and 80B2.

A. Ventral (medial) view of 7961, a right lung of an Ingutuk. The lobar bronchi are removed and segmental bronchi (S) are seen in the hilar region. The superficial location of the veins (V) just below the pleura should be noted. X0.11

B. The dorsal (lateral) surface of 79B1 demonstrates creases in the thick pleura (arrows) which are fixation related and not signs of lobation. X0.12

C. The dorsal (lateral) surface of 80B2. External creases in the pleura (arrows) are fixation artifact and not lobar septa. The principal bronchus (C). The opening (0) where the cranial lobar bronchus is torn away can be seen. Medial view is in Fig 13-47A. X0.13

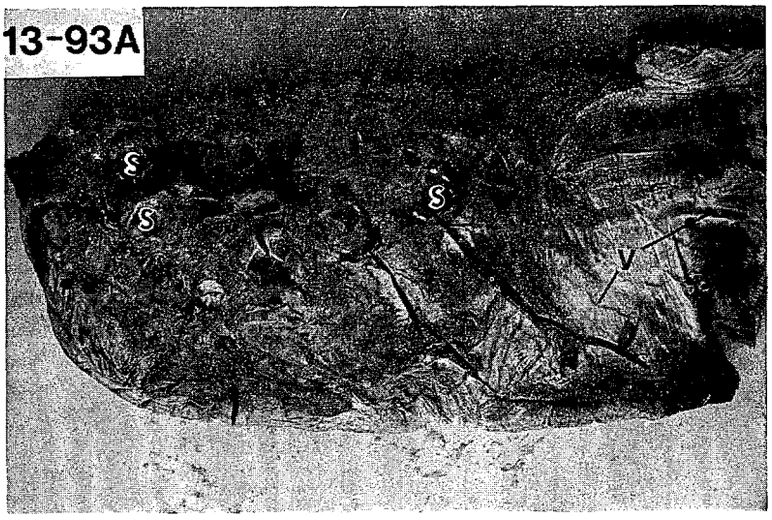
13-93A
§
§
§
V

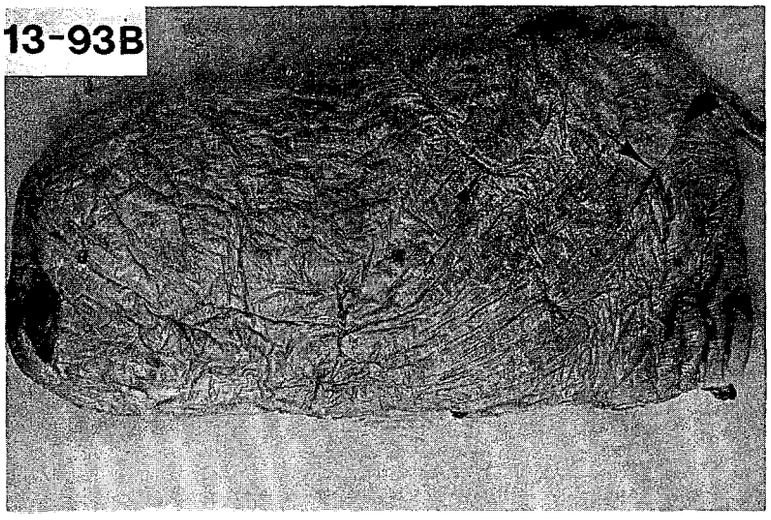
13-93B

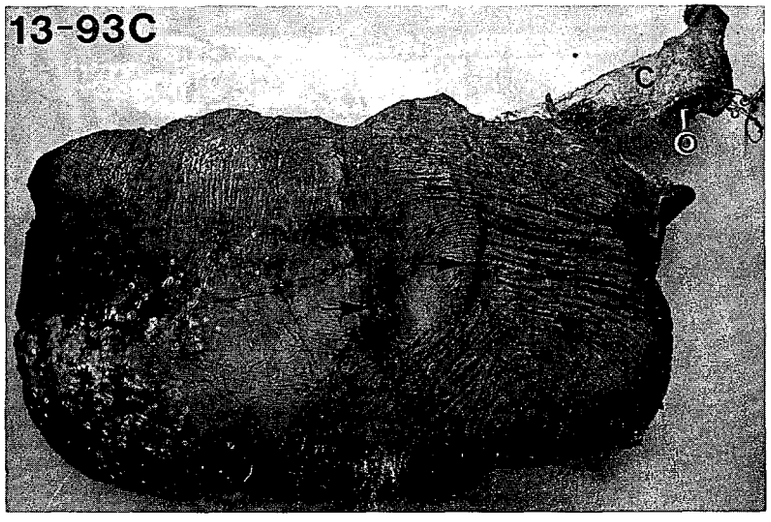
13-93C
C
I
O

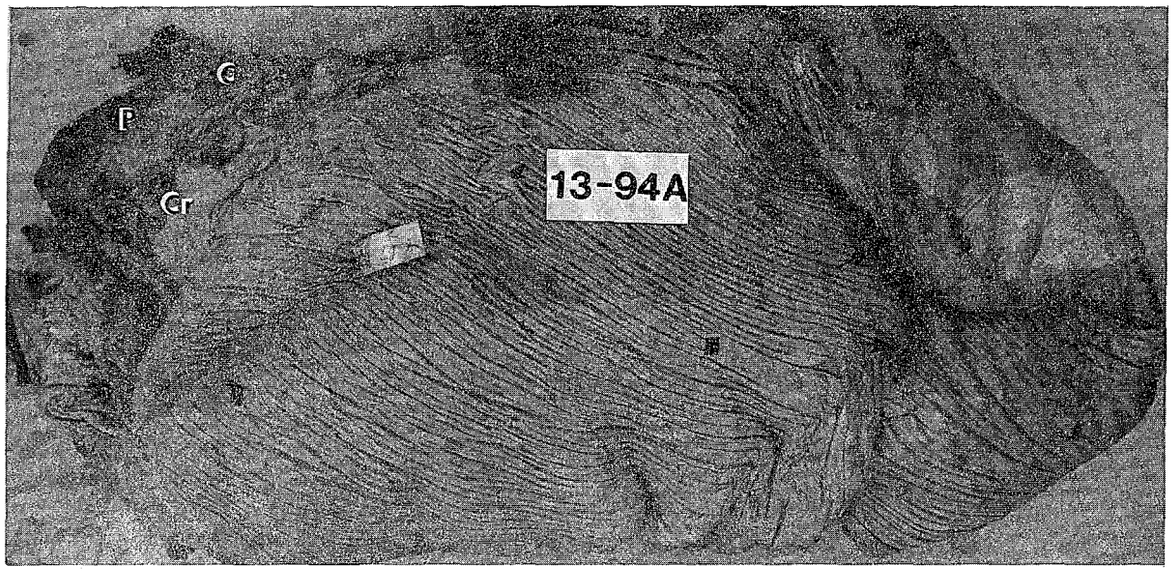

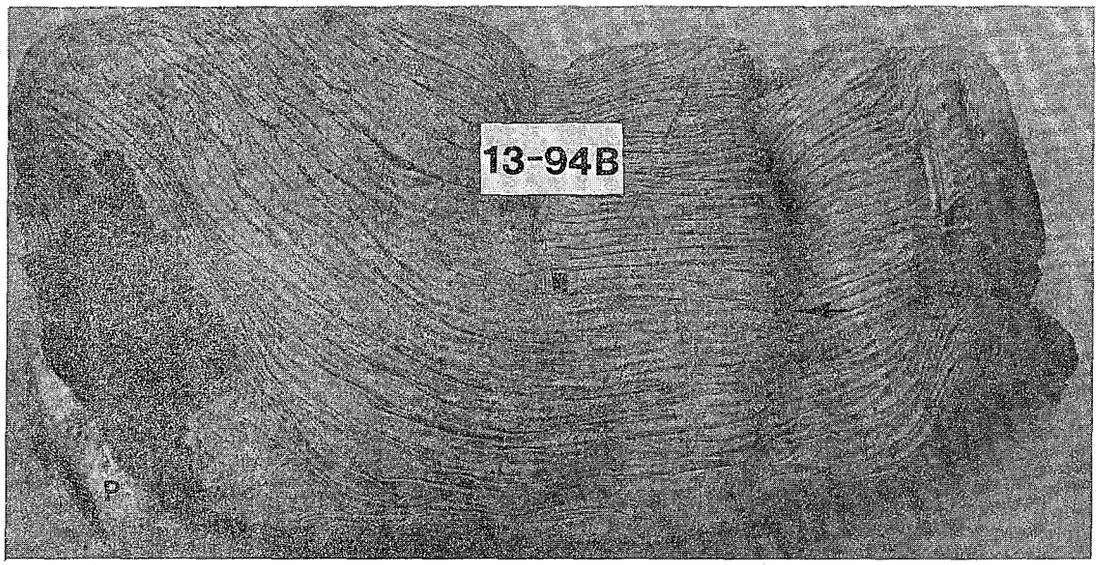

Figure 13-94. Photographs of the lung of 8067 and 80B8.

A. The dorsal (lateral) surface of 8067. The principal bronchus (P) can be seen dividing into cranial (Cr) and caudal (C) lobar bronchi. The thick pleura covering is wrinkled due to its high elastic content and fixation. The large crease (arrows) is fixation and shipping artifact. The medial view can be seen in Fig 13-46A. XO.18

B. The dorsal (lateral) surface of 8068. Note the thick wrinkling of the pleura is cut away near the principal bronchus (P) showing the underlying parenchyma. The large groove (arrow) is from shipping. XO.21

II. Kidney

Owing to the fact that all the specimens received were small chunks of kidney tissue and not the whole organ, it was not possible to determine the general morphology of the kidney of the bowhead whale. Thus, no description is given of the peritoneal investment of the organ, the existence and location of the hilus and renal sinus, overall measurements, or the pattern of entrance or emergence of arteries, veins and ureters. All samples received had one or two surfaces invested with a layer of fascia that contained yellowish colored adipose tissue. When this fascia was pulled away from the kidney tissue, a thin layer remained adherent to the surface (Fig 13-95). This surface fascia did not contain any large blood vessels.

None of the samples demonstrated any of the main renal arteries, veins or ureters. Only smaller branches were represented in the specimens received. Maximum diameters of branches of the renal artery were 5 mm, renal veins 15 mm, and ureteral branches 8 mm. These structures were completely invested by loose fascia that also joined the many kidney lobules together.

In one specimen (80B7) the sample was taken from the margin of the left kidney. The artery, vein and ureteral branch, with their fascia covering, were located in an indentation on the surface of the specimen. The indentation looked like the renal sinus (Figs 13-96, 13-97), however, the small diameter of the vessels indicated that it might be the tip of the sinus. This also implied that the main renal artery branched as it approached the sinus, while the main renal vein and ureter were formed from smaller branches in the sinus. From this we may speculate that the kidney of the bowhead whale has an elongate hilus that extends the whole length of its medial surface.

The kidney of the bowhead whale is highly lobated. It is divided into small lobes or renicules. They were found to exist individually or in clusters of three to five (Figs 13-98, 13-99, 13-100, 13-101). Individual renicules had a complete fascial investment while those in a cluster shared a common investment of fascia with incomplete partitions between renicules (Fig 13-99).

Dissection of the fascia of various clusters exposed the branches of the ureter, renal artery, and renal vein which were completely embedded in it (Figs 13-101, 13-102). A striking feature of the kidney of this whale was the eleborate network of very thin walled veins that surrounded the arterial and ureteral branches (Figs 13-102, 13-103, 13-105). These veins had large lumina, being as much as 8 mm in diameter as compared to 2 mm for arteries and

3 mm for ureters. The veins filled most of the space between renicules and clusters of renicules (Figs 13-103, 13-104, 13-105). When opened there were no discernible valves, but tributaries opened into larger veins on raised folds of the tunics intima (Fig 13-106).

Renicules Each renicule was made of a conical shaped unit. The base of the cone was superficial and the tip of the cone was directed towards the center of the kidney. The cortical parts of the renicules were the only visible structures on the surface (Fig 13-98). The medullary parts were not visible because they were surrounded by large thin walled veins and fascia (Fig 13-101). The outline of the base of the cone was polyhedral and the sides of the renicule were flattened owing to their crowding by neighboring renicules. Blood vessels entered and left the renicules at the corticomedullary junction (Figs 13-107, 13-108). The ureteral branch or infundibulum left the calyx at the tip of the renicule (Fig 13-109). The renicular cortex was narrower than the medulla. It capped the medulla and extended about half of the width on the sides. The cortex was covered by a very thin transparent capsule (Fig 13-110). Subcapsular veins were easily demonstrated as a network of thin walled vessels filled with brown coagulated blood. When branches of the renal veins were injected with colored latex or Microfil, some of the subcapsular 'veins became filled with the injection mass (Figs 13-111, 13-112; 13-113). The largest diameter of a renicule was at its base, ranging from 7.8-14.1 mm. The smallest diameter was represented by a line extending from the base to the apex of the renicule which ranged from 7-10.1 mm (Figs 13-114, 13-115).

Microdissection of renicules revealed that two or more units in a cluster could have fused cortices but retained separate renal papillae (Fig 13116) . Each renal papilla was intimately surrounded by a calyx. A latex rubber cast of calyces clearly demonstrated the chalice shape of these structures (Fig 13-117) . More than one calyx could join to empty in one infundibulum (Fig 13-118). The majority, however, emptied independently. On vertical sections of renicules, the cortex, medulla and intermedullary regions were clearly demonstrated. The cortex of the formalin fixed renicule was dark brown in color and represented the outer one-fifth to one-third of the thickness of the renicule. The medulla was dark toward the cortex but was much lighter distally and occupied the remainder of the parenchymal thickness of the renicule (Figs 13-109, 13-110, 13-114, 13-115.).

The corticomedullary junction (sporta perimedullaris) was represented by a very thin, white connective tissue band between cortex and medulla which contained arteries and veins (Figs 13-109, 13-110, 13-114, 13-118). The cortex measured 2-3 mm in thickness while the medulla occupied the other two-thirds of the renicule (9-11.5 mm). The sporta measured 0.3-0.5 mm in thickness (Fig 13- 115).

When a renicule was serially sectioned transversely starting at the surface of the cortex and proceeding to the level of the corticomedullary junction, it was evident that the connective tissue of the sporta started about 0.5 mm from the surface as a thickening of the stroma of the central zone of the cortex. It was perforated by ascending and descending renal tubules (medullary rays). Deeper sections demonstrated further expansion of the sporta which was perforated by larger bundles of tubules. At the corticomedullary junction it became a wavy connective tissue circle with thickenings accommodating arcuate vessels (Fig 13-119).

The calyx of each renicule had a wall that measured 0.3 mm in thickness; however, it got thicker by blending with walls of neighboring calyces, or by being continuous with the walls of veins in the vicinity (Figs 13-110, 13-120). The wall of the calyx was continuous with the sporta at the corticomedullary junction.

Calyces became continuous with an expansion of a ureteral branch or infundibulum (Figs 13-109, 13-110, 13-114, 13-115). Sometimes more than one calyx shared an infundibulum (Fig 13-118). Ureteral branches draining several clusters joined to form larger branches. This pattern of union was repeated through the specimen and terminated in the formation of two or three ureteral branches draining each piece.

On examination of kidney tissue under the light microscope, it was obvious that the renicule was the morphological unit of the whale kidney. Each renicule was covered by a very thin 20 µm capsule made of loose connective tissue. Deep to the capsule, the parenchyma was divided into cortical and medullary regions with an obvious corticomedullary zone of collagenous connective tissue, the sporta perimedullaris. The renal papilla of each renicule was surrounded by a calyx. The wall of the calyx either blended with the wall of a neighboring one or with the wall of a vein that surrounded it (Fig 13- 120).

Cortex The cortex of the bowhead kidney renicule is of the typical mammalian type consisting of renal corpuscles and

tubules. Renal corpuscles were scattered among the tubules just under the capsule in the middle of the cortex, and were partially embedded in or very close to the corticomedullary connective tissue. Measurements of the corpuscles ranged from 120 x 100 to 170 x 110 μm. Some corpuscles abutted each other to form clusters (Fig 13-121). Parietal epithelial cells of Bowman's capsule, podocytes and glomerular capillaries were easily demonstrated (Fig 13-122). Juxtaglomerular structures were well developed. Maculae densae, afferent arterioles, efferent arterioles and polar cushions were observed. Afferent arterioles were different from efferent arterioles in that they had thicker walls, wider lumina and the majority of smooth muscle cells in their walls were modified. Instead of the normal smooth muscle cell size and staining properties, these cells were stouter and had optically clear, lighter staining cytoplasm. They measured 18 x 8 μm while regular smooth muscle cells measured 25 x 5 μm. The transformation from the normal smooth muscle cell type began as these arterioles originated from interlobular arteries far from the juxtaglomerular areas (Fig 13-123). They also branched toward different glomeruli with their walls already modified (Fig 13-124).

In all the specimens studied (79B1, 79B2, 80B1, 80B2, 80B7, 80B8), no periodic acid-Schiff reaction (PAS) positive renin granules occurred in the juxtaglomerular cells of the afferent arterioles. The diameter of afferent arterioles ranged from 17.5-20 μm. Efferent arterioles emerged from the glomeruli and acquired a smooth muscle wall. They had a comparatively narrower lumen (Fig 13-125).

Macula Densa The part of the distal convoluted tubule that participates in the juxtaglomerular apparatus, the macula densa, was made of light staining, cuboidal epithelial cells with cytoplasm containing fine granules. The part of the tubule next to the glomerulus and its arterioles was characterized by crowding of the cuboidal cells forming a linear cluster of up to 19 cells (Figs 13-125, 13-126). The cells on the other side of the tubule were widely spaced. The polar cushion, or extraglomerular mesangial cells, were represented by a stratification of flattened cells with oval to round nuclei. They filled the triangular area formed by the macula densa, afferent arteriole, and efferent arteriole, and were continuous with the glomerular mesangium (Fig 13-125).

Glomerulus The afferent arteriole entered the renal corpuscle and joined a maze of capillary-like channels lined by endothelial cells. They rested on a basal lamina that was continuous around the channels

in the glomerulus. The channels were arranged into three to five units which were clearly separated from each other. Each unit represented a glomerular lobule. These were easier to observe if the tissue was stained for PAS reaction, owing to the positive reaction of the basal laminae surrounding these channels (Fig 13-127). Glomerular mesangial cells represented connective tissue cells that were an extension of the polar cushion. They were located in the central or axial area of the glomerulus between vascular channels and had an abundant light staining cytoplasm and rounded nuclei (Figs 13-122, 13-125).

Parietal epitheliums of the renal corpuscle was made of simple squamous epitheliums with large oval nuclei that protruded into the urinary space. The epitheliums rested on a complete basal lamina that surrounded the corpuscle except at the vascular and urinary poles (Fig 13-128). The visceral cells, or podocytes, had thicker nuclei and their cytoplasm rested on the basal lamina of the glomerular capillaries. They had more abundant cytoplasm than parietal cells and they stained more darkly than mesangial cells (Figs 13-122, 13-125).

At the ultrastructural level, the renal glomerulus and capsule were similar to those seen in other mammals. The parietal epitheliums of Bowman's capsule was simple squamous while the visceral epitheliums consisted of podocytes with numerous primary and secondary (foot) processes. The foot processes rested on the basal lamina of the capillaries of the glomerulus and interdigitated to form 25-50 nm filtration slits (Figs 13-129, 13-130, 13-131). Diaphragms bridging filtration slits were not observed (Figs 13-130, 13-131). The basal lamina extending between the foot processes and the capillary endothelium measured approximately 0.18 µm in thickness. The parietal epitheliums rested against a basal lamina which separated the capsule from the connective tissue between nephrons (Figs 13-129, 13-132). Mesangi al cells were also evident on the capillary side of the basal lamina (Fig 13-129).

Renal Tubules (uriniferous tubules) Due to poor preservation, the study of cellular detail was not possible. Proximal, distal, ascending and descending limbs, and collecting tubules could be identified, however.

Proximal convoluted tubules were identifiable throughout the cortex from just under the capsule to the corticomedullary junction. The epitheliums in these tubules was dark staining, granular columnar cells (Fig 13-123). The brush border was not fixed well and was not visible even after the PAS reac-

tion, although the basal lamina was easily demonstrated (Fig 13-127). The tubules measured 30-50 μm in diameter. The lumen of the tubules was the narrowest among those seen in the cortex.

Distal convoluted tubules had a wider lumen because the lining epithelium was cuboidal in shape. The cells stained lighter, were less granular (Fig 13-123) and the lumen measured 30-40 μm in diameter. Descending and ascending thick limbs of Henle's loop formed the medullary rays. The descending one resembled proximal convoluted tubules, while ascending limbs resembled distal convoluted tubules. The only difference was their straight course through the cortex (Fig 13-121).

Collecting tubules or ducts were lined by optically clear cuboidal epithelial cells. The cells bulged into the lumen, almost occluding it. Proximal and distal tubules as well as the collecting ducts were poorly preserved, making fine structural observations with the electron microscope impossible (Figs 13-133, 13-134).

Interlobular arteries were easily recognized in the cortex and averaged 75 μm in diameter. An obvious morphological feature of the kidney cortex of the bowhead whale was the presence of large, thin walled subcapsular veins that had large lumina. These were easily demonstrated by subgross and microscopic means (Figs 13-111, 13-112, 13-113). These subcapsular veins drained the capillary networks of the outer cortex, then led into interlobular veins which traversed the cortex to join larger arcuate veins in the sporta perimedullaris. The arcuate veins then left the renicule and drained into the veins that surrounded th'e renicular structures (Fig 13-135).

Connective Tissue Stroma The cortex of the kidney of the bowhead had a well developed dense connective tissue stroma that surrounded all structures. It was most abundant around arteries and renal corpuscles in the cortex (Fig 13-136) and ranged from 2.5-7.5 μm around tubules, and from 10-20 μm around corpuscles. As described above in macroscopic studies, the connective tissue that formed the sporta perimedullaris actually had its origin in the middle layer of the cortex. It was a connective tissue sheet through which medullary rays ascended and descended between cortex and medulla (Fig 13-119 B). Close to the corticomedullary junction, more connective tissue stroma surrounded the cortical elements (Figs 13-119C, 13-119E).

The corticomedullary junction was characterized by this well developed sheet of connective tissue that physically separated the cortex from the medulla except where tubules and blood vessels descended and ascended between

them. The corticomedullary tissue was made of dense white fibrous connective tissue with very few elastic fibers. No smooth muscle fibers were identified as part of this tissue, even with such differentiating stains as Masson's and Milligan's techniques (Figs 13-137, 13-138). The only muscle fibers observed in the corticomedullary tissue belonged to the walls of blood vessels. At the periphery of the renicule, the corticomedullary tissue, or sporta perimedullaris, became continuous with the wall of the calyx. Blood vessels entered and exited through this junction between the sporta and calyx wall (Fig 13-120). When two adjacent calyces shared the same wall, usually the sportae of both renicules were continuous at the junction of the combined calyx wall (Figs 13-139, 13-143).

Medulla The medulla consisted of outer and inner zones. The outer zone was composed mainly of medullary rays and vasa rectae among the straight tubules of Henle's loop. It is important to differentiate between thin segments of Henle's loop and vasa rectae. In the bowhead the arterial segments of the vasa rectae had the thickest walls with simple squamous endothelial lining and one smooth muscle layer. The venous segment had a very thin wall made of endothelial cells and looked like a large lumened capillary. Both of these frequently contained blood elements which made the identification easy.

Henle's thin loop was intermediate in size. It was made of very flat, low cuboidal or even simple squamous epitheliums. In the latter type, it was very difficult to differentiate between it and the venous segments of the vasa rectae. The only clue was that the nuclei of the thin segment epitheliums did not bulge into the lumen as much as in the venous segments. The thick segments of Henle's loop had the same morphology as their related convoluted tubules (Figs 13-140, 13-141). Collecting ducts were easily differentiated from the rest of the medullary structures. They were lined with optically clear cuboidal epithelial cells with sharply demarcated cellular membranes and centrally located nuclei (Figs 13-140, 13-141). Close to the tip of the renal papilla only collecting ducts and thin segments prevailed (Fig 13-142). It was difficult to differentiate interstitial medullary cells in light microscopic observations. The surface of the medulla and papilla that faces the calyx was covered by a very low transitional epitheliums.

Two renal papillae may be fused and open into a common calyx that leads to a common infundibulum (Fig 13-143) without fusion of the cortices. In other renicules, the cortices may be fused but the papillae and calyces

remained separate (Fig 13-144). A third variation was the presence of separate cortices, papillae and calyces, but the calyces communicated to empty into a common infundibulum (Fig 13-145). The calyx wall was made of dense white fibrous connective tissue which was rich in capillaries. There were no smooth muscle fibers in the wall of the calyx or infundibulum. Smooth muscle fibers were present in the walls of ureteral branches 'only. The calyx, infundibulum and ureteral branches were lined with transitional epitheliums (Figs 13-145, 13-146, 13-147).

The ureteral branch wall had a lamina propria-submucosa which was combined peripheral to the transitional epithelium. An outer circular smooth muscle layer and a tunics adventitia completed the wall. A unique feature in the bowhead was the presence of large thin walled veins that surrounded and sometimes shared walls with ureteral branches (Fig 13-148).

Urinary Bladder

Macroscopic Dissection Two samples of urinary bladder were received from whales 7961 and 8067. The lining mucous membrane was smooth and highly folded in an irregular manner. The outer surface was covered by a loose tunics serosa that measured 4 mm in thickness. The complete thickness of the wall of the bladder was 3.7 cm in 7961, a 8.7 m male Ingutuk variant and 6.5 cm in 80B7, a 10.0 m female ordinary bowhead. Other than the mucosal lining and tunics serosa, the rest of the wall, was made of a very tough and vascular fibromuscular tissue. Due to the highly folded mucous membrane it was presumed that the samples were taken from contracted bladders.

Microscopic Anatomy The tunics mucosa had a lamina epithelialis of transitional epitheliums. It varied between four and nine cell layers in thickness. Epithelial cells were missing from parts of the lining surface as a result of handling and processing of the specimens (Fig 13-150). In both specimens, a fine capillary network occurred adjacent to the basal cell layer (Figs 13-149, 13-150). The lamina propria was' vascular, reasonably dense, f ibroel astic connective 'tissue (Figs 13-149, 13-150)'. It terminated with a lamina muscularis mucosae of circularly arranged bundles of smooth muscle fibers in the male Ingutuk (79B1) (Fig 13-151). Peripheral to these bundles, the tunics submucosa consisted of highly vascular, much looser, fibroelastic connective tissue. Bundles of "circularly arranged smooth muscle fibers were scattered with some longitudinally arranged fibers located around large thin walled veins (Fig 13-151). In sections taken from the bladder of the female

bowhead (80B7), the wall had a propria-submucosa without intervening muscularis mucosae. Bundles of smooth muscle fibers were scattered among the vascular connective tissue of both layers of the wall, The tunics muscularis was made of thick multidirectionally arranged bundles of smooth muscle fibers very loosely connected by loose connective septa in 79B1. In 80B7 the bundles were thicker and tightly packed together. Bundles of nerve fibers (Fig 13-152), autonomic nerve ganglia and blood vessels were also present within the tunics muscularis. The tunics adventitia consisted of loose fibroelastic connective tissue.

Figure 13-95. Photograph of a kidney sample covered with fascia, 80B7. Loose fascia (LF) is pulled away to expose a thin layer of fascia (AdF) adherent to renicules. X0.5

Figure 13-96. Photograph of a specimen from the margin of the left kidney, 80B7. The renal artery (A) and vein (V) branches and ureteral branch (U) are located in an indentation on the surface of the specimen. Structures are invested with loose fascia. X0.5

Figure 13-97. Photograph of the same specimen in Fig 13-96 with vessels and ureteral branch pulled away to expose indentation (H) on the surface of the kidney. This indentation probably represents the tip of the renal sinus. The part of this sinus where the blood vessels enter and leave the kidney is the hilus. X0.5

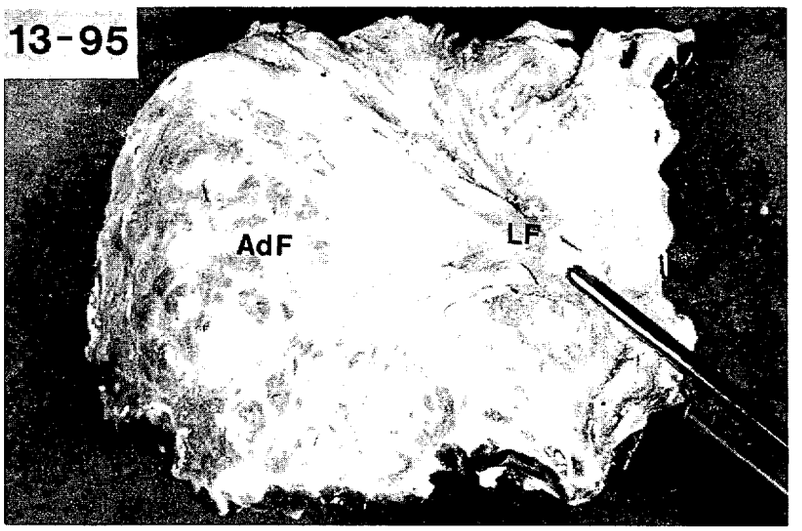
13-95
AdF
LF

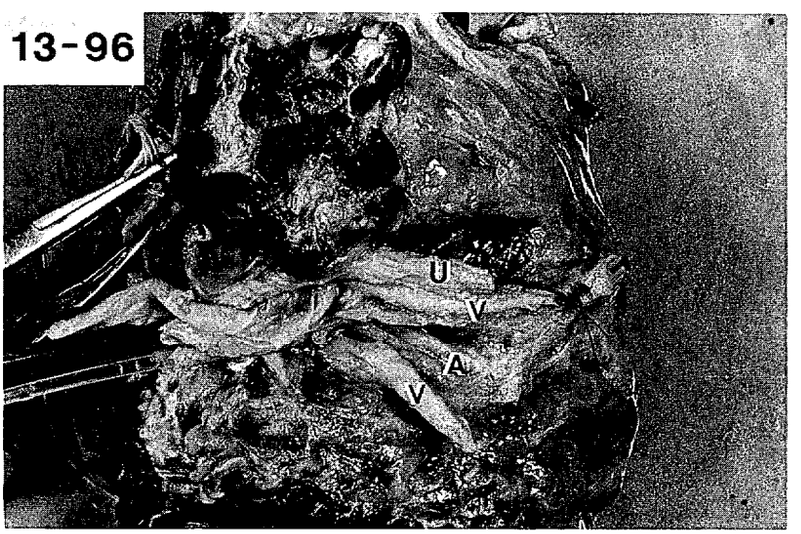
13-96
U
V
A
V

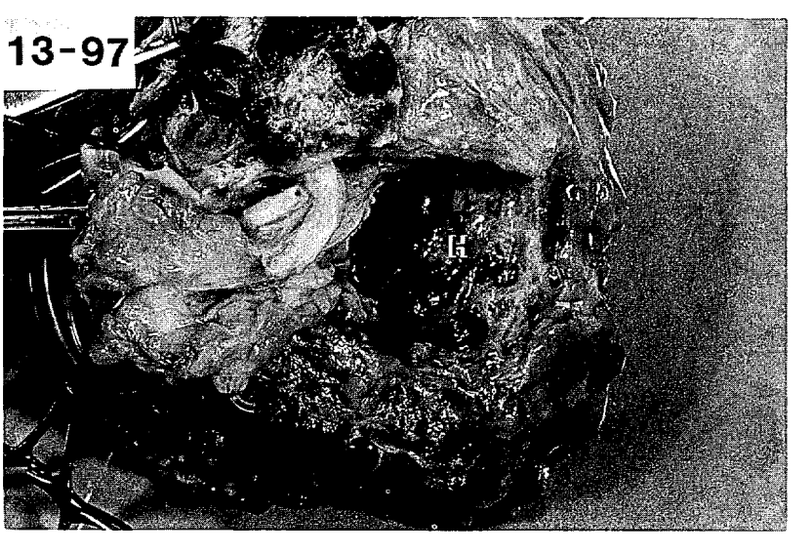
13-97
H

Figure 13-98. Photograph of a kidney specimen after removal of surface fascia, 80B7. Renicules are arranged in clusters (C). Only the bases of renicules represented by cortex surfaces are showing. xl

Figure 13-99. Photograph of fascial compartments (arrows) surrounding individual renicules of a cluster after removing the renicules, 80B7. X4.5

Figure 13-100. Photograph of the cortical surface of a cluster made of four renicules (R), 80B1. X4.5

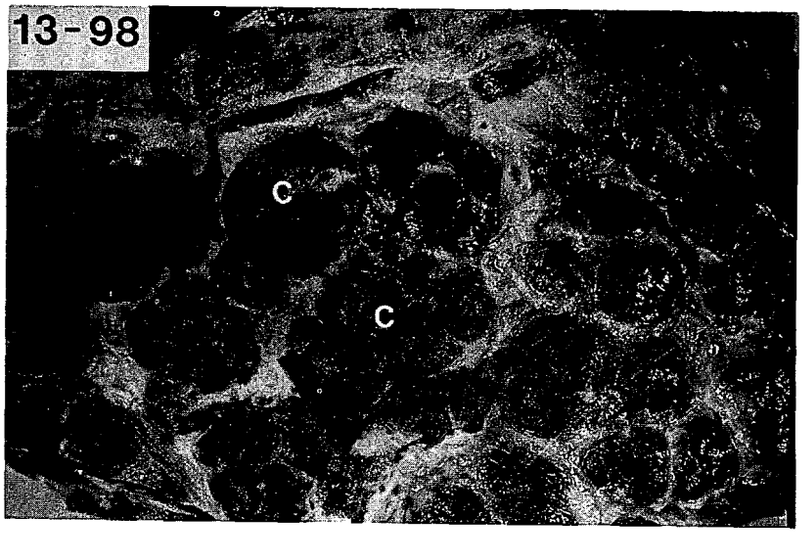
13-98
C
C

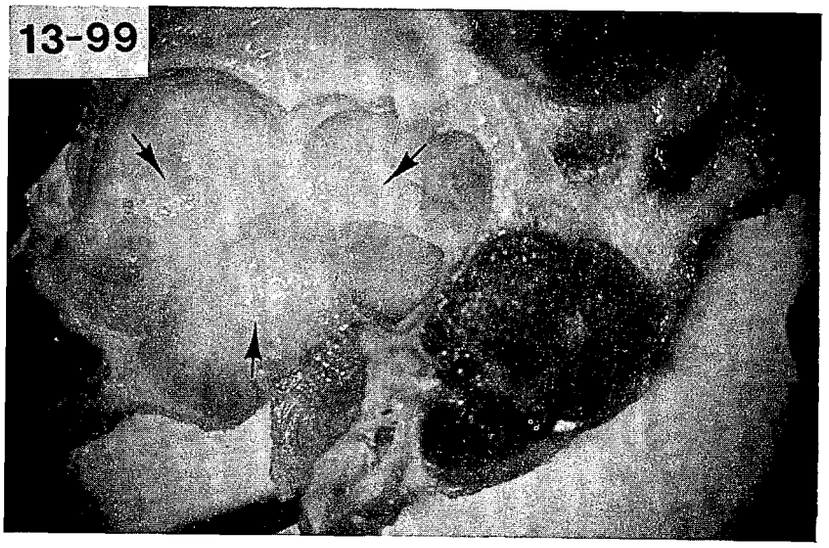
13-99

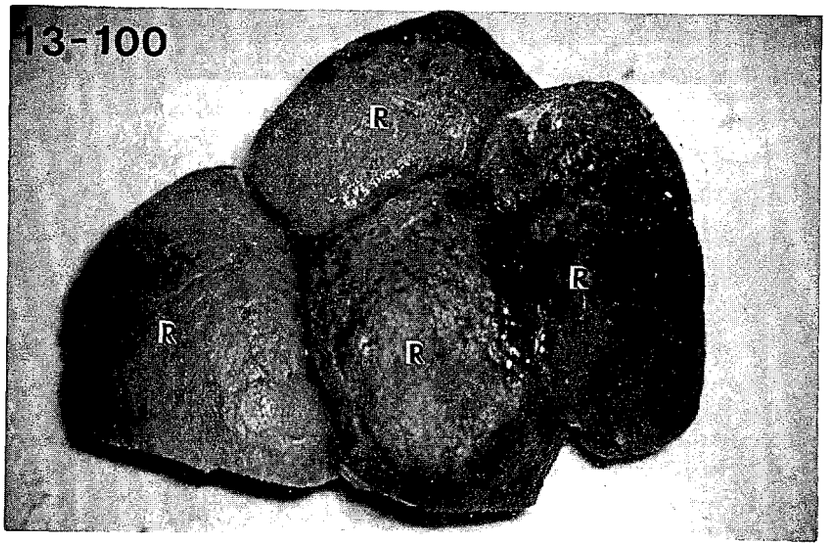
13-100
R
R
R
R

Figure 13-101. Photograph of the deep surface of same cluster in Fig 13-100. The minor calyces are completely hidden by fascia (F) and thin walled veins (V). A small artery (arrow) is entering the renicule at the corticomedullary junction. Superficial subcapsular veins are seen under cortical capsule (arrowheads). x7.5

Figure 13-102. Photograph of the deep surface of same cluster in Fig 13-101 with fascia cleaned. Ureteral branch (U), renal artery (A) and veins (V) are exposed. Veins and ureter are cut transversely. One vein contains Microfil (white) mass that was injected into larger vein in the specimen. X5

Figure 13-103. Photograph of the deep surface of a cluster of renicules, 79B1. Fascia is cleaned away very carefully to expose very large thin walled vein (V) that fills the space (arrows) between renicules and hides an artery and ureteral branch. A cannula inserted through a hole in the venous wall is directed towards the renicule. X6

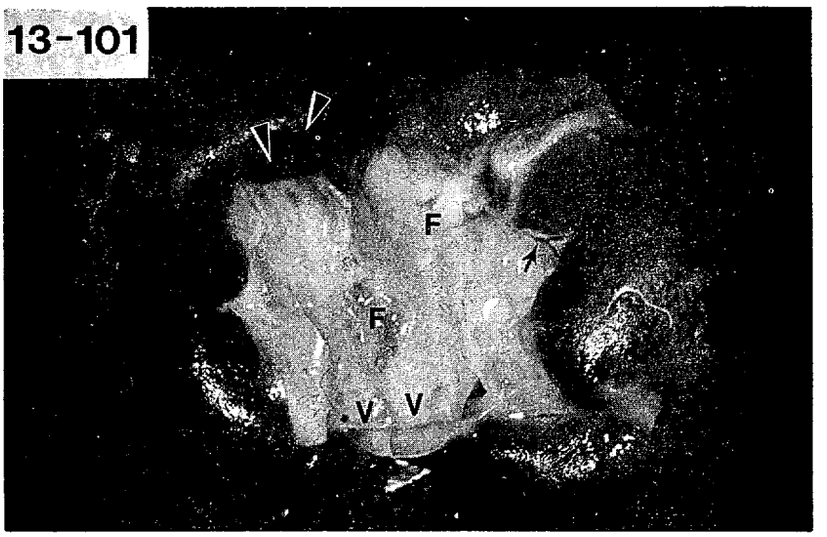
13-101
F
F
V
V

13-102
V
V
U
A

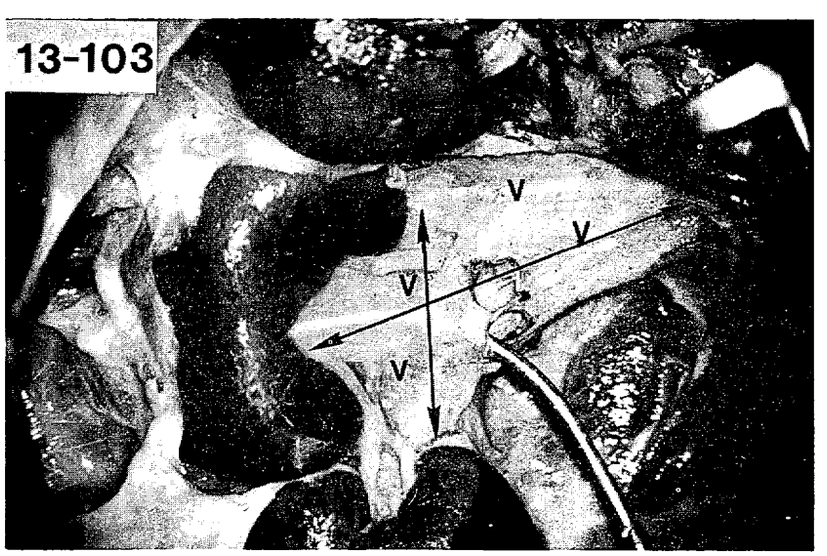
13-103
V
V
V
V

Figure 13-104. Photograph of the same specimen in Fig 13-103. The cannula in the vein is directed away from the renicule to show how extensive the veins (V) are. X4

Figure 13-105. Photograph of a microdissection of the deep surface of a cluster of renicules (80B1). Most of the fascia is cleaned away. A ureteral branch (U) is surrounded by large thin walled veins (V) while an artery (unopened) (.4) crosses the area. Other thin walled veins (V) can be seen. X4

Figure 13-106. Higher magnification photograph of specimen in Fig 13-102 (80B1). It demonstrates how smaller veins open into larger ones on raised folds of the tunics intima (arrow). U = ureter; V = vein; A = artery X20

13-104
V
V
V

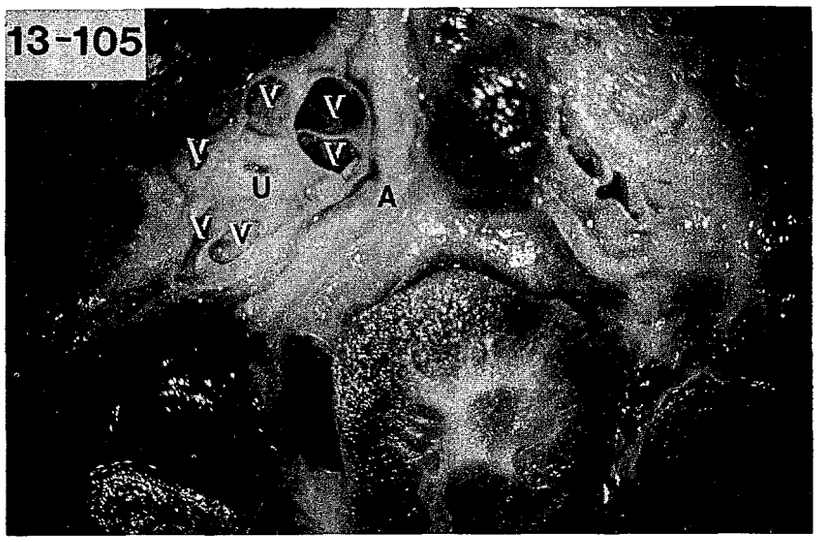
13-105
V
V
V
V
U
A
V
V

13-106
V
V
V
U
A
V
V

Figure 13-107. Photograph of a small artery (arrow) injected with 1 atex entering a renicule at the corticomedullary junction, 79B1. The medulla is covered by cortex (C). The calyx is covered by fascia and thin walled veins (FV). X7.5

Figure 13-108. Drawing of the distribution of arterial branches to a cluster of renicules. 79B2.
A = artery; V = veins; U= ureteric branch; R= renicule

Figure 13-109. Photograph of a vertical section of a renicule to demonstrate how a calyx (Cl) leads into an infundibulum (I) at the tip of the renicule (arrow), 80B8. Notice that the papilla (P) protrudes into infundibulum. Cortex (C), medulla (M), and sporta perimedullaris (Sp) are demonstrated in this photograph. Cortex is shown to cover calyx on right side. X7.5

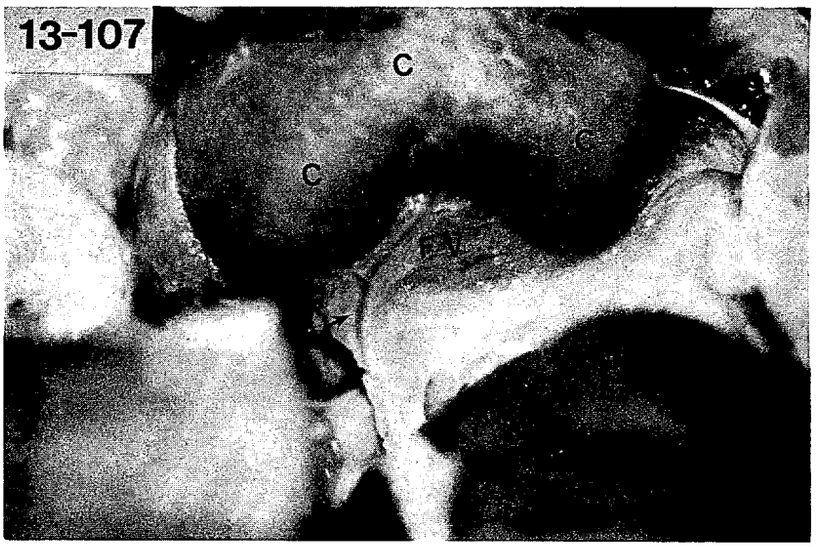
13-107
C
C
C

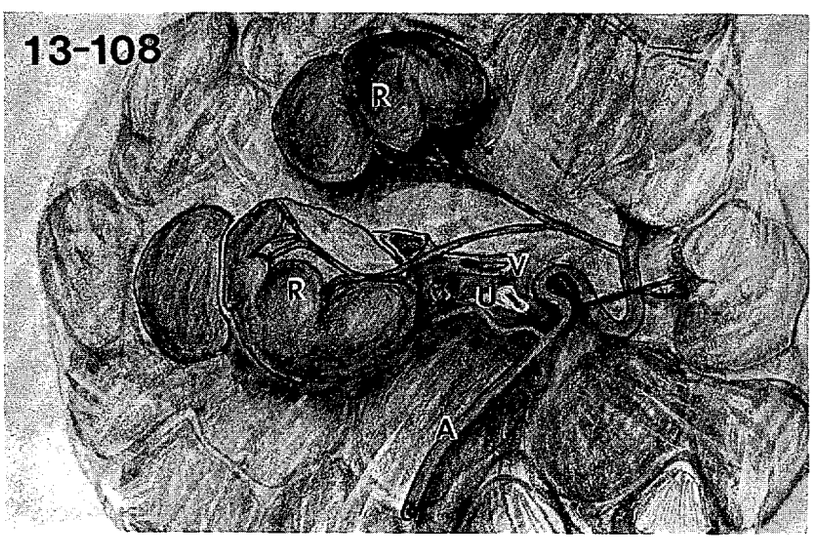
13-108
R
R
V
U
A

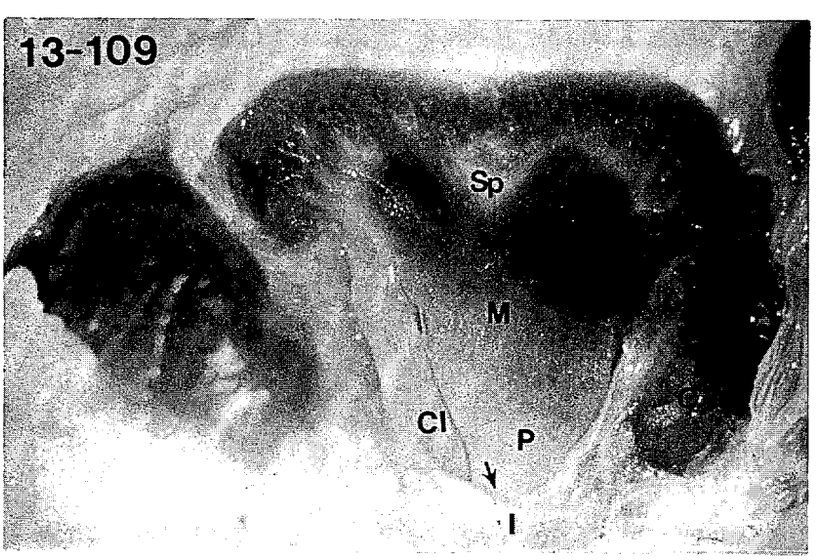
13-109
Sp
M
Cl
P
I

Figure 13-110. Photograph of a vertical section of a renicule from 79B2 demonstrates the cut surfaces of cortex (C) and medulla (M). The cortex is superficial and caps the medulla covering about half of its lateral surface. The thickness of the cortex is about 1/4 that of the medulla. Cortex and medulla are separated at the corticomedullary junction by a sheet of connective tissue, the sporta perimedullaris (arrowheads). An arcuate vessel (AV) is embedded in the sporta. The medulla tapers and forms a renal" papilla (P). A calyx (Cl) surrounds the medulla and leads into an infundibulum (I). Large veins (V) surround the calyx and infundibulum. X20

Figure 13-111. Photograph of the outer surface of cortex of a renicule from 80B1 . Subcapsular veins show under the thin reflective capsule as a dark network (arrowheads). X20

Figure 13-112. Photograph of the surface of the cortex of a renicule from 80B1 . After an injection of yellow colored Microfil, a subcapsular vein is well demonstrated (arrowhead). X20

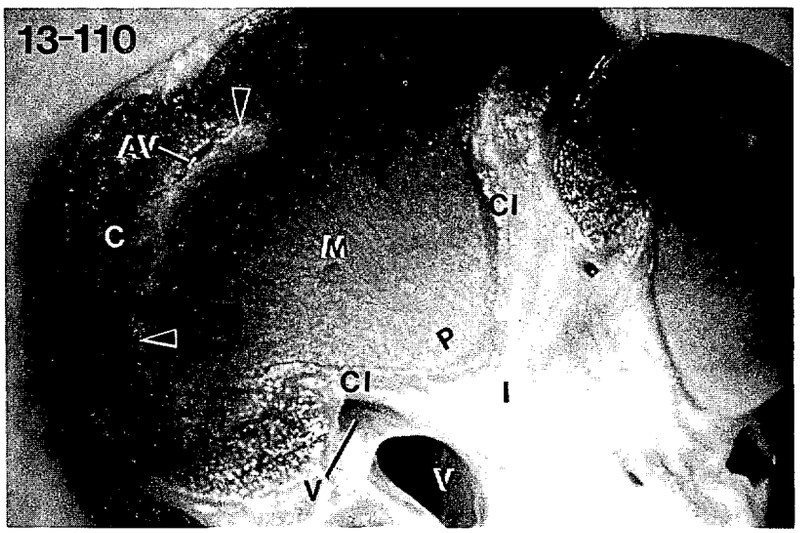
13-110
AV
C
M
CI
P
CI
I
V
V

13-111
V
V
V

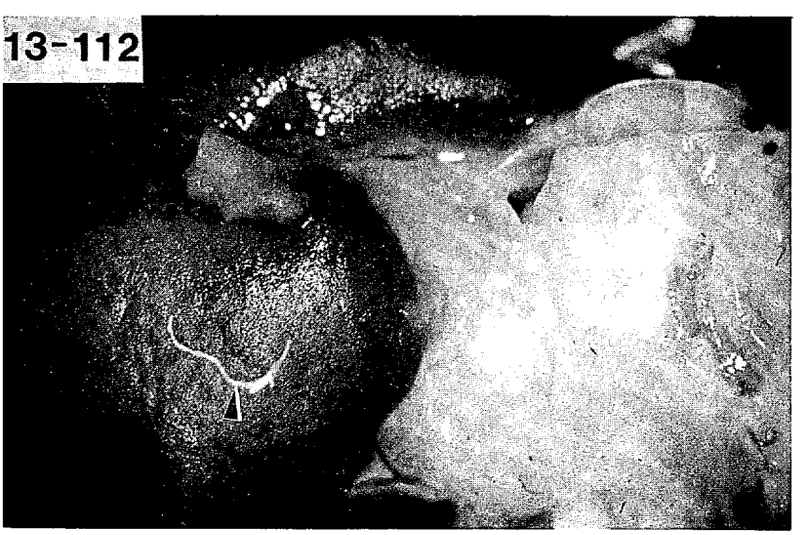
13-112

Figure 13-113. Higher magnification photograph of the subcapsular area of a sectioned cortex from 80B1. Microfil was injected into one of the veins leading from the renicule. Subcapsular veins are demonstrated on the outer surface of the cortex (arrowhead). Deeper veins filled with Microfil can be seen on the cut surface of the cortex (arrows). X20

Figure 13-114. Photograph of a vertical section of a renicule from 80B8. The millimeter scale demonstrates measurement of the longest diameter at the base of renicule. It measures 13 mm.

Figure 13-115. Photograph of a vertical section of a renicule from 80B8. The millimeter scale demonstrates measurement of the shortest diameter of the renicule which extends from the tip of the medulla to the surface of the cortex. It measures 10 mm.

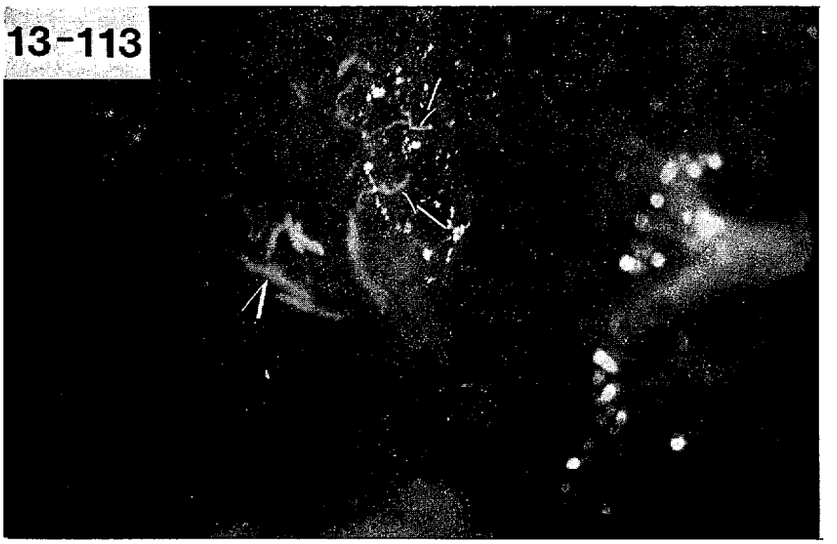
13-113

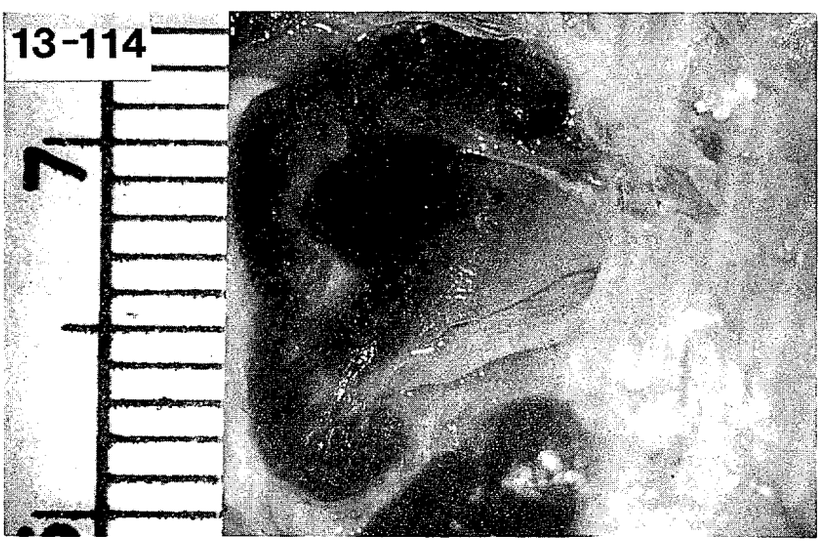
13-114
7

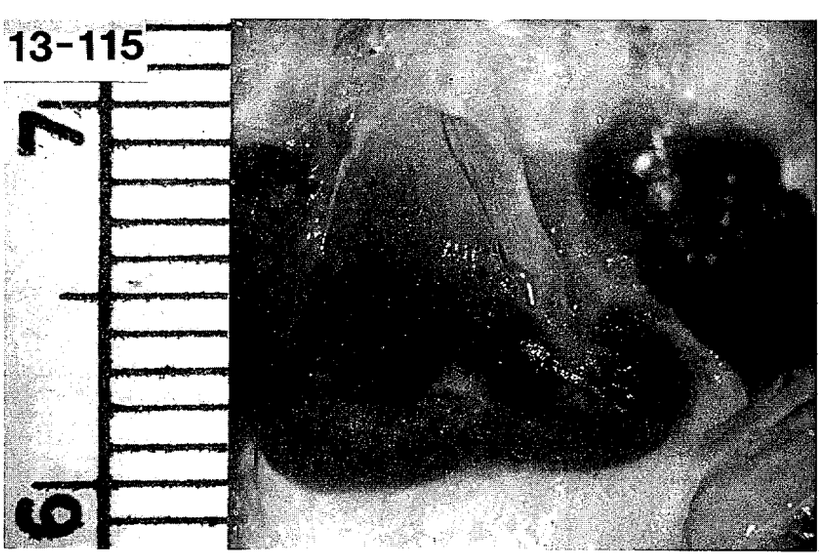
13-115
7
6

Figure 13-116. Photograph of a transverse section of two renicules in a cluster from 79B2. The cortices (C) of the two renicules are fused at this level. The fibrous sporta perimedullaris (Sp) is represented by a white sheet perforated by medullary rays (arrowheads). X7.5

Figure 13-117. Photograph of a latex cast of calyces from the renicule clusters from 79B1. The chalice shape of the calyces (Cl) is well represented. Infundibula (arrowheads) lead into ureteral branches. X15

Figure 13-118. Photograph of a dissection of renicules demonstrates two renal papillae (A) and (B) protruding from two calyces which lead into one common infundibulum (arrows), 79B1. Notice large veins (V) surrounding calyces and infundibulum. Some of the veins' walls are fused with the wall of the calyx (Cl). X4

13-116

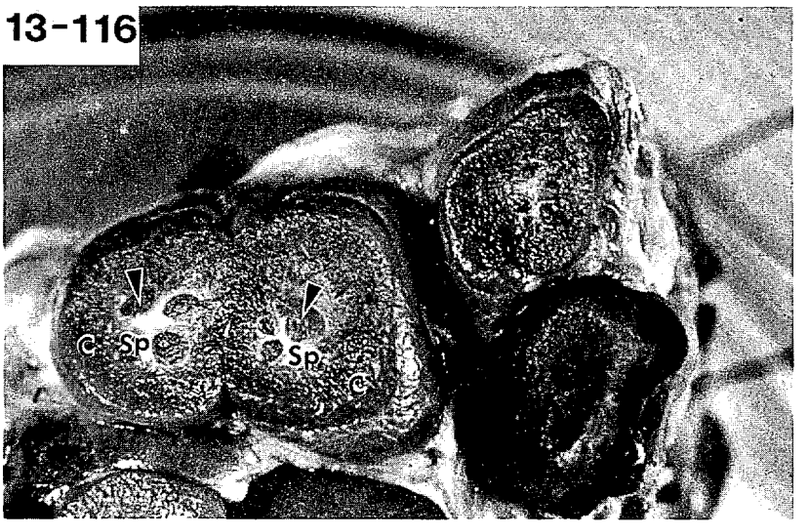

13-117

13-118

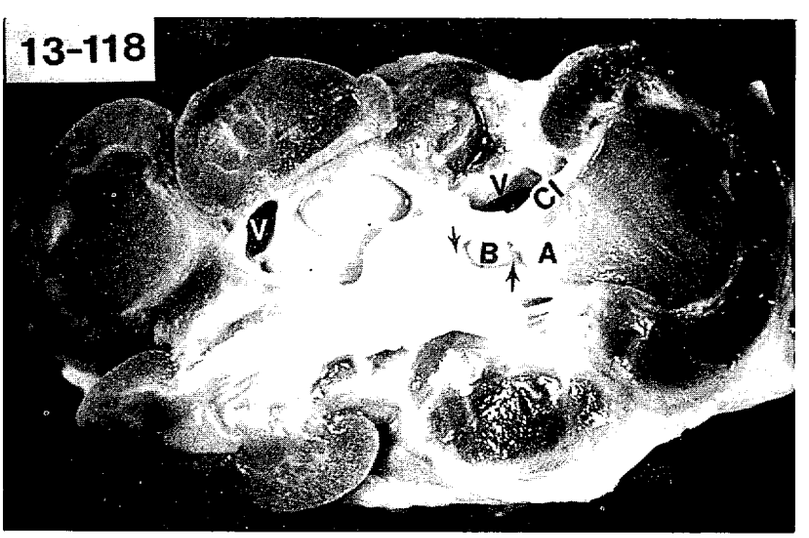

Figure 13-119. Photographs of a renicule isolated and serially sectioned transversely at one millimeter thick slices starting at the surface of the cortex inward toward the medulla, 79B1. X7.5

A. About 0.5 mm of the cortex is sliced away. Increase of connective tissue stroma among cortical parenchyma is evidenced by increase of pale whitish tissue (Ct). Medullary rays are also evident as small rounded areas (arrowheads) that penetrate through the connective tissue st roma.

B. One millimeter deep into the cortex, the connective tissue (Ct) becomes more dense with more obvious medul lary rays (arrowheads).

C. About two millimeters deep into the cortex, a definite sheet of connective tissue (Ct) is formed with larger medullary rays penetrating it. This is definitely part of the sporta perimedullaris. At this level or at the above levels there is no evidence of arcuate vessels.

D. At the corticomedullary junction, the sporta (Sp) is broken down into an interrupted line of connective tissue with medullary tissue in between. Arcuate vessels are shown embedded in the tissue of the sporta (arrowheads).

E. Deepest layer of the sporta (Sp) bordering on the medulla (M). Cortical tissue (C) at this level represents the lateral extension of the cortex down onto the outer surface of the medulla. The arcuate vessels (arrowheads) are definitely in the deepest layer of the sports.

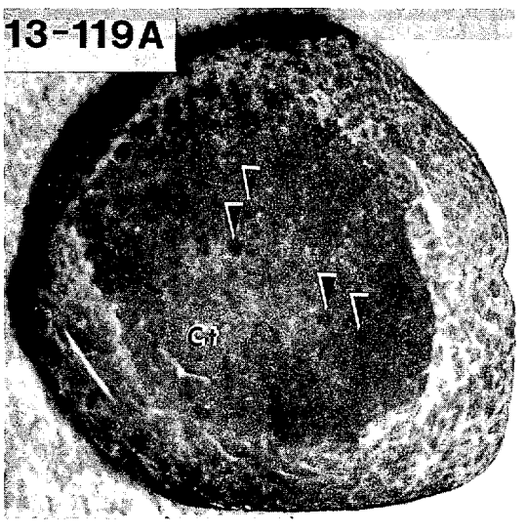
13-119A
Ct

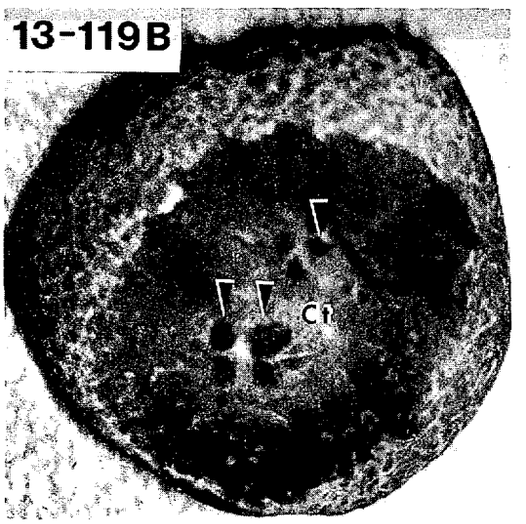
13-119B
Ct

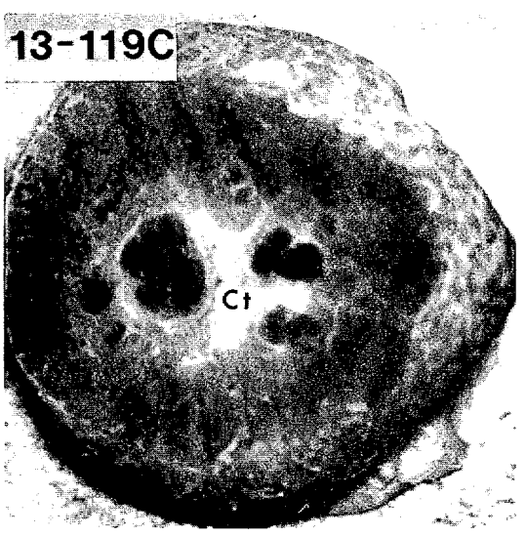
13-119C
Ct

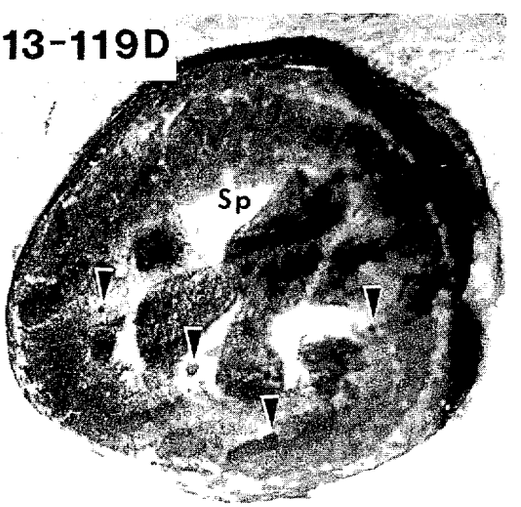
13-119D
Sp

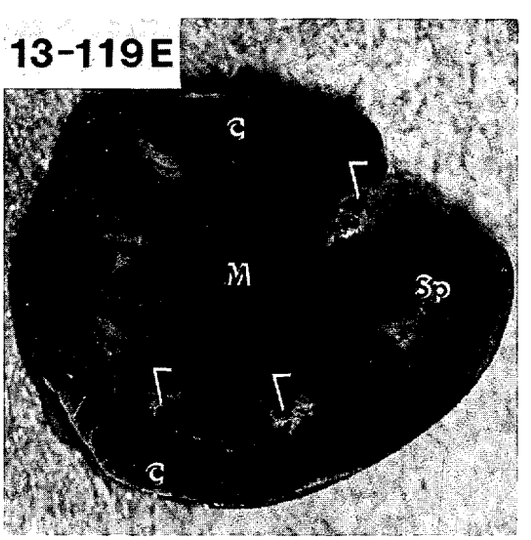
13-119E
C
M
Sp
C

Figure 13-120. Photomicrograph of a parasagittal section of a renicule, 79B1. Cortex (C) is on top of a part of medulla (M) and the renal papilla (P) is surrounded by the calyx (Cl). The calyx wall in the top part of the field joins the wall of another calyx. The other side of the calyx shares the wall of large lumen veins (V). An artery (A) enters the renicule at the corticomedullary junction. The sporta perimedullaris (Sp) is broken into five segments separated by medullary rays. L.S., Verhoeff stain. X7.5

Figure 13-121. Photomicrograph of the renicular cortex, 79B1. Three renal corpuscles (Rc) are clustered together in midcortex. PAS reaction stains the basal lamina around tubules. The proximal convoluted tubule (Pt) epitheliums is not well preserved. Distal convoluted tubules (Dt) have wider lumina. A medullary ray (Mr) made of ascending and descending thick parts of Henle's loops is well demonstrated. L.S., PAS stain, X300

Figure 13-122. Photomicrograph of a semi-thin section of renicule cortex, 80131. A renal corpuscle demonstrates Bowman's capsule (Be) lined with parietal simple squamous epithelial cells. Urinary space (Us) surrounds the glomerulus. Podocytes (arrows) representing the visceral layer of Bowman's capsule are next to glomerular capillaries. Mesangial cells (M) have lighter staining cytoplasm and roundish nuclei. Epon, X.S., Azure blue-methylene blue stain, X300

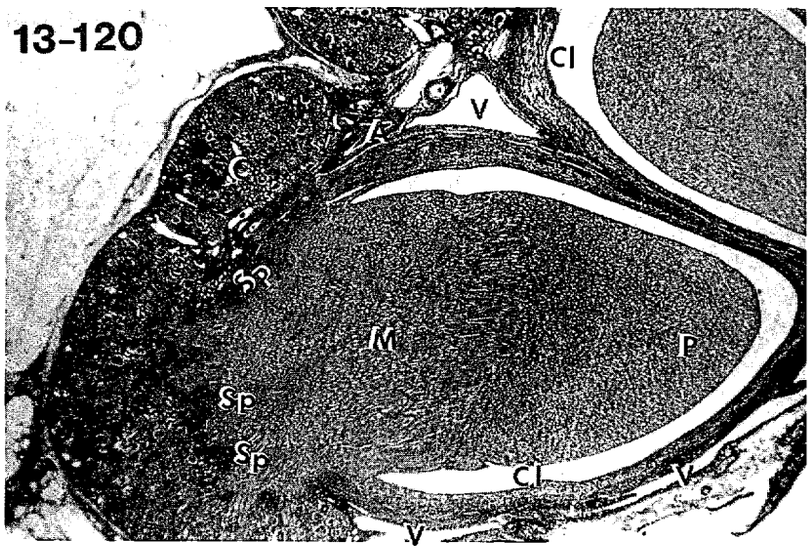
13-120
Cl
V
C
M
P
Sp
Sp
Cl
V
V

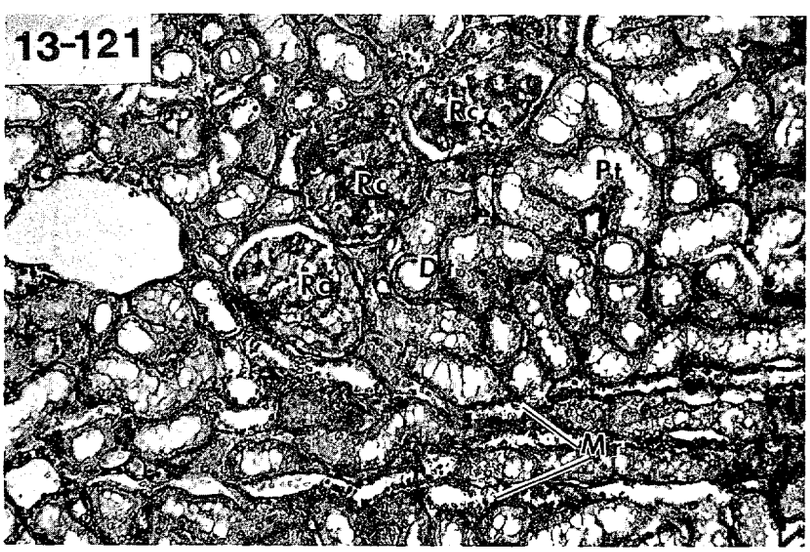
13-121
Rc
Rc
Pt
Rc
D
Mr

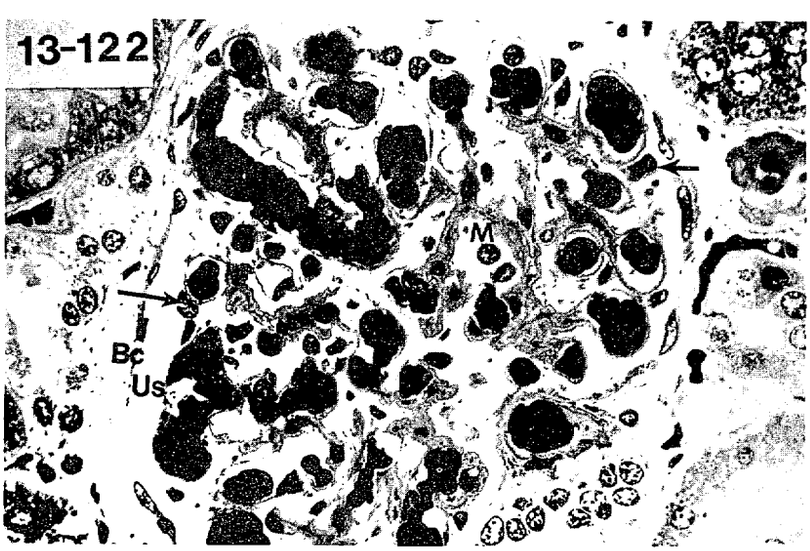
13-122
M
Bc
Us

Figure 13-123. Photomicrograph of a semi-thin section of renicular cortex, 80B1 . An afferent arteriole (As) branches off an interlobular artery (IL). The smooth muscle fibers in the afferent arteriole are optically clear and stouter than those in the wall of the interlobular artery. The lumen of the arteriole is also wide., Proximal convoluted tubules (Pc) (poorly fixed) are lined with darker staining cells as compared with the lighter staining cells lining the distal convoluted tubules (De). Epon, X.S., Azure blue-inethylene blue stain, X470

Figure 13-124. Photomicrograph of a semi-thin section of renicular cortex, 80B1. Two arterioles (A) branch from a common trunk (T). Each arteriole is directed toward a renal corpuscle becoming its afferent arteriole. Arteriolar trunk and branch arterioles have modified muscle cells in their walls. Epon, X.S., Azure blue-methylene blue stain, X470

Figure 13-125. Photomicrograph of a semi-thin section of a renal corpuscle with a complete juxtaglomerular apparatus, 80B1. The afferent arteriole (As) is on the right side of the corpuscle. Its wall is made of modified smooth muscle cells and has a wide lumen as it enters the glomerulus. The efferent arteriole (Es) is on the left side and has regular smooth muscle cel in its walls and a narrower lumen. A polar cushion {Pc) and a macula densa (Md) complete the J.G. apparatus. A mesangial cell is easily seen in the center of the glomerulus (arrow). Epon, X.S., Azure blue-methylene blue stain, X470

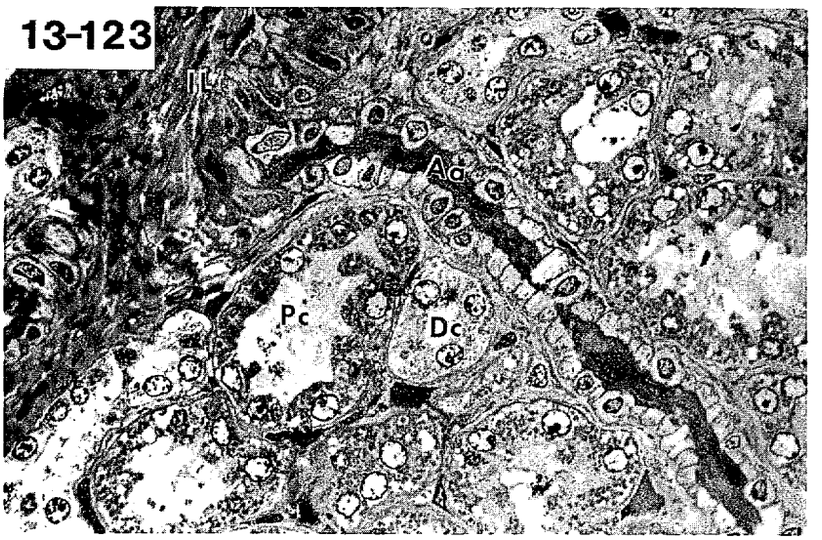
13-123
Ll
Ac
Pc
Dc

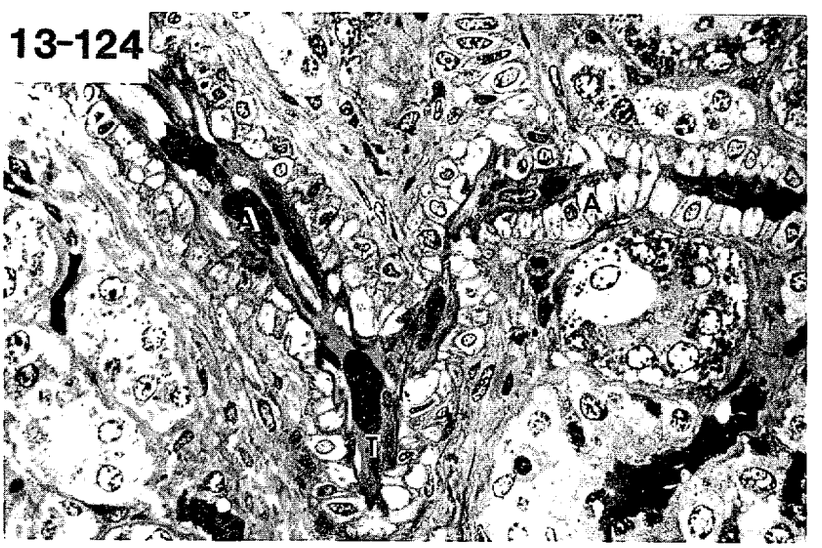
13-124
A
A
T

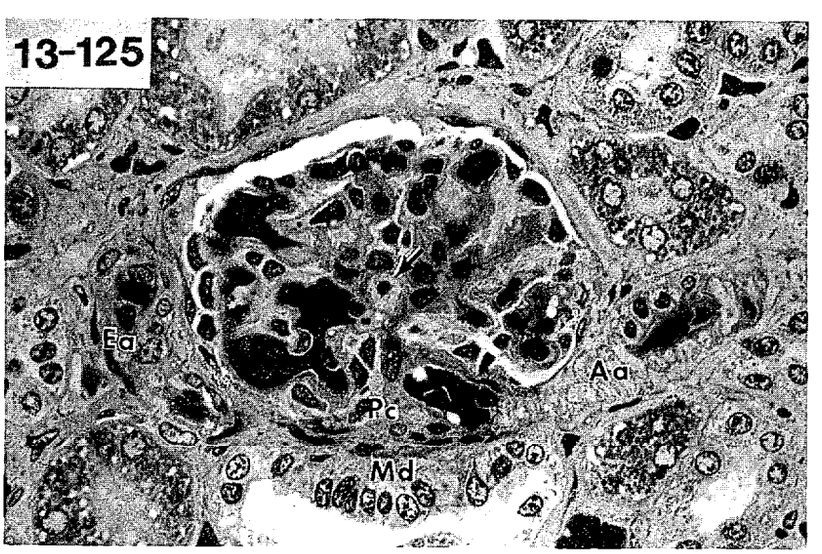
13-125
Ea
Aa
Pc
Md

Figure 13-126. Photomicrograph of a semi-thin section of a renal corpuscle (Rc), 80B1. The macula densa (Md) is the part of the distal convoluted tubule that is in contact with the glomerulus. The nuclei of the lining epitheliums are crowded in this part of the wall of the tubule. Epon, X.S., Azure blue-methylene blue stain, X470

Figure 13-127. Photomicrograph of renicular cortex, 79B1. A renal corpuscle has three glomerular lobules (arrowheads). Part of the capsule of the cortex (Cp) is showing. Smal 1, thin walled tubules (T) are located directly under the capsule and represent connecting tubules that connect distal convoluted tubules to collecting ducts. X.S., PAS, X375

Figure 13-128. Photomicrograph of renicular cortex, 79B1. Renal corpuscles show a thin dark" staining basal lamina (arrowheads) positive for the periodic acid-Schiff reaction. The vascular pole (Vp) and urinary pole (Up) of one corpuscle are demonstrated. x.-s., PAS, x375

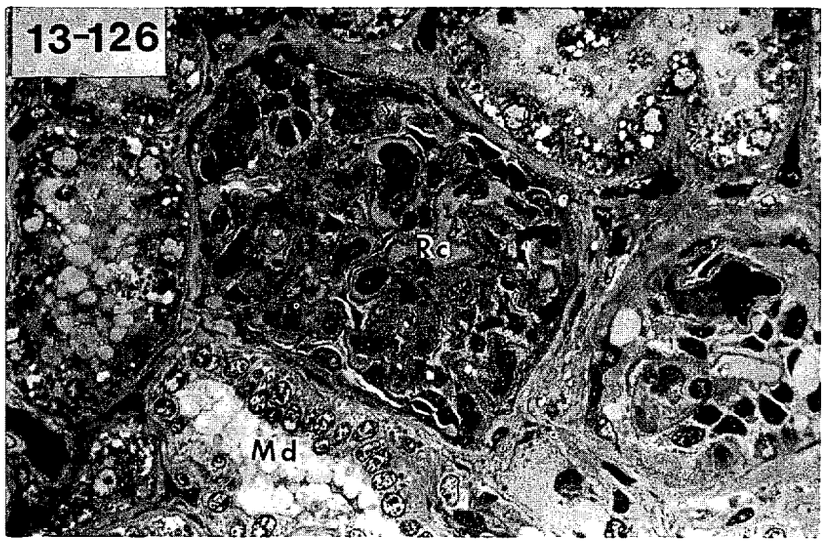
13-126
Rd
Md

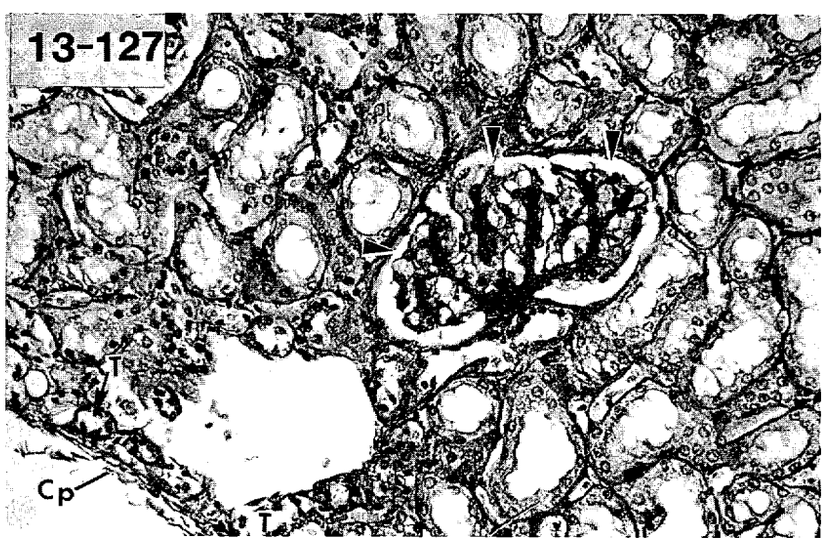
13-127
T
Cp
T

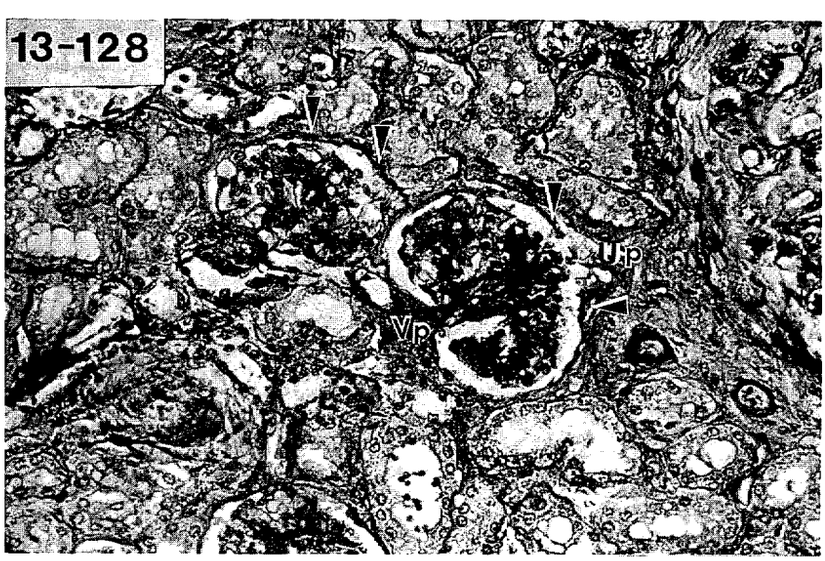
13-128
Up
Vp

Figure 13-129. Transmission electron photomicrograph of a portion of a renal corpuscle, 80B1. Endothelial cells (EC) of capillaries are evident resting on their basal lamina (BL). The foot processes (FP) of podocytes (P) are seen on the opposite surface of the basal lamina. A mesangial cell (M) is seen within the basal lamina surrounding a capillary. Cells of the parietal epitheliums (PE) are seen resting on the basal lamina of the renal corpuscle (BLR). Outside the renal corpuscle a heavy concentration of collagen (C) is seen. X4,400

Figure 13-130. Higher magnification transmission electron photomicrograph of a glomerular capillary and associated podocyte from the renal corpuscle shown in Fig 13-129. A red blood cell (RBC) may be seen closely appressed to the surface of an endothelial cell (EC). The basal lamina (BL) separates the endothelial cell from the foot processes (FP) of a podocyte (P). X30 ,000

13-129
M
EC
BL
EC
FP
P
P
PE
BLR

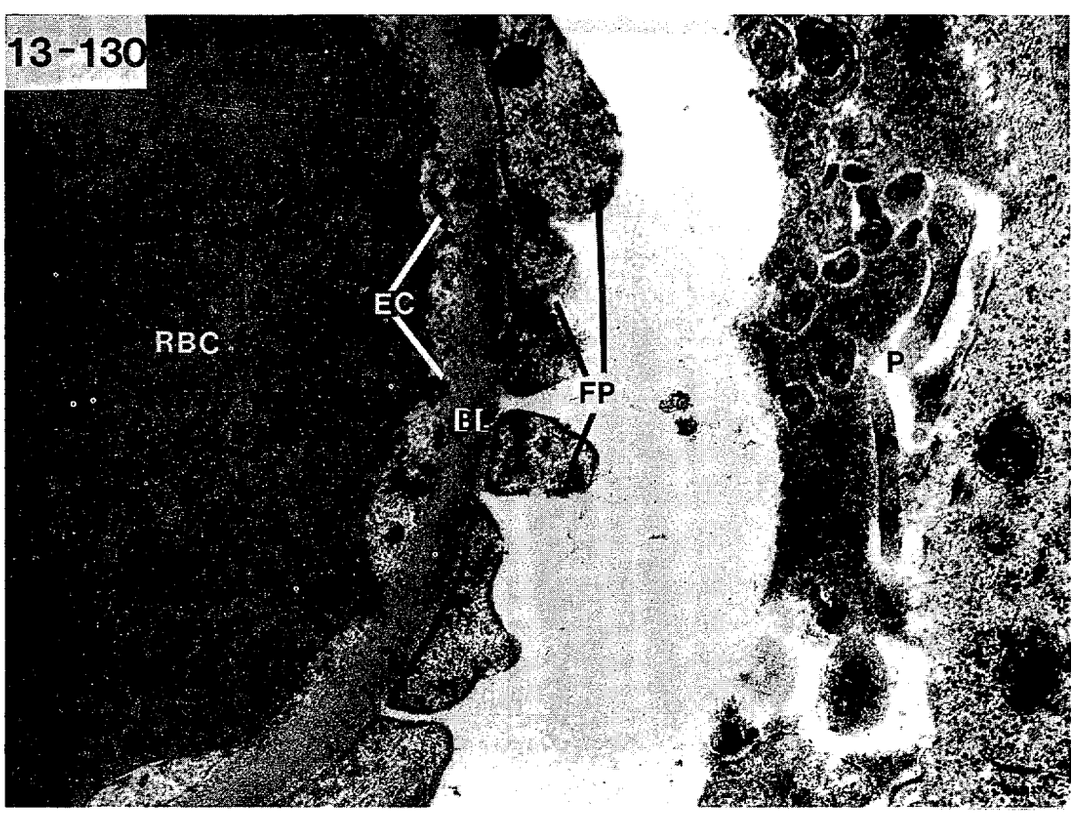
13-130
EC
RBC
FP
BL
P

Figure 13-131. Very high magnification transmission electron photomicrograph of a region of podocyte-basal lamina contact from the renal corpuscle shown in Fig 13-129. Podocyte foot processes (FP) may be seen resting on the basal lamina (BL) of a glomerular capillary. The, foot processes are separated from each other by a filtration slit (FS). No diaphragm across the filtration slit is evident. Mitochondria (M), microfilaments (MF) and a microtubule (MT) are evident in the foot process. X90,900

Figure 13-132. High magnification' transmission electron photomicrograph of a region near the edge of the renal corpuscle seen in Fig 13-129. The basal lamina of the renal corpuscle (BLR) is evident as is the cytoplasm of a parietal cell (PC) on the interior of the corpuscle. Concentrations of collagen (C) may be seen exterior to the BLR. A fibroblast (F) is also evident. X36 ,000

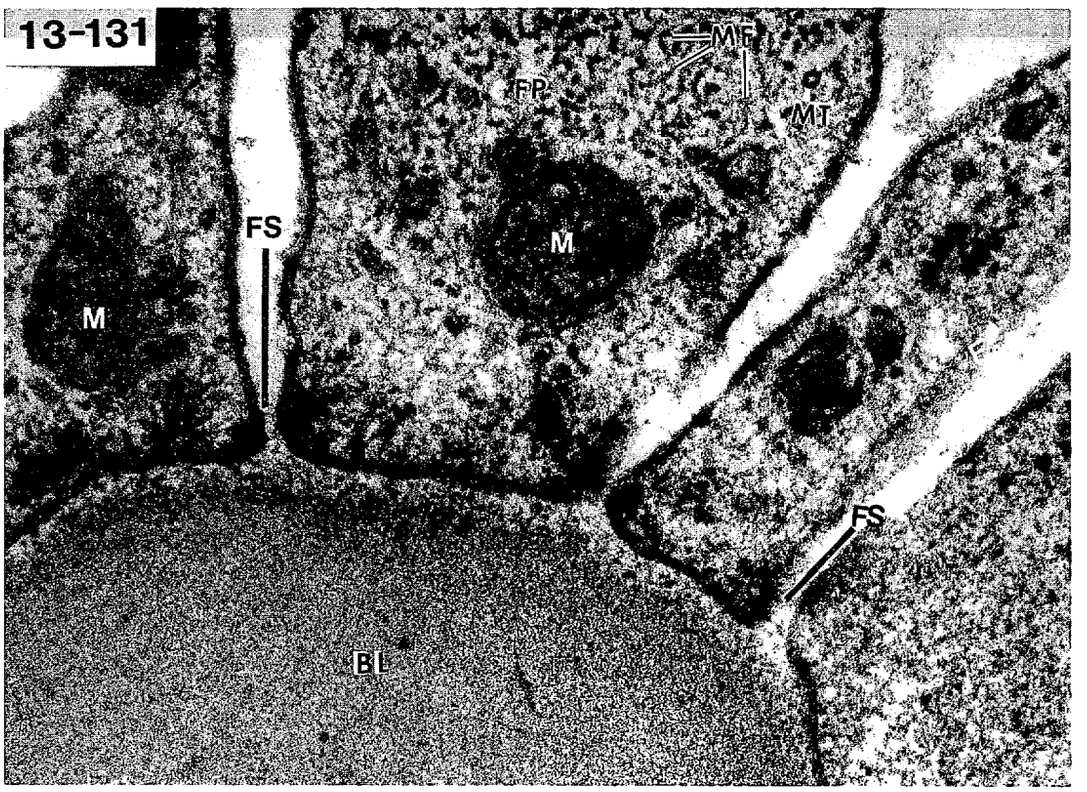
13-131
MF
FP
MT
FS
M
M
FS
BL

13-132
C
C
F
BLR
PC

Figure 13-133. Transmission electron photomicrograph of a typical renal tubule taken from a kidney of 80B1. The basal lamina (BL), mitochondria (M) and nuclei (N) are visible but preservation is poor. X4,600

Figure 13-134. Higher magnification electron photomicrograph of the edge of the tubule shown in Fig 13-133. The fibrous structure of the basal lamina (BL) is evident but cytoplasmic constituents other than mitochondria (M) are not discernible. X36,600

13-133
BL
N
M
N
BL
N

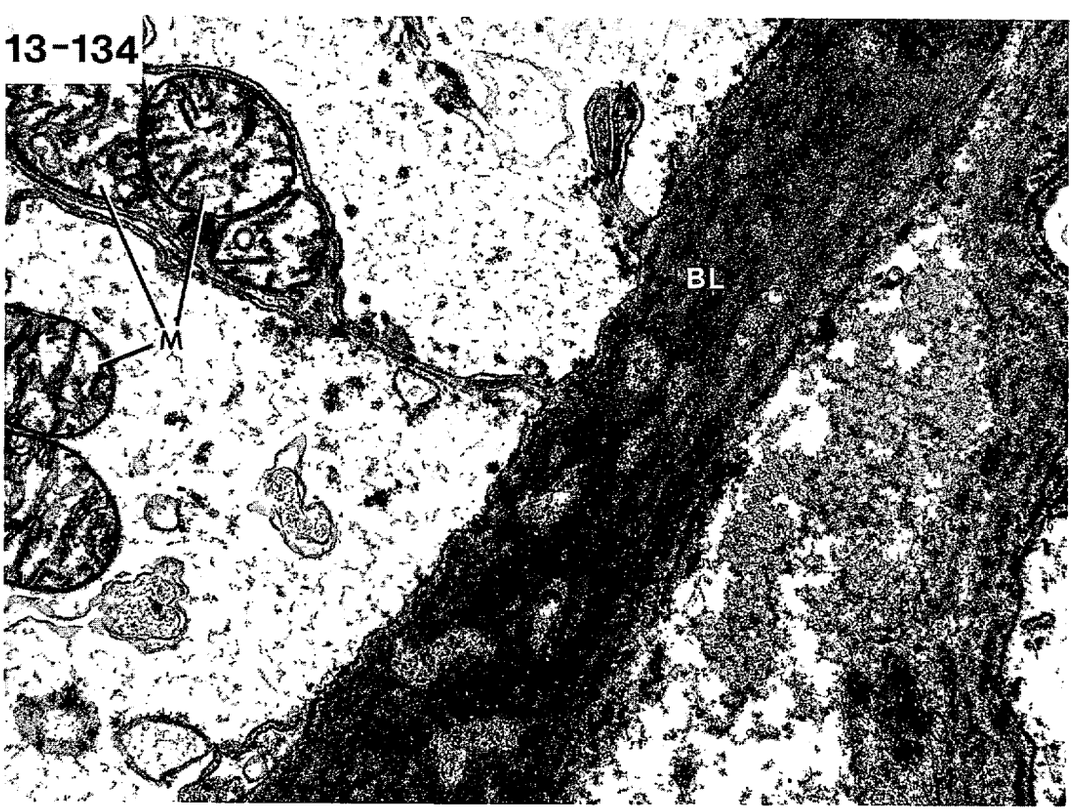
13-134
M
BL

Figure 13-135. Photomicrograph of the cortices of two renicules, 79B1. Cortical veins are very wel 1 demonstrated (SCV and ILV). The flow of venous return from the cortex to the corticomedullary junction and then outside the renicule can be followed in the left renicule. Subcapsular veins (ScV) continue as a straight interlobular vein (ILV) across the cortex to larger veins at corticomedullary junction (CmV), to the renicular vein (Rv) between renicules. X.S., Verhoeff stain, X9

Figure 13-136. Photomicrograph of a renal corpuscle, tubules and connective tissue stroma, 80B1. The stroma (Ct) is most abundant around the corpuscle. This is typical of the bowhead kidney. Epon, X.S., Azure blue-methylene blue stain, X470

Figure 13-137. Photomicrograph of the sporta perimedullaris (Sp) at lower magnification, 80B1. The tissues were stained with Milligan's trichrome technique which stains white fibrous connective" tissue green and smooth muscle fibers purplish red. In this photograph the smooth muscle fibers in the arterial wall (A) are dark while the connective tisssue sporta is lighter in color. There is no evidence of smooth muscle fibers in the sporta in this preparation or from other samples. Cortical tubules (T) indicate that the sporta extends into the cortex and is not limited to the corticomedullary junction. L.S., Milligan's stain, X19

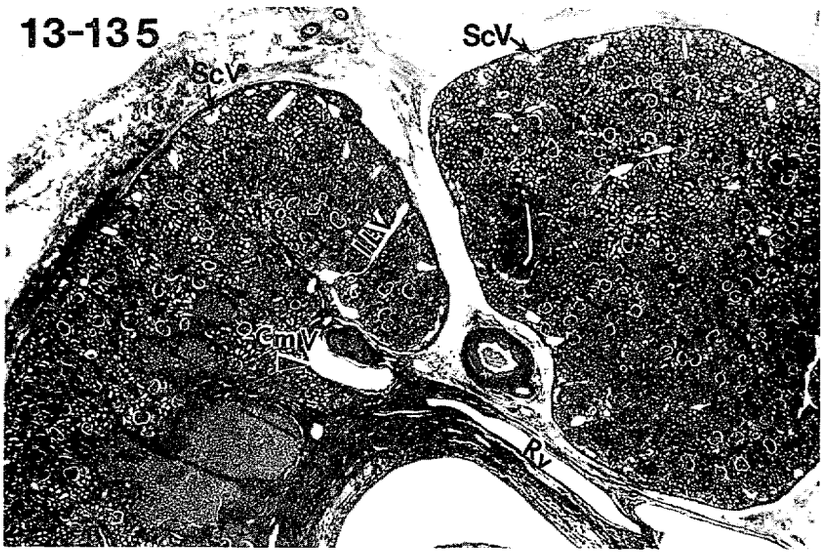
13-135
ScV
ScV
CmV
Rv

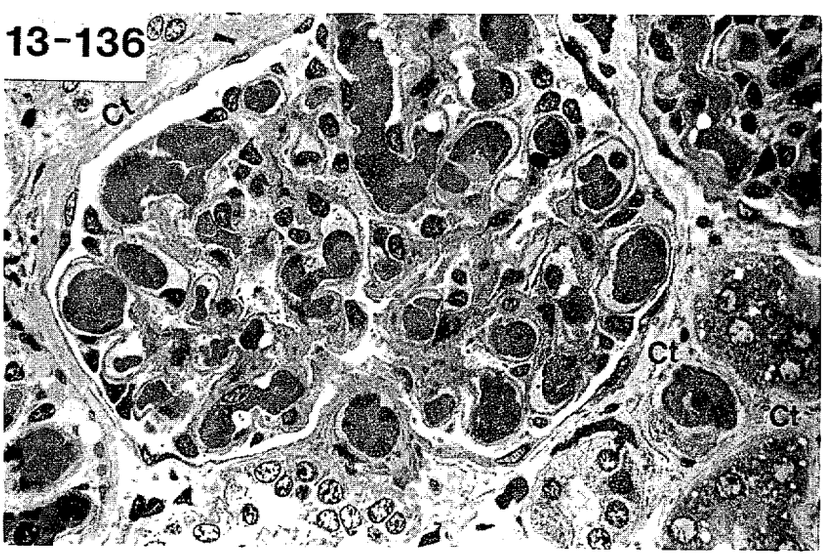
13-136
Ct
Ct
Ct

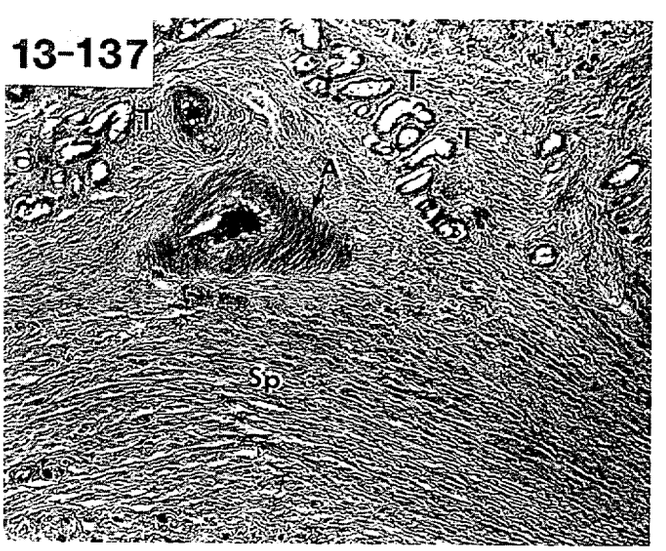
13-137
T
T
T
A
Sp

Figure 13-138. High magnification photomicrograph of tissue of the sporta perimedullaris, 79B1. The sporta is composed of dense white fibrous connective tissue with collagenous fibers (Cf) irregularly arranged, elastic fibers (not obvious with this staining technique) and connective tissue cel 1s (mainly fibroblasts) whose nuclei only are showing (arrows). There are no smooth muscle fibers. If there were any, they would have stained darker and their nuclei would be larger and with more open chromatin than those of the fibroblasts. A lymphatic vessel (Lv) crosses through the tissue. L. S., Masson's stain, X375

Figure 13-139. Photomicrograph of sections of two renicules to demonstrate the continuation between calyx wall (Clw) and the sporta perimedullaris (Sp), 79B1. Arteries (A) enter and veins (V) leave the renicule at the level of the sporta. This photomicrograph demonstrates the presence of large vessels (arcuate in the sporta). L.S., Verhoeff's stain, X30

Figure 13-140. Photomicrograph of a semi-thin longitudinal section of outer medulla (medullary rays), 79B2. It demonstrates descending thick segment (Dt), ascending thick segment (At), thin segment of Henle's loop (Tht), collecting ducts (Cd), arterial vasa rectae (Avr) and venous vasa rectae (filled with dark staining red blood corpuscles) (Vvr). Epon, L.S.. Azure blue-methylene blue stain, X300

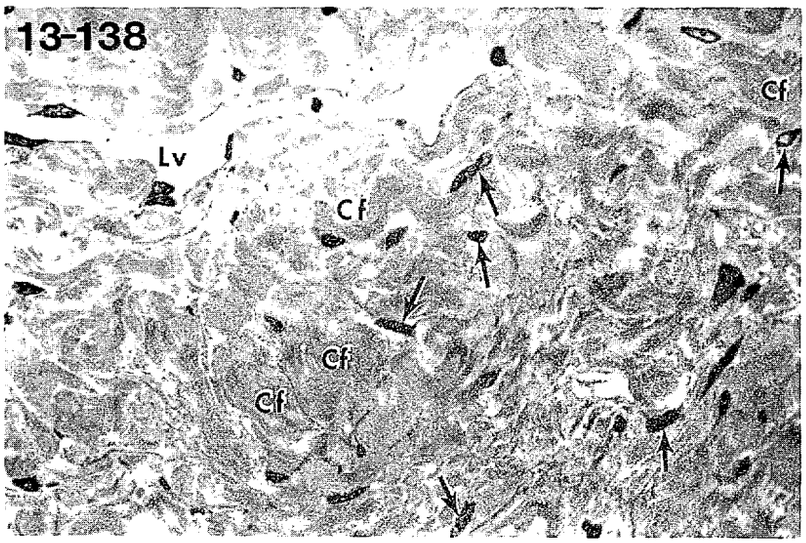
13-138
Lv
Cf
Cf
Cf
Cf

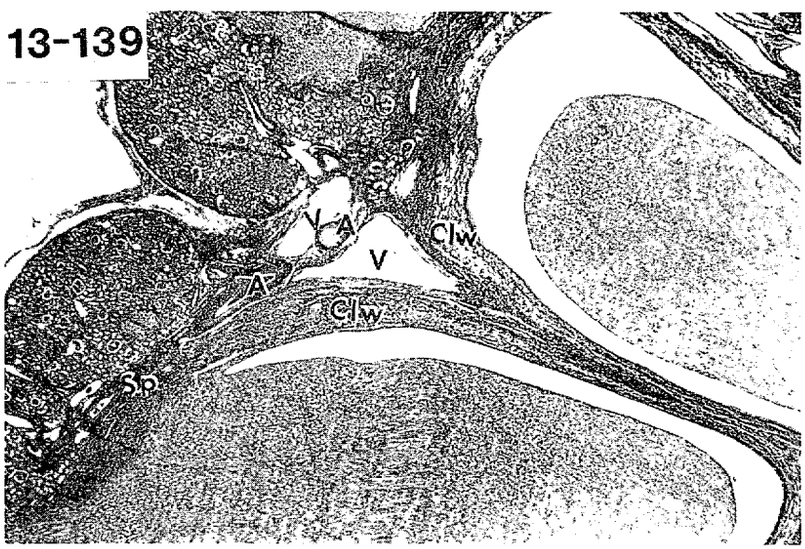
13-139
Cf
V
A
V
Clw
A
Clw
Sp

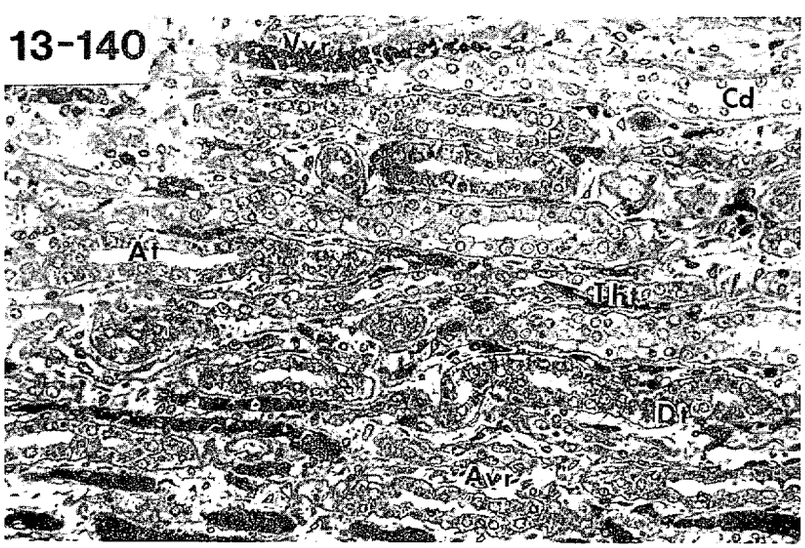
13-140
Vvr
Cd
Af
Ilt
Dr
Avr

Figure 13-141. Photomicrograph of a semi-thin transverse section of outer medulla (medullary rays), 79B2. It demonstrates descending thick segment (Dt), ascending thick segment (At), thin segment of Henle's loop (Tht), arterial vasa rectae (Avr) and venous vasa rectae (Vvr). X.S., Azure blue-methylene blue stain, X300

Figure 13-142. Photomicrograph of a renicular renal papilla, 79B2. It mainly consists of cross sections of collecting ducts (Cd) and thin segments of Henle's loop (Tht). It is covered at the calyx (Cl) surface by a low transitional epitheliums (Te). X. S., H and E, X300

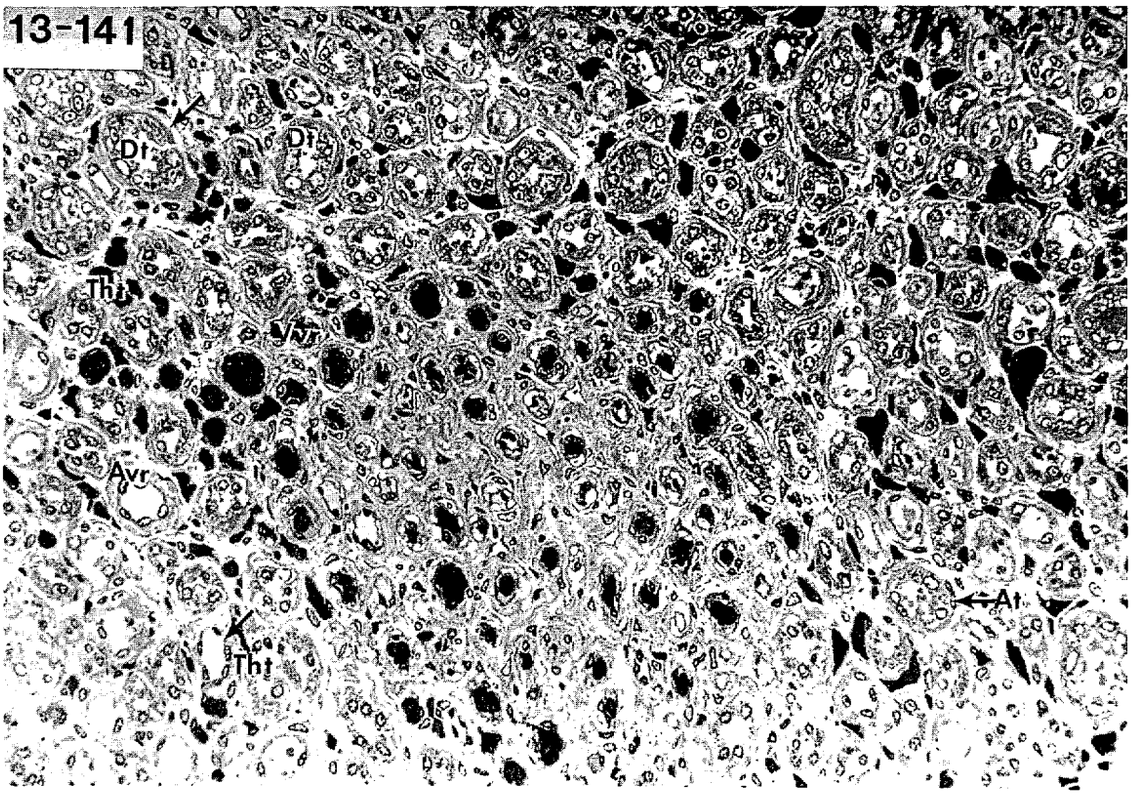
13-141
Dt
Dt
Tht
Vvr
Avr
At
Tht

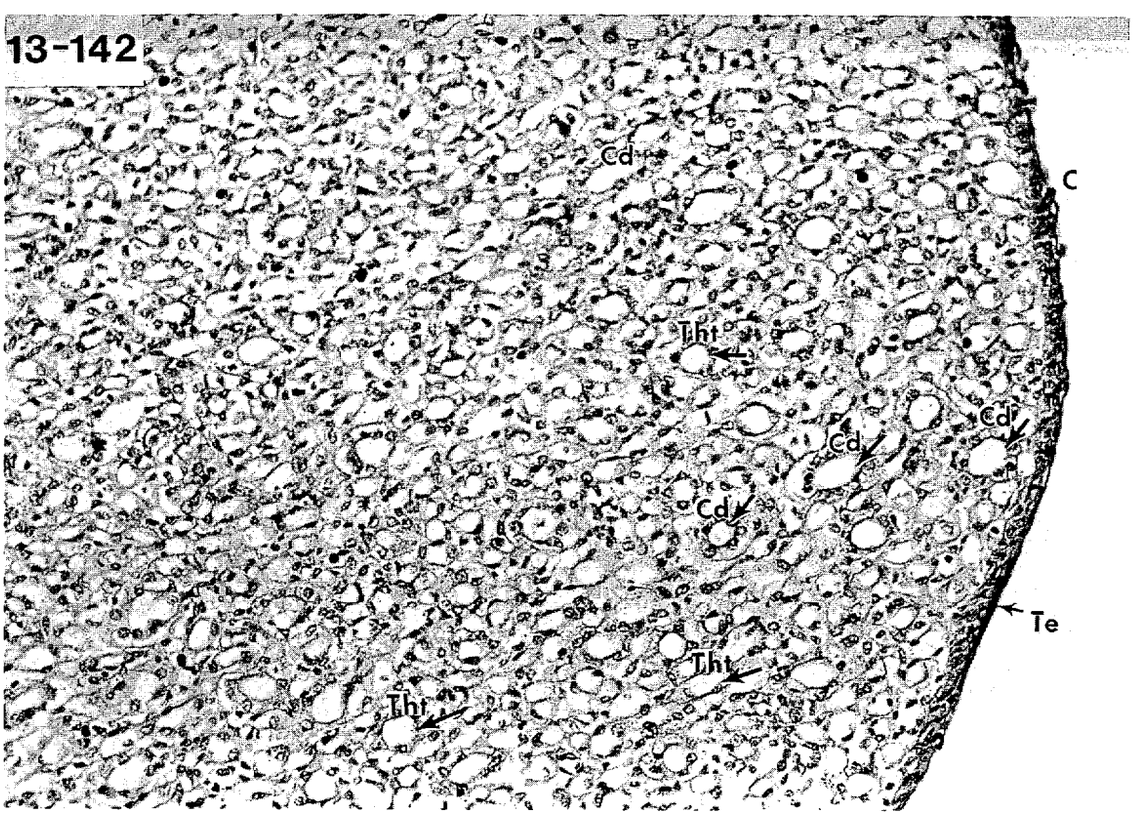
13-142
Cd
C
Tht
Cd
Cd
Cd
Te
Tht
Tht

Figure 13-143. Photomicrograph of a section of two reniculi with fused papillae (P), 80B1. They share a common calyx (Cl) and infundibulum (In). The sporta (Sp) is continuous across the two renicules. L.S., Milligan's stain, X19

Figure 13-144. Photomicrograph of two renicules with fused cortices (C) but separate renal papillae (P) and calyces (Cl), 80B1. The two calyx walls are fused with the sporta (Sp) which is continuous from one renicule to the other. L.S., Milligan's stain, X19

Figure 13-145. Photomicrograph of two renicules, 79B2. The two calyces (Cl) communicate to empty into the same infundibulum (arrow). Om-outer medulla; P-papilla. Calyx wa"l1s are fused. L.S., H and E, X30

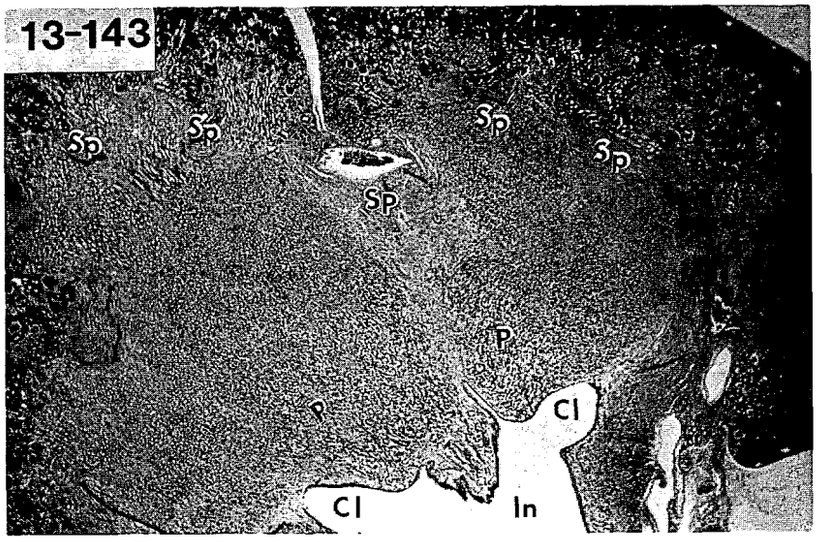
13-143
Sp
Sp
Sp
Sp
Sp
P
P
Cl
Cl
In

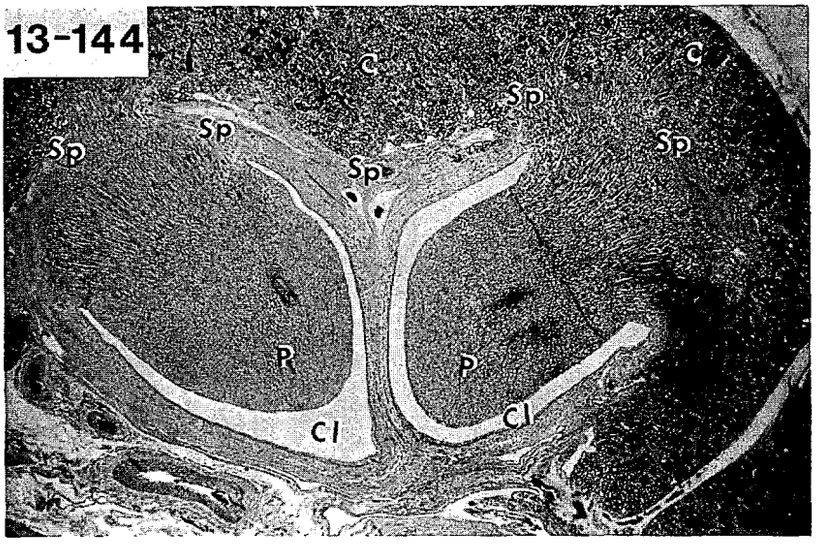
13-144
C
C
Sp
Sp
Sp
Sp
Sp
P
P
Cl
Cl

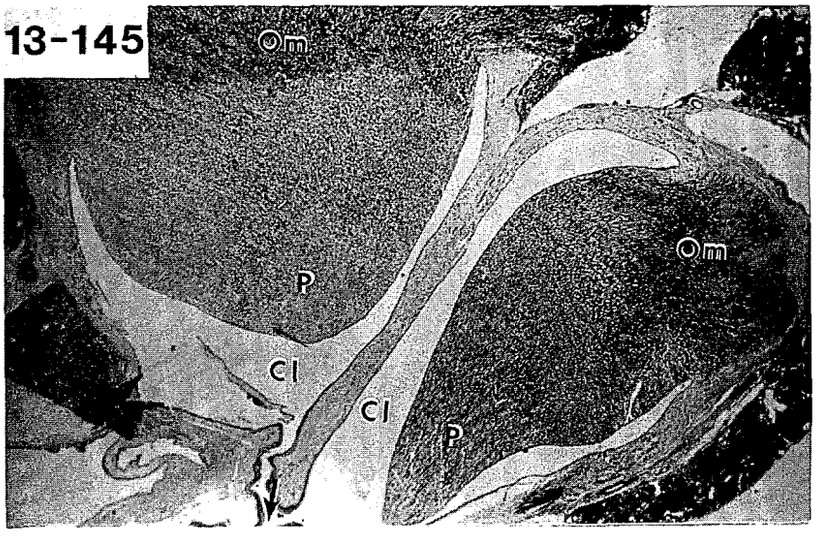
13-145
Om
Om
P
Cl
Cl
P

Figure 13-146. Photomicrograph of a section through part of a calyx wall (Clw) and part of renal papilla (P) with the cavity of the calyx (Cl) separating them, 79B1. The wall of the calyx is composed of dense white fibrous connective tissue. Capillaries (Cap) filled with red blood corpuscles show the vascularity of the tissue. The wall contains no smooth muscle. L.S., H and E, X1000

Figure 13-147-. Higher magnification photomicrograph of structures in Fig 13-146. Transitional epitheliums lining the calyx (Cl) has optically clear ballooned superficial, cells (arrows). The remainder of the calyx wall (Clw) is made of fibrous connective tissue. The papilla (P) consists mainly of collecting ducts (Cd) and thin tubules of Henle's loop (Tht). X1,000

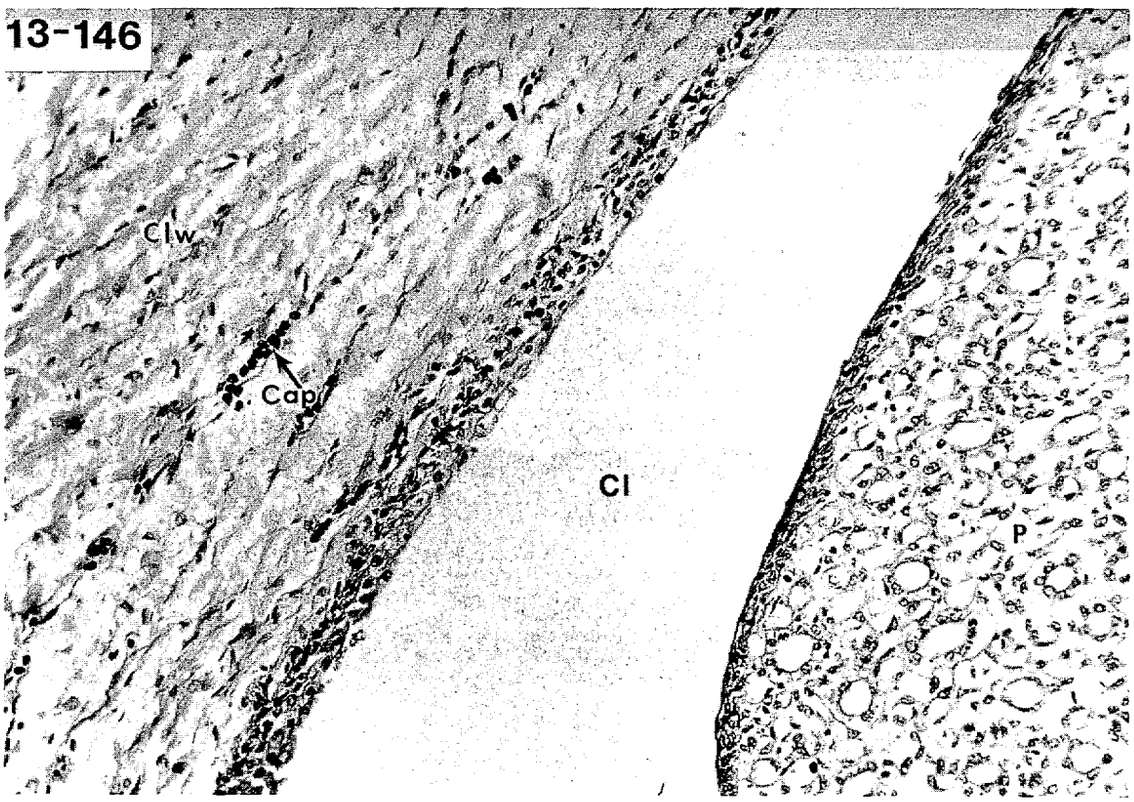
13-146
Clw
Cap
Cl
P

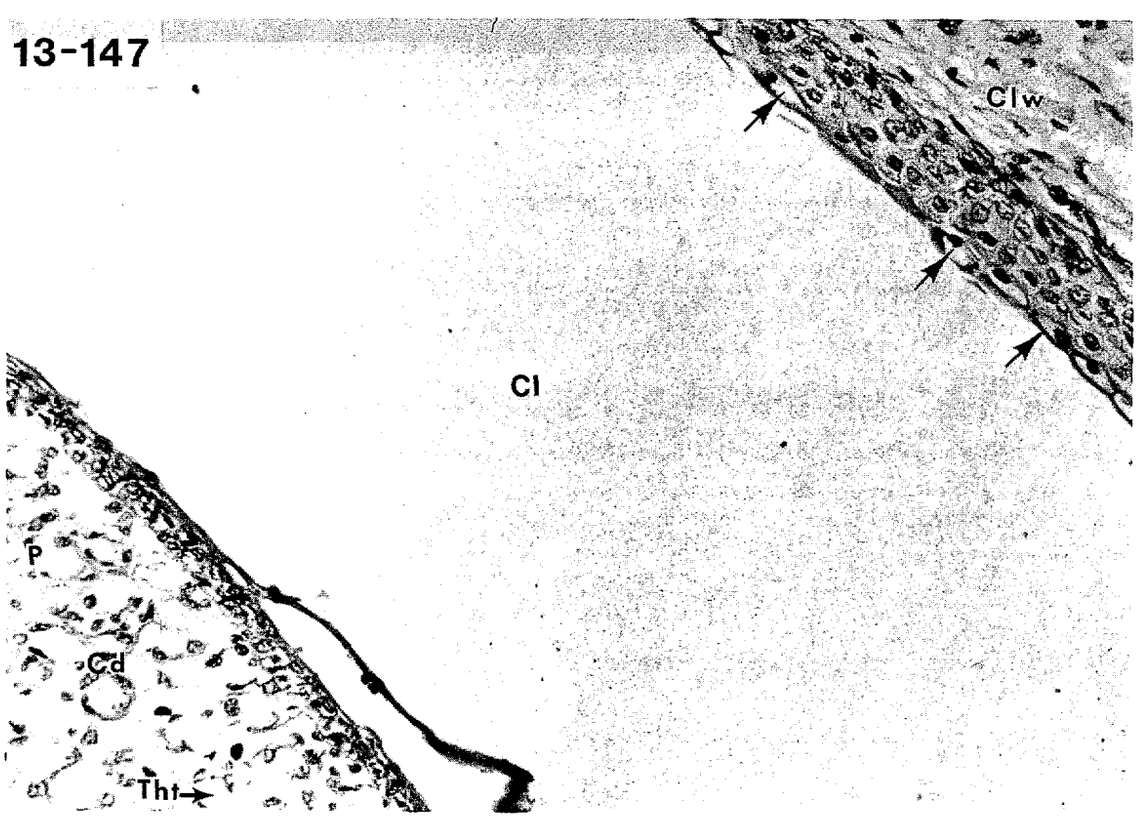
13-147
Clw
Cl
P
Cd
Tht

Figure 13-148. Photomicrograph of a ureteral branch, 79B1. The lining transitional epitheliums (Te), propria-submucosa layer (Ps), and smooth muscle layer (M) form the wall. The tunics adventitia (Ta) blends with the walls of surrounding veins (V). X. S., Verhoeff's stain, X30

Figure 13-149. Photomicrograph of the wall of the urinary bladder, 79B1. The lining epitheliums is of the transitional type (Te). Small and large blood capillaries (Cap) lie next to the basal lamina of the epitheliums. The lamina propria (Lp) is composed of dense white fibrous connective tissue and contains large veins (V). X.S., Verhoeff's stain, X475

Figure 13-150. Photomicrograph demonstrating the same structures described in Fig 13-149, 80B7. Transitional epitheliums (Te), lamina propria (Lp), and blood capillaries (Cap) are labelled. In this photomicrograph lymphatic (L) are shown instead of veins. X.S., Hand E, X475

13-148
V
V
V
Te
Ps
M
Ta
V
V
V

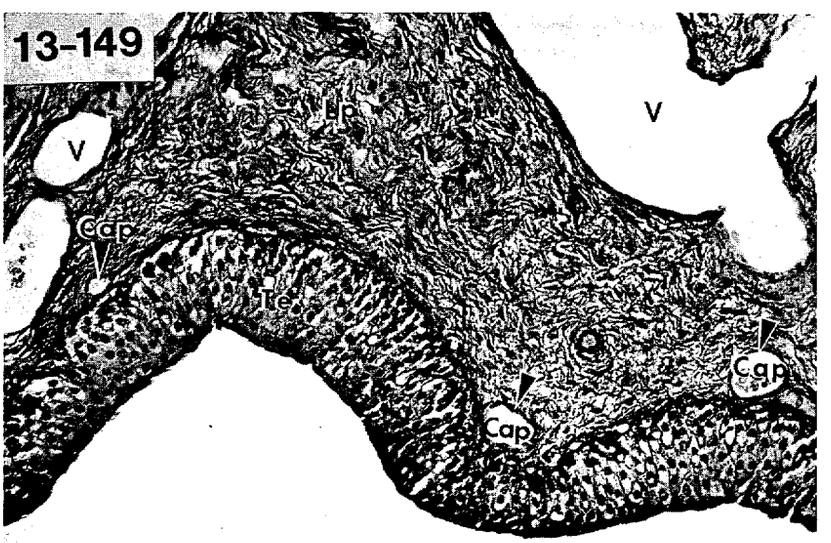
13-149
Lp
V
V
Cap
Te
Cap
Cap

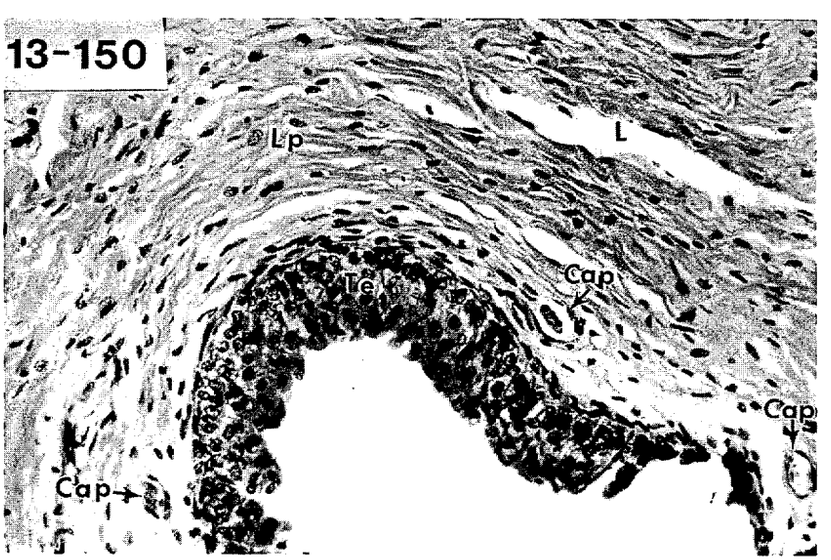
13-150
Lp
L
Te
Cap
Cap
Cap

Figure 13-151. Photomicrograph of a section in the wall of the urinary bladder, 7961. The transitional epithelial lining is missing in the section. The lamina propria (LP) , lamina muscularis mucosae (Mm), tunics submucosa (Sin), veins (V) and beginning of tunics muscularis (Tin) are wel 1 demonstrated. The submucosa consists of a looser connective tissue than that of the lamina propria and is also more vascular. X.S., Verhoeff's stain, X19

Figure 13-152. Photomicrograph of a section through the tunics muscularis (M) of urinary. bladder, 80B7. A nerve fiber bundle (arrows) 1s located between muscle bundles. X.S., H and E, X300

Figure 13-153. Photomicrograph of a section of the tunics muscularis of the wall of the urinary bladder, 8067. An autonomic nerve ganglion is located between muscle bundles (M) . Ganglion cells (arrows) exhibit the typical eccentric location of nuclei. Bundles of nerve fibers (N) are nearby. X.S., H and E, X475

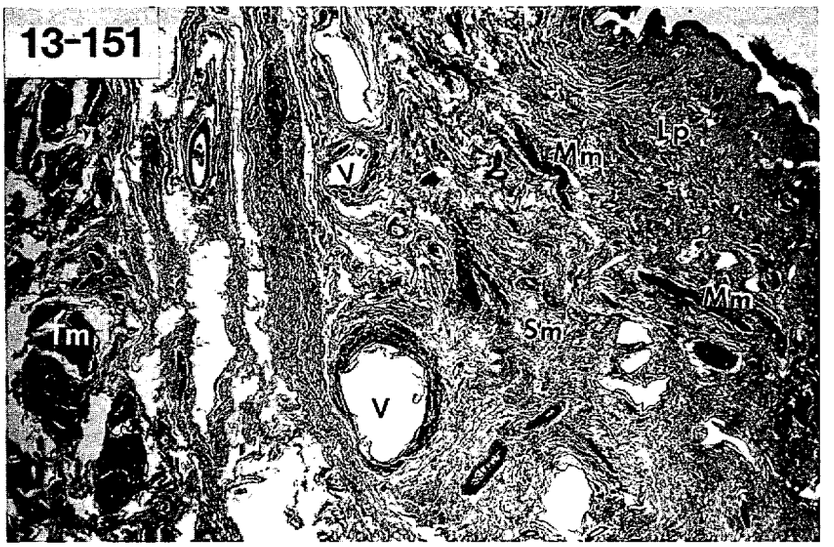
13-151
V
Mm
Lp
Mm
Sm
Tm
V

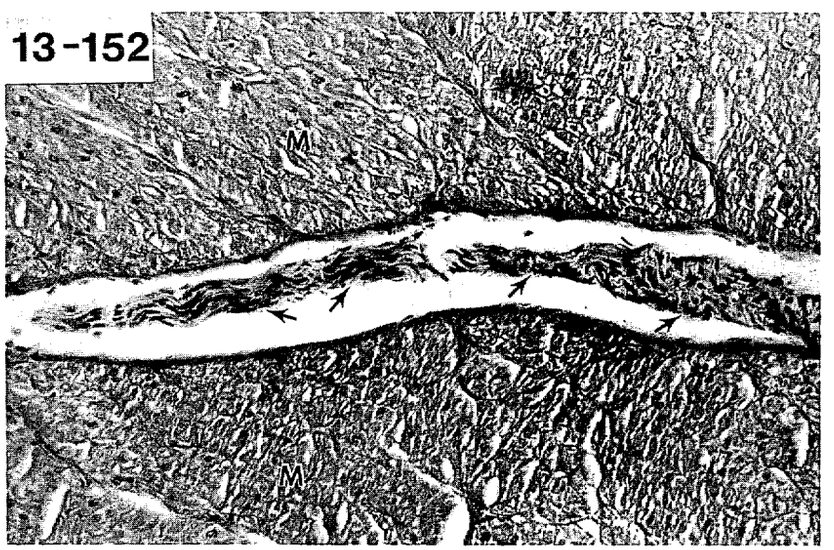
13-152
M
M

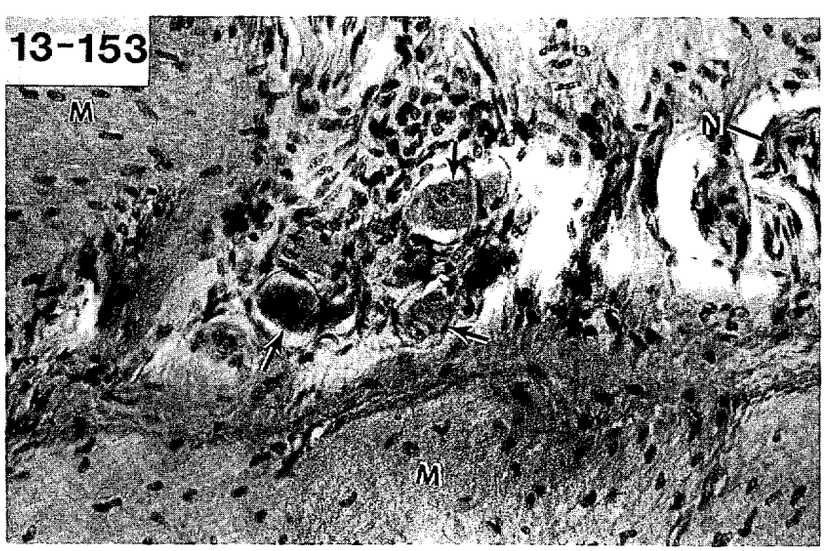
13-153
M
N
M

III. Brain

Cetacean brains retain their embryonic cervical, pontine, and mesencephalic flexures in the definitive state, whereas only the mesencephalic flexure is retained in the human brain, and all three flexures are lost in the course of development in the brains of domestic mammals (McFarland et al 1969, Morgane et al 1980). By means of these flexures, the brain is shortened by a sort of "accordian folding" and is widened laterally so that it presents a globoid appearance. The basal forebrain lies close to the intercrural fossa and the optic tract forms a very acute angle with the crus cerebri. The usual directional terms used for terrestrial mammals hardly apply. The "frontal lobe" is directed more ventrally than rostrally, the "occipital" area is directed more dorsally than caudally, and the temporal pole is directed more ventrally than rostrally. The lateral (Sylvian) fissure is oriented almost vertically (Morgane et al 1972, 1980).

The cerebral hemispheres of the bowhead brain exhibited deep sulci and convoluted gyri as is characteristic of cetacean brains (Figs 13-154, 13-155). Since no intact bowhead brains were received, no attempt was made to identify sulci and gyri either in comparison to those of ungulates and carnivores or according to the scheme of Morgane et al (1980). Ridgway has observed that there are fewer sulci and gyri in the hemispheres of the bowhead brain than in brains of some toothed whales (Appendix IV).

The "rhinic lobe" or rhinencephalon has been defined by Morgane et al (1980) as the portion of the telencephalon limited by the "rhinic cleft." Their rhinic cleft is a continuous sulcus made up by the rostral (anterior), and caudal (posterior) rhinal sulci, rhinohippocampal sulcus, hippocampal sulcus, the sulcus of the corpus callosum, and the caudal (posterior) parolfactory sulcus. The rhinic lobe is described as consisting of archicortical and paleocortical parts which meet in the median plane through the septal area and bilaterally through the unci.

The paleocortex (olfactory) is separated from the neocortex by the rhinal sulcus. Olfactory peduncles and olfactory bulbs have been described on brains from other mysticete whales, but none were observed on the bowhead brains examined, probably because of the method of removal. The lateral olfactory gyrus, which lies just medial to the rhinal sulcus on some cetacean brains, was not identified on the bowhead brains. The most prominent feature of the bowhead paleocortex was the olfactory tubercle (Fig 13-156). This region overlies the head of the caudate nucleus (Breathnach 1955). Caudal and

medial to the olfactory tubercle is the diagonal area which extends from the septum to the periamygdalar area. Its caudolateral part is perforated by blood vessels. The uncus, consisting of the gyrus semilunaris medially and the gyrus ambiens laterally, lies medial to the temporal pole (parahippocampal gyrus) separated from the latter by the caudal rhinal sulcus. The rostral part of the uncus is the periamygdalar area and is essentially identical with the corticomedial complex of the amygdalar nuclei (Morgane et al 1972). The stria terminals, which arises from the amygdaloid nuclei, could be easily identified medial to the caudate nucleus (Figs 13-158, 13-160, 13-166).

The archicortex (hippocampal formation) began as the subcallosal gyrus under the rostrum and genu of the corpus callosum in the septal area (Fig 13-162). It continued dorsal to the corpus callosum, limited laterally by the sulcus of the corpus callosum, as the indusium griseum (Figs 13-162, 13-158) and around the splenium of the corpus callosum as the fasciola cinerea. At this point began the hippocampus major (or proper). Part of the temporal lobe was missing on the brain of 80B1, so its full extent was not observed (Fig 13-158). The temporal part of the hippocampus did protrude into the temporal horn of the lateral ventricle in the bowhead brain (Fig 13-165). Note in this figure that there is no occipital horn of the lateral ventricle.

The septum lay between the rostral horns of the lateral ventricles below the rostrum of the corpus callosum. Caudally it was traversed by the rostral commissure, which is characteristically small in cetaceans. It was separated from the neocortical parolfactory area (of Broca) by the caudal parolfactory and rostral rhinal sulci. It can be seen in Fig 13-162.

Several of the basal nuclei were identified on the bowhead bra ins. The caudate nucleus can be seen in Figs 13-158, 13-160, 13-164. The putamen is also seen in Figs 13-164 and 13-166. The claustrum is seen between the external and extreme capsules in Fig 13-166.

The caudolateral part of the thalamus was very well developed. The medial geniculate body was very large compared to domestic terrestrial mammals, but not necessarily so for cetaceans (Figs 13-156, 13-158). The lateral geniculate body could be identified easily but was not large compared to the medial geniculate body. The stria habenularis was easily identified but the habenula was not easily seen grossly (Fig 13-160). The pineal body was not seen and may not have been present. The interthalamic adhesion (massa intermedia) was not present in the bowhead thalamus. The rostral thalamic tubercle was recognizable, but was not prominent (Figs 13-166, 13-161).

The hypothalamus in cetacean brains is short rostrocaudally and deep dorsoventrally. The mammillary bodies are usually not readily identifiable grossly, and this was true of the bowhead. Most of the hypothalamus remained with the meninges when they were separated from the brain of 80B1 prior to its arrival at our lab. The optic chiasm and proximal parts of the optic tracts can be seen in Figs 13-167 and 13-168.

In many cetaceans, the adenohypophysis and neurohypophysis are not closely associated distally. This must be true of the bowhead, because the neurohypophysis came out with the meninges of 80B1 and can be seen in Figs 13-169 and 13-170, but the adenohypophysis apparently remained in the dura mater in the skull. See RU 580 also.

One of the most remarkable features of the brain of cetaceans is the great size of the cerebellum, particularly the paraflocculus. The ratio of the cerebella weight to the total brain weight for the bowhead brain is at the upper end of the range given for cetacean brains (Ridgway, Appendix IV). To a veterinary anatomist, the cerebellum of the bowhead brain is comparable to the cerebellum of domestic terrestrial mammals and has been labeled accordingly in this report. This does not coincide with the designations "given by Jansen (1950) for the cerebellum of the fin whale (Balaenoptera rostratus) and the bottle nose whale (Hyperoodon rostratus). Most authors describing the cerebellum of cetacean brains have followed the format used by Jansen in '1950. The cerebellum of the bowhead whale is shown in the accompanying figures. One could substitute the labels most frequently used for cetaceans if preferred.

Like the rest of the brain, the cerebellum was very fragile. The only picture that shows it completely intact is Fig 13-167, which was taken before the leptomeninges were removed. The nomenclature for the mammalian cerebella vermis and hemispheres was established by Larsen (1970). The numbered hemispheric lobules are continuous with like-numbered vermal lobules. However, in these bowhead specimens the connections which were deep within sulci could not be investigated in detail because of the fragility of the brains, so the designations given the hemispheric lobules were based only on their appearance.

The cerebellum is shown from the dorsal aspect in Figs 13-171 and 13-172. The primary fissure is relatively far forward, so most of the cerebellum is the caudal lobe, as is true for other cetaceans. The culmen of the rostral lobe is rostral to the primary fissure. The lobulus simplex and declive are limited by the primary fissure rostrally and the posterior super-

ior or preansiform fissure caudally. The large region of the cerebellum limited rostrally by the posterior superior or preansiform fissure, laterally by the parafloccular fissure, and caudally by the ansoparamedian fissure is the ansiform lobule. The ansoparamedian fissure appears as a dark line in Fig 13-167, where the meninges extend down into it, and as a wide cleft in Fig 13-172. Most authors describing the cerebellum of cetaceans have designated only the oval-shaped rostral portion of this area as the ansiform lobule and the remainder as the paramedian lobule even though it is not near the median plane. The vermis separated where the ansoparamedian fissure crosses it. The vermal portion between this fissure and the posterior superior fissure is thought to be the folium vermis, which is supposed to be continuous with the ansiform lobule.

The prominent lobule caudal to the ansoparamedian fissure is the paramedian lobule. These lobules resemble the paramedian lobules of domestic terrestrial mammals and lie on either side of the median plane next to the vermis. The paramedian lobules are supposed to be attached to the tuber vermis and the rostral part of the pyramis, but this could not be confirmed on these specimens.

The ventral part of the hemisphere of the caudal lobe of the cerebellum consists of the dorsal and ventral parafloccular lobules. The dorsal paraflocculus can be seen in Figs 13-167, 13-171, and 13-175 from the caudal view. The division between the paramedian lobule and the dorsal paraflocculus is hard to determine in Fig 13-175 but is readily seen in Fig 13-167 on the right side. Here the parafloccular fissure can be followed passing ventral to the paramedian lobule.

The ventrolateral aspect of the cerebellum is presented in Figs 13-176 and 13-177. The convoluted dorsal paraflocculus, which is separated from the ansiform and paramedian lobules by the parafloccular fissure, can be traced around to the rostral aspect of the cerebellum, where it can also be seen in Fig 13-173 on the right side of the picture (left side of the cerebellum). The ventral paraflocculus is separated from the dorsal paraflocculus by the intraparafloccular fissure and lies ventromedial to the dorsal paraflocculus (Figs 13-176, 13-177, 13-178, and 13-179). It too, is convoluted. Various portions of it have been designated as the accessory paraflocculus by authors describing the cerebellum of other cetaceans.

The caudolateral (posterolateral) fissure and the flocculonodular lobe were not identified on these specimens. The caudal vermis was in pieces, so that the pyramis, uvula, and nodule could not be identified.

The rostral lobe of the cerebellum of cetaceans is small compared to the caudal lobe and also compared to the rostral lobe of domestic terrestrial mammals, especially carnivores. Most of the rostral lobe is seen in the rostroventral views of the cerebellum in Figs 13-180, 13-181, 13-182, and 13-183. The hemispheres of the rostral lobe were more extensive laterally than in most domestic mammals.

The sagittally sectioned cerebellum of 80B1 is shown in Figs 13-181, 13-182, and 13-183. The vermis disintegrated caudal to the folium vermis, so the caudal lobules could not be identified. The primary fissure and the posterior superior or preansiform fissure were determined by comparison with the surface, where they limit the very obvious lobulus simplex and declive. The other lobules were determined by the branching of the arbor vitae and by the depth of the fissures.

Almost all of the available brains appeared to have been rather violently separated through the mesencephalon with resulting distortions, so not too much can be said about this region. In other cetaceans the mesencephalic (cerebral) aqueduct is said to be voluminous caudally at the level of the caudal colliculus. This is probably true for the bowhead brain, so the aqueduct is depicted as expanding caudally in Fig 13-160. The only brain stem fragment that included both the rostral and caudal colliculi is pictured in Fig 13-184. Superficially, the rostral and caudal colliculi appeared to be about the same size. The rostral colliculi did not appear as massive as in domestic ruminants, but would not be regarded as small. The caudal colliculi appeared somewhat larger relative to other brain stem structures in the bowhead brain than is the case in carnivores, but were probably not larger than the caudal colliculi of other cetaceans. The lateral lemniscus was very prominent and so was the brachium of the caudal colliculus (Fig 13-184 and 13-185). The large medial geniculate body has already been mentioned with the thalamus.

The rhombencephalon appeared to be wide and shallow, especially in the brain of 80B1 (Figs 13-186, 13-187, 13-188, and 13-189). The transverse fibers of the pens formed a massive structure, as would be expected with the large cerebellum (Figs 13-188 and 13-189). The middle cerebella peduncle (brachium pontis) was twice as large as the rostral or caudal cerebella peduncle, but neither of the latter two structures appeared to be particularly small (Figs 13-186, 13-187). The large trigeminal nerve (V) exited through the transverse fibers of the pens, as in the human brain and unlike the

arrangement in domestic mammals, where it exits caudal to the transverse fibers or middle cerebella peduncle (Figs 13-188, 13-189). The vestibulocochlear nerve (VIII) can be seen caudal to the cerebella peduncles in Figs 13-186 and 13-187 and at the lateral border of the trapezoid body (CT) in Figs 13-188 and 13-189. It was not larger than the trigeminal nerve in the bowhead, which is typical for baleen whales, although the vestibulocochlear nerve has been reported to be larger than the trigeminal nerve in some toothed whales (Pilleri and Gihr 1970).

The superficial origins of some other cranial nerves can be seen on the ventral surface of the brain stem in Figs 13-188 and 13-189. The facial nerve (VII) exited between the trigeminal and vestibulocochlear nerves (V and VIII). The glossopharyngeal nerve (IX) exited caudal to the vestibulocochlear nerve (VIII). The rootlets of the hypoglossal nerve (XII) could be seen exiting lateral to the pyramids. The rootlets of the vagus nerve (X) and the accessory nerve (XI) were not identified on the bowhead brain stems, but on other cetacean brains, both motor and sensory rootlets of the vagus nerve have been described caudal to the glossopharyngeal nerve, with the rootlets of the accessory nerve continuing in line with the vagal motor rootlets (Breathnach 1955, 1960, Pilleri 1964, 1966a).

The oculomotor nerve (III), trochlear nerve (IV) and abducent nerve (VI) , which innervate the extraocular muscles, have been described for most cetacean brains (Pilleri and Gihr 1970), but were not identified with certainty on these bowhead specimens. The band of fibers drawn in ventral to the mesencephalic aqueduct in Fig 13-150, but not labeled, may be the oculomotor nerve. This band can be seen on the other half of the brain of 80131 in Fig 13-159, but is not depicted in Fig. 13-158. A smaller band of fibers was seen exiting the brain stem of 79B1 between the rostral cerebella peduncle and the lateral lemniscus which may have been the trochlear nerve, since this is the site of superficial origin given for it in the humpback whale by Breathnach (1955). The abducent nerve is always pictured in its normal location exiting through the trapezoid body just lateral to the pyramid, but it was not identified on any of the bowhead brain stems examined.

The olives are seen on either side of the ventral median fissure in Figs 13-188 and 13-189. This protuberance, which is characteristic of cetacean brains, was the surface representation of the very large medial accessory olivary nucleus. The pyramids emerged caudal to the pontine transverse fibers

and passed ventral to the trapezoid body and around the lateral sides of the olives and decussated caudal to them.

The dorsal median sulcus and the dorsolateral sulcus can be seen on the dorsal surface of the brain stem in Figs 13-186 and 13-187. The fasciculus cuneatus and the cuneate tubercle could be seen. The nucleus gracilis was visible at the caudal extremity of the fourth ventricle, but a fasciculus gracilis was not visible on the dorsal surface. The bulge lateral to the dorsolateral sulcus in the caudal part of the medulla oblongata was probably the spinal tract of the trigeminal nerve.

The pontine flexure was at the level of the vestibulocochlear nerve and trapezoid body, and the cervical flexure was approximately at the junction between the brain stem and spinal cord.

Abbreviations Used for Labeling Figures 13-154 through 13-189

AC	Commissura rostralis
ALC	Ala lobuli centralis
APB	Area parolfactoria (Brocae)
Aq	Aqueducts mesencephali (A. cerebi)
AS	Area septal is (Area subcal loss)
BCdC	Brachium colliculi caudalis
c1	Claustrum
Cu	Culmen
cc	Corpus callosum
CdC	Colliculus caudalis
CrC	Crus cerebri
CE	Capsula externa
CEm	Capsula extrema
CI	Capsula interna
CT	Corpus trapezoideum

D	Decl i ve
F	Fornix
FAPM	Fissura ansoparamediana
FC	Fasciculus cuneatus
FD	Fascia dentata
FH	Fimbria hippocampi
FIPf	Fissura intraparafloccularis
FP	Fissura prima
FPf	Fissura parafloccularis
FPS	Fissura preansiformis (F. posterior superior)
FPrC	Fissura preculminata
FoV	Folium vermis
GA	Gyrus ambiens
GD	Gyrus diagonals
GS	Gyrus semilunaris
H	Hippocampus
I	Infundibulum
IG	Indusium griseum
L	Lingula (cerebelli)
LA	Lobulus ansiformis
LC	Lobulus centralis
LG	Corpus geniculatum laterale
LL	Lemniscus lateralis
LPM	Lobulus paramedianus
LQ	Lobulus quadrangularis
LS	Lobulus simplex
MG	Corpus geniculatum mediale

NC	Nucleus caudatus
NH	Neurohypophysis
N 11	Nervus opticus
N V	Nervus trigeminus
N VII	Nervus facialis
N VIII	Nervus vestibul ocochlearis
N IX	Nervus glossopharyngeus
N XII	Nervus hypoglossus
o	Oliva
OC	Chiasma optics
OT	Tractus opticus
Pcc	Pedunculus cerebellaris caudalis
PCM	Pedunculus cerebellaris medius
PCR	Pedunculus cerebellaris rostralis
P fD	Paraflocculus dorsalis
PfV	Paraflocculus ventralis
Pul	Pulvinar
P Ut	Putamen
Py	Pyramis (medullae oblongatae)
RC	Colliculus rostralis
RTT	Tuberculum rostrale thalami
SH	Sulcus hippocampi
SLD	Sulcus lateralis dorsalis
SMD	Sulcus medianus dorsalis
SP	Septum telencephali (pellucidum)
SPfA	Substantial perforata rostralis (anterior)
SRhA	Sulcus rhinalis rostralis (anterior)
Spcc	Splenium corporis callosi
StH	Stria habenularis thalami
StT	Stria terminals

TC	Tuberculum nuclei cuneati
TO	Tuberculum olfactorium
V	Vinculum lingulae
VL	Ventriculus lateralis

Figure 13-154. Photograph of an intact brain of bowhead whale. Photograph obtained from Dr. Sam Ridgway, NOSC. It is purposely mounted upside down to facilitate comparison with brains of other species.

Figure 13-155. Photograph of the dorsal aspect of the intact brain of 80B2. Photograph obtained from Dr. Sam Ridgway, NOSC.

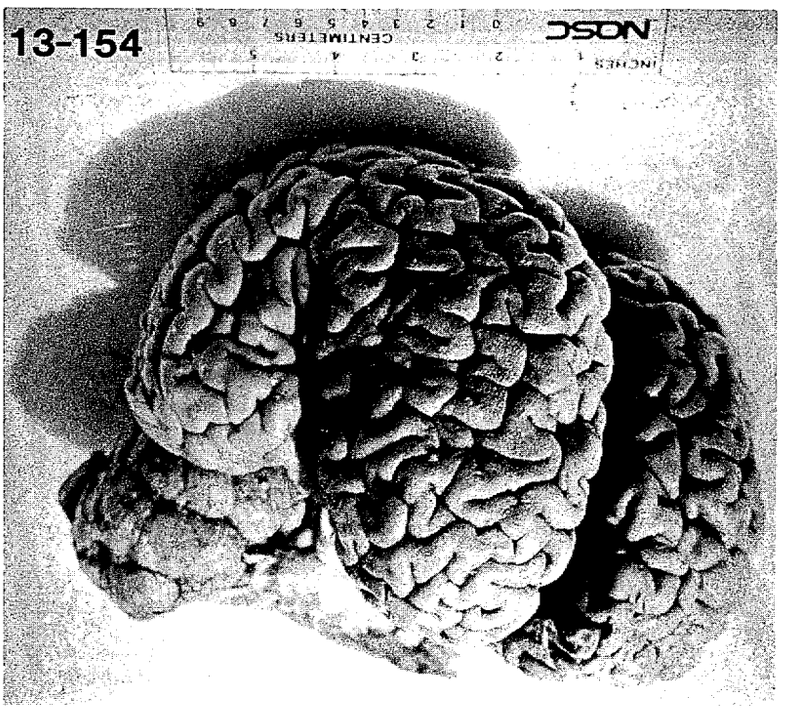
13-154
NOSC
CENTIMETERS
INCHES

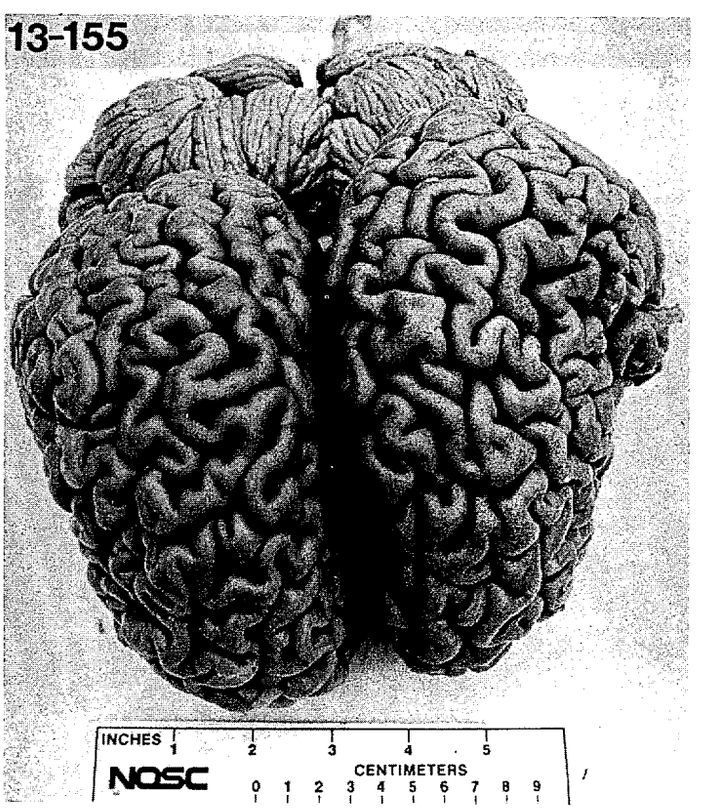
13-155
INCHES 1 2 3 4 5
NOSC
CENTIMETERS
0 1 2 3 4 5 6 7 8 9

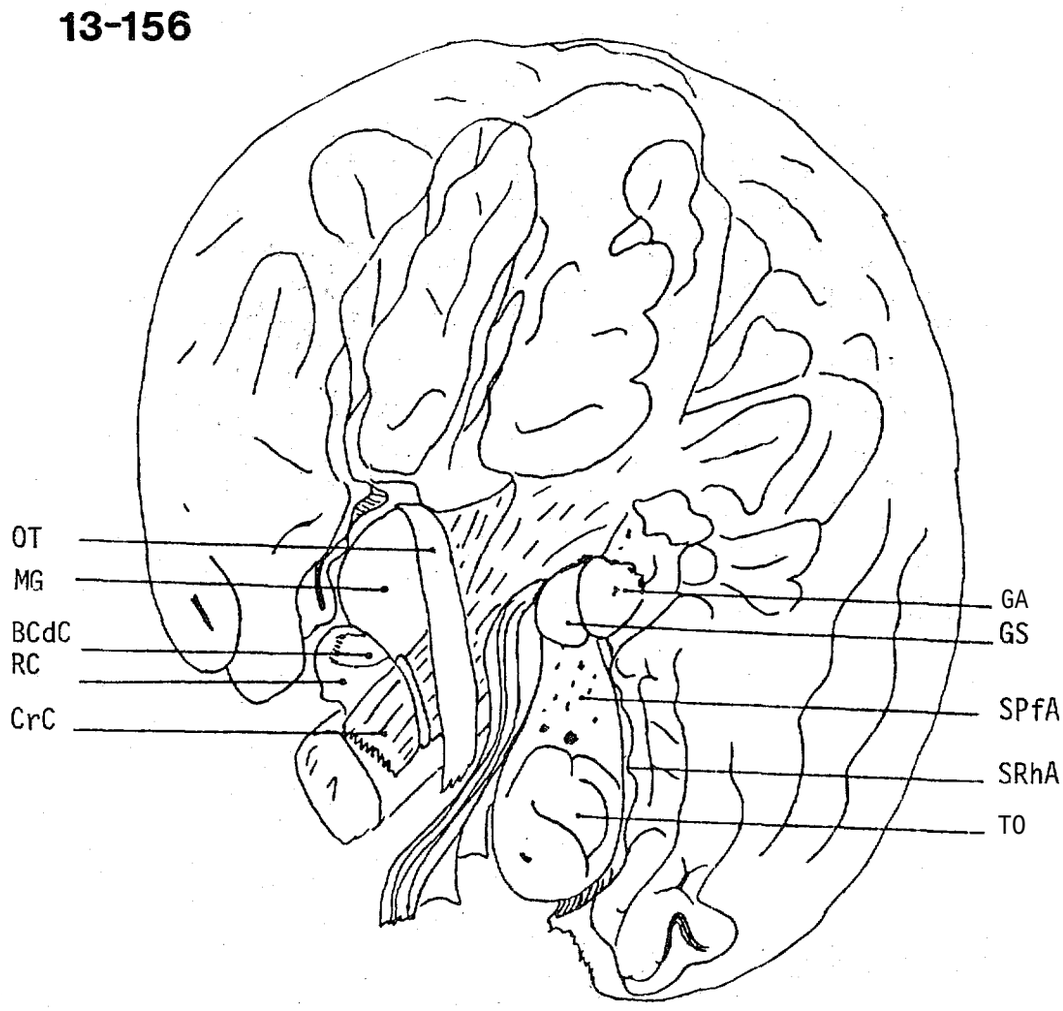

Figure 13-156. Sketch of the ventrolateral aspect of the "forebrain" of 80B1 ("damaged in removal"). Compare to Fig 13-157. Drawn from the same brain fragment shown in Fig 13-157, but not from the .photograph. BCdC - Brachium colliculi caudalis; CrC - Crus cerebri; GA - Gyrus ambiens; GS - Gyrus semilunaris; MG - Corpus geniculatum mediale; OT - Tractus opticus; RC - Colliculus rostralis; SPfA - Substantial perforata rostralis (anterior); SRhA - Sulcus rhinalis rostralis (anterior)"; TO - Tuberculum olfactorium.

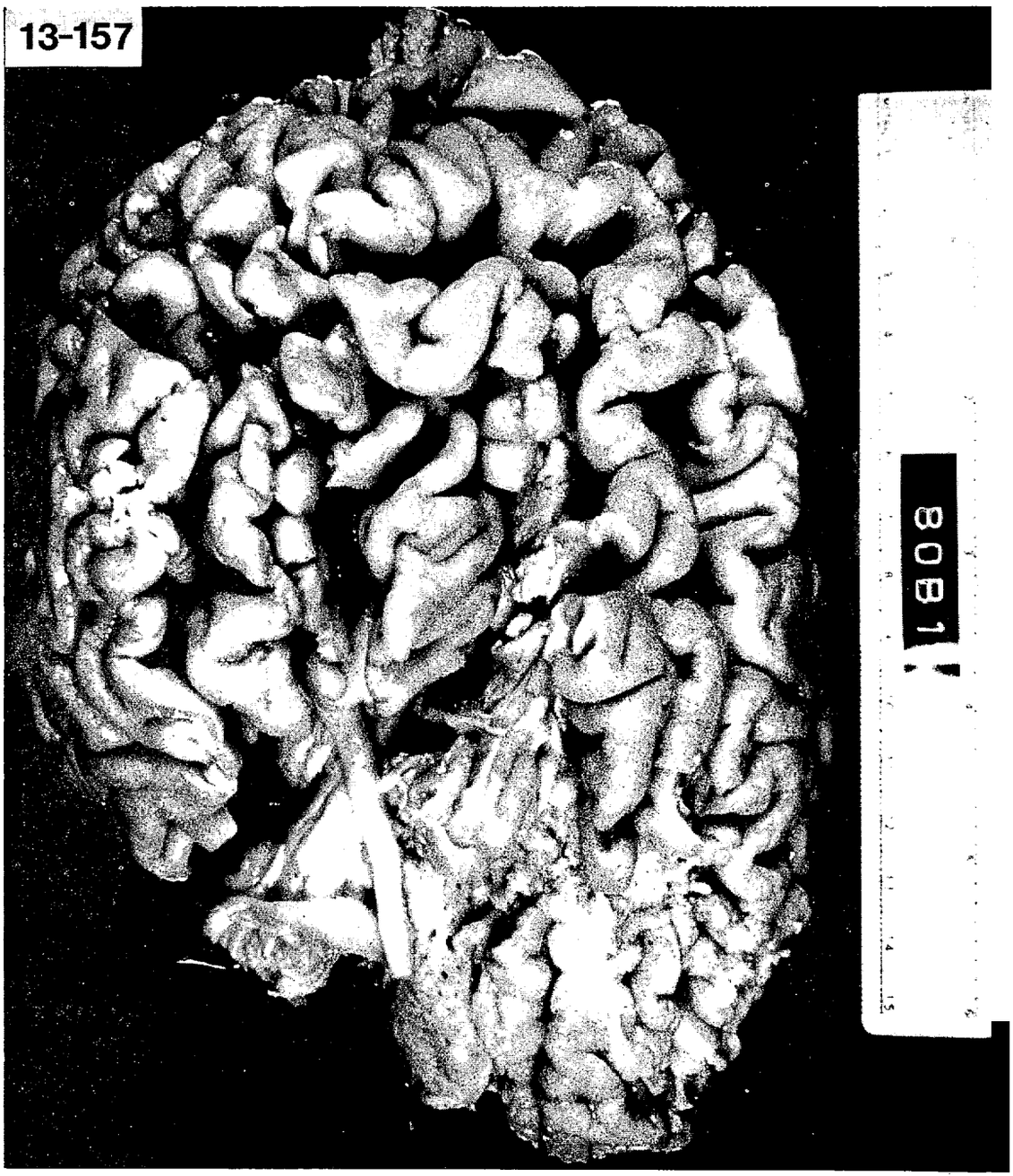

Figure 13-157. Photograph of the ventrolateral aspect of the forebrain of 80B1 (right side). Compare to Fig 13-156.

13-158

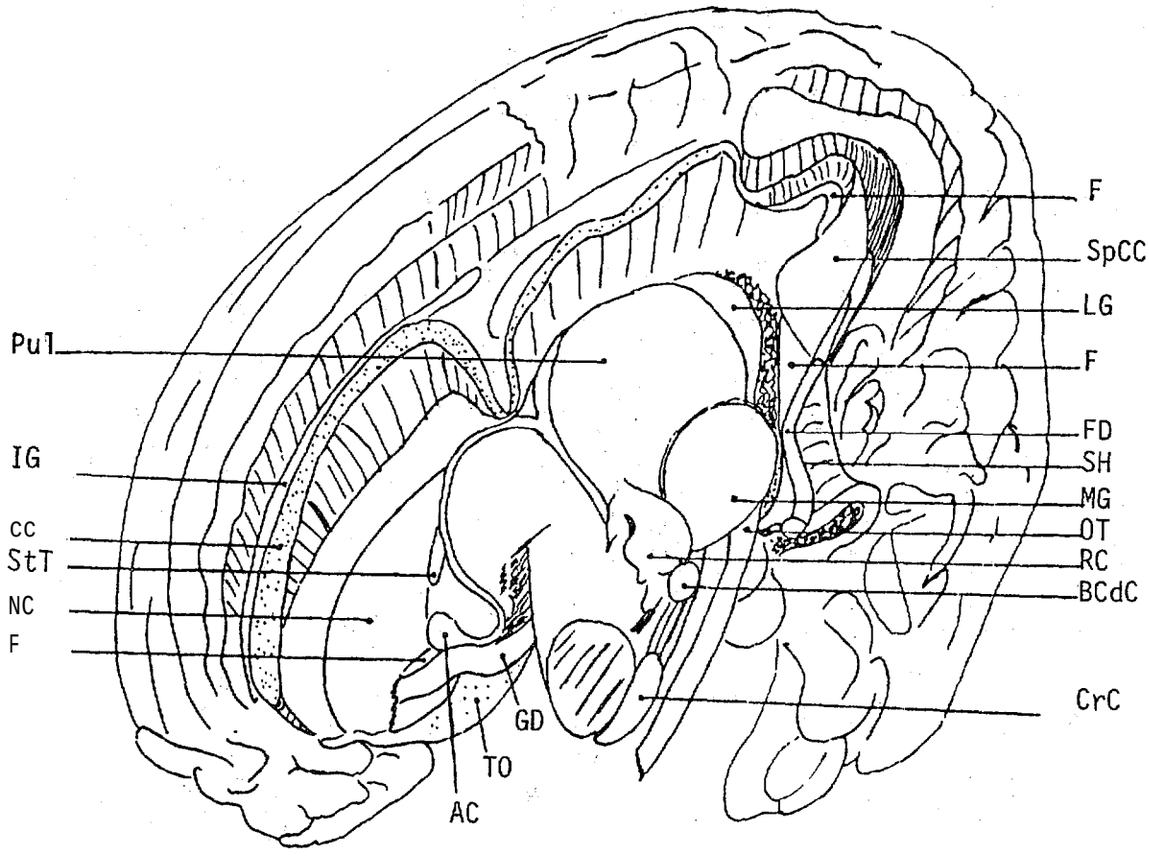

Figure 13-158. Sketch of the ventromedial view of the right "half" of the forebrain of 8061. Compare to Fig 13-159. Orientation not exactly the same as in the photograph. AC - Commissura rostralis; BCdC - Brachium colliculi caudalis; CC - Corpus callosum; CrC - Crus cerebri; F - Fornix; FD - Fascia dentata; GD - Gyrus diagonals; IG - Induseum griseum; LG - Corpus geniculatum laterale; MG - Corpus geniculatum mediale; NC - Nucleus caudatus; OT - Tractus opticus; Pul - Pulvinar; RC - Colliculus rostralis; SH - Sulcus hippocampi; SpCC - Splenium corporis callosi; StT - Stria terminal-is; TO - Tuberculum olfactorium.

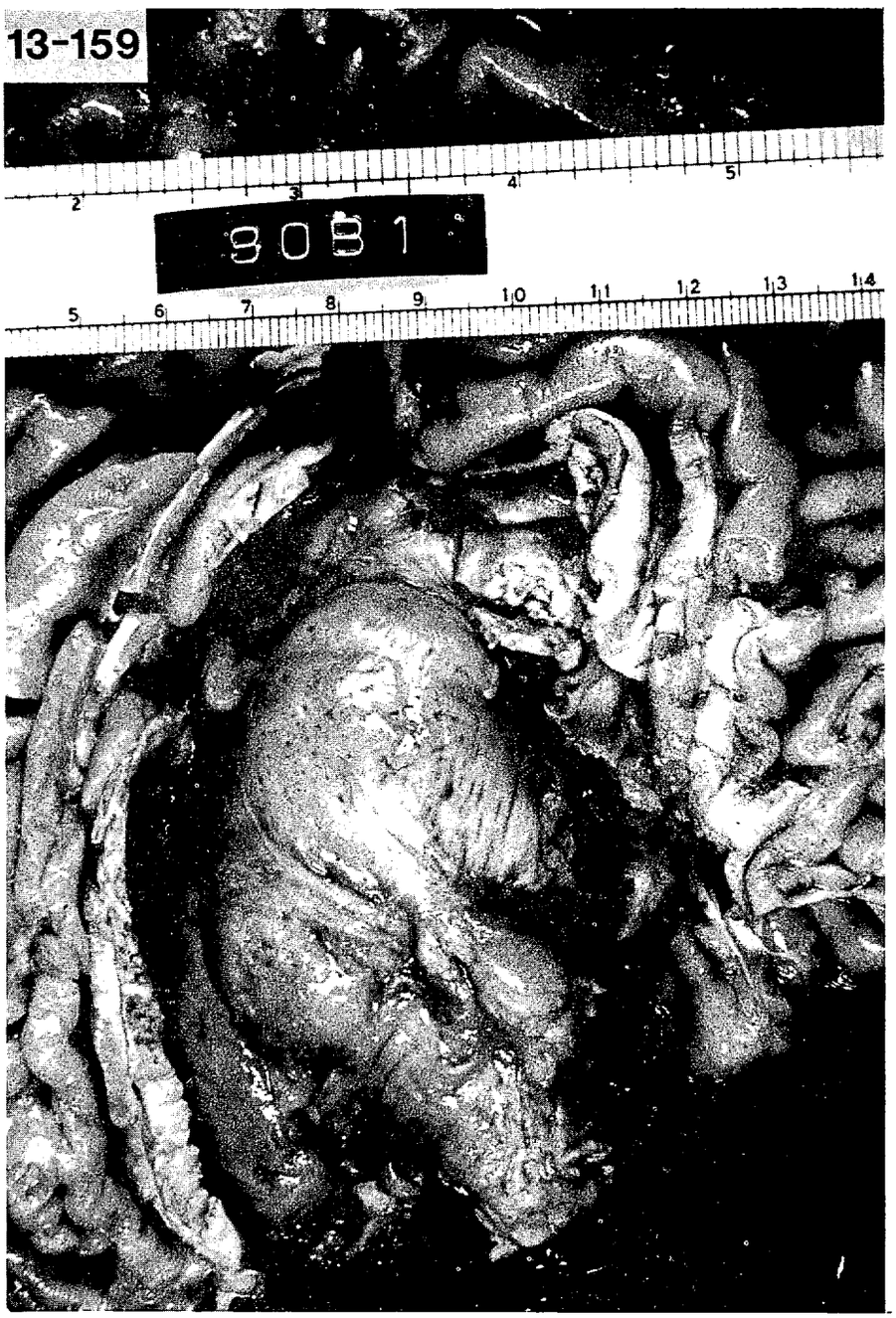

Figure 13-159. Photograph of the medial aspect of the right half of the forebrain of 80B1. Compare to Fig 13-158. Orientation not exactly the same as in the sketch.

13-160

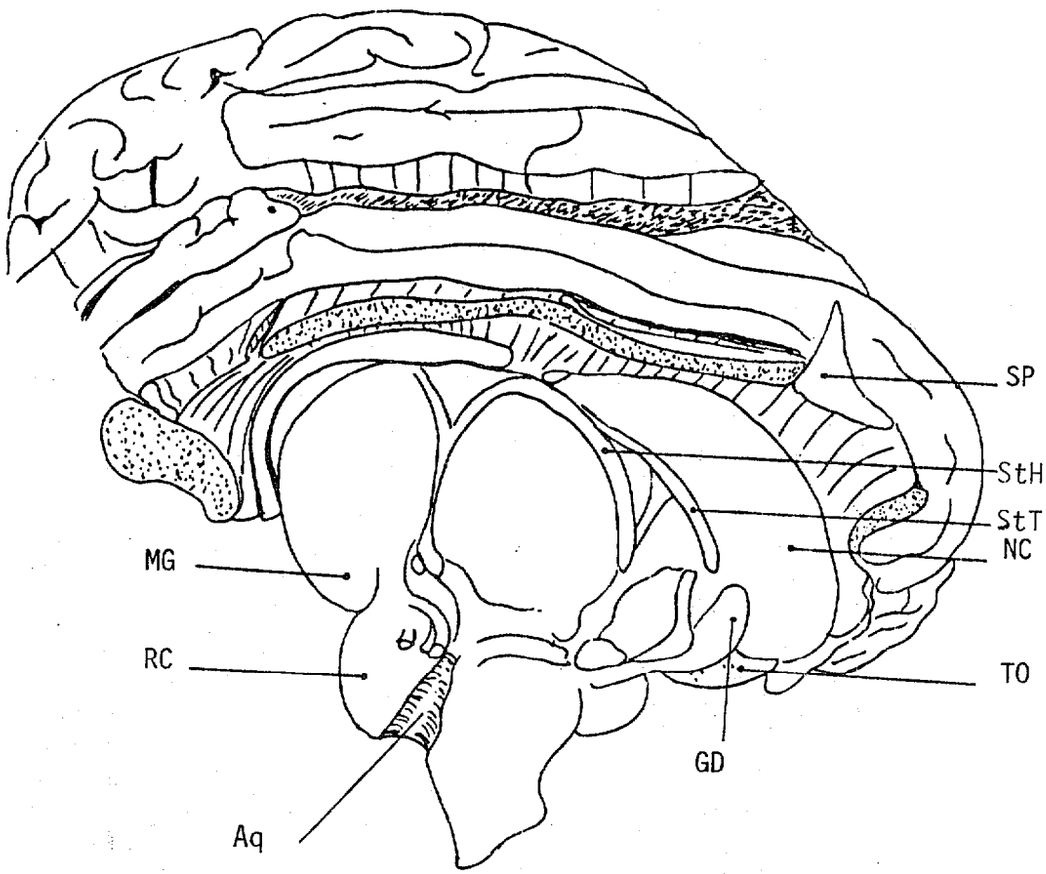

Figure 13-160. Sketch of the ventromedial aspect of the left "half" of the "forebrain" of 80B1. Compare to Fig 13-161. Drawn from the same brain fragment shown in Fig 13-161, but not from the same orientation. Aq - Aqueducts mesencephali (A. cerebri); GD - Gyrus diagonals; MG - Corpus geniculatum mediale; NC - Nucleus caudatus; RC - Colliculus rostralis; SP - Septum telencephali (pellucidum); StH - Stria habenularis; StT - Stria terminals; TO - Tuberculum olfactorium.

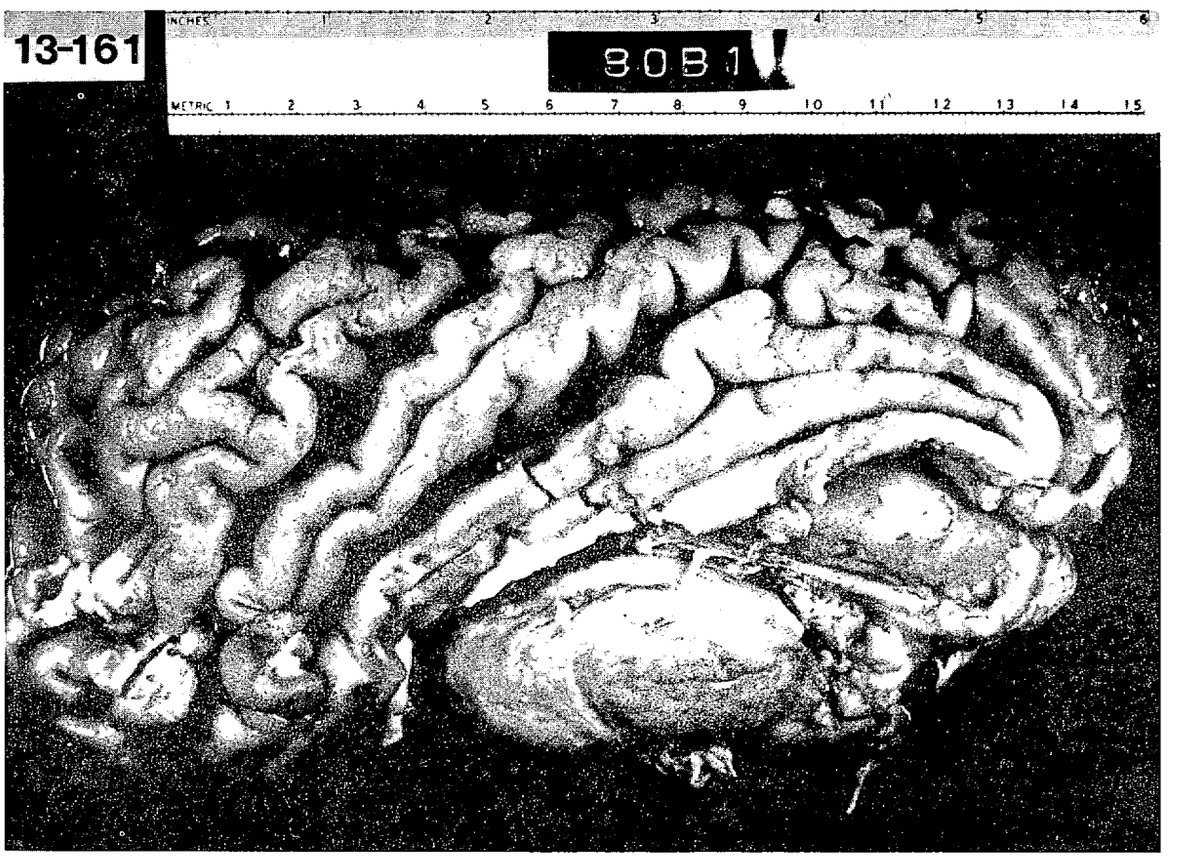

Figure 13-161. Photograph of the medial aspect of the left “half” of the “forebrain” of 80B1. Compare to Fig 13-160.

Figure 13-162. Photograph of the medial aspect of a slice of the right cerebral hemisphere of 80B2, showing the septal area. AC - Commissura rostral is; APB - Area parolfactoria (Brocae); AS - Area septalis; CC - Corpus callosum; F - Fornix; IG - Indusium griseum.

Figure 13-163. Photograph of the reapproximated slices of the left half of the "forebrain" of 79KK2.

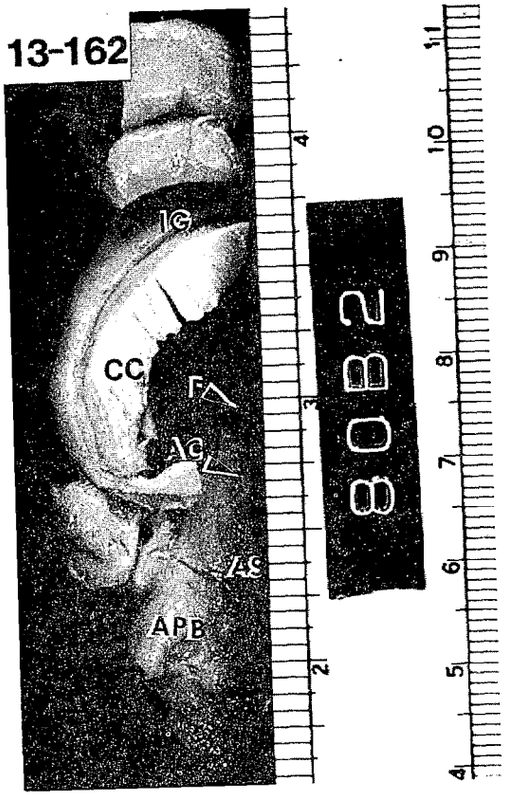
13-162
IG
CC
F
AC
AS
APB
8082

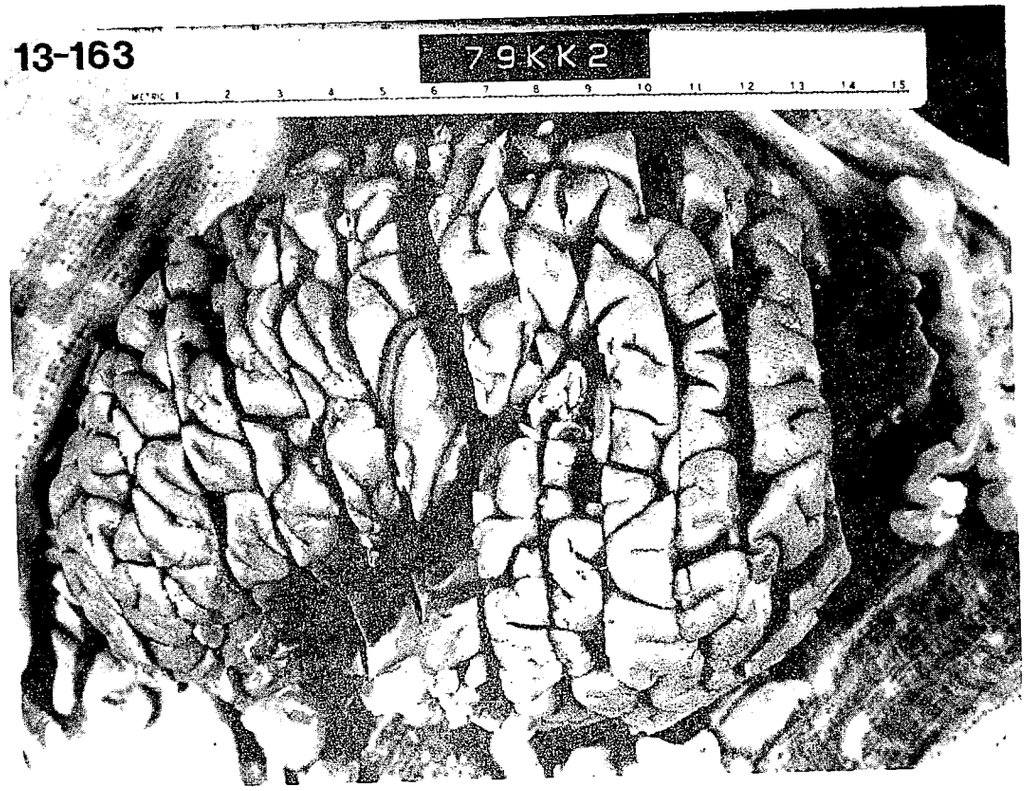
13-163
79KK2

Figure 13-164. Photograph of the caudal surface of the fourth slice from the "frontal" pole of the left hemisphere of 79KK2. See Fig 13-163. CC - Corpus callosum; CE - Capsula externa; CI - Capsula interns; NC - Nucleus caudatus; Put - Putamen; TO - Tuberculum olfactorium; VL - Ventriculus lateral is.

Figure 13-165. Photograph of the rostral surface of the tenth slice from the "frontal" pole of the left hemisphere of 79KK2 (through the temporal horn of the lateral ventricle). Compare to Fig 13-163. The hippocampus does protrude into the lateral ventricle. FH -' Fimbria hippocampi; H - Hippocampus; VL - Ventriculus lateral is.

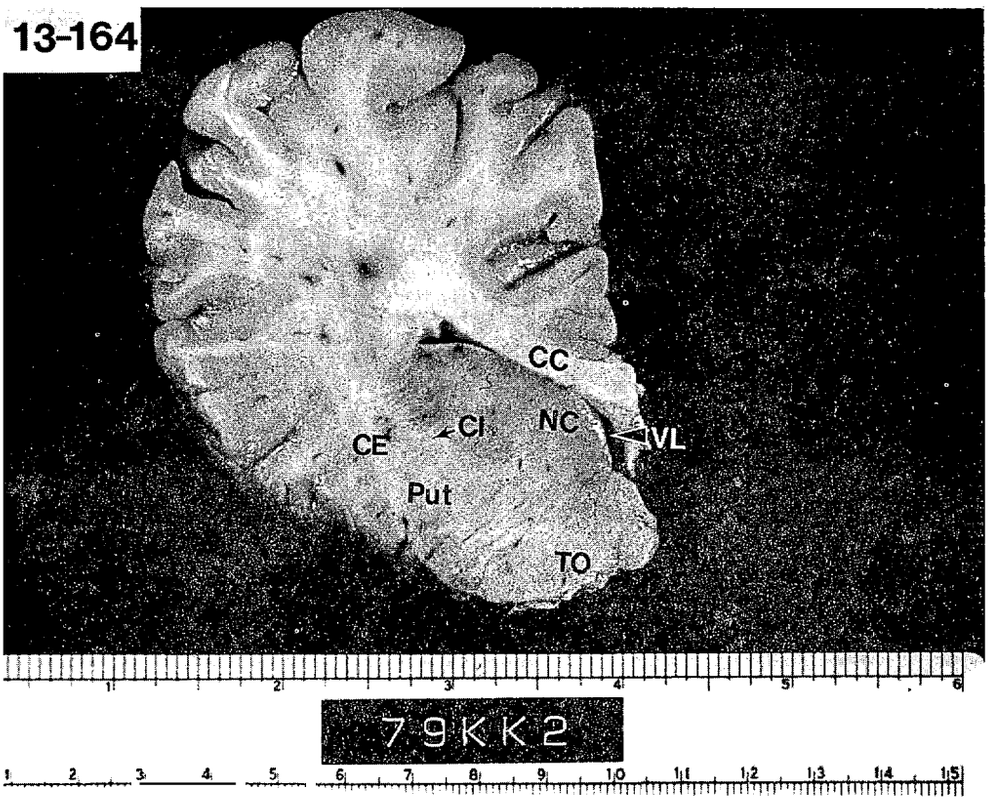
13-164
CC
CI
NC
VL
CE
Put
TO
79KK2

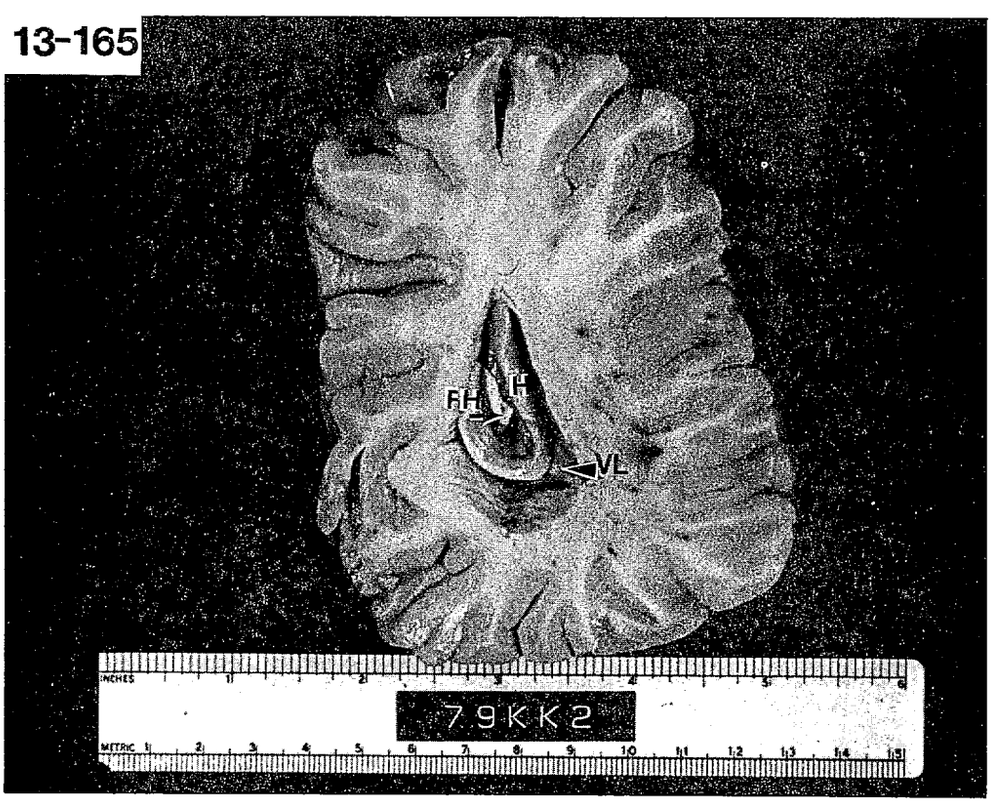
13-165
RH
LH
VL
79KK2

Figure 13-166. Photograph of the rostral surface of a slice of the left hemisphere of 79KK4 at the interventricular foramen. The plane of sectioning is different than in 79KK2. CC - Corpus callosum; CE - Capsula externa; CEm - Capsula extrema; CI - Capsula interna; Cl - Claustrum; NC - Nucleus caudatus; Put - Putamen; RTT - Tuberculum rostrale thalami; StT - Stria terminals.

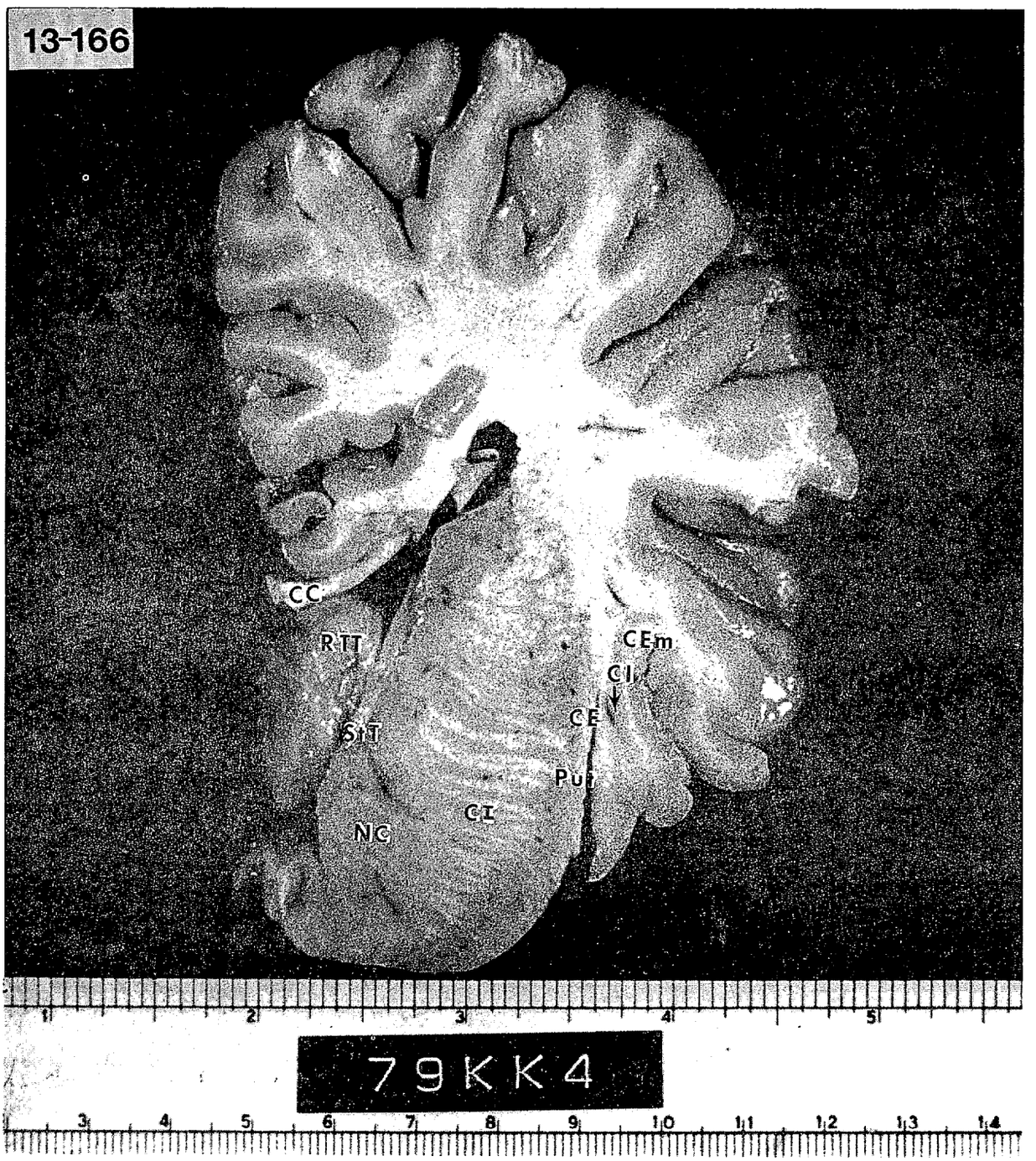
13-166
CC
RTT
SiT
Nc
CI
Put
CE
CI
CEm
79KK4

Figure 13-167. Photograph of a dorsal view of the detached leptomeninges of the forebrain and the cerebellum and brain stem of 8061 still covered by leptomeninges. The optic chiasm and parts of the optic tracts are visible. Compare to Fig 13-168. LPM - Lobulus paramedianus; OC - Chiasma optics; PfD - Paraflocculus dorsalis.

Figure 13-168. Photograph of a closer view of the optic chiasm, optic tracts, and ventral hypothalamus of 80B1 in the leptomeninges. I - Infundibulum; OC - Chiasma optics; OT - Tractus opticus.

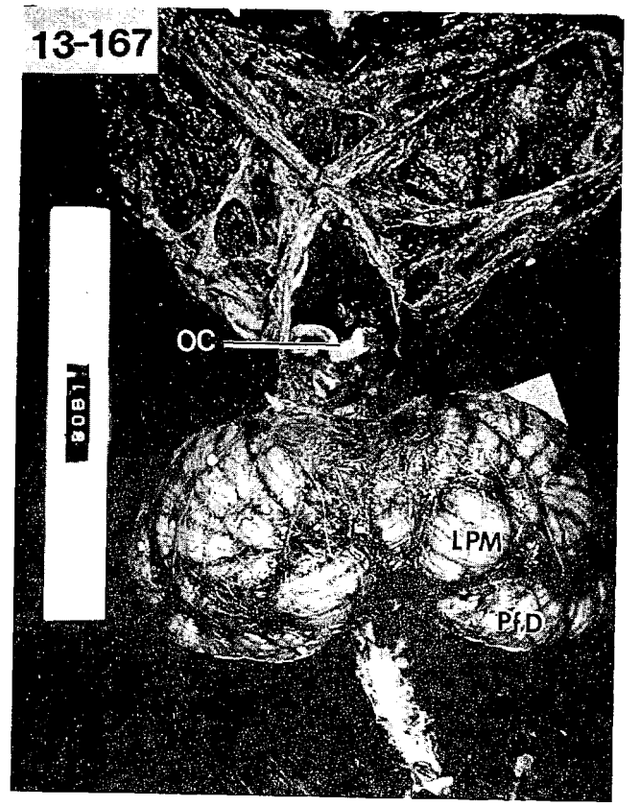
13-167
OC
LPM
PfD

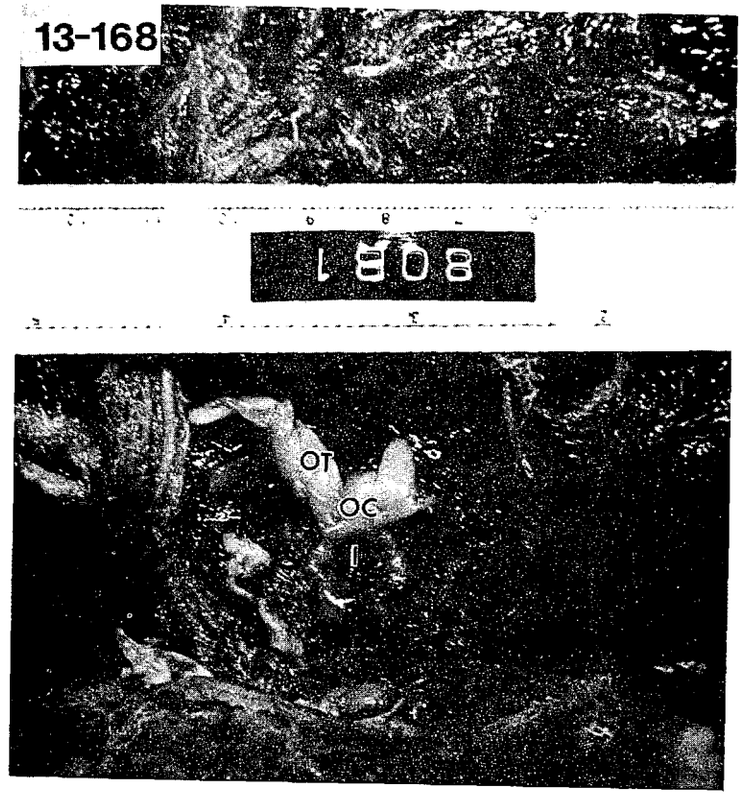
13-168
OT
OC

Figure 13-169. Photograph of a ventral view of the leptomeninges, cerebellum and brain stem of 80B1. The optic nerves (N II) and neurohypophysis (NH) are visible. Compare to Fig 13-170.

Figure 13-170. Photograph of a closer view of the optic nerves and neurohypophysis of 80B1. N II - Nervus opticus; NH - Neurohypophysis.

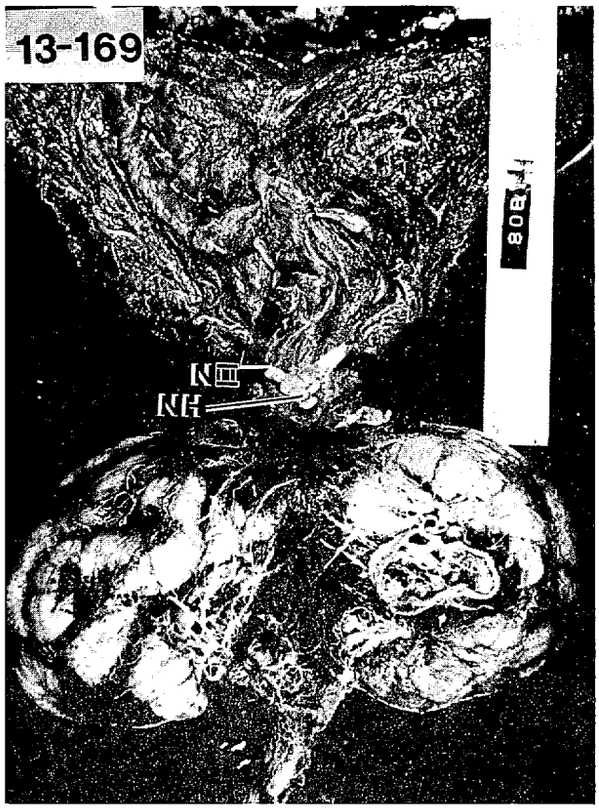
13-169
HN
IIN
808

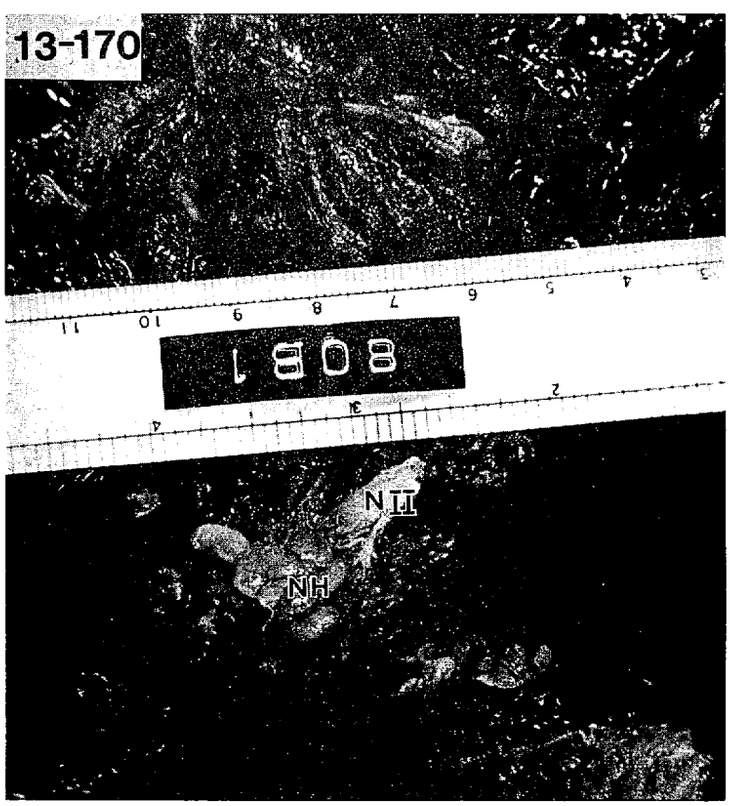
13-170
HN
IIN
808 1

13-171

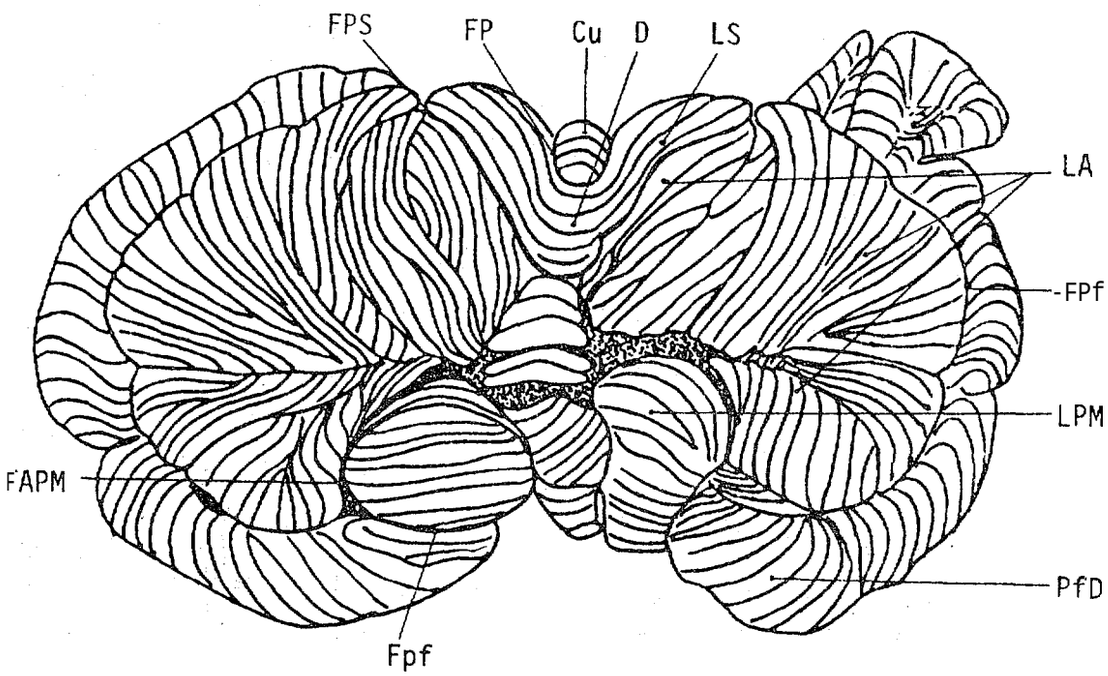

Figure 13-171. Sketch of the dorsal aspect of the cerebellum of 80B1. Note the ansiform lobule (LA). Cu - Culmen; D - Declive; FAPM - Fissura ansoparamediana; FP - Fissura prima; FPS - Fissura preansiformis (F. posterior superior); FPf - Fissura parafloccularis; LA - Lobulus ansiformis; LPM - Lobulus paramedianus; LS - Lobulus simplex; PfD - Paraflocculus dorsal is.

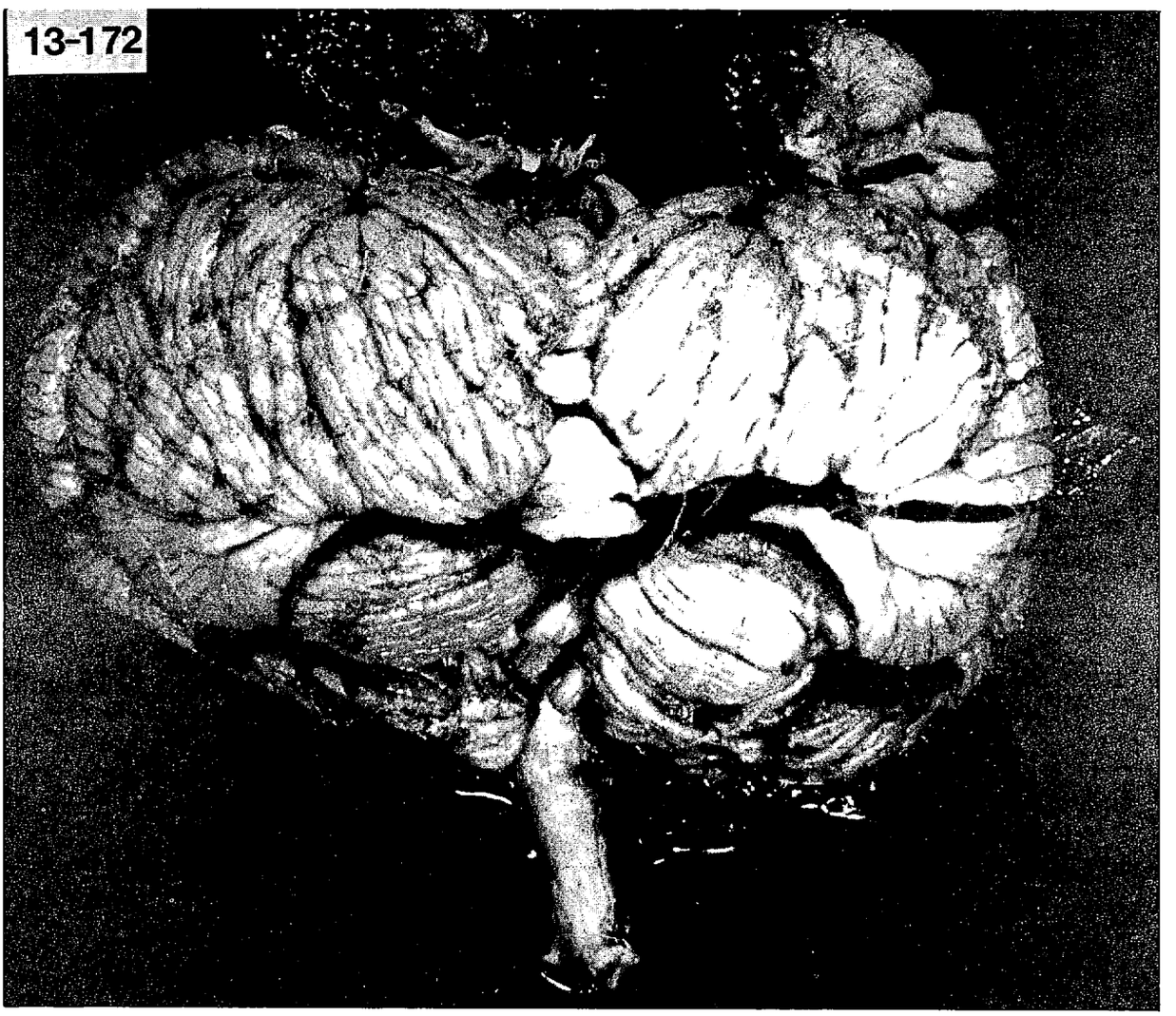

Figure 13-172. Photograph of the dorsal aspect of the cerebellum of 8061. Compare to Fig 13-171. XO.85

13-173

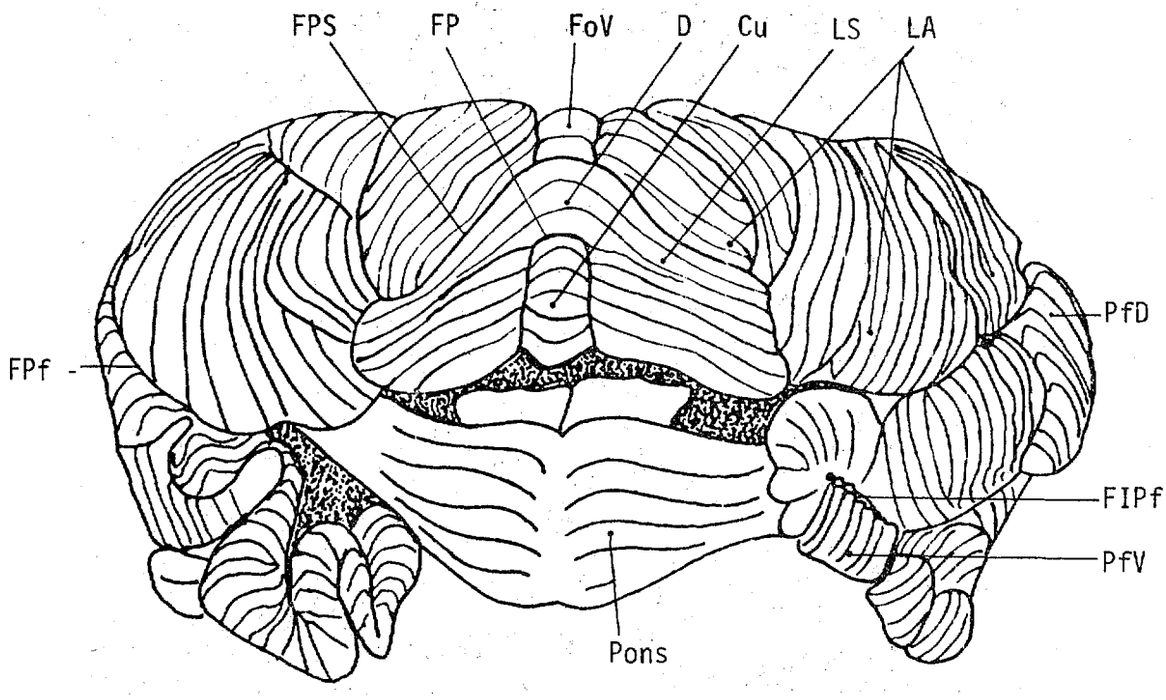

Figure 13-173. Sketch of the rostral aspect of the cerebellum of 80B1 (still attached to the brain' stem). Cu - Culmen; "D - Declive; FIPf - Fissura intraparafloccularis; FP - Fissura prima; FPf - Fissura parafloccularis; FPS - Fissura preansiformis (F. posterior superior); FoV - Folium vermis; LA - Lobulus ansiformis; LS - Lobulus simplex; PfD - Paraflocculus dorsalis; PfV - Paraflocculus ventralis.

Figure 13-174. Photograph of the rostral aspect of the cerebellum of 80B1. Compare to Fig 13-173. X1

Figure 13-175. Photograph of the caudal aspect of the cerebellum of 80B1. Note the paramedian lobules (LPM) on either side of the vermis and the dorsal paraflocculus (PfD). FAPM - Fissura ansoparamediana; FPf -. Fissura parafloccularis; LA - Lobulus ansiformis. X0.85

13-175
LA
LA
FA
PM
LPM
FPf
PfD

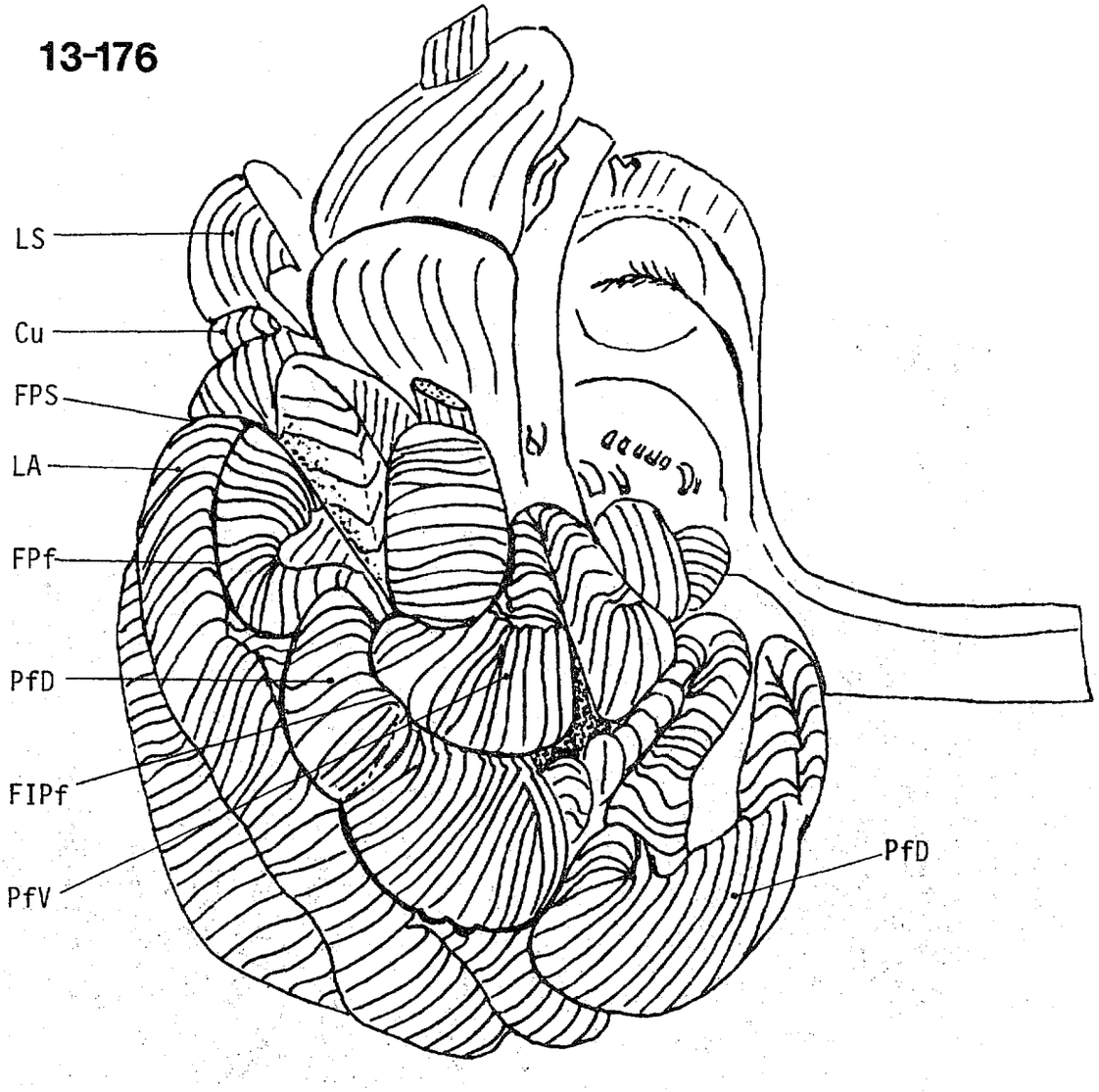

Figure 13-176. Sketch of the ventrolateral aspect of the cerebellum of 80B1. Note the dorsal paraflocculus (PfD). Cu - Culmen; FIPf - Fissura intraparafloccularis; FPf - Fissura parafloccularis; FPS - Fissura preansiformis (F. posterior superior); LA - Lobulus ansiformis; LS - Lobulus simplex; PfD - Paraflocculus dorsalis; PfV - Paraflocculus ventralis.

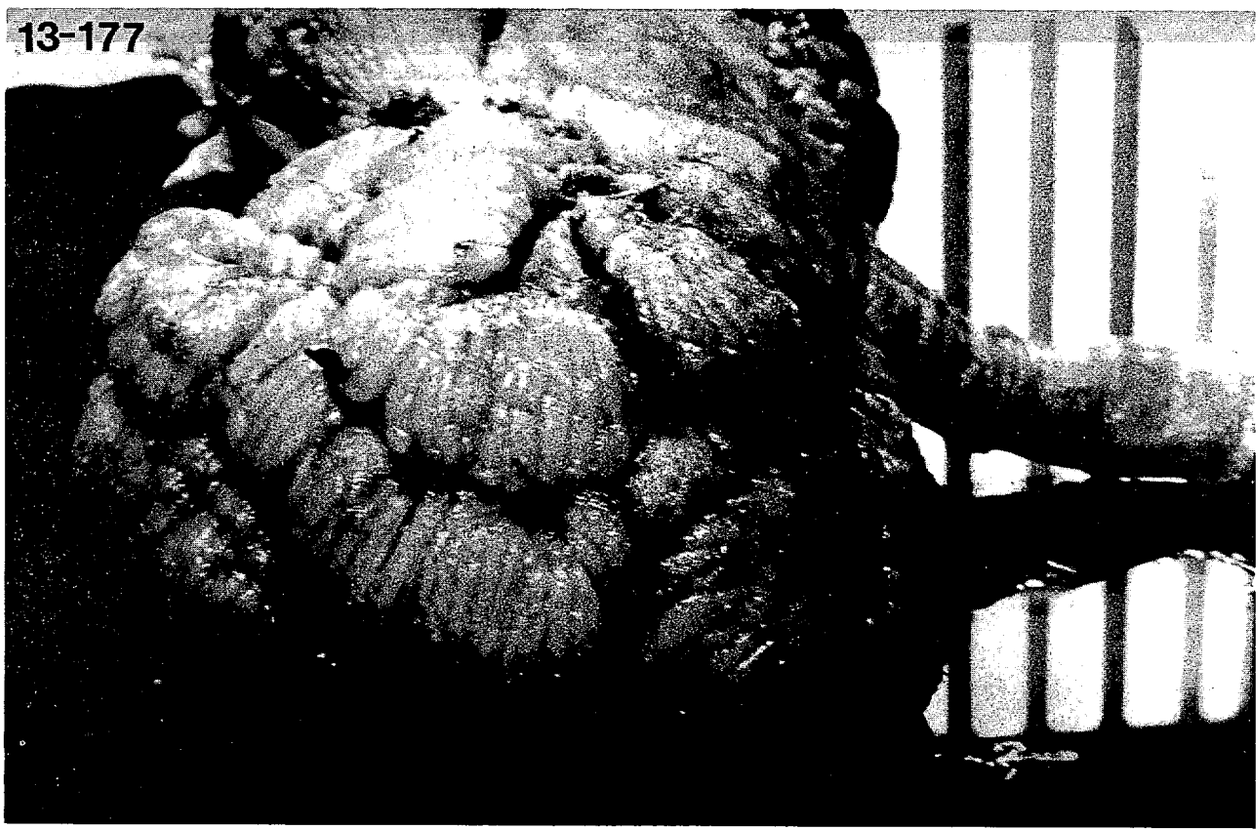

Figure 13-177. Photograph of the ventrolateral aspect of the cerebellum of 80B1 . Compare to Fig 13-176. Xl

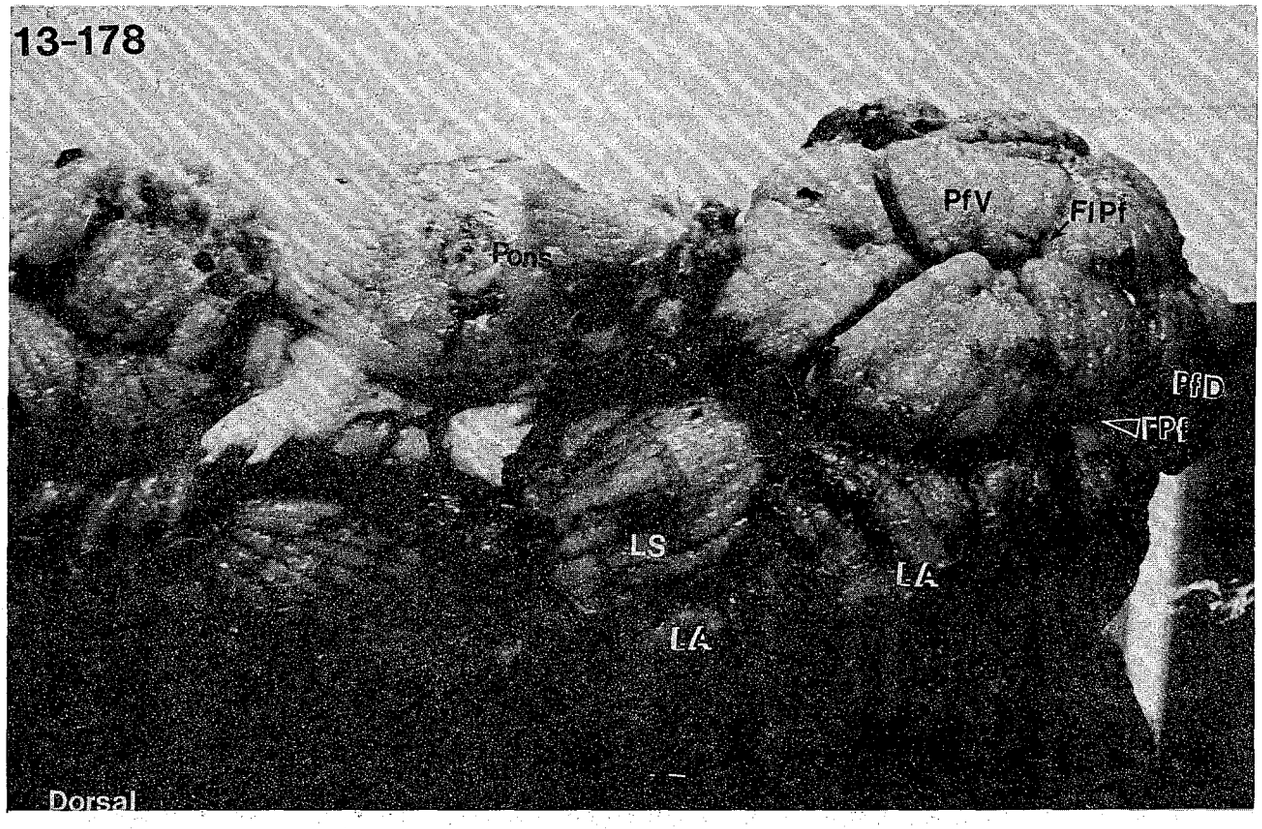

Figure 13-178. Photograph of the rostroventral aspect of the cerebellum of 80B1. Note the intraparafloccular fissure (FIPf). FPf - Fissura parafloccularis; LA - Lobulus ansiformis; LS - Lobulus simplex; PfD - Paraflocculus dorsalis; PfV - Paraflocculus ventral is. Xl

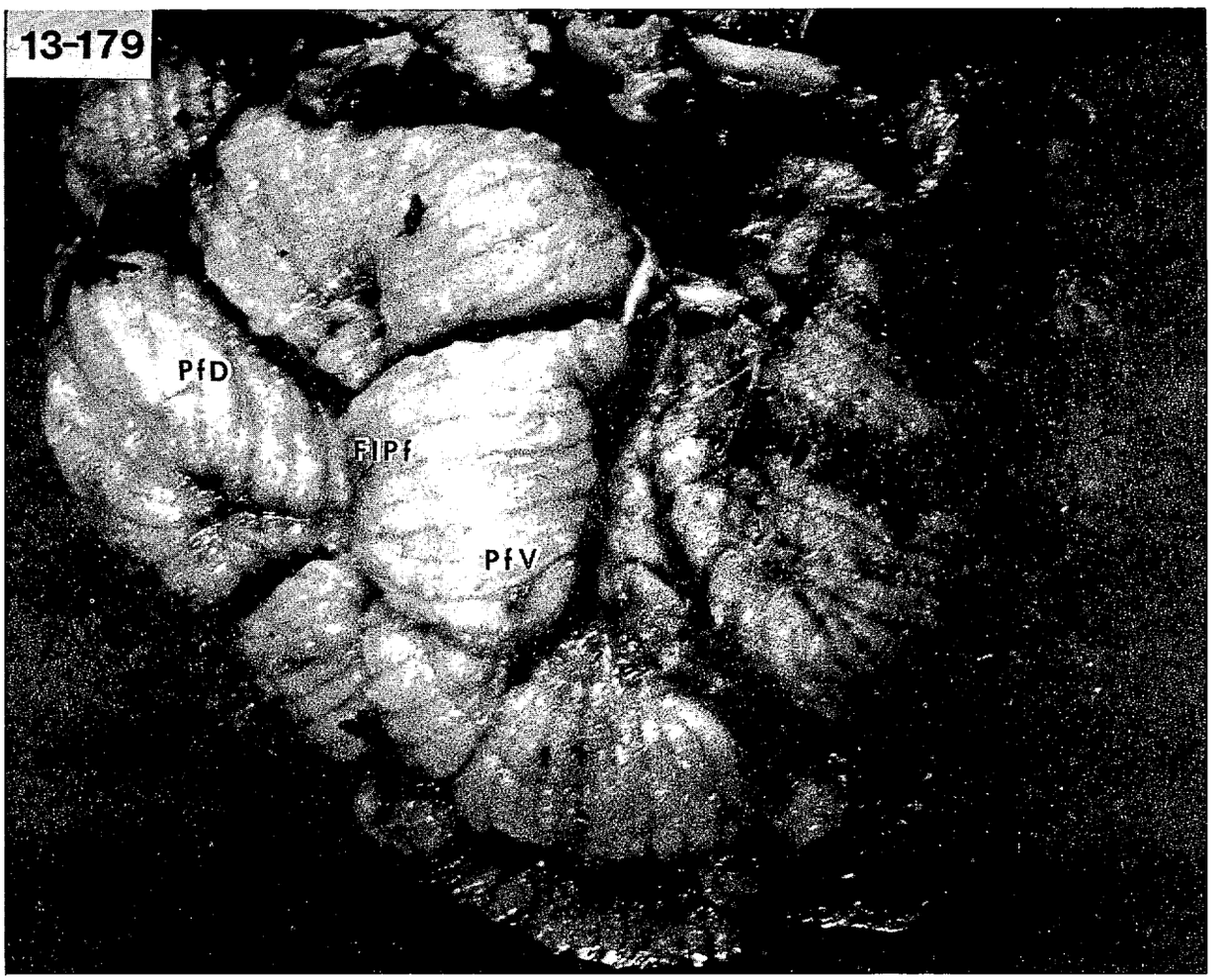

Figure 13-179. Photograph of the ventral aspect of the right cerebella hemisphere of 80B1. Note the ventral paraflocculus (PfV). FIPf - Fissura intraparafloccularis; PfD - Paraflocculus dorsal is. X1.55

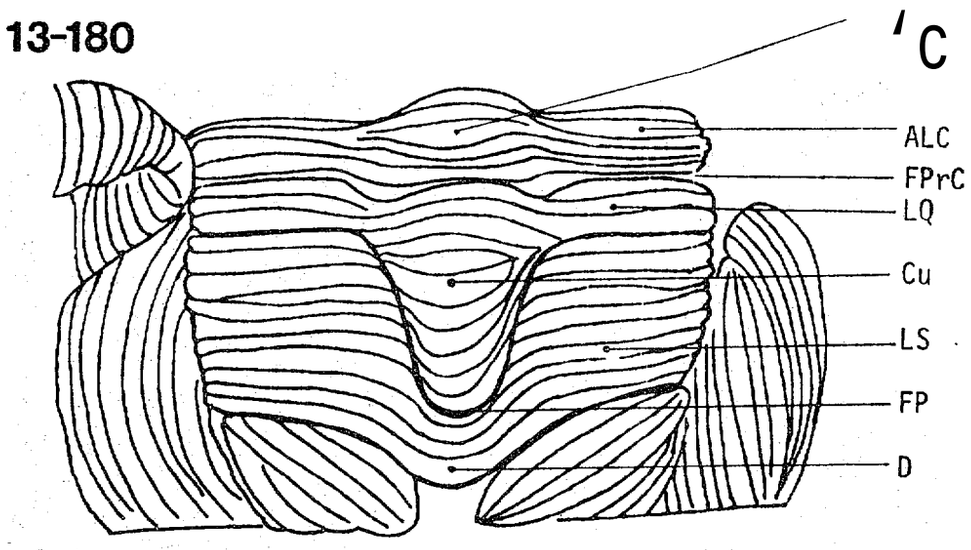

Figure 13-180. Sketch of the rostral aspect of the cerebellum of 80B1 with the brain stem removed. ALC - Ala lobuli centralis; Cu - Culmen; D - Declive; FP - Fissura prima; FPrC - Fissura preculminata; LC - Lobulus central is; LQ - Lobulus quadrangularis; LS - Lobulus simplex.

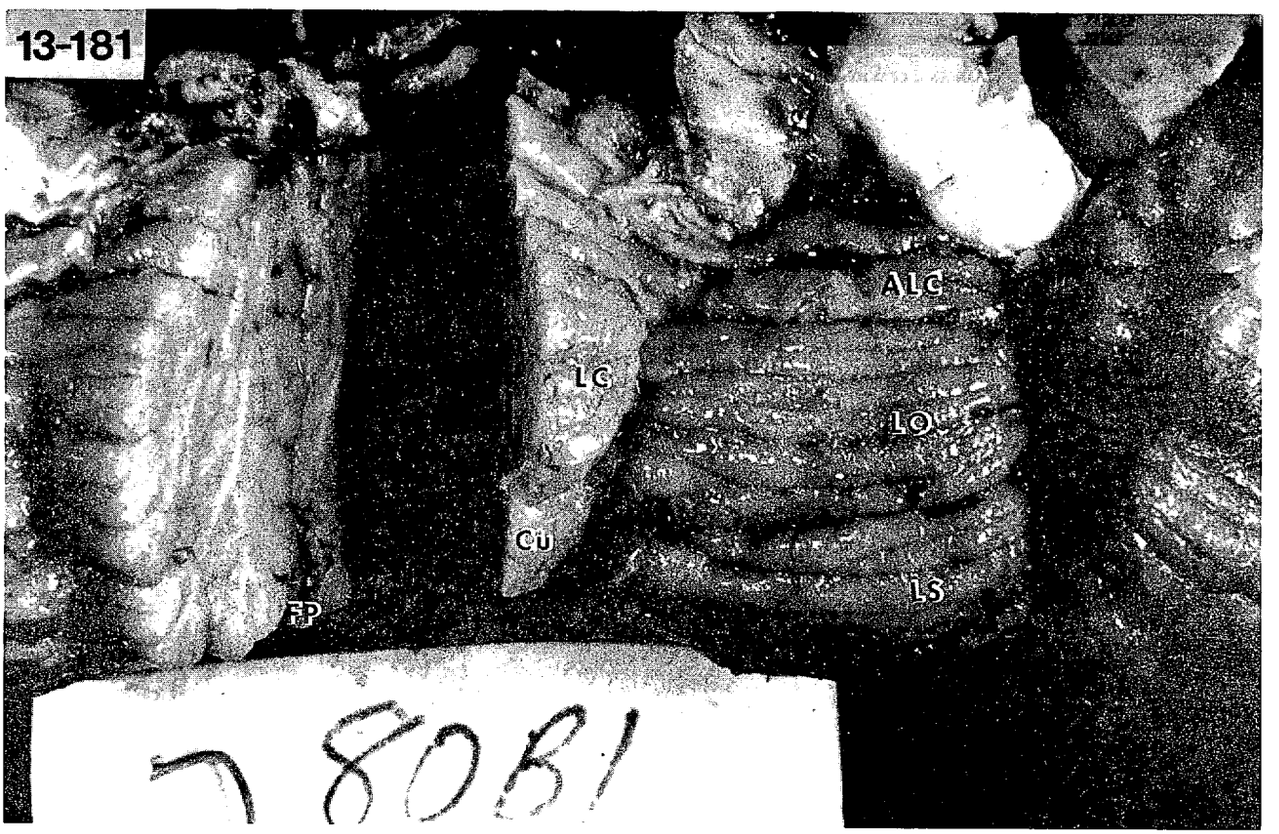

Figure 13-181. Photograph of the rostroventral aspect of the cerebellum of 80B1. The cerebellum has been sectioned sagittally. Note the lateral extent of the rostral lobules. Compare to Figs 13-180 and 13-182. ALC - Ala lobuli centralis; Cu - Culmen; FP - Fissura prima; LC - Lobulus central is; LQ - Lobulus quadrangularis; LS - Lobulus simplex. X1.83

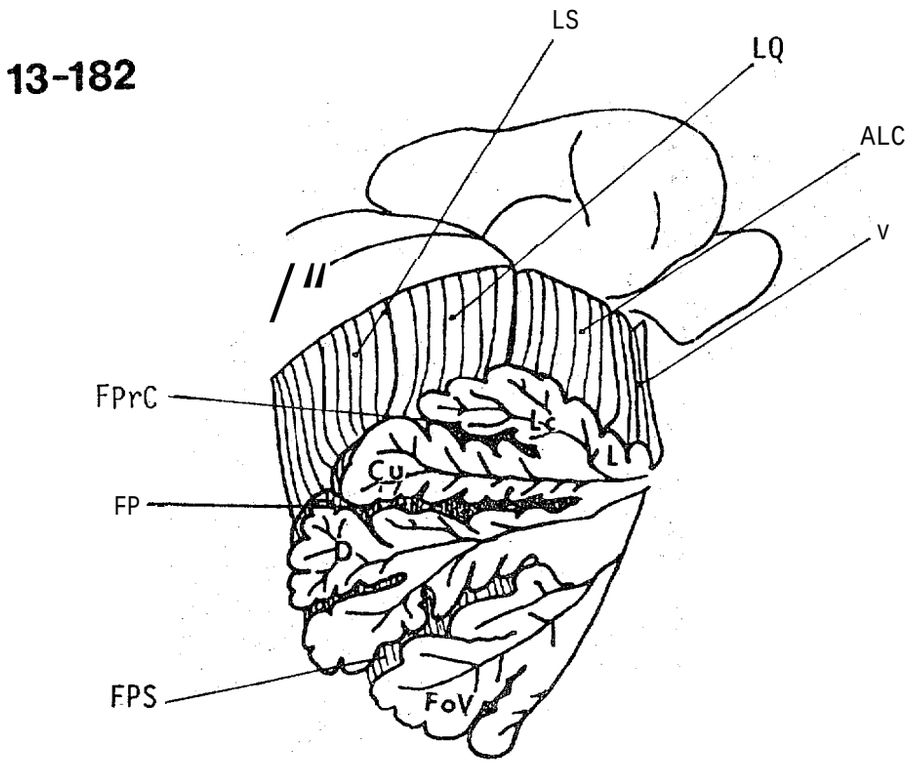

Figure 13-182. Sketch of the sagittal section of the cerebellum of 80B1 oriented as in Figs 13-181 and 13-183. ALC - Ala lobuli centralis; Cu - Culmen; D - Declive; FP - Fissura prima; FPrC - Fissura preculminata; FPS - Fissura preansiformis (F. posterior superior); FoV - Folium vermis; L - Lingula; LC - Lobulus centralis; LQ - Lobulus quadrangularis; LS - Lobulus simplex; V - Vinculum lingulae.

Figure 13-183. Photograph of the sagittal section of the cerebellum of 80B1. Compare to Fig 13-182. X1.83

Figure 13-184. Photograph of the dorsal aspect of the brain stem of 79KK3, showing the rostral colliculi, and lateral lemniscus, caudal colliculus and the brachium colliculi caudalis on the right side. The left caudal colliculus is also present. BCdC - Brachium colliculi caudalis; CdC - Colliculus caudalis, LL - Lemniscus lateralis; RC - Colliculus rostralis.

Figure 13-185. Photograph of the lateral aspect of the left half of the brain stem of 79KK2, showing the lateral lemniscus and caudal colliculus. BCdC - Brachium colliculi caudal is; CdC - Colliculus caudalis; LL - Lemniscus lateral is.

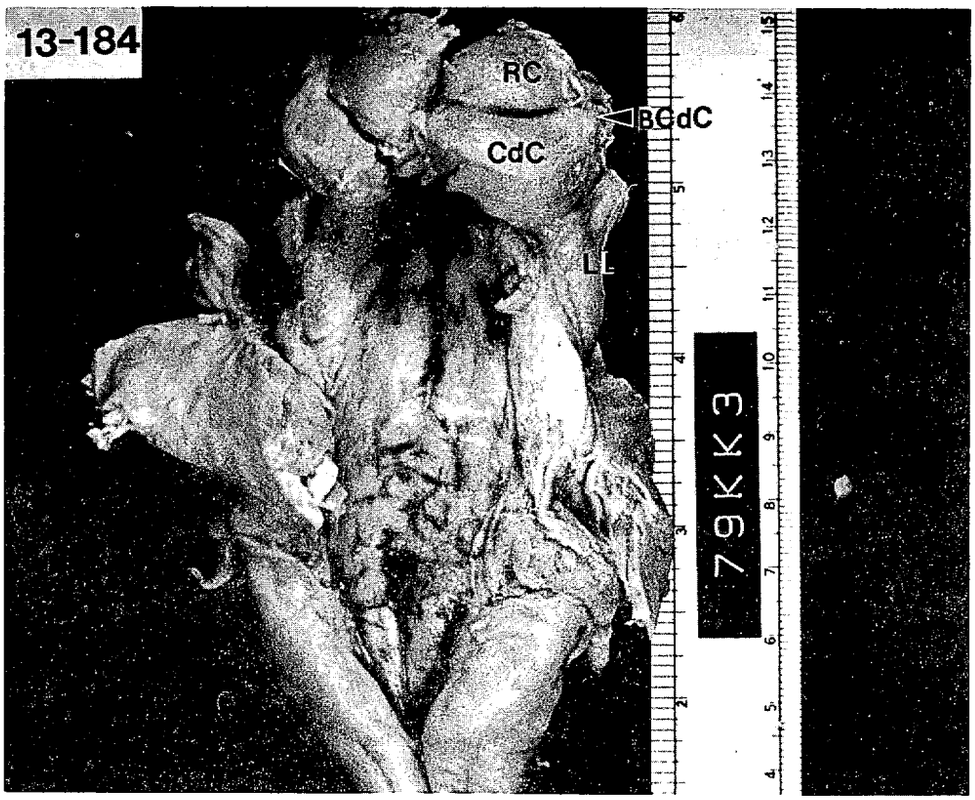
13-184
RC
BCdC
CdC
LL
79KK3

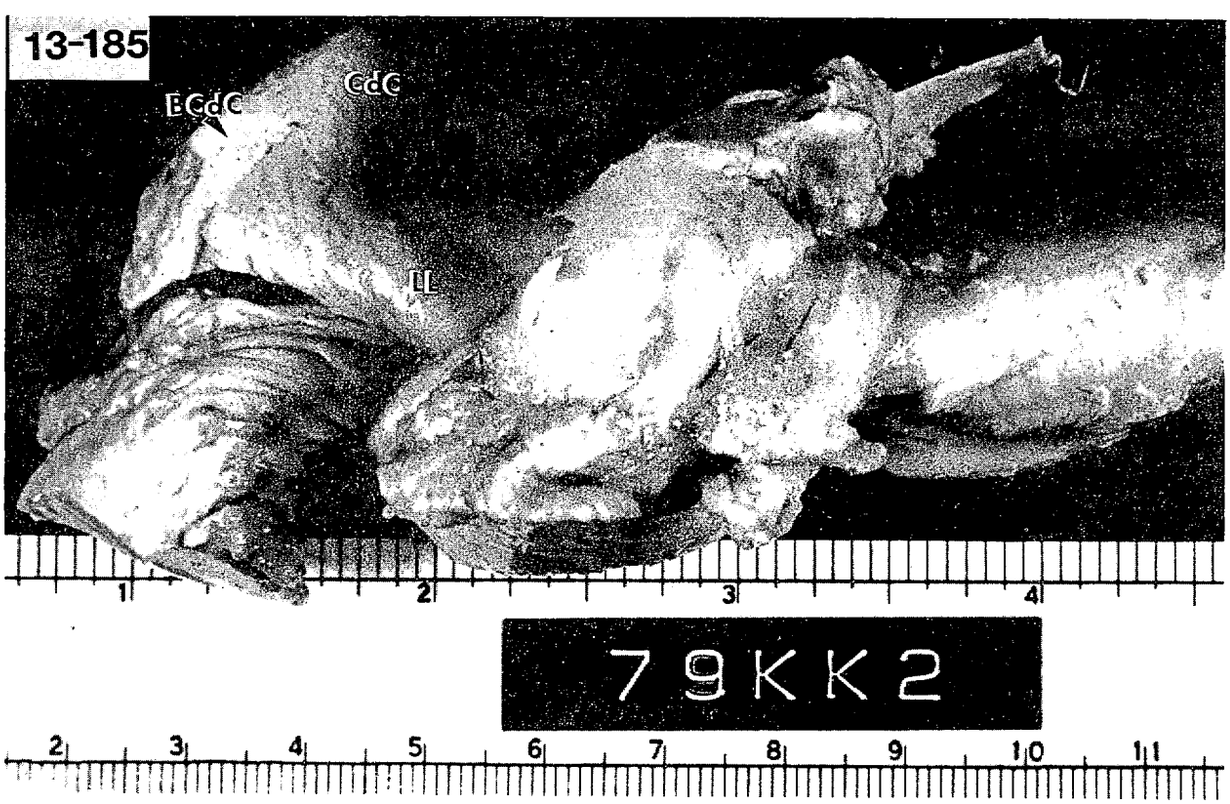
13-185
BCdC
CdC
LL
79KK2

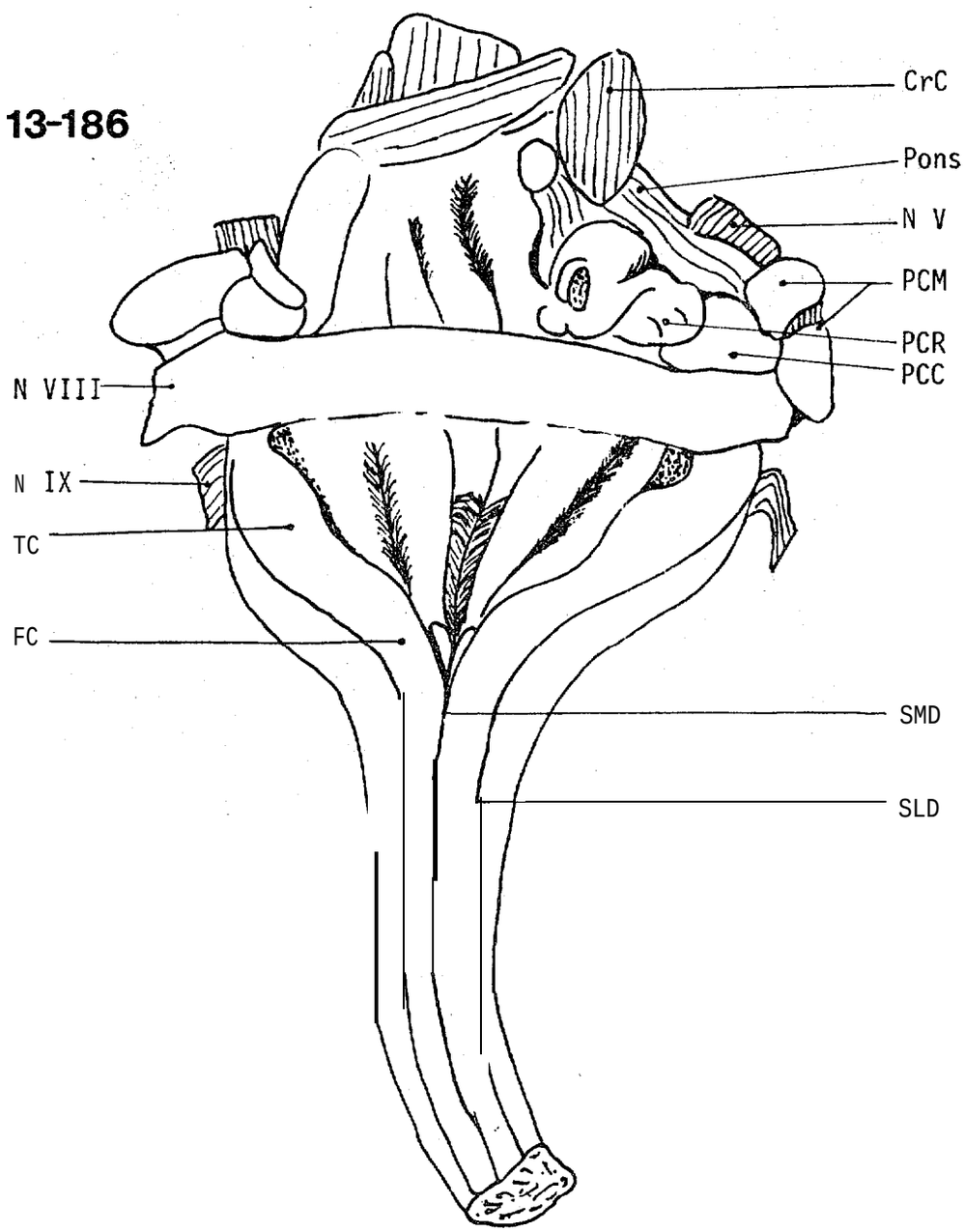

Figure 13-186. Sketch of the dorsal aspect of the brain stem of 80B1. CrC - Crus cerebri; FC - Fasciculus cuneatus; N V - Nervus trigeminus; N VIII - Nervus vestibulocochlearis; N IX - Nervus glossopharyngeus; PCC - Pedunculus cerebellaris caudalis; PCM - Pedunculus cerebellaris medius; PCR - Pedunculus cerebellaris rostralis; SLD - Sulcus lateralis dorsalis; SMD - Sulcus medianus dorsalis; TC - Tuberculum nuclei cuneati.

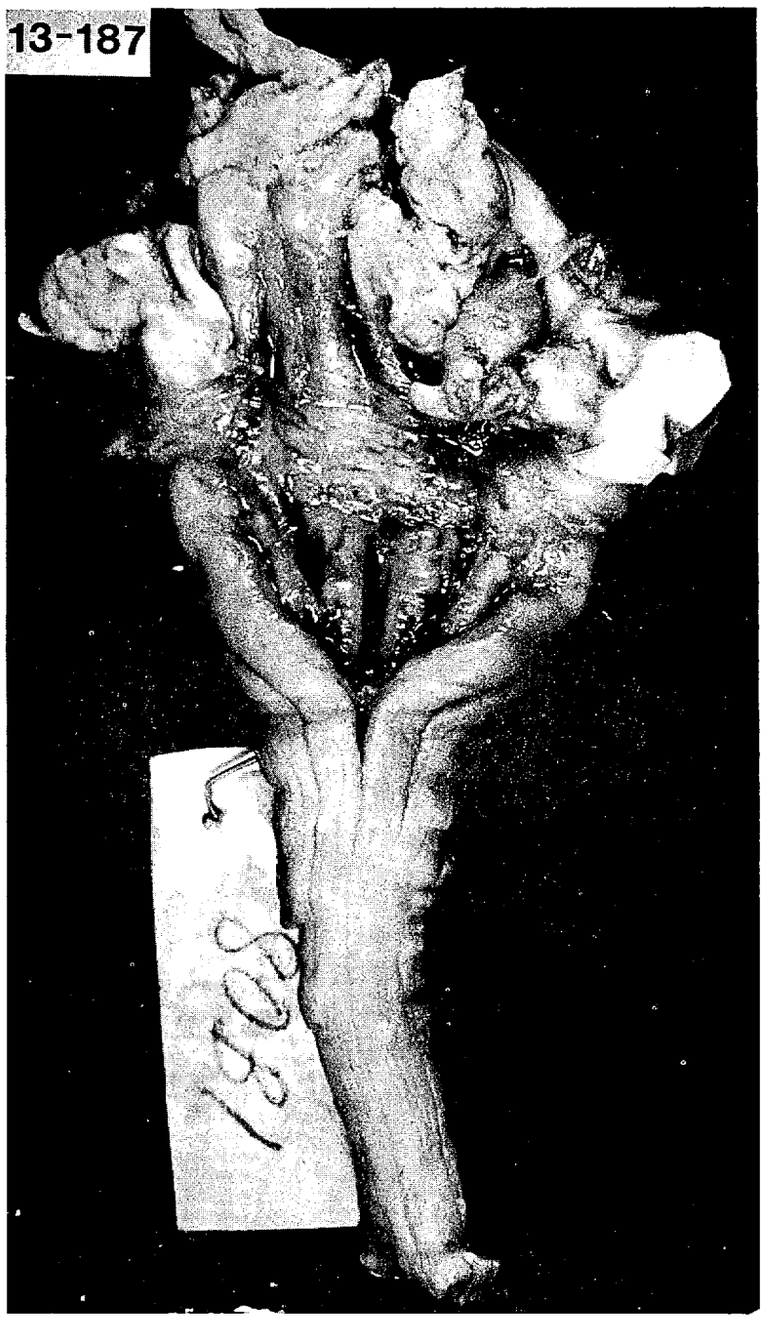

Figure 13-187. Photograph of the dorsal aspect of the brain stem of 80B1. Compare to Fig 13-186. X1.14

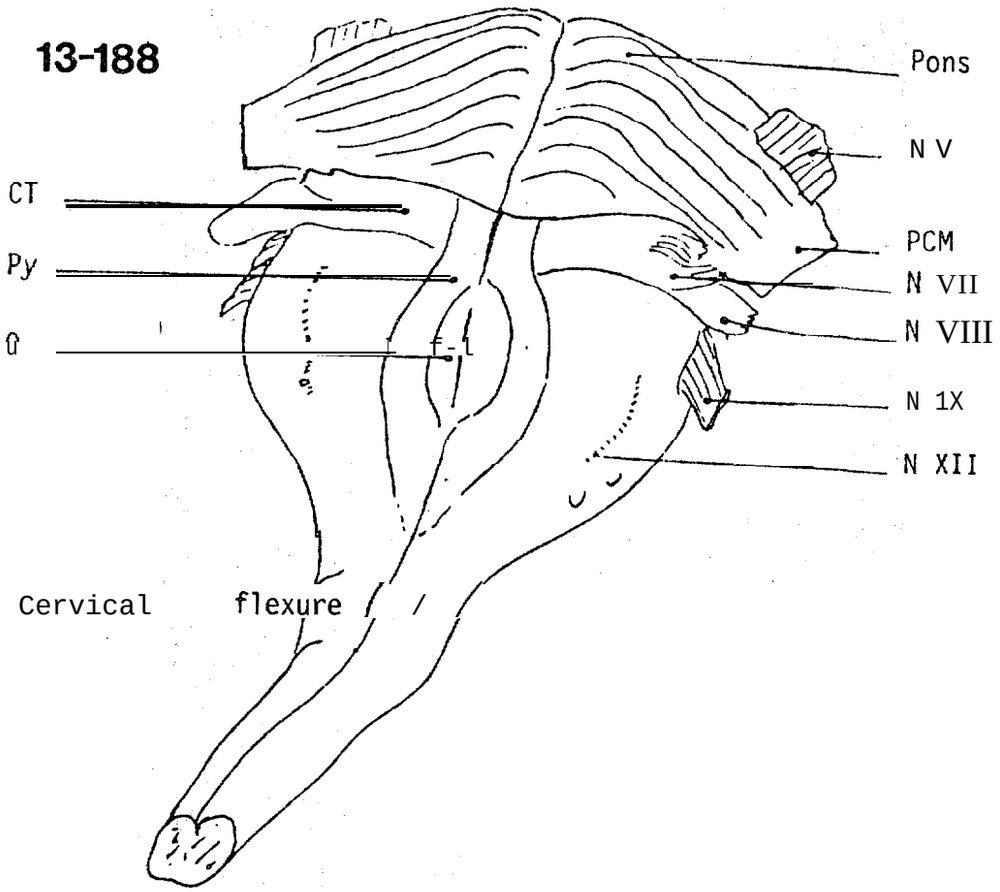

Figure 13-188. Sketch of the ventral aspect of the brain stem of 80B1. Note the trigeminal (V) and vestibulocochlear (VIII) nerves and the olive (0). CT-Corpus trapezoideum; N V - Nervus trigeminus; N VII - Nervus facialis; N VIII - Nervus vestibulocochlearis; N IX - Nervus glossopharyngeus; N XII - Nervus hypoglossus; O - Oliva; PCM - Pedunculus cerebellaris medius; Py - Pyramis (medullae oblongatae).

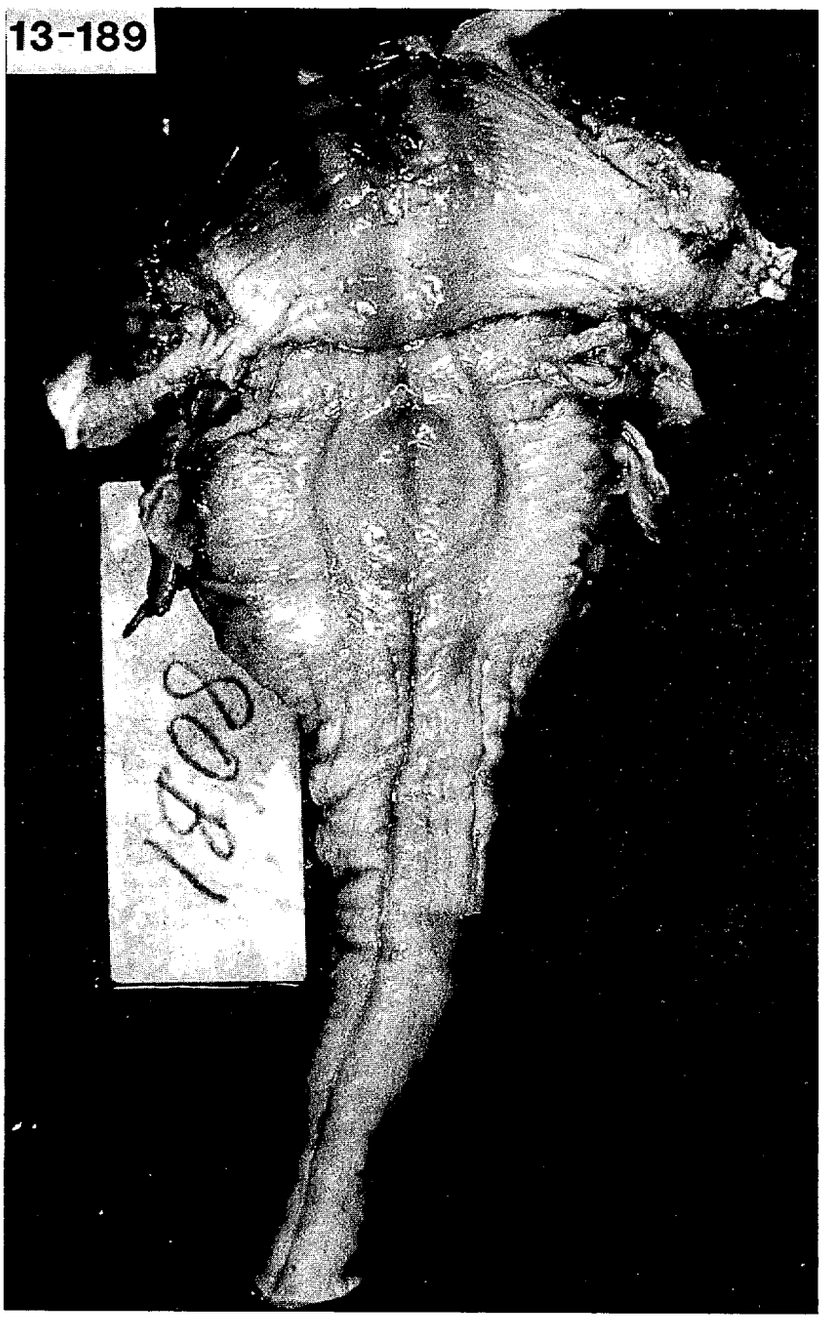

Figure 13-189. Photograph of the ventral aspect of the brain stem of 80B1. Compare to Fig 13-188. X1.14

Iv. Skin

General Characteristics The ordinary bowhead skin samples collected and supplied by RU 180 (79B3, 80B1, 80B2, 80B7) represented most of the various body regions (Fig 13-190). Samples obtained from Ingutuk variants (79B1, 79B2, 80B8) were also from most body regions (Fig 13-191), but more limited in quantity. The areas sampled included: the lower jaw; lower lip (inner and outer surfaces); upper lip (inner and outer surfaces); upper and lower eyelids; flipper (dorsal and ventral surfaces); fluke (dorsal and ventral surfaces); and dorsal, lateral, and ventral body wall regions. Most samples of the hard palate included parts of the gums (gingivae) containing many rows of baleen hairs and a very few small baleen plates. The surface area of the samples ranged between 1-7 cm by up to 15 cm. The dermis and some blubber of variable thicknesses were also present.

The formalin fixed skin of the bowhead whale was shiny and black over the dorsal surface and gradually changed to dark gray ventrally (Fig 13-192). Cream colored skin was present around the chin and to a variable extent on the ventral surface of the body (Fig 13-193) extending to near the urogenital orifice in some individuals. The preserved epidermis was thick with a rubbery consistency and ranged from 1 mm thick at the eyelid to 24 mm thick on the dorsal midline (Figs 13-190, 13-191). A yellowish coating of diatoms was present on most samples.

The skin samples obtained from the lower jaw showed rounded epidermal depressions between 1-3 mm in diameter at the surface (Fig 13-194) which extended inward about 4-8 mm. The apex of each funnel-shaped depression was directed toward the dermis (Fig 13-195) with a simple tactile hair emerging from the center. The tactile hairs were few in number with distances of 3-20 mm between them. Tactile hairs were present only on the margins of the upper and lower jaws, the chin, and in a V-shaped arrangement just caudal to the blowhole. They always emerged from black epidermis areas even in generally cream colored regions (Fig 13-196).

The epidermis of the bowhead was covered by a macroscopic, thin superficial layer of cells between 0.25 and 1 mm thick (the parakeratotic stratum corneum). This layer was present on both creamy and black skin and also on the mucosa of the hard palate and inner lips although thinner.

The epidermis of the flippers and the flukes varied in thickness in the various regions of their dorsal and of their ventral surface (Figs 13-

197, 13-198; Table 13-4). Deep macroscopic dermal papillae were visible on cut surfaces.

The epidermis of bowheads varied slightly in thickness (Table 13-5) and color in different regions. In general the trunk had the thickest epidermis. The epidermis of the head region was mostly a black to dark gray color with a variably sized area of cream colored skin on the chin (Figs 13-193, 13-194) caudally. Epidermal thickness also varied in different regions of the head (Table 13-6).

Variable numbers and sizes of epidermal lesions occurred in the skin of the various body regions. At least six morphological types were present on the samples received: (1) elevated smooth areas (7962 chin), (2) even granular areas (8068, Tag 96 dorsal midline), (3) elevated granular areas (80B2 lower eyelid), (4) shallow depressions (80B7, Tag 12A, chin ventral midline), (5) granular deep depressions (8068, Tag 84 ventral midline), (6) smooth deep depressions (80B8, Tag 3A outer upper lip). Table 13-7 lists the approximate sizes and morphological types. The data are biased by the large number of samples from one whale which was indicative only of the cooperation of one whaling captain and his crew in sampling. Data concerning the abundance of lesions on other whales was not available.

The gross appearance of the various lesions was distinct. Fig 13-200 shows both a depression lesion and a depression lesion with a granular raised central mass. Depression lesions also occurred in areas with even granular lesions (Fig 13-201). A granular depression lesion is shown in Fig 13-202 with an adjacent depression lesion with raised center. Shallow depression lesions are most noticeable in the cream colored areas (Fig 13-203) since they were frequently darker in color. The eyelids were also subject to lesions (Figs 13-204, 13-205) . Scanning electron microscopy showed that the simple depression lesions actually had a slightly elevated rim with a rather smooth interior (Figs 13-206, 13-207) which was occupied by an extensive and varied microflora of bacteria and diatoms (*Cocconeis* and *Navicula*). Depression lesions with raised centers (Fig 13-208) had a totally different group of microorganisms (bacteria, *Stauroneis* and *Navicula* diatoms) present (Fig 13-209) . Some lesions were fuzzy or filamentous in appearance (Fig 13-210). Increased magnification showed that the filaments were primarily chains of diatoms and bacteria (Fig 13-211). The smooth areas in the floor of some depression lesions (Fig 13-212) proved to be primarily chains of large bacilli with a few filamentous diatoms (Fig 13-213). Finally, the granular depression

TABLE 13-4 AVERAGE PRESERVED EPIDERMAL THICKNESS OF THE SKIN OF THE FLIPPERS AND FLUKES OF BOWHEADS

Region	Sample Numbers	Average Preserved Epidermal Thickness (mm)
Dorsal Flipper	80B1 : Tag 57, Tag 60, Tag 64, Tag 68. Tag 70, Tag 71, Tag 73	12.57
	80B7 : Tag 1A, Tag RF3, Tag 5A, Tag 7A Tag lOA, Tag TRF, Tag RF1	12.14
Ventral Flipper	80B1 : Tag 57, Tag 64, Tag 68. Tag 70, Tag 71, Tag 73	11.16
Dorsal Fluke	79B3; 80B2: Tag 11, Tag 30, Tag 32, Tag 34, Tag 35, Tag 38, Tag 40	11.86
	80B7 : Tag 2A, Tag 4A, Tag 3A	
Ventral Fluke	80B2 : Tag 35, Tag 40	9.66
	80B7 : Tag 4A	

TABLE 13-5 AVERAGE PRESERVED EPIDERMAL THICKNESS OF THE BODY SKIN OF BOWHEADS

Region	Sample Numbers	Average Preserved Epidermal Thickness (mm)
Dorsal 1/3 *	80B7 Tag 1/3 D 80B8 Tag 87	20
Dorsal 2/3	80B7 Tag 2/3 D 80B8 Tag 85	18
Lateral 1/3	80B6 Tag 1/3 L 80B8 Tag 86	20.5
Lateral 2/3	80B7 Tag 2/3 L 80B8 Tag 93	20.5
Ventral 1/3	80B7 Tag 1/3 V 80B8 Tag 98	20.75
Ventral 2/3	80B7 Tag 2/3 V 80B8 Tag84	18
Ventral 1/2	80B8 Tag 27, Tag 98	21.25
Lower Jaw	80B8 Tag 25, Tag 26	20.5

* 1/3 = 1/3 the distance from flipper to fluke.
1/2 = 1/2 the total body length.
2/3 = 2/3 the distance from flipper to fluke.

TABLE 13-6 AVERAGE PRESERVED EPIDERMAL THICKNESS OF THE SKIN OF HEADS OF BOWHEADS

Region	Sample Numbers	Average Preserved Epidermal Thickness(mm)
Blowhole	79KK1 80B8 Tag 96	20
Outer Upper Lip	79B3 80B7 Tag 1 80B8 Tag 3A, Tag 9	15.5
Outer Lower Lip	80B1 Tag 42, Tag 43, Tag 44, Tag 53, Tag 66 80B7 Tag 5, Tag 38 80B8 Tag 20, Tag 35, Tag 37, Tag 42	12.77
Eyelids	80B2 80B7 Tag LLEL, Tag LUEL 80B8-Tag 8	11.75
Lower Jaw	79B1 79B2 80B1 Tag 45, Tag 54 80B7 Tag 8A, Tag 12A, Tag 13A 80B8 Tag 22, Tag 28, Tag 30	17.55

TABLE 13-7 RELATIVE SIZES AND TYPES OF EPIDERMAL LESIONS ON BOWHEAD SKIN SAMPLES

Region	Sample Number	Lesion	
		Size*	Type
Lower Lip	8061 Tag 53	Medium	Depression
Chin	8067 Tag 11A	Small	Depression
Chin	80B7 Tag 12A	Small	Depression
Chin	7961 Tag 1	Large	Elev Smooth
Chin	7961 Tag 2	Large	Elev Smooth
Chin	79B1 Tag 2	Small	Elev Smooth
Lower Jaw 1' Caudally	80B8 Tag 22	Very Small	Depression
Lower Jaw 6' Caudally	8068 Tag 28	Medium	Depression
Lower Jaw 6' Caudally	8068 Tag 28	Large	Depression
Lower Jaw 4' Caudally	8068 Tag 30	Very Large	Depression
Outer Lower Lip	8068 Tag 37	Large	Deep Depression
Outer Upper Lip	80B8 Tag 3A	Large	Depression
Blowhole	79KK1	Large	Irregular Depression
Blowhole	79KK1	Large	Raised Granular
Blowhole	79KK1	Very Large	Raised Granular
Blowhole	79KK1	Very Large	Raised Granular
Blowhole	79KK1	Very Large	Raised Granular
Blowhole	79KK1	Very Large	Raised Granular
Blowhole	79KK1	Very Large	Raised Granular

(continued)

TABLE 13-7 RELATIVE SIZES AND TYPES OF EPIDERMAL LESIONS ON BOWHEAD SKIN SAMPLE (continued)

Region	Sample Number	Lesion Size*	Lesion Type
Lower Eyelid	80B2	Smal 1	
Dorsal Eyelid	80B8 Tag 11	Very Large	Depress w/ Raised Center
l/2a Ventral Body Wall	80B8 Tag 27	Medium	Even
l/2a Ventral Body Wall	80B8 Tag 27	Smal 1	E v e n
l/2a Ventral Body Wall	80B8 Tag 27	Med i urn	Depression
2/3 Dorsal Body Wall	80B8 Tag 85	Large	Depress w/ Raised
2/3 Dorsal Body Wall	80B8 Tag 85	Medium	Depress w/ Raised
2/3 Dorsal body Wall	80B8 Tag 85	Smal 1	Depression
1/3 Dorsal Body Wall	80B8 Tag 87	Large	Depression Gran
1/3 Dorsal Body Wall	80B8 Tag 87	Medium	Depression
Dorsal Midline 1 m Caudal of Blowhole	80B8 Tag 96	Very Large	Even Granular
Dorsal Midline 1 m Caudal of Blowhole	80B8 Tag 96	Large	Even Granular
Dorsal Midline 1 m Caudal of Blowhole	80B8 Tag96	Large	Even Granular
Dorsal Midline 1 m Caudal of Blowhole	80B8 Tag 96	Medium	Even Granular
1/3 Dorsal Body Wall	80B8 Tag 87	Large	Granular Depression
2/3 Dorsal Body Wall	80B8 Tag 85	Smal 1	Depress w/ Raised Center

(continued)

TABLE 13-7 RELATIVE SIZES AND TYPES OF EPIDERMAL LESIONS ON BOWHEAD SKIN SAMPLES (continued)

Region	Sample Number	Lesion	
		Size*	Type
2/3 Lateral Body Wall	80B8 Tag 93	Large	Depression
2/3 Lateral Body Wall	80B8 Tag 93	Small	Granular Depression
2/3 Lateral Body Mall	80B8 Tag 84	Large	Granular Depression
2/3 Ventral Body Wall	80B8 Tag 84	Small	Granular Depression
2/3 Ventral Body Wall	80B8 Tag 84	Large	Granular Depression
2/3 Ventral Body Wall	80B8 Tag 84	Small	Granular Depression
2/3 Ventral Body Wall	80B9 Tag 84	Medium	Granular Depression
1/3 Ventral Body Wall	80B9 Tag 88	Very Small	Depression
Dorsal Fluke	80B2 Tag 32	Very Large	Irregular Depression

* Very Small - about 1 mm; Small - 2-4 mm; Medium = 5-8 mm; Large = 10-15 mm; Very Large = 20 mm or more.

[a] 1/3 = 1/3 the distance from flipper to fluke.

1/2 = 1/2 the total body length

2/3 = 2/3 the distance from flipper to fluke.

TABLE 13-8 QUALITATIVE ESTIMATES AND TYPES OF MICROORGANISMS OCCURRING ON AND IN BOWHEAD UNBLEMISHED SKIN

Region	Sample Number	Organisms*	Abundance
Inner Upper Lip	80B8 Tag 9	None	
Inner Upper Lip	80B8 Tag 37	None	
Inner Upper Lip	80B8 Tag 34	None	
Outer Upper Lip	80B8 Tag 9	Gom or Staur	few
Outer Upper Lip	80B8 Tag 37	Bat, Coc and Gom or Staur	many, few, several
Inner Lower Lip	80B8 Tag 42	None	
Outer Lower Lip	80B8 Tag 42	Coc and Gom or Staur	few, several
Outer Lower Lip	80B1 Tag 53	Gom or Staur	few
Outer Lower Lip	80B1 Tag 66	None	
Lower Jaw	80B1 Tag 43	Bac and Pro	many, few
Upper Eyelid	80B9 Tag 11	None	
Lower Eyelid	80B8 Tag 11	None	

(continued)

TABLE 13-8 QUALITATIVE ESTIMATES AND TYPES OF MICROORGANISMS OCCURRING ON AND IN BOWHEAD UNBLEMISHED SKIN (continued)

Region	Sample Number	Organisms*	Abundance
1/3 Dorsal Body Wall	80B8 Tag 87	Coc and Gom or Staur	few, many
1/3 Dorsal Body Wall	80B8 Tag 1/3D	None	
1/3 Lateral Body Wall	80B7 Tag l/3L	Coc and Gom or Staur	few, several
1/3 Ventral Body Wall	80B7 Tag l/3V	Gom or Staur	several
2/3 Dorsal Body Wall	80B7 Tag 2/3D	Gom or Staur	few
2/3 Dorsal Body Wall	80B7 Tag 85	Coc and Gom or Staur	few, several
2/3 Lateral Body Wall	80B7 Tag 2/3L	None	
2/3 Lateral Body Wall	80B8 Tag 93	None	
Cranial Dorsal Fluke	80B2 Tag 17	Coc and Nav	
Caudal Dorsal Fluke	80B2 Tag 35	Coc and Nav	

* Bac = Bacteria - unknown; Coc = *Cocconeis* sp.; Gom = *Gomphonema* sp.; Nav = *Navicula* sp.; Pro = Protozoan - possible; Staur = *Stauroneis* sp.

TABLE 13-9 QUALITATIVE ESTIMATES AND TYPES OF MICROORGANISMS OCCURRING ON AND IN BOWHEAD SKIN EPIDERMAL LESIONS

Lesion Type	Sample Number	Organisms*	Abundance
Depression with Raised Center	80B8 Tag 85	Bac and Poss Pro	many, few
Depression with Raised Center	80B8 Tag 84	Bac and Gom or Staur	many, several
Shallow Depression	80B8 Tag 84	Bac	many
Granular Depression	80B8 Tag 87	Nav and Bac	many, many

* Bac = Bacteria - unknown; Coc = *Cocconeis* sp.; Gom = *Gomphonema* sp.; Nav = *Navicula* sp. ;
Pro = Protozoan - possible; Staur = *Stauroneis* Sp.

TABLE 13-10 NUMBER OF DERMAL PAPILLAE PER mm2 IN DIFFERENT REGIONS OF BOWHEAD WHALE SKIN

Regional	Sample Number	Ordinary Bowheads		Ingutuk Variant		Sample Number
		Dermal	Sensory	Dermal	Sensory	
Inner Upper Lip	80B1 Tag 100	8	4	4	1	80B8 Tag 9
Outer Upper Lip				5		80138 Tag 9
Inner Lower Lip	80B1 Tag 43	5	1	22	3	80B8 Tag 34
Inner Lower Lip	80B1 Tag 53	11	1	4	1	80B8 Tag 37
Inner Lower Lip	80B1 Tag 66	5		16		80B8 Tag 42
Outer Lower Lip	8061 Tag 43	7		9		80B8 Tag 20
Outer Lower Lip	80B1 Tag 53	6		7		80B8 Tag 37
Outer Lower Lip	8061 Tag 66	8		9		80B8 Tag 42
Caudal Dorsal Flipper	80B1 Tag 57	5				
Caudal Ventral Flipper	80B1 Tag 57	9				
l/3a Dorsal Body Wall	80B7 Tag 1/3D	6		10		80B8 Tag 87
1/3 Lateral Body Wall	80B7 Tag l/3L	7		5		80B8 Tag 86
1/3 Ventral Body Wall	80B7 Tag l/3V	5		6		80B8 Tag 88
2/3[b] Dorsal Body Wall	80B7 Tag 2/3D	5		5		80B8 Tag 85
2/3 Lateral Body Wall	80137 Tag 2/3L	6		7		80B8 Tag 93
2/3 Ventral Body Wall	80B7 Tag 2/3V	5		5		80B8 Tag 84
Cranial Ventral Fluke	80B2 Tag 17	7				
Upper Eyelid					10	8068 Tag 11
Lower Eyelid					6	80B8 Tag 11

a 1/3 the distance from flipper to fluke.

[b] 2/3 the distance from flipper to fluke.

TABLE 13-11 REGIONAL VARIATION OF DISTANCE OF DERMAL PAPILLAE TIPS FROM THE BOWHEAD EPIDERMAL SURFACE

Region	Sample Number	Papilla Type	Distance (mm)
Lower Eyelid Skin	8068 Tag llLL	Sensory	0.070
Lower Eyelid Conjunctival	8068 Tag 11LL	Dermal	0.005
Upper Eyelid Skin	80B8 Tag 11LU	Sensory	0.090
UpperE yelid Conjunctival	8068 Tag llLU	Dermal	0.010
Inside Upper Lip	8057 Tag 12	Sensory	0.100
Outside Upper Lip	8067 Tag 12	Sensory	00170
Chin	8067 Tag lL	Dermal	7*5
Caudal Dorsal Flipper	8061 Tag 57	Dermal	5.0
Caudal Ventral Flipper	8061 Tag 57	Dermal	4*375
Cranial Dorsal Fluke	80B2 Tag 17	Dermal	4.750
Cranial Ventral Fluke	80B2 Tag 17	Dermal	3.750
1/3 Dorsal Body Wall[a]	8068 Tag 87	Dermal	10.250
2/3 Dorsal Body Wall	80B8 Tag 85	Dermal	9.0
2/3 Ventral Body Wall	80B8 Tag 84	Dermal	15.625*
2/3 Ventral Body Wall	8068 Tag 84	Dermal	13.5**

* Adjacent to shallow depression lesion.

** Adjacent to depression lesion with raised center.

a 1/3 or 2/3 the distance from flipper to fluke.

lesions also had a rim, but the interior was rough (Fig 13-214). High magnification revealed a still different floral composition of Cocconeis only (Fig 13-215). Based on the limited sampling that was possible from most of the bowheads of this study, it appeared that epidermal lesions occurred on all regions of the body with higher concentrations located on the lower lips, chin, and jaw caudally onto the ventral body wall (Fig 13-216). See RU 780 for description of the general pathology of lesions of the head.

The epitheliums of the hard palate was about 1 mm thick, black to gray in color and appeared granular with very small rounded elevations. The baleen hairs and plates extended from the right and left sides of the upper jaws (Fig 13-217) lateral to the narrow hard palate. The baleen emerged from smooth gray tissue which represented the gums (gingivae) of the whale. The epitheliums which bore the baleen was much thicker than the epitheliums of the hard palate. The baleen at the medial epithelial elevation of the gingiva consisted of many rows of fine white baleen hairs which ranged from 6-30 mm in length. This type of baleen resembled the coarse hair of some mammals in being simple with one small baleen hair emerging from each orifice in the gingiva. Toward the upper lip (laterad), the baleen became denser, coarser and darker in color (Fig 13-217). This second type of baleen was both longer and compound, i.e., several simple baleen hairs fused into one large hair emerged from each orifice in the gingiva. Such compound baleen hairs were 0.5-1 mm in diameter at the gum line. Further laterad the fusion of the compound hairs produced baleen plates (Fig 13-217) .

In front of the baleen, the upper lips and snout had a restricted area of well defined, elevated, light colored, papillae about 1 mm in diameter and about 0.5 mm tall (Fig 13-218). The epidermis thickened rostrad and laterad to the papillary area becoming similar to the skin of other body regions.

Dermal papillae were abundant throughout the integument and interdigitated with the epidermis (Figs 13-193, 13-219). The superficial (reticular) dermis was dense irregular white fibrous connective tissue which varied from 2-4 mm in thickness. The underlying hypodermic or blubber was largely adipose connective tissue laced with distinct strands of more regularly arranged dense white fibrous connective tissue and blood vessels (see RU 480). The blubber between the dorsal and ventral epidermises of the flippers and flukes possessed more abundant coarse white fibers than other regions (Fig 13-

220) with the flukes having more than the flippers (Figs 13-196, 13-220, 13-221) .

Microscopic Characteristics The epidermis of bowhead skin was covered by a continuous layer of stratified squamous epithelial cells, the stratum corneum, consisting of between 12-60 rows of flattened to oval cells (Fig 13- 222). Their long axes were parallel to the skin surface. For the most part, they retained their nuclei and their cytoplasm contained abundant keratin. Their nuclei were varied in shape, but were generally flattened and oval with the cytoplasm containing small amounts of fibrillar material. The stratum corneum showed keratinization, but was parakeratotic. The parakeratotic stratum corneum was thinnest on the inner surface of the lips and outer eyelids and was thickest on the epidermis of the chin. The stratum corneum which extended into the funnel-shaped depressions around the tactile hairs showed several rows of cells with few nuclei (Fig 13-223) and was more typically keratinized. Most regions of the parakeratotic stratum corneum showed concentrations of epidermal rods arising from the stratum basale cells around the tips of the dermal papillae. Most of the cells of the parakeratotic stratum corneum also exhibited variable numbers of melanin granules within the pigmented epidermis.

Although the gross appearance of bowhead skin was smooth and shiny, scanning electron microscopy clearly showed flaking of the surface squamous cells. One of the most highly keratinized regions was the inner lip epithe-1 ium (Figs 13-224, 13-225). The surface cells apparently were desquamating individually with the" cells showing close apposition to each other and surface ridges similar to those seem in terrestrial mammals. The epidermal surface of the outer lip (Fig 13-226) showed more flaking with aggregates of desquamating cells. Fig 13-227 illustrates some of the normal inhabitants of the minute cracks and crevices that occur in normal whale skin exposed to the marine environment. The epidermis on the dorsal, lateral and ventral aspects of the body trunk (Figs 13-228 through 13-233) had a somewhat rougher texture with a more varied population of microorganisms (see Table 13-8). See RU 1280 also for diatom analysis. The epidermal rods that arose from the stratum basale cells covering the ends of the dermal papillae maintained their rodlike configuration through the stratum corneum and showed on the surface as rosettes of squamous cells.

The epidermal cells deep to the parakeratotic stratum corneum comprised a typical stratum spinosum. The cells were rounded, oval, or poly-

hedral with oval to round nuclei (Fig 13-234). The nuclei showed scanty, marginally placed, clumped chromatin. Many of the cells had melanin granules in their cytoplasm (Fig 13-234). All cells of this region had a distinct fibrous texture with cell boundaries appearing thick under the light microscope. This "thickness" was the result of highly folded cell membranes and desmosomes, clearly demonstrated by transmission electron microscopy (Fig 13-235). All cells in the stratum spinosum contained tonofilaments arranged in parallel bundles as well as large numbers of ri bosomes and pol yribosomes (Fig 13-235). Keratohyalin granules of variable diameter were scattered throughout the cytoplasm (Figs 13-236, 13-237) . At the ultrastructural level , the nuclei of the spinosal cells were large and irregular (Fig 13-237) with eccentric to centrally located nucleoli and marginal heterochromatin. Some cells contained melanin granules near the nucleus (Figs 13-237, 13-238). The deeper cells of the stratum spinosum were rounder and smaller than the more superficial cells. More cellular fibrous elements were seen in the cells of the stratum spinosum of flukes and flippers than elsewhere.

The number of keratohyalin granules in the. epidermis decreased in the spinosal cells as they were pushed toward the stratum corneum. The number of keratohyalin granules varied in different body regions, being most abundant in the stratum spinosum of the 'chin and outer lip. The cytoplasm of most spinosal cells contained a considerable number of melanin granules (Fig 13-239) . Melanin granules were most abundant in the stratum basale, but were also present in cells of the parakeratotic stratum corneum (Fig 13-222).

The stratum basale consisted of a single layer of columnar cells with basally located oval nuclei. The PAS reaction showed a basement membrane between the dermis and the epidermis. Melanocytes were present between the basal cells and occasionally in the first layers of the stratum spinosum. They were very well developed, large and possessed dendritic processes (Figs 13-239, 13-240) . Numerous cytoplasmic undulations of the basal cells interdigitated with the superficial layer of the dermis (Fig 13-241) and maintained contact with the basal lamina that separated epidermis from dermis (Fig 13-242) . The basal cells also had lateral interdigitations with adjacent cells which produced wide areas of apparent intercellular space. These wide areas were merely the interfolding of the undulating adjacent cell membranes with more desmosomes than occurred in the other two strata (Fig 13-243).

Histologic examination of a shallow depression lesion 13 mm diameter X 1.875 mm deep showed that the parakeratotic stratum corneum was intact

and 375 µm thick. The parakeratotic layer had small Gram positive bacilli between cells and on the surface. Occasional bacteria and diatoms (Stauroneis and/or Gomphonema) were present in the parakeratotic stratum corneum around the lesion (Fig 13-244). A granular depression lesion 6 mm in diameter X 2.75 mm deep showed the parakeratotic layer missing and a V-shaped area of the stratum spinosum also gone (Fig 13-245). The outer 875 µm of spinosal cells on the depression surface were different in appearance than those located deeper below the depression. The modified layer was penetrated to its full depth in several loci by chains of large Gram positive bacilli. The surface of the depression was also coated with bacilli, some Stauroneis and/or Gomphonema, and many spherical cells about 3.74-7.5 µm in diameter. Some of the spherical cells were in between the cell layers with the bacilli. Flaking of the modified spinosal layer in the depression resulted in exposure of the tips of the epidermal rods. A depression lesion of 11 mm diameter X 3.6 mm deep with a raised center 3.2 mm high X 2.5 mm in diameter undercut all around except at the attached basal area, is shown in Fig 13-246. The central mass sat upon a small pedestal-like, 0.5 mm diameter portion of the spinosum which maintained contact with the underlying spinosal layers. No exposed epithelial rods were present within the lesion. The depression surface and, particularly, the raised mass had several foci of Stauroneis and/or Gomphonema and small Gram positive bacilli which extended inward penetrating most of the raised mass. Occasional 21 x 55 µm nucleated protozoan-like cells were also on the central mass surface with concentrations of these cells in the clefts of the parakeratotic mass as well. A 6 mm diameter X 2 mm deep lesion with raised center had the central mass permeated with chains of large Gram positive bacilli and Stauroneis and/or Gomphonema between the cells with some bacteria inside the cells. No exposure of epithelial rods was visible. The central mass was also undercut almost completely around except at the small pedestal-like basal attachment to the underlying spinosal layers (Fig 13-247). Cocconeis and Navicula (diatoms) also occurred in some of the other types of lesions, either separately or in conjunction with other diatoms or bacteria (Table 13-9).

Long dermal papillae (Fig 13-239, 13-240) interdigitated with the epidermis exhibiting definite regional variations in number of papillae per square millimeter (Table 13-10). The regions with the greatest numbers were the upper lip where the majority were large and sensory and the lower lip where fewer sensory papillae were mixed with ordinary papillae. The eyelids

possessed an intermediate number of both types of papillae. The general body wall had the lowest number, all of which were of the non-sensory type. The ordinary dermal papillae varied in basal diameter and tended to be oval in cross section. Secondary papillae arose from the basal portions of large dermal papillae. Above the origin of the secondary papillae, the main dermal papilla became smaller and smoother resembling the secondary papillae. All papillae within a given area ended at about the same level, but the level of papillary termination varied in distance from the epidermal surface according to epidermal thickness (Table 13-11).

Blood vessels occurred in all dermal papillae, but consisted of only arterioles, capillaries, and venules at the most distal levels. Even the smallest secondary papillae contained capillaries. Nerve fibers also occurred in the basal portions of the dermal papillae with the papillae of the inner lips and eyelids possessing numerous nerve fibers (Fig 13-248) and Herbsti-like encapsulated sensory nerve endings.

The reticular dermis consisted of dense irregular connective tissue with collagen fibers continuing into the loose connective tissue of the dermal papillae (Figs 13-222, 13-239). Elastic fibers were present throughout this tissue which also contained many arteries, veins, large venous sinuses and nerve fiber bundles (Fig 13-240).

Tactile hair structure Tactile hairs were present in specimens from 79KK1 (blowhole); 7961, 79B2, 80B1, and 80B7 (chin); and 80B7 (upper lip). The tactile hairs extended above the surrounding epidermal surface 1-1.5 cm after exiting the epidermis in the center of a funnel-shaped depression which was 4 mm in depth. Some hairs among our specimens appeared to be broken off which may have introduced errors into our measurements. The dermal sheath surrounding the tactile hair follicle continued into the hypodermic for 20-30 mm (Figs 13-194, 13-196). The hairs emerged singularly, but occasionally split above the epidermal surface into two or three small units.

Longitudinal and frontal serial sections through tactile hairs and follicles from 80B1 and 80B7 were examined. The hair follicle had the usual components: a central shaft (tactile hair) surrounded by an epidermal sheath which was enveloped in a dermal sheath (Fig 13-249). In longitudinal sections the hairs were seen exiting through the center of the funnel-shaped depression of the epidermis. Midway between the rim of the funnel and the base of the funnel (Fig 13-250), the typically mammalian stratum corneum thinned. Close

to the shaft the stratum corneum became thinner resembling stratum disjunctum and housed bacteria, diatoms and possibly protozoa (Fig 13-251). The free shaft extended through the epidermal layer and 3-3.2 cm below the superficial dermis level into the hypodermic (Fig 13-252) . The epidermis surrounded the free shaft down through the superficial dermis and was in turn surrounded by a dense, vascular dermal sheath. The dense irregular connective tissue of the dermal sheath contained numerous nerve fibers and what appeared to be receptor organs. These structures were seen lying 2.8-4.1 mm below the general dermal-epidermal junction (Fig 13-253). A few nerve fiber bundles were seen surrounding the follicle as well as near the base of the follicle. The receptor organs appeared similar to the Herbsti-type. The majority of these structures lay 0.5 mm superficial to the sinus area. Arteries and nerves appeared to enter the follicle at its base in the hypodermic (Fig 13-254). The nerves coursed superficially and branched within the dermal sheath. " The blood vessels entered sinuses which formed a complete sinusoidal network surrounding the epidermal portion of the tactile hair follicle (Fig 13-255). The sinuses extended only three-fifths of the way up the follicle toward the dermal-epidermal junction. The hair shaft originated at the bulb which surrounded the dermal papilla of the follicle (Fig 13-254) . No glands were seen associated with the follicle.

Serial frontal sections near the dermal-epidermal junction of the surrounding skin showed the hair shaft with a thin cortex and solid medulla (Fig 13-249). The epidermal layer of the follicle had a heavily keratinized stratum corneum adjacent to the shaft. The epidermis of the funnel shaped depression extended below the surrounding dermal-epidermal junction forming an extension of the epidermis into the hypodermic (Fig 13-252). Frontal sections through this depressed area showed the same epidermal-hair shaft relationship (Fig 13-249).

Baleen Serial sections of the baleen hairs showed that individual hairs started as single tube-like structures arising from the epithelial cells in contact with the connective tissue papillae. Each single tubule consisted of a medulla of vascularized loose connective tissue surrounded by the stratum basale. Spinosal cells produced hard keratin peripherally around the tubule (Fig 13-256) forming several layers which increased in number as the tubules extended beyond the papillae to approach the surface of the gingiva (Fig-257). The medulla of a baleen hair consisted

of an outer cellular zone and an inner highly vascular zone (Fig 13-258) with little loose connective tissue. The medulla continued into the free shaft of the baleen hairs occupied with a reticulum of dead avascular connective tissue (Fig 13-258).

Further laterad in the gingiva, single baleen hairs arising in clusters joined each other with fusion of their cortices to form compound baleen hairs consisting of three to twelve tubules (Fig 13-259). As compound baleen hairs approached the gingival surface, their common, hard keratin, outer cortex became more circular forming a single layer of hard keratin around several originally single tubules (Fig 13-260) which emerged from the gingival surface as a large compound baleen hair with several medullary spaces (Fig 13-261).

Skin-oil Interactions Prudhoe Bay crude oil was cohesive enough at room temperature that the oil formed a thick film on a nonagitated artificial sea water surface. This cohesiveness permitted only a portion of the aquarium surface to be coated. After slow cooling to 3°C, the oil slick was 4 mm thick and covered 3/4 of the water surface. When a piece of preserved whale skin cooled to 3°C at the clear end of the aquarium was lifted through the cold oil slick, the film of oil remained intact over the entire piece until the skin surface was lifted more than 10 mm above the water surface after which the oil film separated and drooped over the sides of, the piece of skin. Submerging the oil coated skin back through the oil film left most of the oil film on the water surface or it floated free of the skin shortly after full submergence leaving small patches of oil on all preserved skin samples tested. This minor agitation of the oil slick broke up the film leaving oil patches on the water surface surrounded by the undisturbed film. Oil globules of varying sizes were carried beneath the surface with the skin samples, but did not remain suspended beneath the water surface of the undisturbed aquarium. They floated upward beneath the surface oil film and patches making them thicker (up to 10 mm) producing an undulating water-oil interface while the oil-air interface remained smooth. Alternatively they created additional oil patches on the water surface that was clear. No globs or globules remained suspended within the water column after a few minutes.

The number and size of the small patches of oil adhering to the various types of preserved skin samples after a simulated breathing cycle of 3 surfacings and submergence (breathing rolls) seemed to be in direct propor-

tion to (1) the number of cycles and (2) the roughness of the skin sample. Oil adtiered to the vibrissae and their surrounding epidermal depressions (Figs 13-262, 13-263) and various other rough areas (Figs 13-264, 13-265). The epidermal lesions and abrasion (Figs 13-266, 13-267, 13-268) showed variable degrees of "oil adhesion. Diatom covered regions around vibrissal depressions, and in some cases even the normal smooth appearing skin seemed to show oil adhesion'. The least amount of oil adherence seemed to occur in the smoothest areas, i.e., those areas where the sea water film tended to be maintained with the least disruption as contact was made with the oil slick. These results are only valid for formalin fixed skin samples in an undisturbed cold artificial sea water situation in a laboratory.

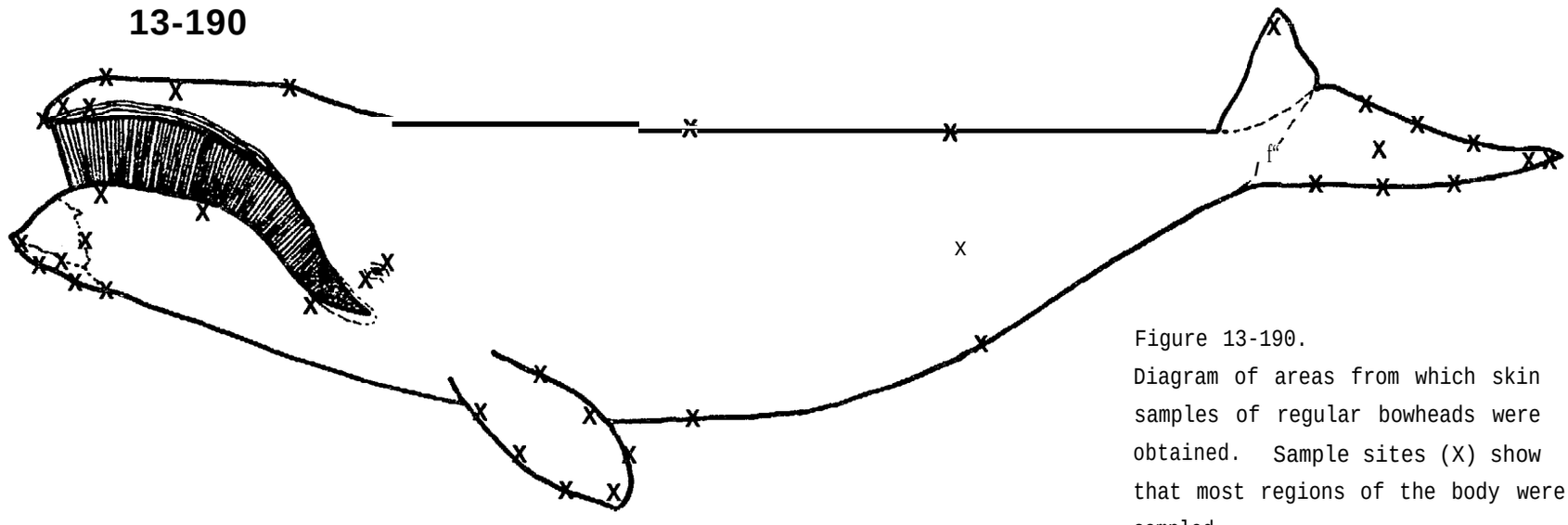

Figure 13-190.
Diagram of areas from which skin samples of regular bowheads were obtained. Sample sites (X) show that most regions of the body were sampled.

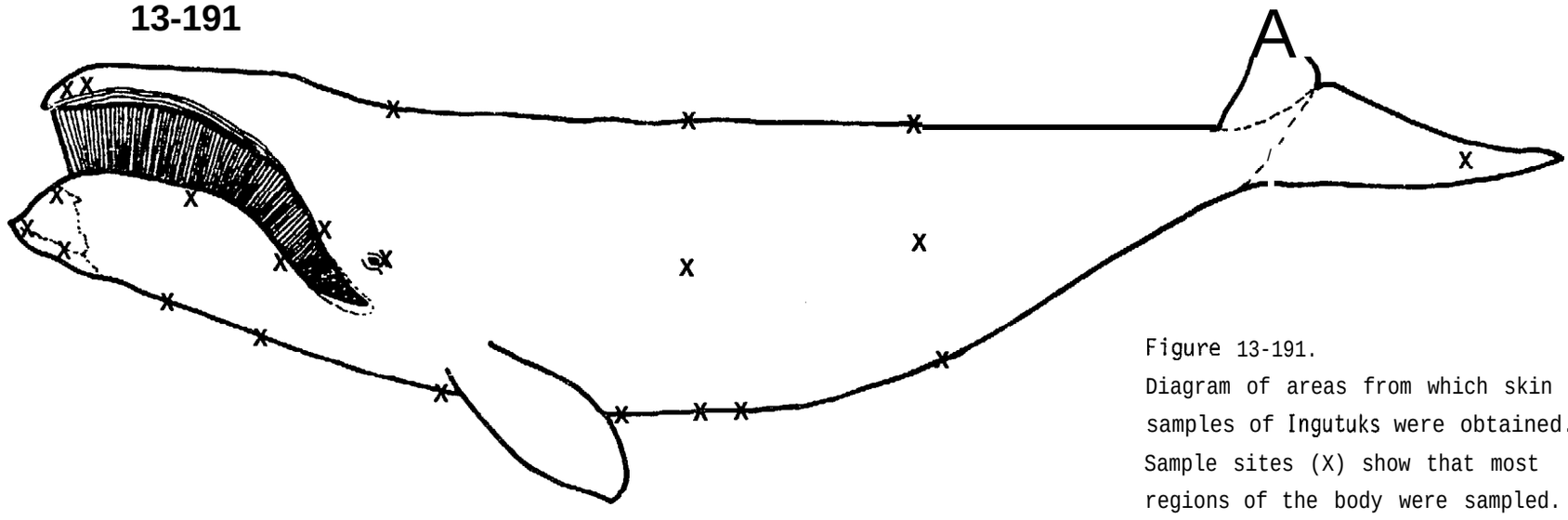

Figure 13-191.
Diagram of areas from which skin samples of Ingutuks were obtained. Sample sites (X) show that most regions of the body were sampled.

Figure 13-192. Photograph of the upper lip, 79B3. The cut edge slightly visible toward the ruler shows the thin epitheliums of the inner lip (left) with the gradual change to thicker epidermis of the outer surface (right).

Figure 13-193. Photograph of the cut edge of chin skin, 80B1. The nonpigmented areas of the chin are creamy in color. Without pigment in the epidermis, the pigmentation in the vascular dermal papillae clearly shows the extent of the papillary interdigitation with the epidermis (arrows). Immediately beneath the epidermis is the dense irregular connective tissue of the dermis (1)) and beneath this the hypodermic (Ii) or blubber. The surface of this sample is more desquamated (flaky) than usual.

Figure 13-194. Photograph of a skin sample with vibrissa from the upper lip, 79B2. The outer upper lip, the outer lower lip, and the chin have distinct regions in which vibrissae are located. Each vibrissa emerges from a funnel shaped depression (arrowheads) which is surrounded by a slightly elevated portion of the epidermis. The elevations are not light colored as they appear here, but are as dark as the surrounding epidermis. The white area (Se) is an apparent healed scar (See RU 780).

Figure 13-195. Photograph of the cut surface of the same sample in Fig 13-194 showing extent of a tactile hair follicle. The funnel shaped depression from which the hair shaft emerges shows as a triangular black area at the epidermal surface. The epidermis dips below the normal dermal-epidermal junction (arrow) extending" ultimately to the base of the hair follicle. The hair shaft and foilicle were cut off with only the edge of the dermal sheath (DS) surrounding the follicle indicating the extent of the foilicle penetration into the hypodermic (H).

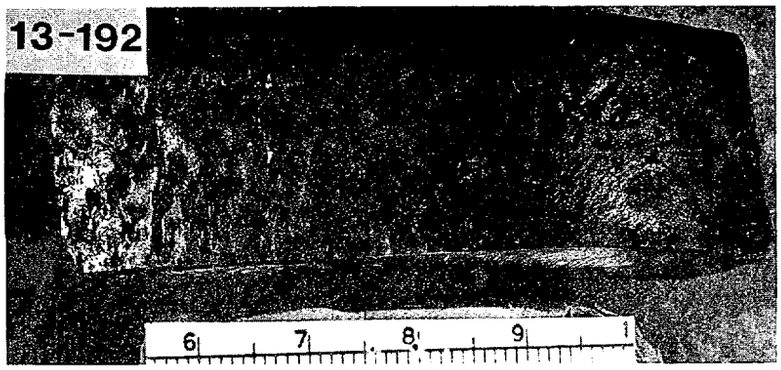
13-192

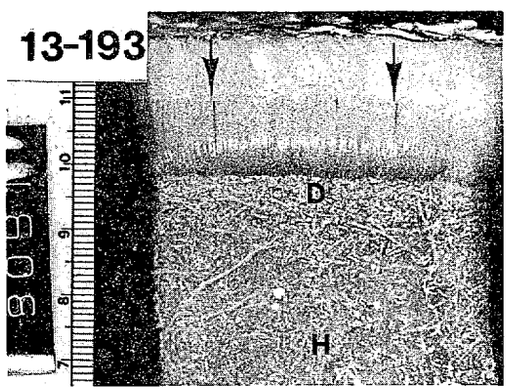
13-193
D
H

13-194
Sc

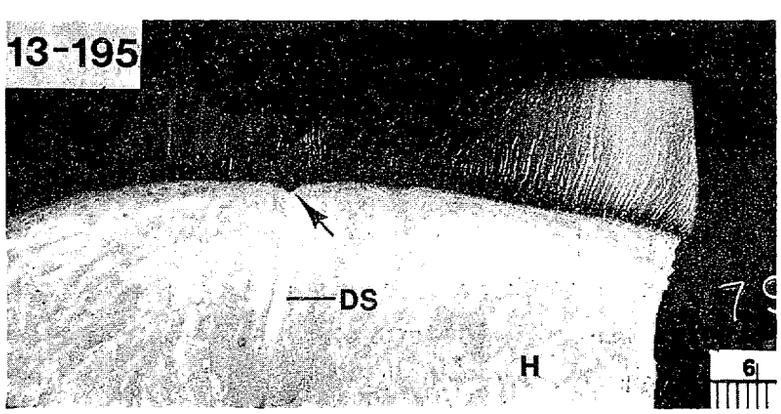
13-195
DS
H

Figure 13-196A. Photograph of chin skin, 8091, Tag 42. Vibrissae (arrows) always emerge from pigmented epidermis even in otherwise non-pigmented regions.

Figure 13-196B. Photograph of the cut surface of the same sample. The vibrissae extend toward the ruler having emerged through the pigmented areas of the epidermis (arrow). Some of the dermal sheath (DS) with pigmented epidermis extending into it is visible.

Figure 13-197. Photograph of the cut edge of the flipper caudal border, 80B7. The skin covering' the dorsal and ventral surface of the caudal border of the flipper unites in a smooth arc rather than meeting at a sharp angle. Dorsal epidermis is toward the top of the picture. The dermis (D) from both layers of skin fuses without hypodermic. Only blood vessels (arrows) mark the theoretical fusion line. Note the irregularly arranged white collagenous fibers in the dermis.

Figure 13-198. Photograph of the cut edge of a plug sample through the left fluke, 8097. The thicker dorsal epidermis (Table 13-1) is up. The dermis (D) of each skin layer shows distinctly with the central portion of the fluke composed of highly tendinous hypodermic (H). The arrow indicates a large artery. The black spot in the hypodermic is a piece of epidermal stratum corneum that flaked off during handling.

13-196A

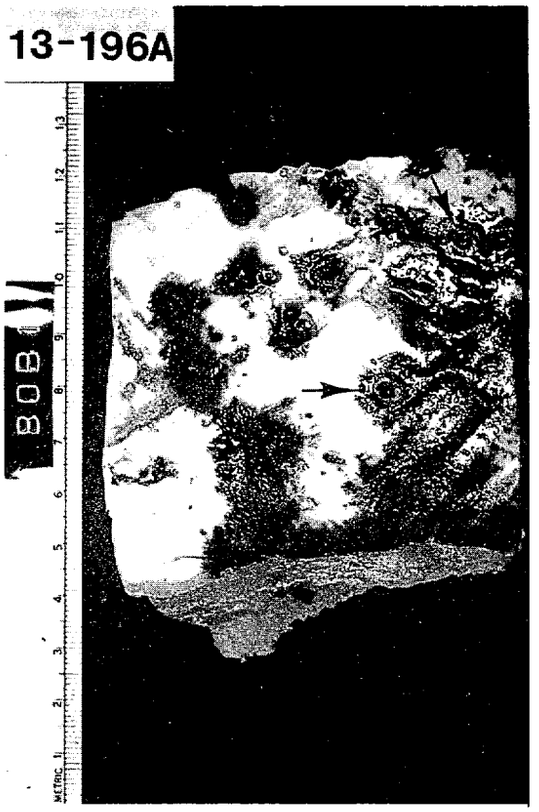

13-196B

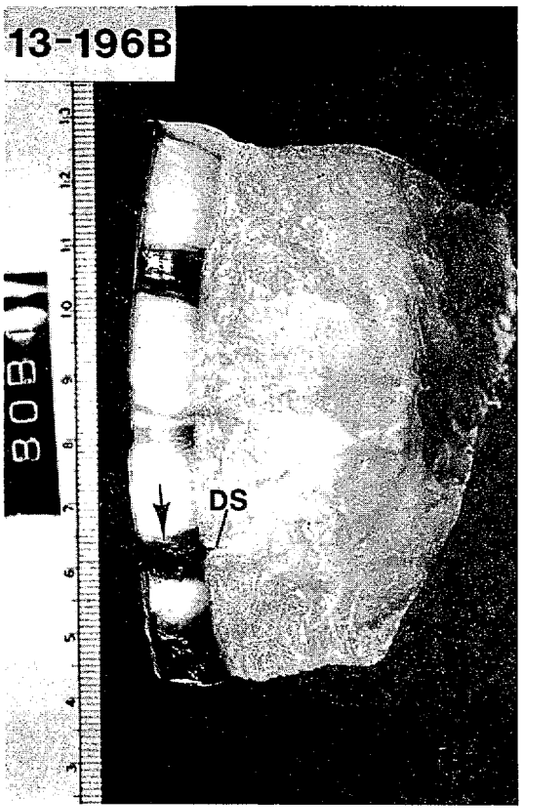

13-197

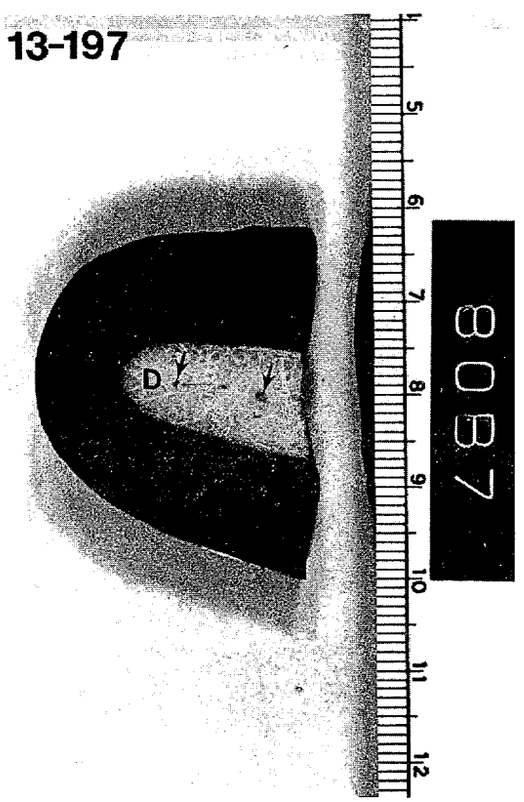

13-198

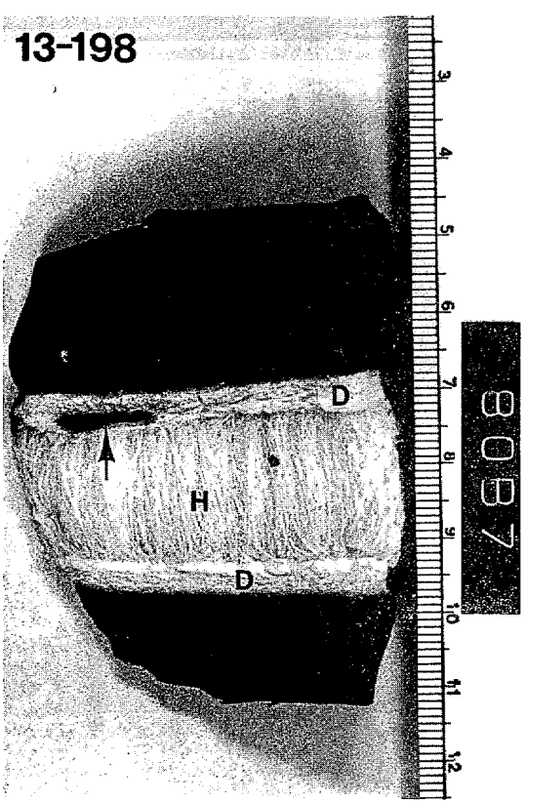

Figure 13-199A. Photograph of dorsal midline skin, 80B7. Sample taken 1/3 the distance from flipper to fluke. The top of the picture is toward the head. Note the transverse ridges of the epidermal surface. Their significance is unknown, but they are found on all formalin fixed samples from the body trunk. The uniform black color is typical. The caudal portion (lower left) has a large area where the stratum corneum was lost during handling.

Figure 13-199B. Photograph of a similar sample from 2/3 the distance from flipper to fluke. The transverse ridges are not as pronounced. The white area is a probable healed scar.

Figure 13-200. Photograph of skin with lesions from ventral midline 80B8, Tag 27. A medium sized, smooth depression lesion (L) is on the left and a small depression lesion with raised center (arrow) is at the right. Note again the transverse ridges in the normal areas. Cranial is toward the left of the photograph.

Figure 13-201. Photograph of the cranial portion of sample 80B8, Tag 93. Sample taken 2/3 distance from flipper to fluke along the lateral midline. The ridge of a smooth depression lesion is above the 7/8" mark, diatom patches are above the 1 1/4" mark and an even granular lesion is above the 2" mark.

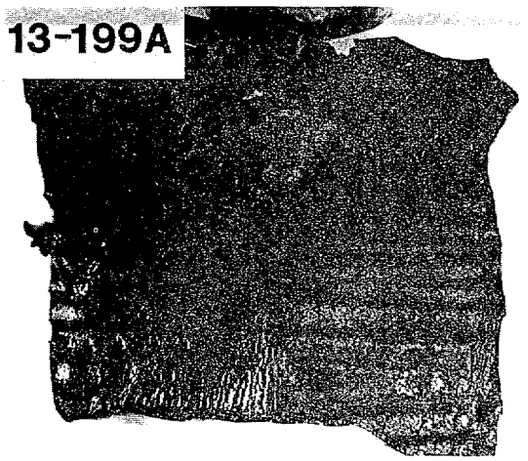
13-199A

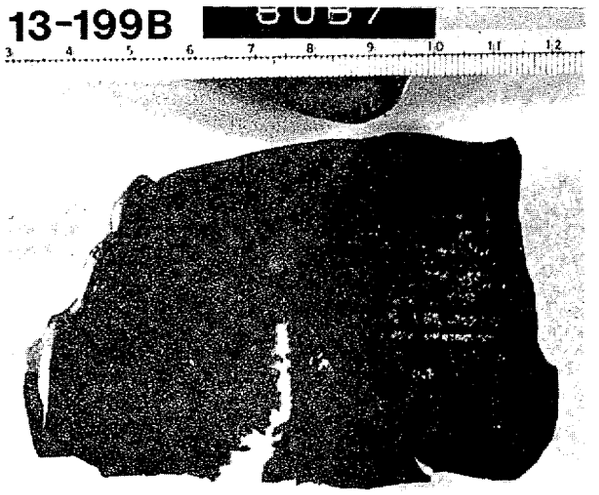
13-199B

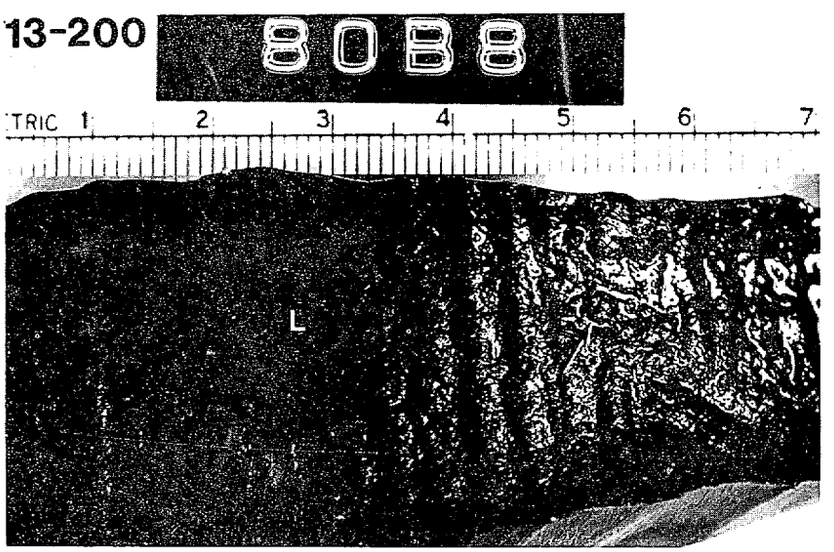
13-200
8088
TRIC 1 2 3 4 5 6 7
L

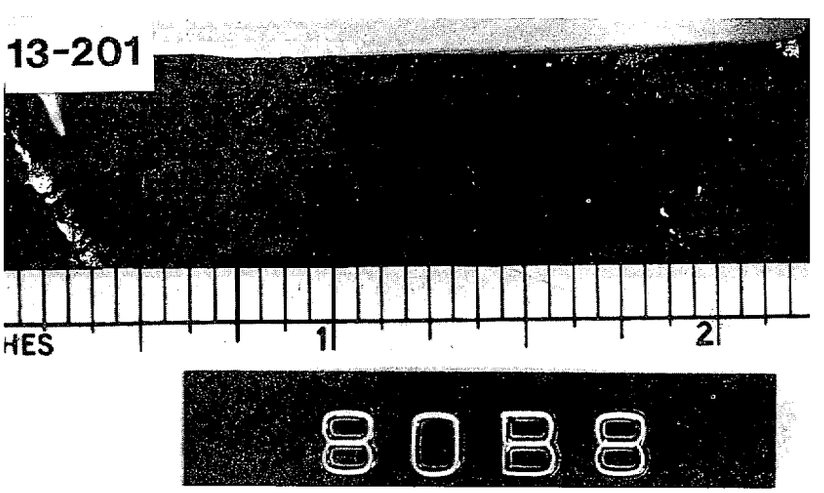
13-201
HES 1 2
8088

Figure 13-202. Photograph of lesions on the ventral midline, 8068, Tag 84. The sample is from 2/3 the distance from flipper to fluke. The left lesion is a small depression with raised center. On the right is a granular depression lesion.

Figure 13-203. Photograph of small, shallow, smooth depression lesions on chin ventral midline, 80B7, Tag 12A. Small depression lesions show most readily on the nonpigmented areas since they are frequently brownish in color (arrows).

Figure 13-204. Photograph of a medium depression lesion with raised center on upper eyelid, 80B8, Tag 11. The central mass is grainy to filamentous in appearance. Note that the ridge and central mass are not affected by the wrinkling of the thin epidermis caused by fixation shrinkage.

Figure 13-205. Photograph of elevated granular and even granular lesions on lower eyelid, 80B8, Tag 11. The even granular lesion appears as a rough area (arrowhead) on the otherwise smooth but folded epidermis; The remainder of the lesions are the elevated granular type.

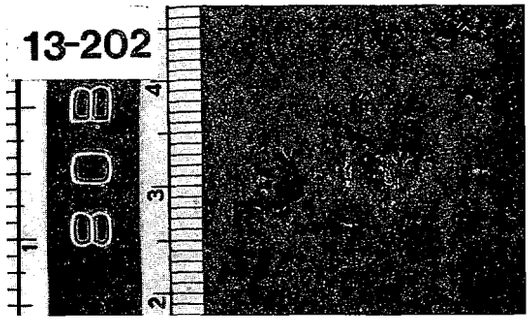
13-202
1
2
3
4

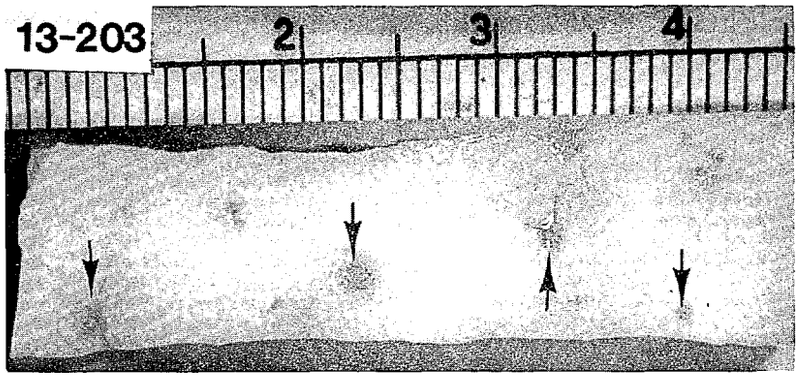
13-203
2
3
4

13-204

13-205

Figure 13-206. Scanning electron photomicrograph of a very small depression lesion on the ventral body wall, 80B8, Tag 86. Location is 1/3 the distance from flipper to fluke. The normal desquamating area around the depression is normal skin. The ridge of the crater appears smoother indicating the cells are not flaking off as fast and, hence, the ridge. The walls and floor of the crater are intermediate in amount of flaking. X35

Figure 13-207. Much higher magnification scanning electron photomicrograph of a portion of the floor of the lesion in Fig 13-206. The roughness of the floor is produced not only by desquamating cells (D), but to a large extent by microorganisms, notably Cocconeis (C) and bacteria (B). X3 ,500

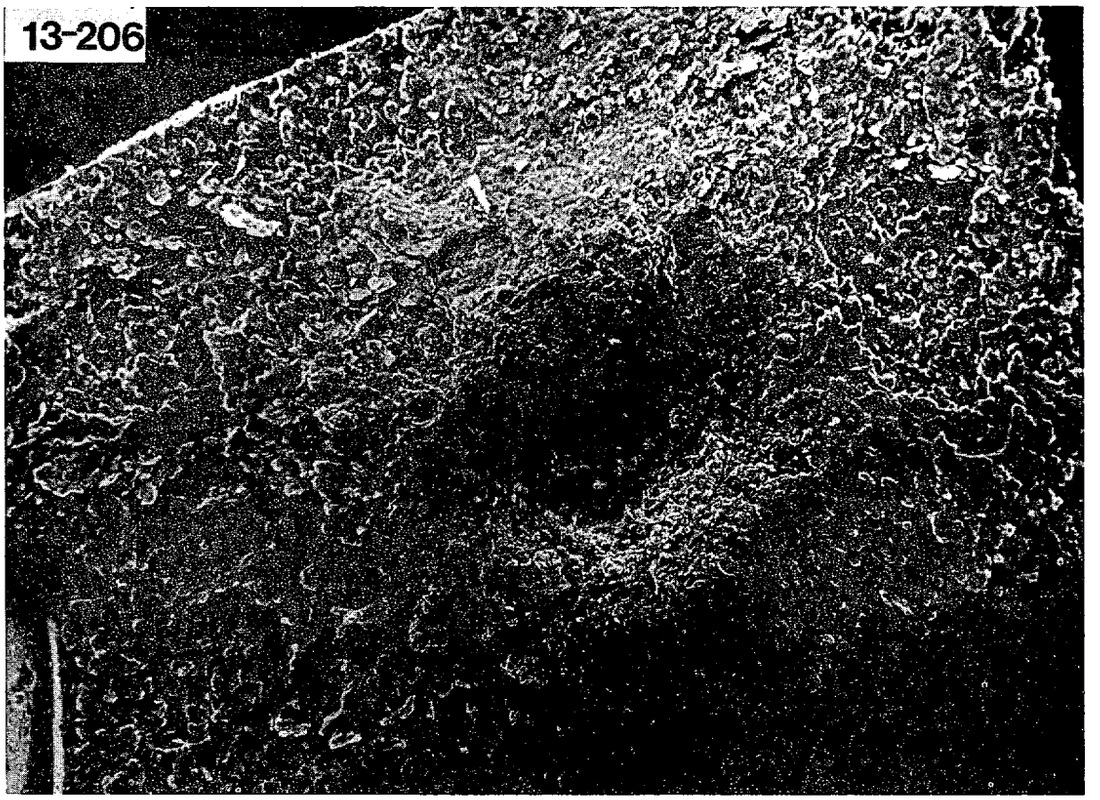
13-206

13-207
B
C
D

Figure 13-208. Scanning electron photomicrograph of a 1/4 piece of a depression lesion with raised center, 80B8, Tag 85. The ridge (R) is the crater rim, but the depression exists mainly as a crevice (arrowhead) undercutting a central mass (M) of cells which fills most of the region. C = cut surfaces. X37

Figure 13-209. Much higher magnification scanning electron photomicrograph of the crevice in Fig 13-208. Desquamating cells are also present, but the microflora is drastically different. than in depression lesions. Probable Stauroneis (S) or Gomphonema (G) plus bacteria are present. X1,700

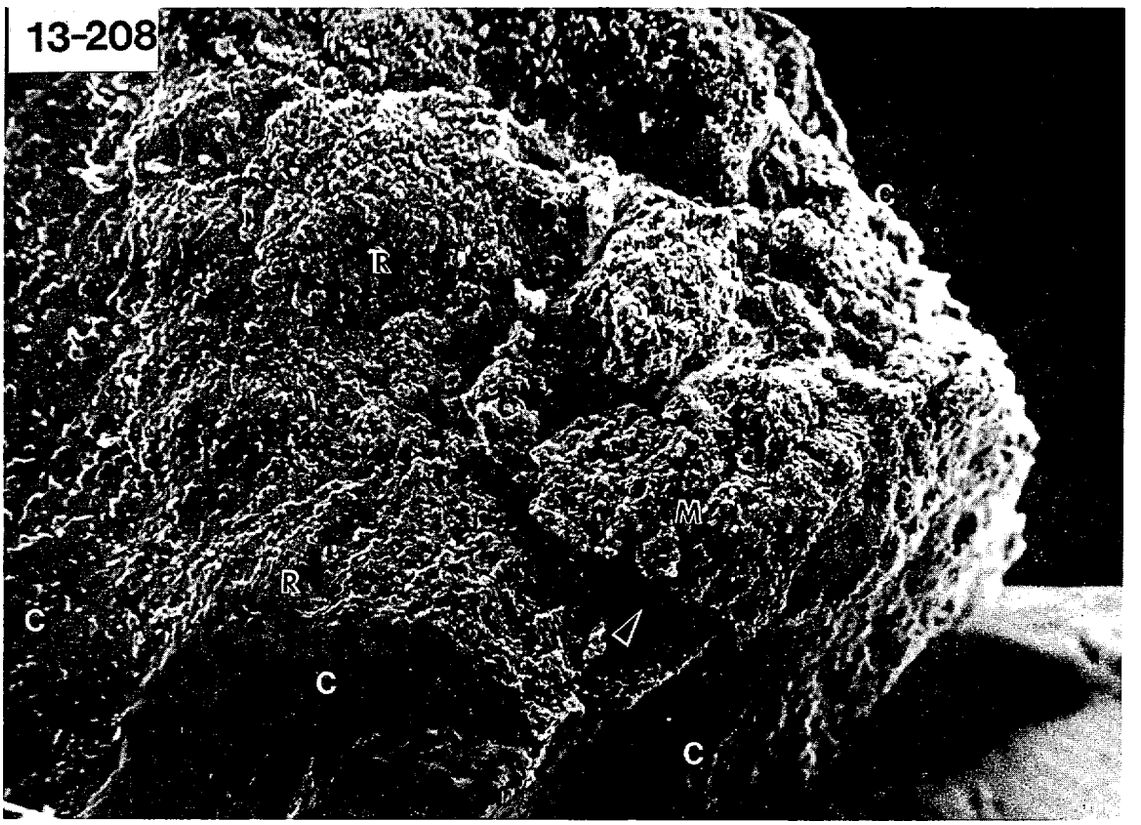
13-208
R
C
M
R
C
C
C

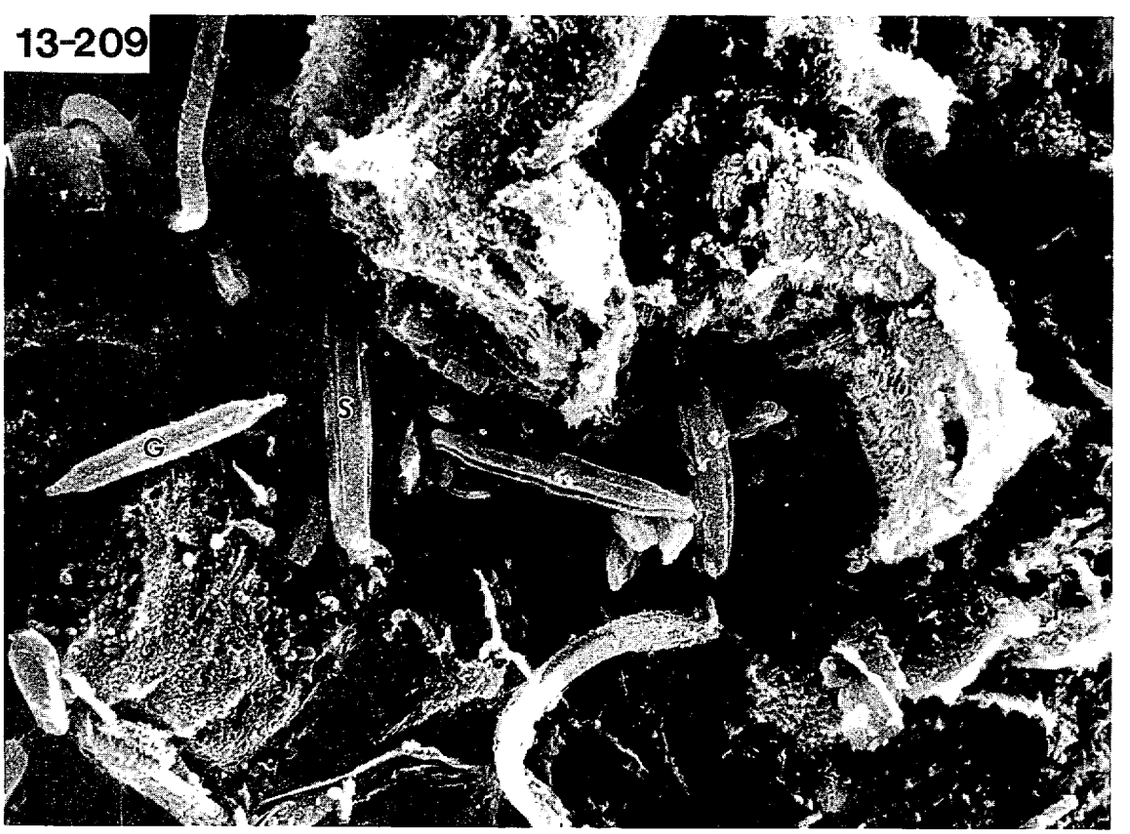
13-209
G
S

Figure 13-210. High magnification scanning electron photomicrograph of a portion of the floor of a large granular depression, 80B8, Tag 87. The granular appearance is produced by increased desquamation of large flakes of epidermal cells (F) and greater than normal exposure of the epidermal rods (R) whose circular cell arrangements produce rosettes. Filamentous masses of microflora (arrows) are spread over some areas. X300

Figure 13-211. Higher magnification scanning electron photomicrograph of microflora in Fig 13-210. Masses of small bacilli (arrows) and filaments of bacteria (B) form the meshwork. The red blood cells (R) are contamination from the collection process. X3,100

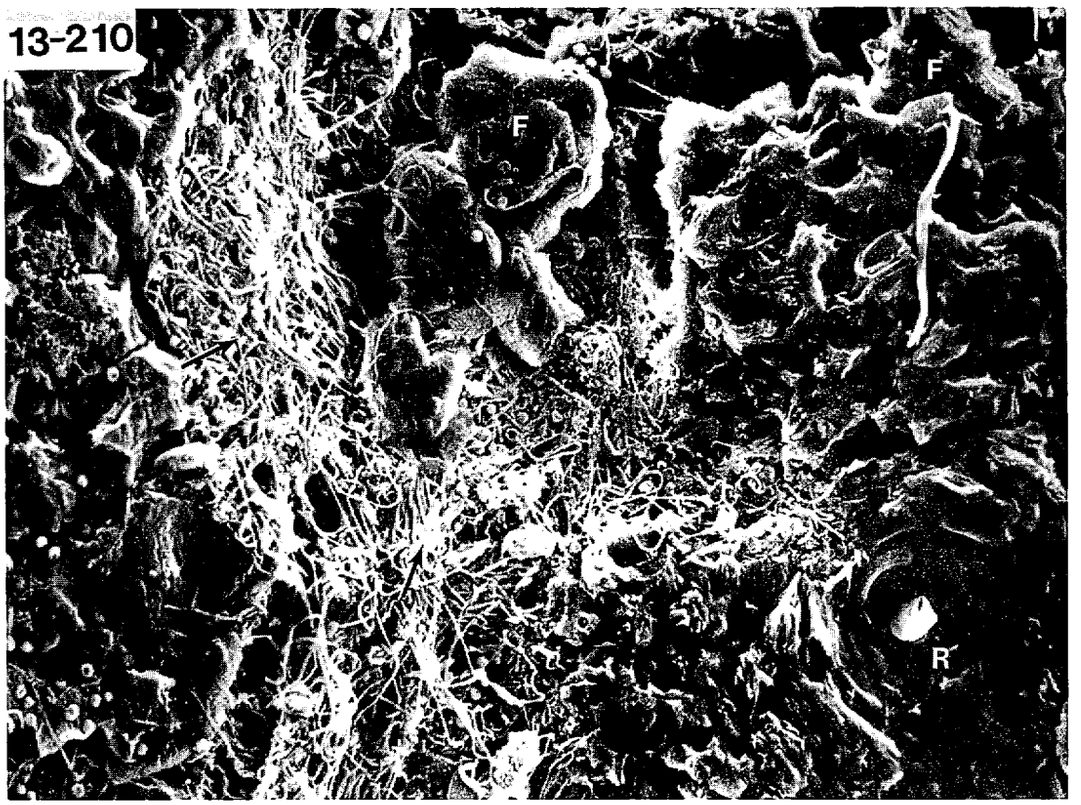
13-210
F
F
R

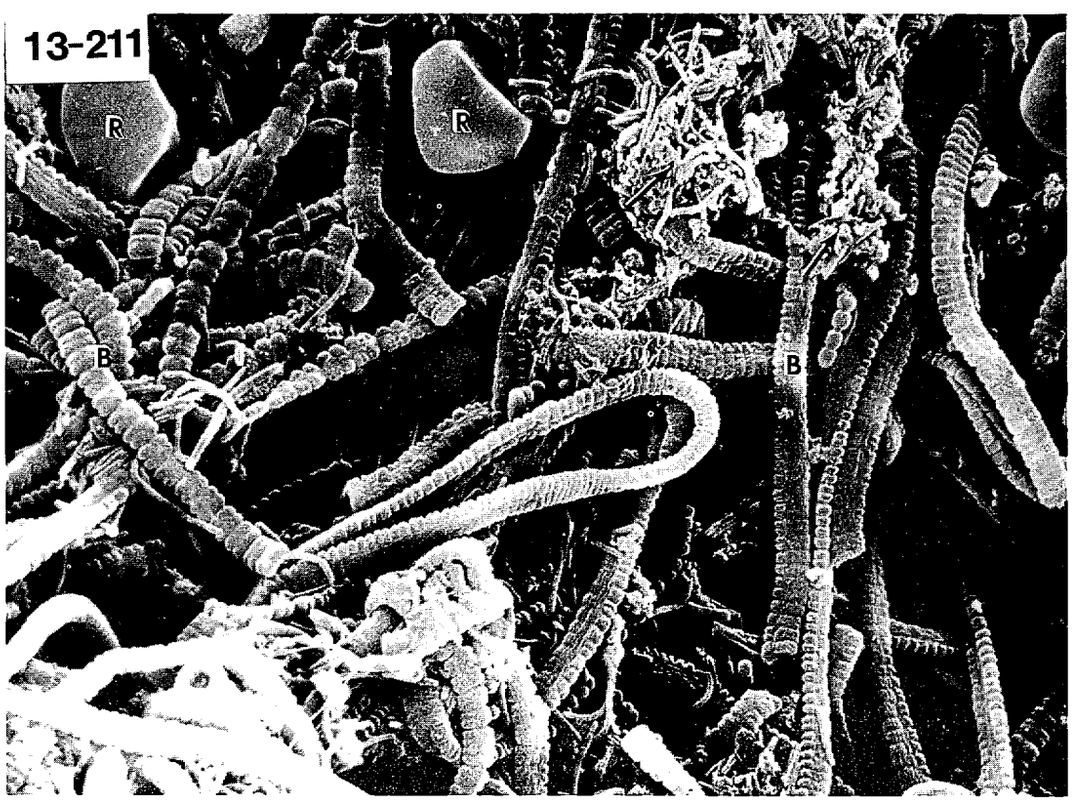
13-211
R
R
B
B

Figure 13-212. Scanning electron micrograph of the floor of a depression lesion, 80B8, Tag 27. The crater wall (W) becomes smoother toward the floor (F) of the depression. Small, much smoother appearing areas (S) occur on the floor surface. The arrowhead indicates a crevice produced by the trimming of the sample. X27

Figure 13-213. Higher magnification scanning electron photomicrograph of a very smooth area in Fig 13-212. The smooth effect is produced primarily by an aggregation of bacteria (B). X2 ,700

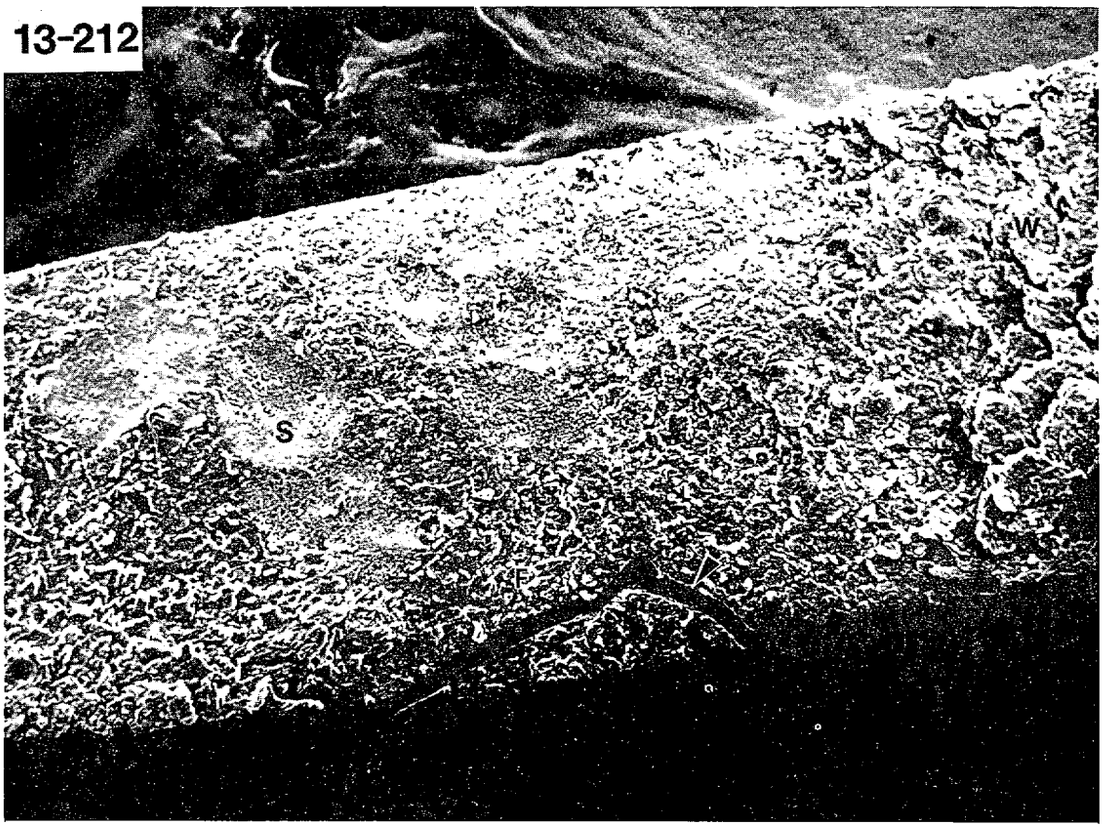
13-212
W
S

13-213
B
B

Figure 13-214. Scanning electron micrograph of a small granular depression lesion, 80B8, Tag 93. The elevated rim (R) is wel 1 demonstrated. Note the granular appearance of the crater floor (F). The crevices are part of the effects of the lesion. X31

Figure 13-215. Higher magnification scanning electron photomicrograph of the outer surface of the elevated rim (R) of Figure 13-214. The desquamating cell surface is occupied by a concentration of Cocconeis diatoms (arrowheads). See label "C" on Fig 13-207 for greater magnification of this diatom. The rosette of an epidermal rod (E) is at the upper right. X370

13-214

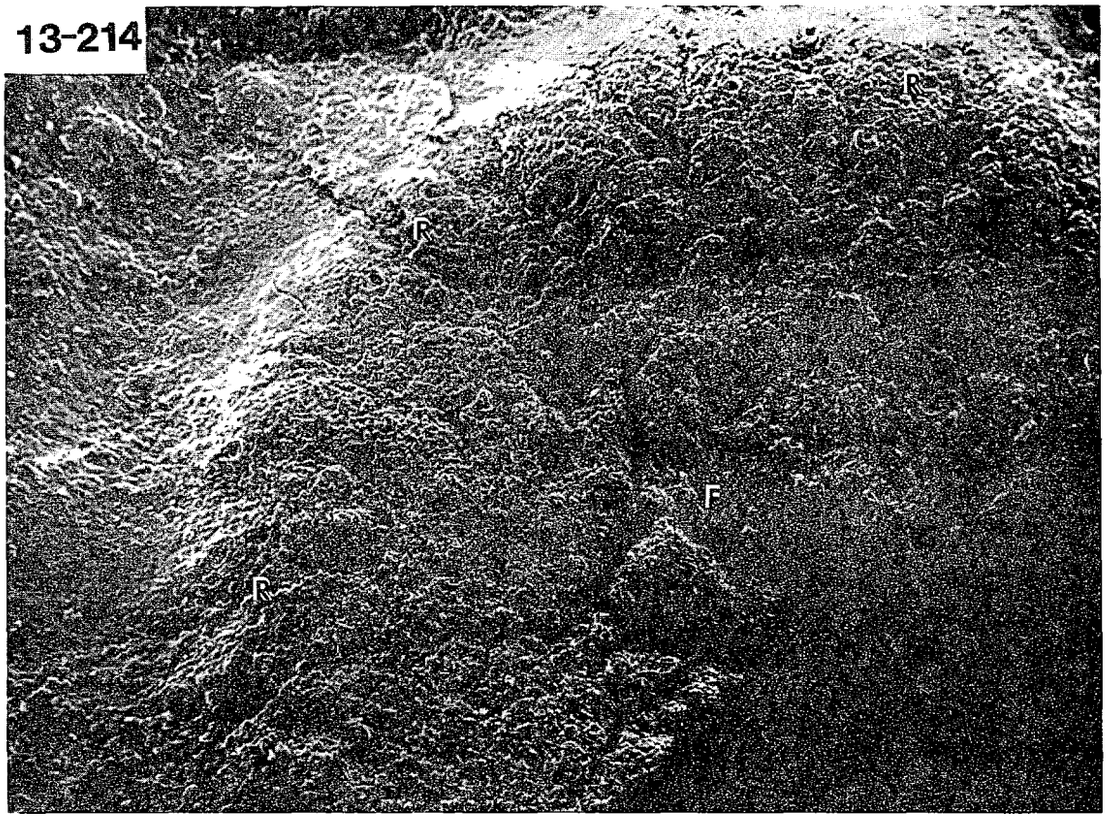

13-215

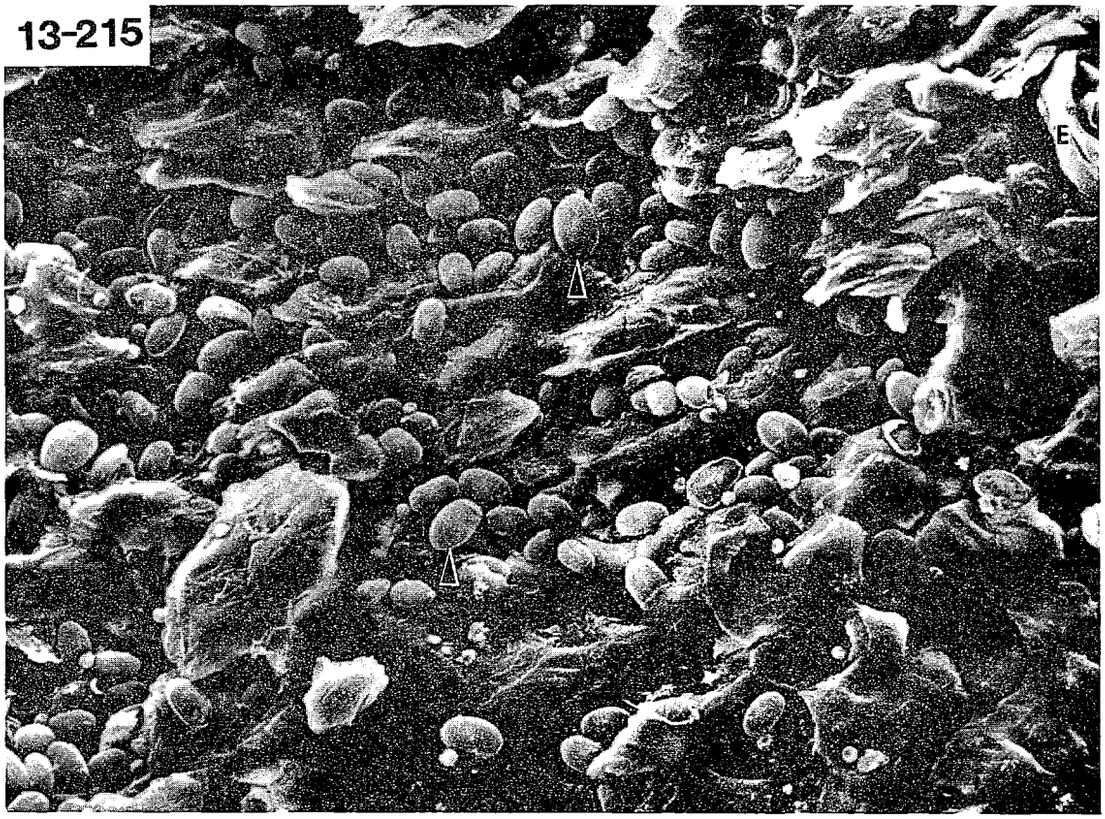

Figure 13-216. Outline of the bowhead illustrating the skin sample locations (X) that have one or more epidermal lesions.

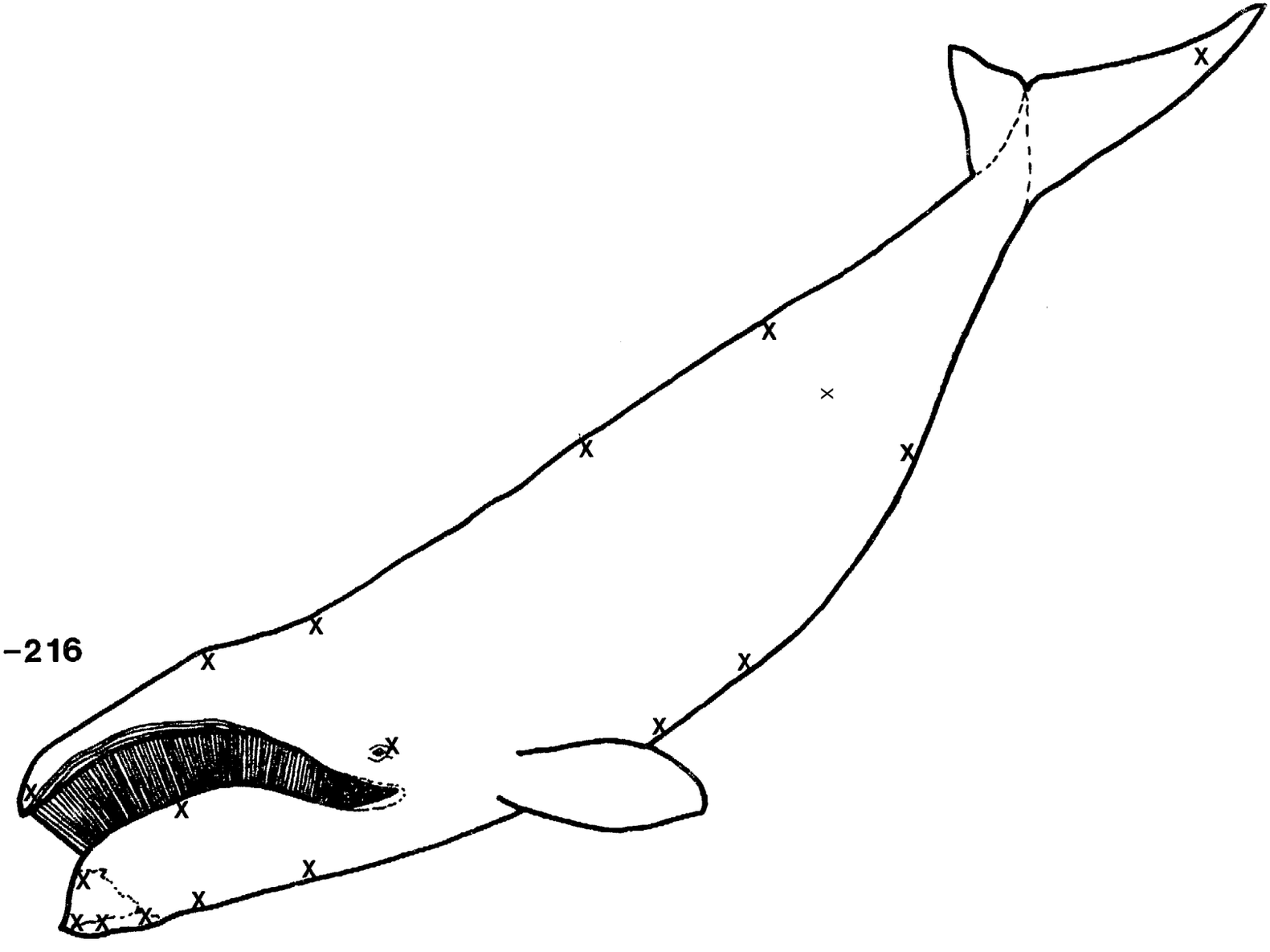

13-216

Figure 13-217. Photograph of the rostralmost baleen, upper left jaw, 80B7, Tag 16. The baleen emerges from the highly thickened epidermis of the gum (G). The medial baleen is made of white simple hair-1 ike structures (S). Laterad (right), the baleen is brownish compound hairs (C) with the most lateral baleen fused into plates [P) whose tips and medial surfaces display filaments (F)-. The thin," medium gray epitheliums of the hard palate (HP) contrasts with the black outer upper lip epidermis (E).

Figure 13-218. Photograph of sensory papillae, snout of 80B7, Tag 12. The thin black epidermis (E) of the outer upper lip on the rostral snout in front of the baleen becomes gray (G) caudally as it becomes thinner covering a distinct region of sensory papillae (arrowheads) just rostral to the hard pal ate (HP).

Figure 13-219. 'Photograph of a vertical cut through upper lip of 79B3. The thick outer lip epidermis gradually thins medially. Dermal papillae can be seen as gray streaks interdigitating with the epidermis. The superficial dermis (D) and hypodermic (H) are the same as in other body regions.

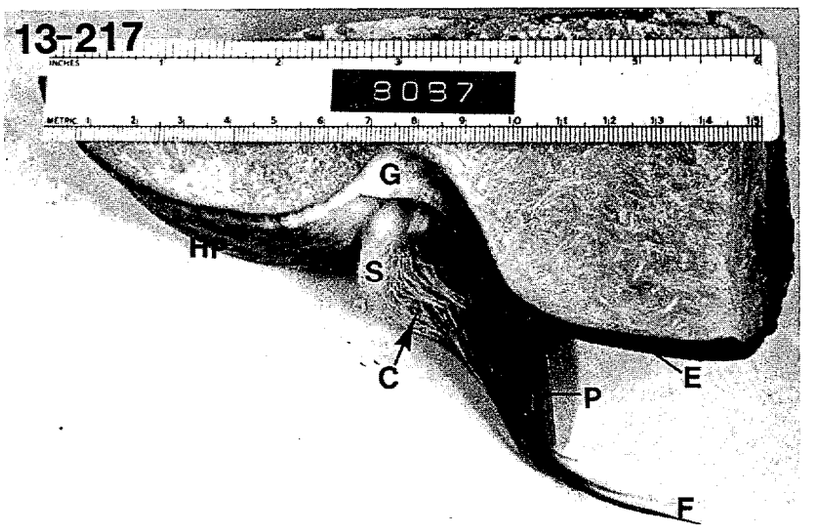
13-217
8087
G
HP
S
C
P
E
F

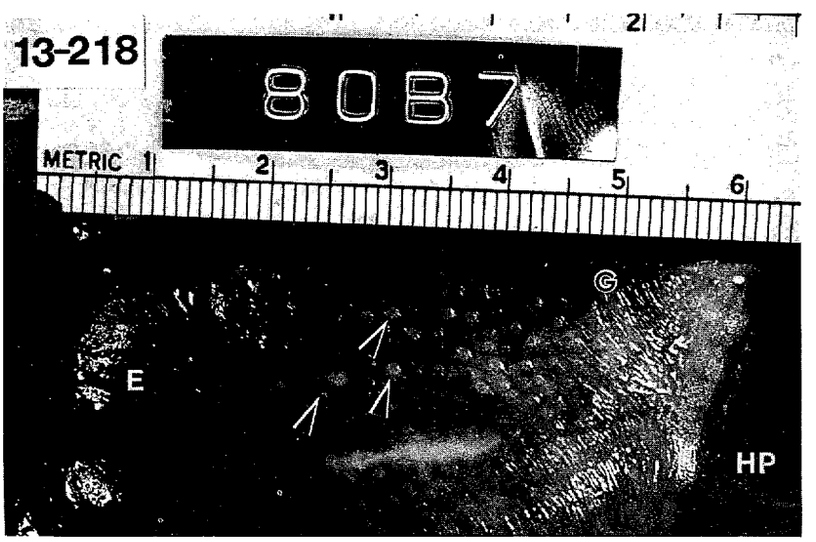
13-218
8087
METRIC 1 2 3 4 5 6
G
E
HP

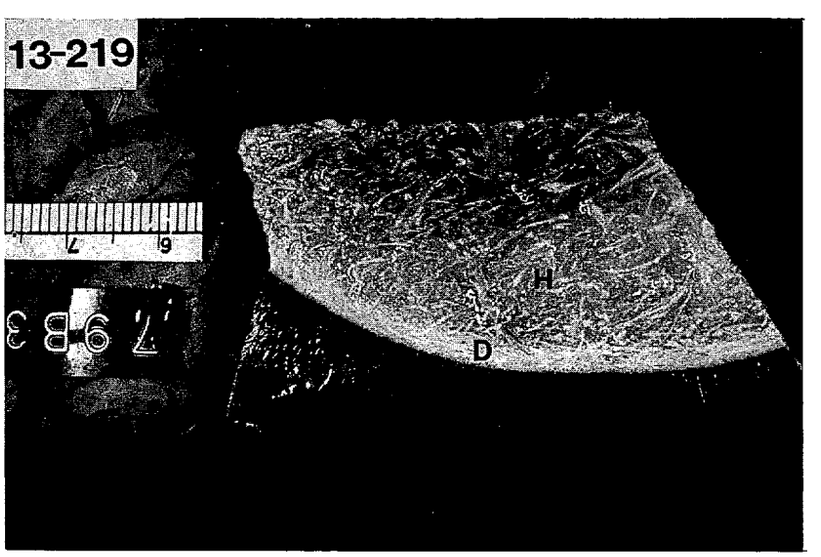
13-219
H
D

Figure 13-220. Photograph of a vertical cut through the dorsal and ventral epidermis, caudal border, fluke, 80B2, Tag 35. The superficial dermis (light) associated with the epidermis is fused without any intervening hypodermic.

Figure 13-221. Photograph of a vertical section through the dorsal and ventral skin, fluke, 7963. Hypodermic (H) rich in collagen fibers occurs between dermis (S) beneath the dorsal (D) and ventral (V) epidermis in the thicker fluke samples. Note the arteries (A), the largest of which is surrounded by a plexus of veins.

Figure 13-222. Photomicrograph of a vertical section, inner lower lip, 8068, Tag 42L. The parakeratotic stratum corneum (SC) forms the epithelial surface covering the stratum spinosum (SS). The retention of nuclei in the keratinized corneal cells is, by definition, parakeratosis. Melanin granules are clustered near the nuclei which overemphasizes them at this magnification. Large sensory papillae (SP) are interspersed between the distal tips of the regular papillae (P) of the lamina propria. X.S., Hand E, X150

Figure 13-223. Photograph of a vertical section through skin with a tactile hair follicle, 80B1, Tag 42. The section is peripheral to the hair shaft, but illustrates the funnel shaped depression that surrounds the follicular orifice. The parakeratotic stratum corneum (SC) extends into the depression becoming thinner and more keratinized which results in production of a stratum disjuncture (arrows) as it continues deeper into follicle. X.S., Verhoeff stain, X40

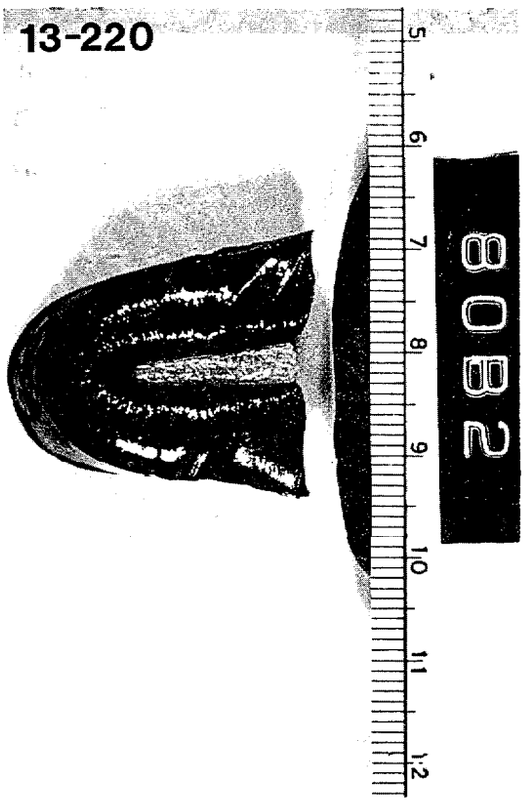
13-220
2808

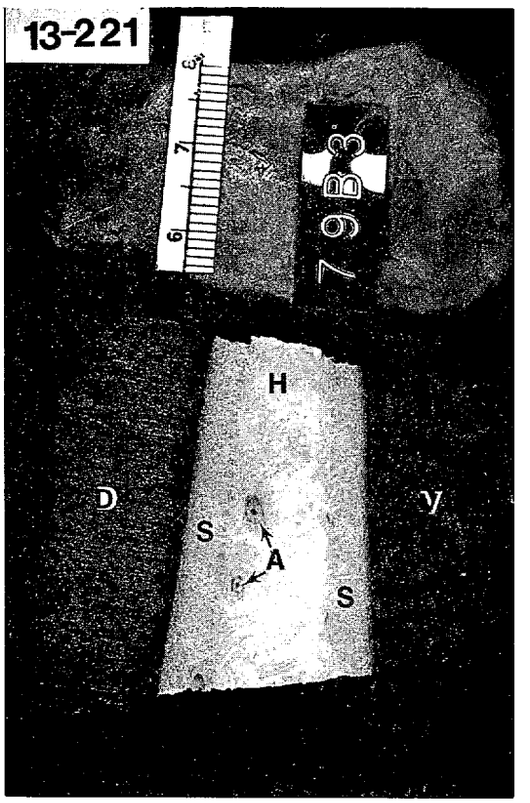
13-221
H
D
V
S
A
S

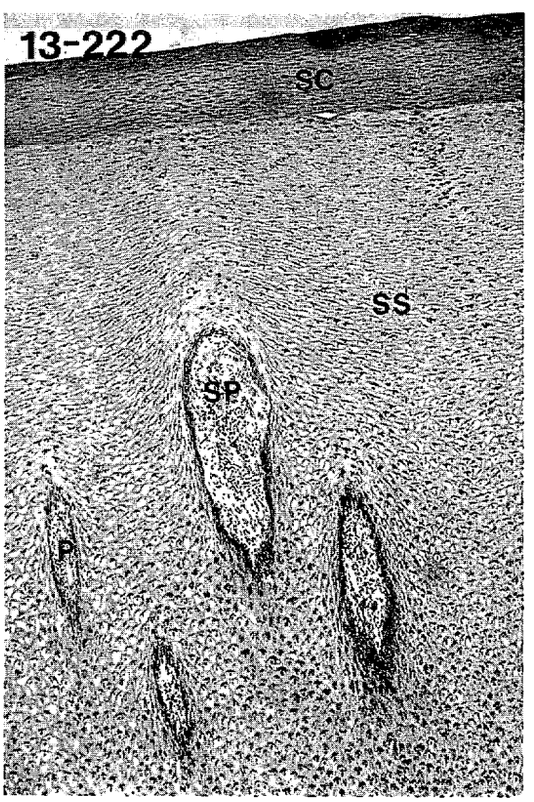
13-222
SC
SS
SP
A

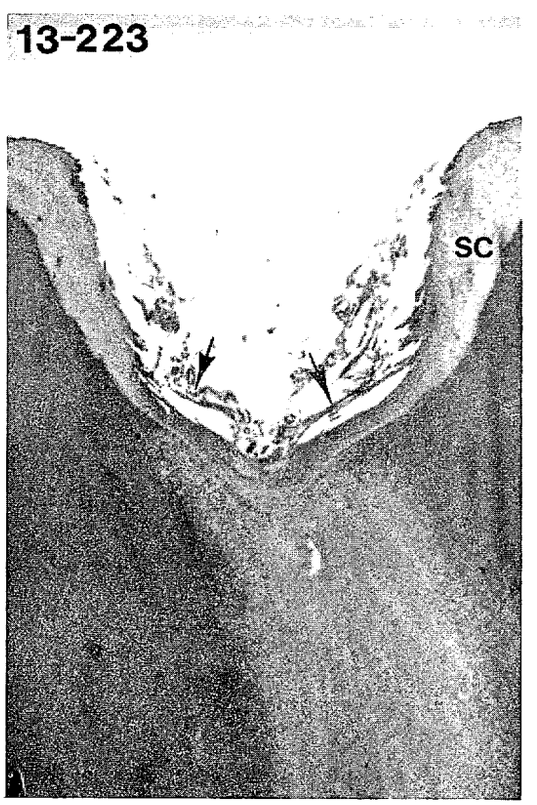
13-223
SC

Figure 13-224. Scanning electron photomicrograph of the inner lower lip surface, 8067, Tag 5. The surface of the parakeratotic stratum corneum is relatively smooth with few cells desquamating (arrowhead). X219.

Figure 13-225. Higher magnification scanning electron photomicrograph of inner lip surface, 80B7, Tag 5. The distinct cell junctions (arrowheads) and surface membrane ridging is normal for keratinized stratum corneum resembling those of terrestrial mammals. X2,700

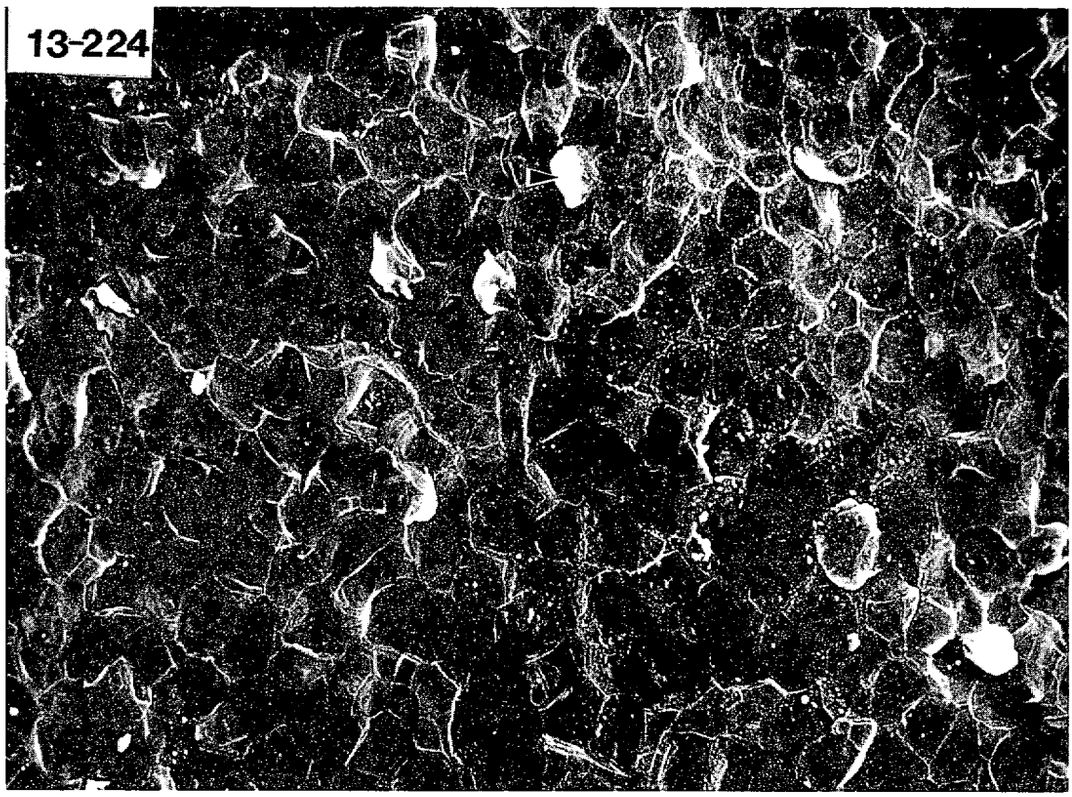
13-224

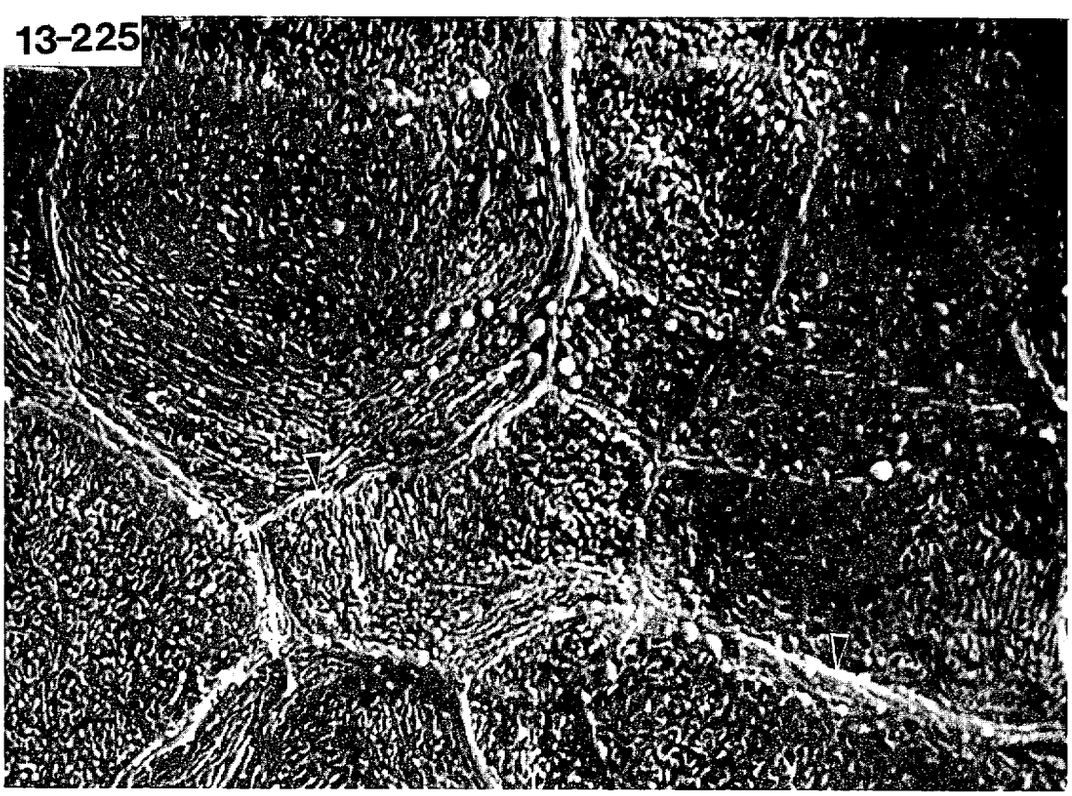
13-225

Figure 13-226. Scanning electron photomicrograph, outer lower lip, 80B8, Tag 35. The normal outer lip skin surface is actually rougher than visible to the unaided eye. The normal sloughing of stratum corneum cells fills the field. Some rosettes (R) of the circularly arranged cells of the epidermal rods are visible. X60

Figure 13-227. Higher magnification scanning electron photomicrograph of Fig 13-226. The squamous cel 1 (S) surfaces have some bacteria (B) and the normal ridging of squamous cells. The normal crevices of desquamation are occupied by Cocconeis (C) and bacteria. xl ,500

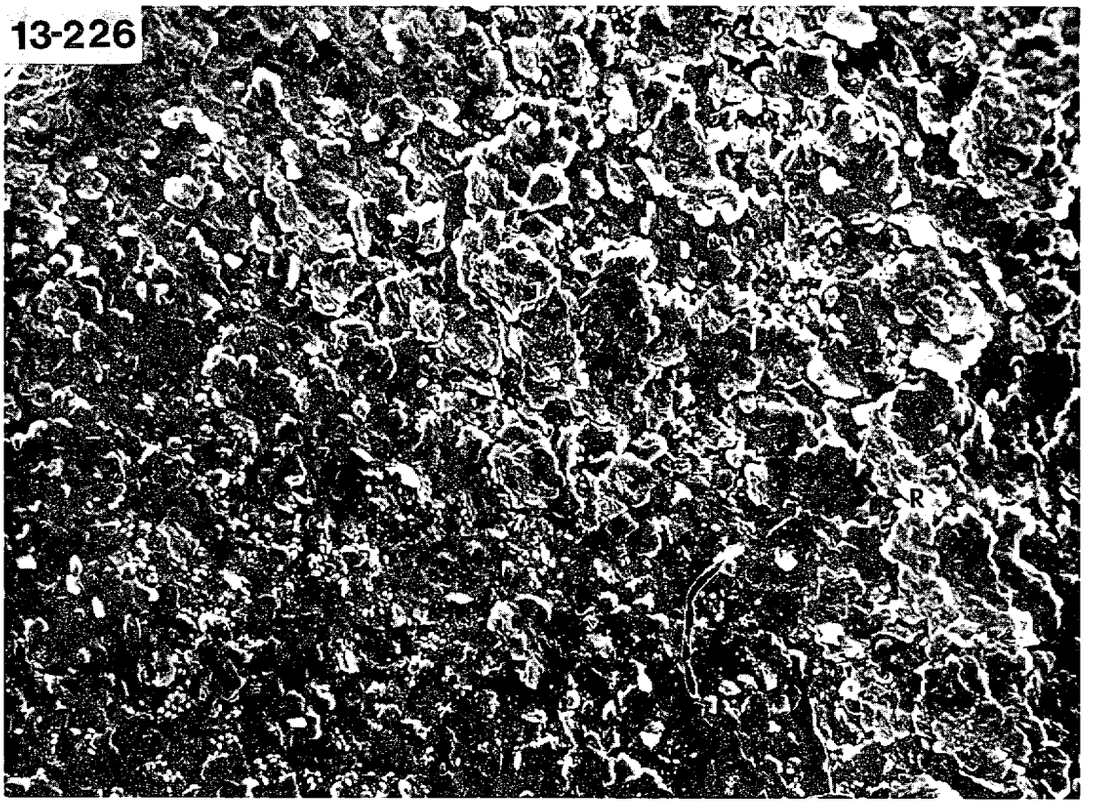
13-226
R

13-227
S
C
S
C
B

Figure 13-228. Scanning electron photomicrograph, skin surface, dorsal midline, 80B8, Tag 87. The normal dorsal body skin surface is actually rougher than it appears to the unaided eye. The normal sloughing of stratum corneum cells fills the field of view. The rosettes (R) of squamous cells owing to the circularly arranged cell layers of the epidermal rods show clearly. X240.

Figure 13-229. Higher magnification scanning electron photomicrograph of Fig 13-228. The crevices that result from normal desquamation of squamous cells (S) are frequently occupied by microflora. Cocconeis (C) and bacteria (B) occur on this sample. The red blood cells (R) are from the collection process. Also note the typical squamous cell ridging. X3,200

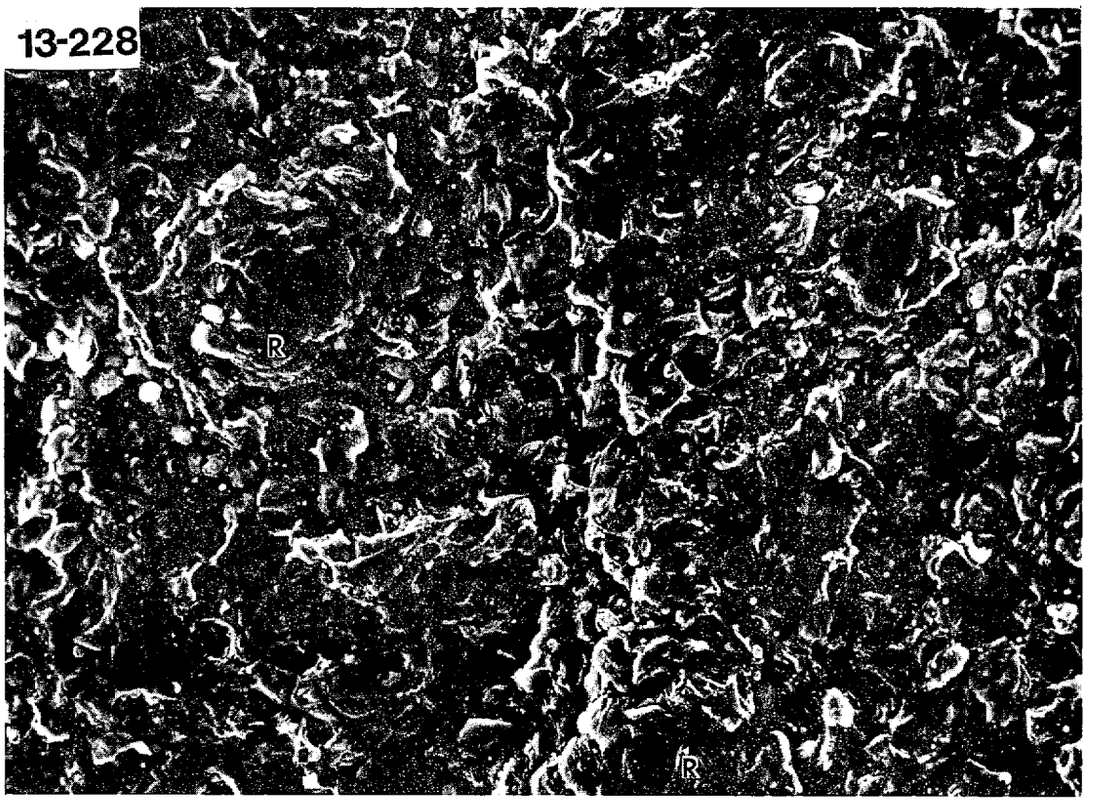
13-228
R
R

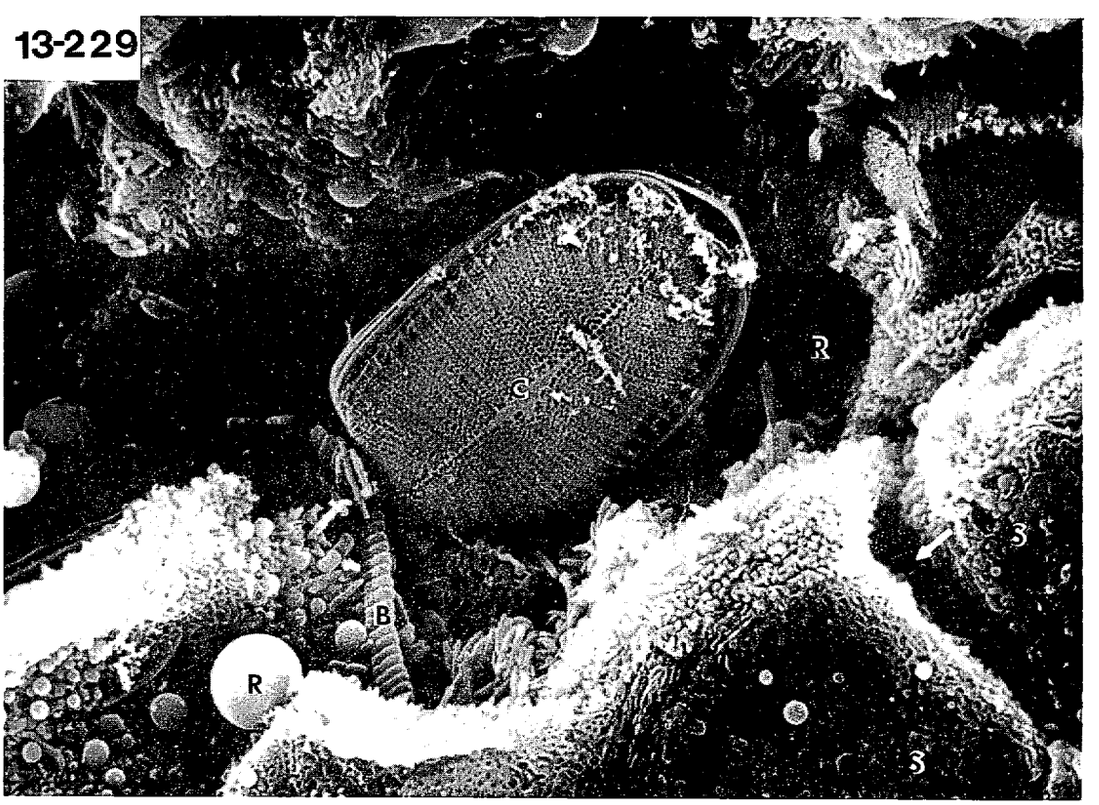
13-229
C
R
S
B
R
S

Figure 13-230. Scanning electron photomicrograph, lateral body wall, 80B8, Tag 86. The normal lateral body wall surface is actually rougher than visible with the unaided eye. The normal sloughing of stratum corneum cells fill the field of view. Rosettes (R) of the circularly arranged cel 1s of the epidermal rods show clearly. Microflora (arrows) are also visible. X230

Figure 13-231. Higher magnification scanning electron photomicrograph of Fig 13-230. The crevices (arrowheads) that normally occur in the desquamation process as well as the cell surfaces harbor Cocconeis (C) and bacteria (B). Debris and red blood cel 1s (R) are from the coll ection process.. Normal ridging of the squamous cells (S) is also visible. X3,600

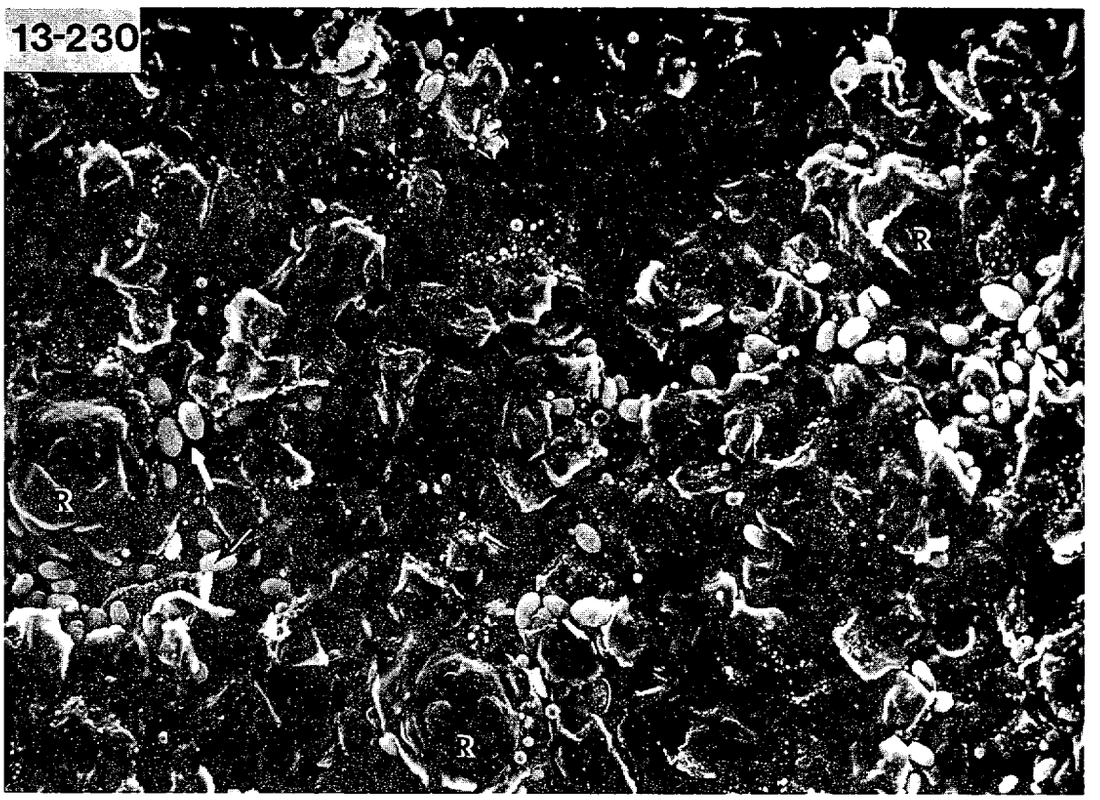
13-230
R
R
R

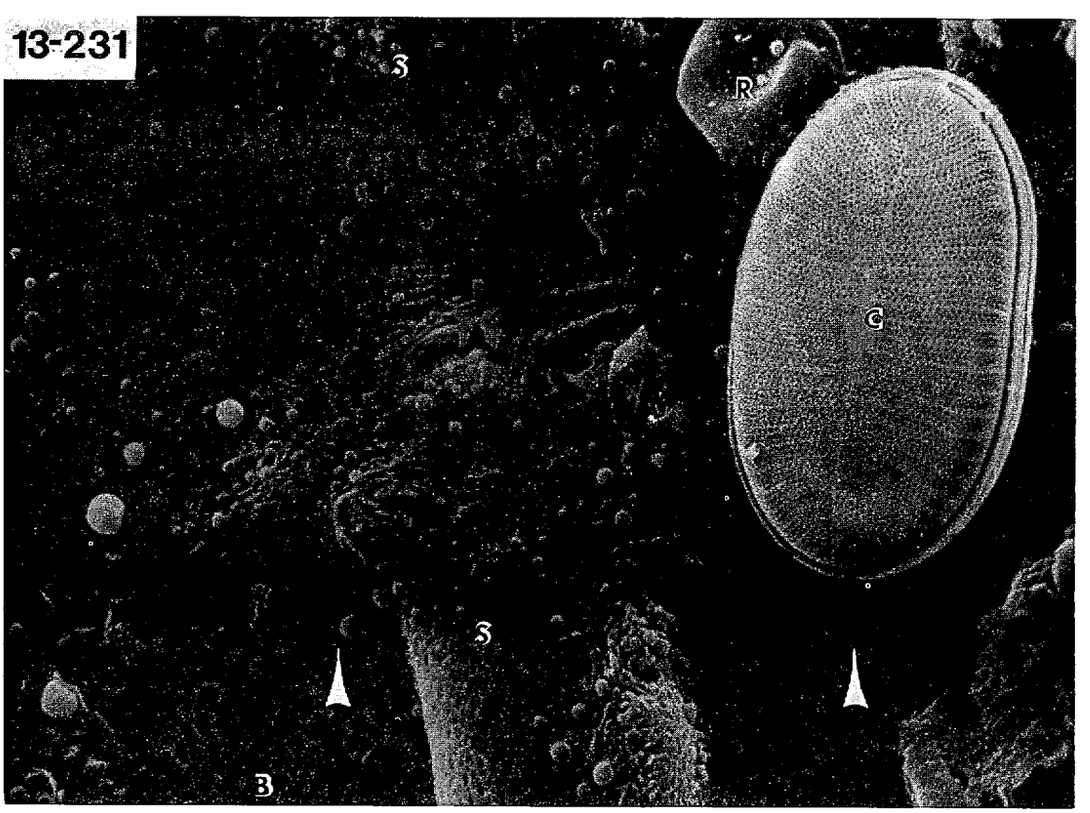
13-231
S
R
C
S
B

Figure 13-232. Scanning electron photomicrograph, ventral body surface, 80B7, Tag 1/3 V. The normal ventral body skin surface is also actually rougher than it appears to the unaided eye. The normal sloughing of stratum corneum cells fills the field of view. The rosettes (R) of circularly arranged cells of the epidermal rods are also visible. X180

Figure 13-233. Higher magnification scanning electron photomicrograph of Fig 13-232. The normal crevices are occupied by Cocconeis (C) and bacteria (B). Note the normal surface ridging of the squamous cells (S). X3,600

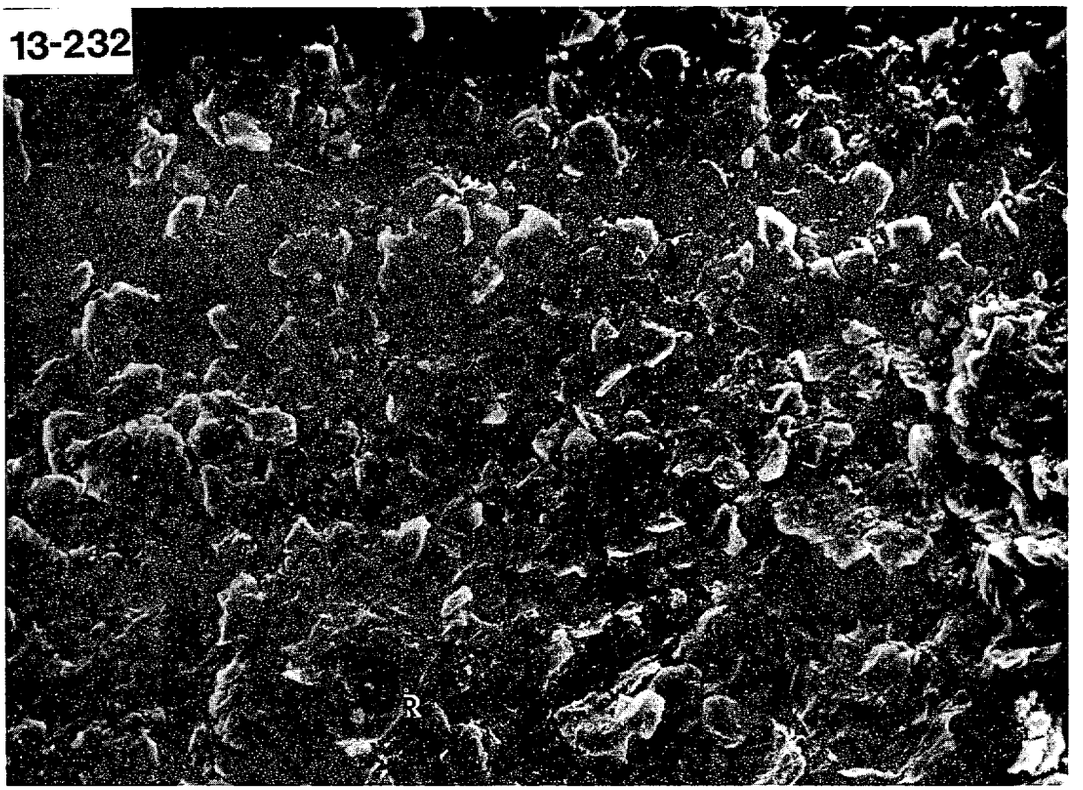
13-232
R

13-233
B
C
C
B
S

Figure 13-234. Photomicrograph of stratum spinosum, 80B1. The spinosal cells are mainly polyhedral, round, or flattened in shape with scanty chromatin in the nuclei (arrows). The major characteristic of this stratum is the prominent cell boundaries (triangles). The black granules are melanin. X.S., H and E, X2,100

Figure 13-235. Transmission electron photomicrograph, stratum spinosum, 80B1. Spinosal cells have numerous tonofilaments (TF) within the cytoplasm. Keratin granules (K) and glycogen granules (G) also occur. Desmosomes (D) and the highly undulating cell membranes account for the thick junctions seen in light microscopy. Uranyl acetate and lead citrate. X19,100

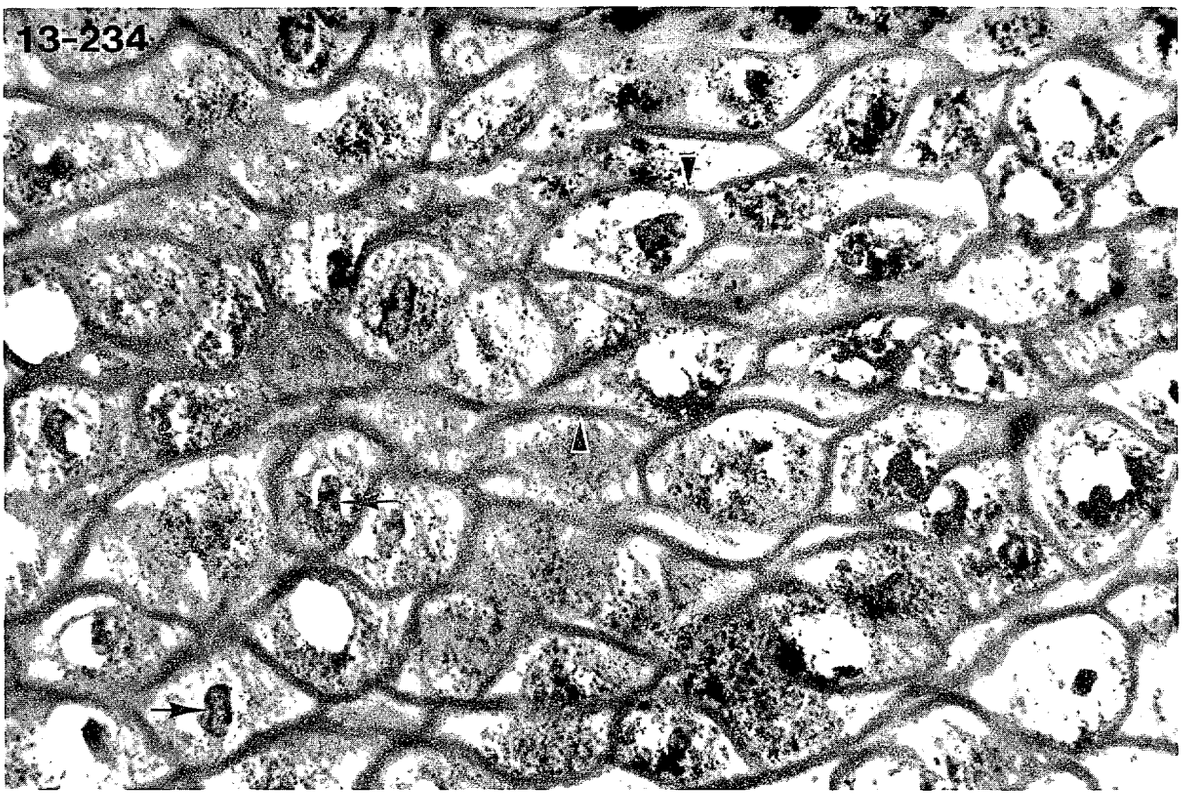
13-234

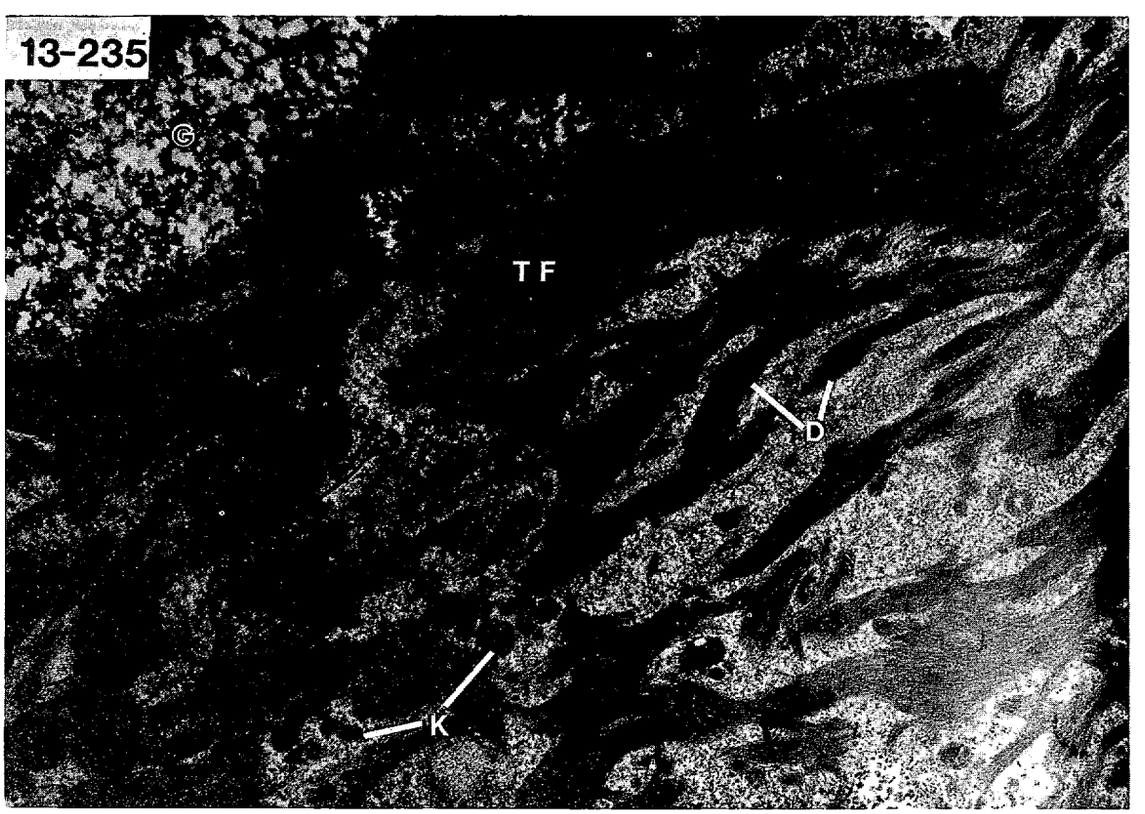
13-235
G
TF
D
K

Figure 13-236. Transmission electron photomicrograph of the stratum spinosum, 80B1 . This spinosal cell cytoplasm has monofilament (TF) bundles, keratin granules (K) and large groups of glycogen granules (G). X23,900

Figure 13-237. Transmission electron photomicrograph of the stratum spinosum, 80B1 . This spinosal cell cytoplasm has an abundance of tonofilaments (TF), keratohyalin (K) and melanin (M) granules. The elongated irregular nucleus (Nu) has a prominent nucleolus (N). X9,400

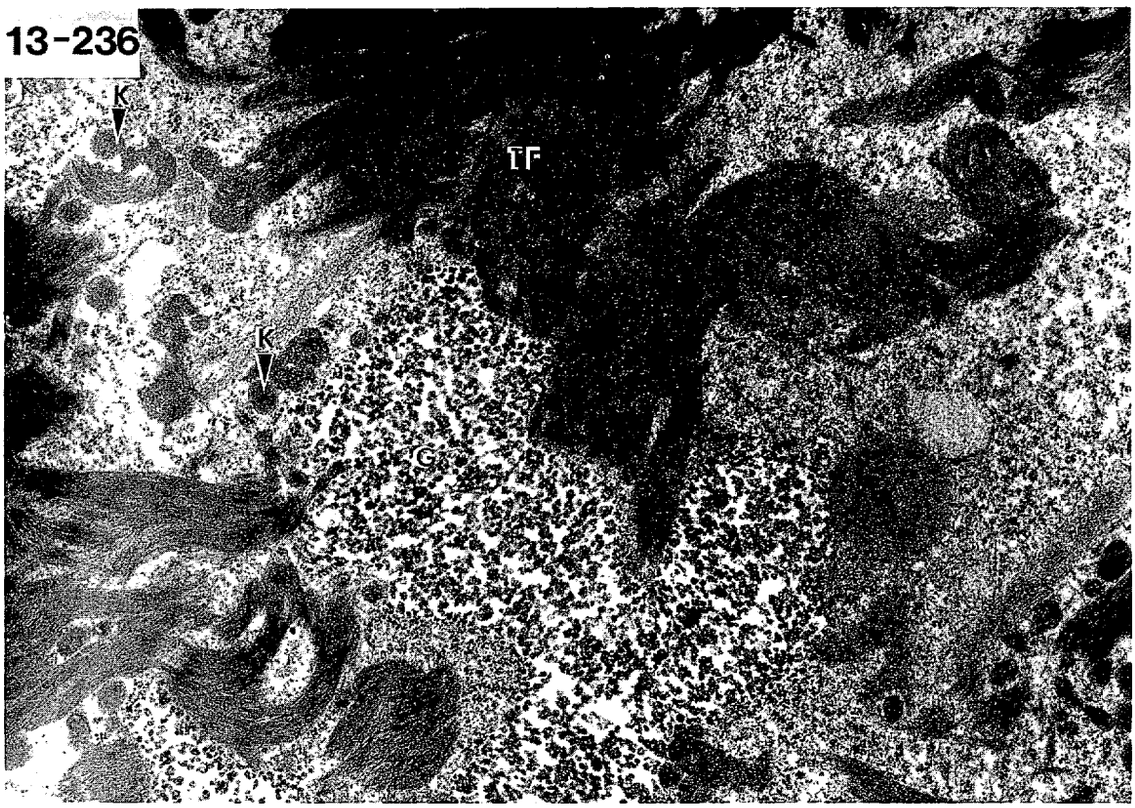
13-236
K
TF
K
G

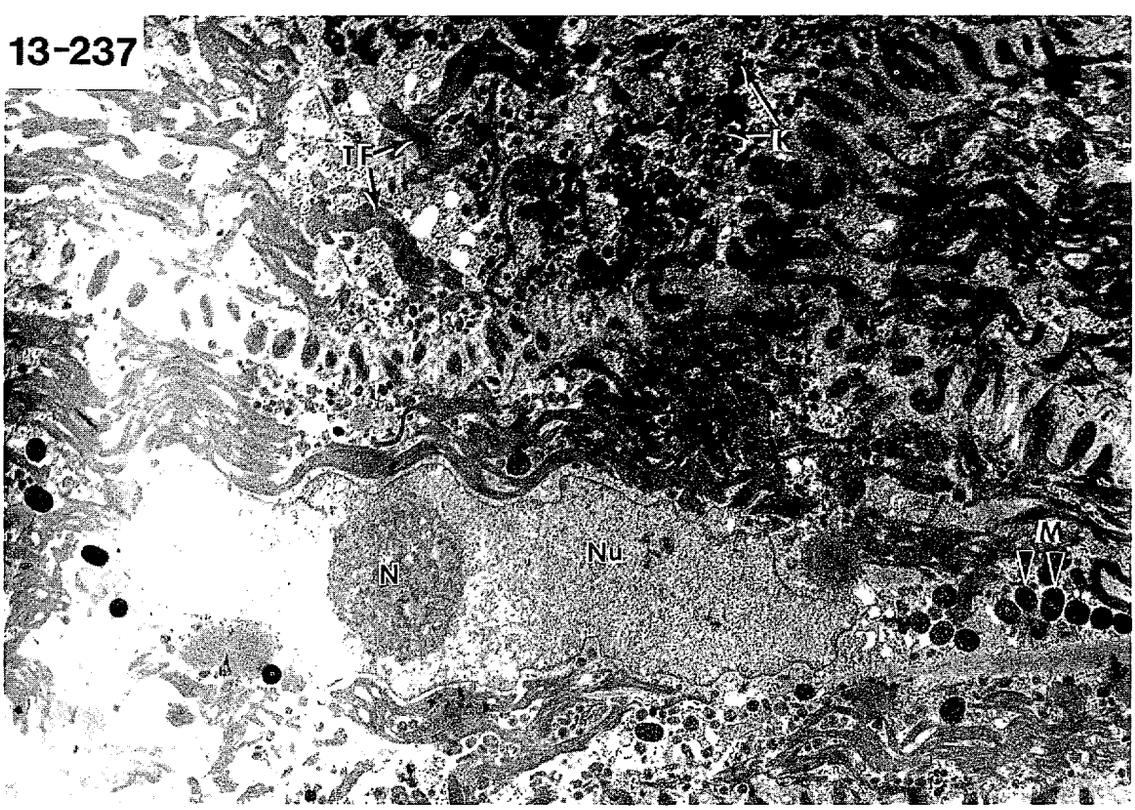
13-237
TF
K
N
Nu
M

Figure 13-238. Transmission electron photomicrograph of stratum spinosum, 80B1. This cell of the spinosum has electron lucent granules (E) and tonofilaments (TF) i n the cytoplasm. Desmosomes (D) are found where cytoplasmic processes interdigitate with those of neighboring cells. The large irregular nucleus (Nu) has a prominent nucleolus (N) and peripheral chromatin (arrowhead). X19 ,100

Figure 13-239. Photomicrograph, basal epidermis and dermis, 80B7. Mel ani n granules produced by melanocytes (M) in the stratum basale primarily are present in the cytoplasm of stratum spinosum cells (S). Extensions of the superficial dermis (D) interdigitate with corresponding extensions of the epidermis forming a papillary layer. Coarse collagen fibers (C), arterioles (A) and venules (V) extend into the resulting dermal papillae (DP) . X.S., Verhoeff stain, X2,100

13-238
T
D
TF
E
Nu
N

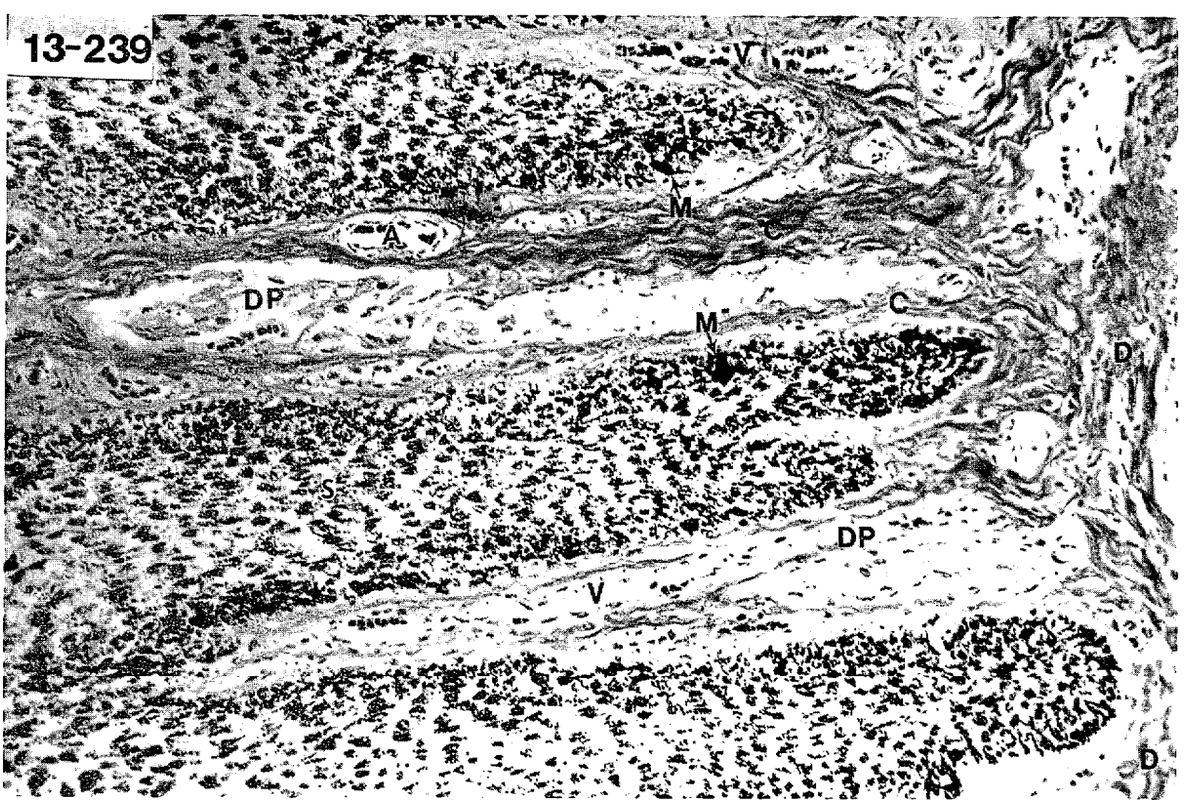
13-239
V
M
A
DP
C
M
D
S
DP
V
D

Figure 13-240. Photomicrograph of bowhead 80B7 dermal-epidermal junction. The deep epidermal stratum spinosum (Sp), stratum basale (B) and superficial dermis (l)) are seen. Note the nerve fiber bundles (N) and collagen fibers (Cf). X2,300

Figure 13-241. TEM photomicrograph of stratum basale, 80B1. Several basal cells-with numerous cytoplasmic processes (Cp) are seen surrounding a melanocyte (M). The melanocyte has prominent melanin granules (Mg). The nuclei (Nu) of basal cells have prominent nucleoli (N) . The basal lamina (BL) separates the cells from the dermis (D). X9,400

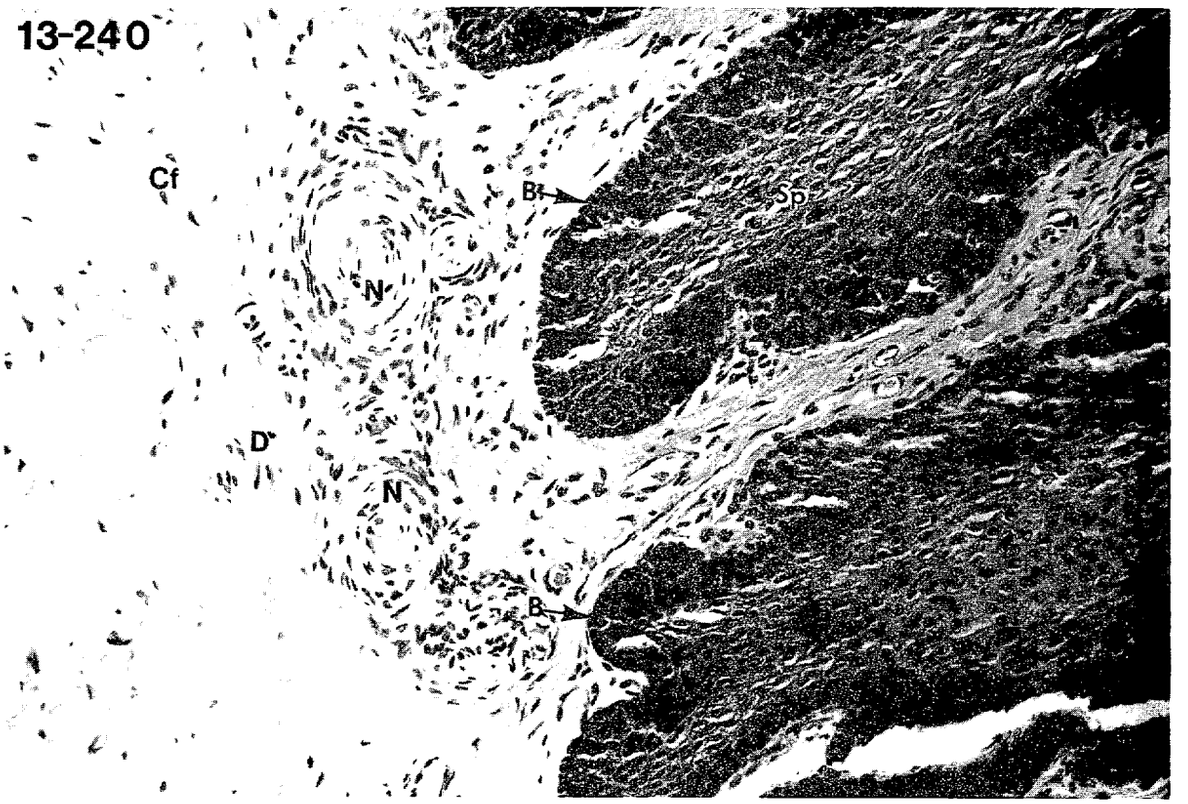
13-240
Cf
Bt
Sp
N
D
N
Bt

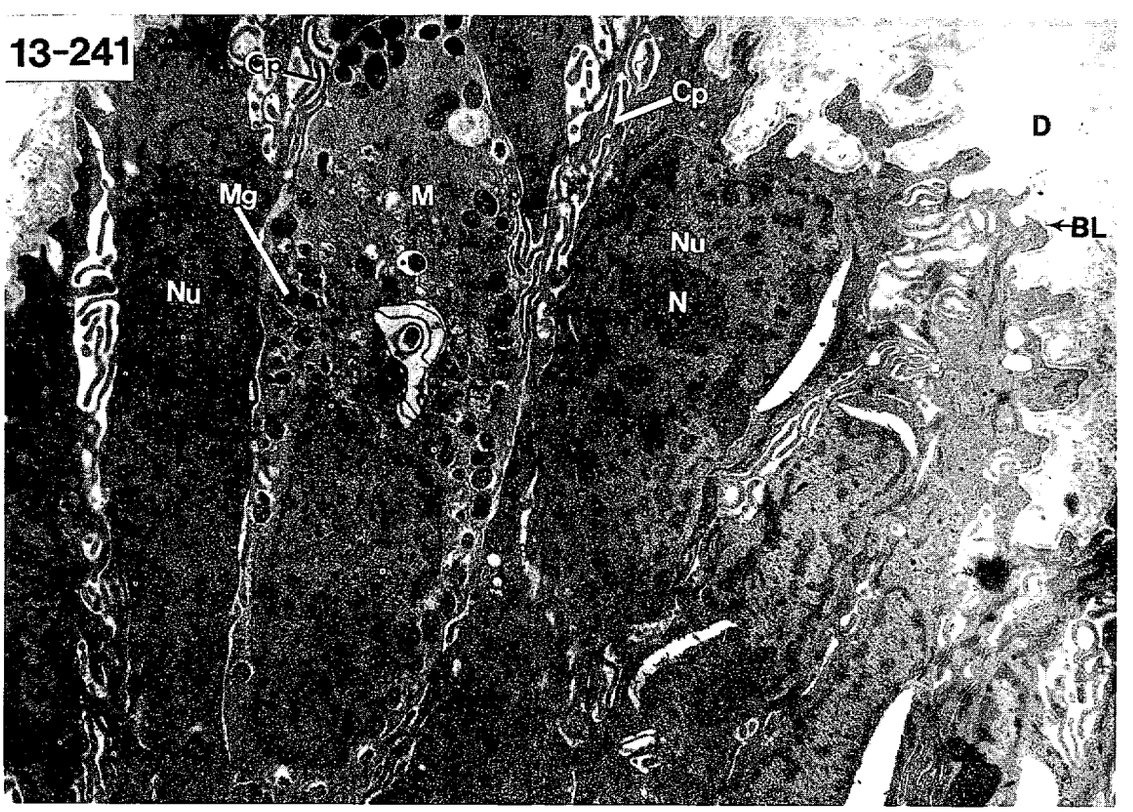
13-241
Cp
Cp
D
Mg
M
BL
Nu
Nu
N

Figure 13-242. TEM photomicrograph of the stratum basale, 80B1. Cytoplasmic processes (Cp) of basal epidermal cells are seen surrounding a melanocyte (M) with melanin granules (Mg). The nucleus (Nu) shows a prominent nucleolus (N) and peripherally clumped chromatin (C). The basal lamina (BL) is seen separating the epidermis from the dermis (l)) with its collagen fibrils (Cf). X23 ,900

Figure 13-243. TEM photomicrograph of the stratum spinosum, 80B1 . Two irregularly shaped and adjacent epithelial cells show numerous desmosomes (D) between their cellular processes. Long bundles of tonofilaments (TF) are seen in the cytoplasm. X19,100

13-242
N
M
Cp
Mg
C
Nu
BL
Cf
Cp
D

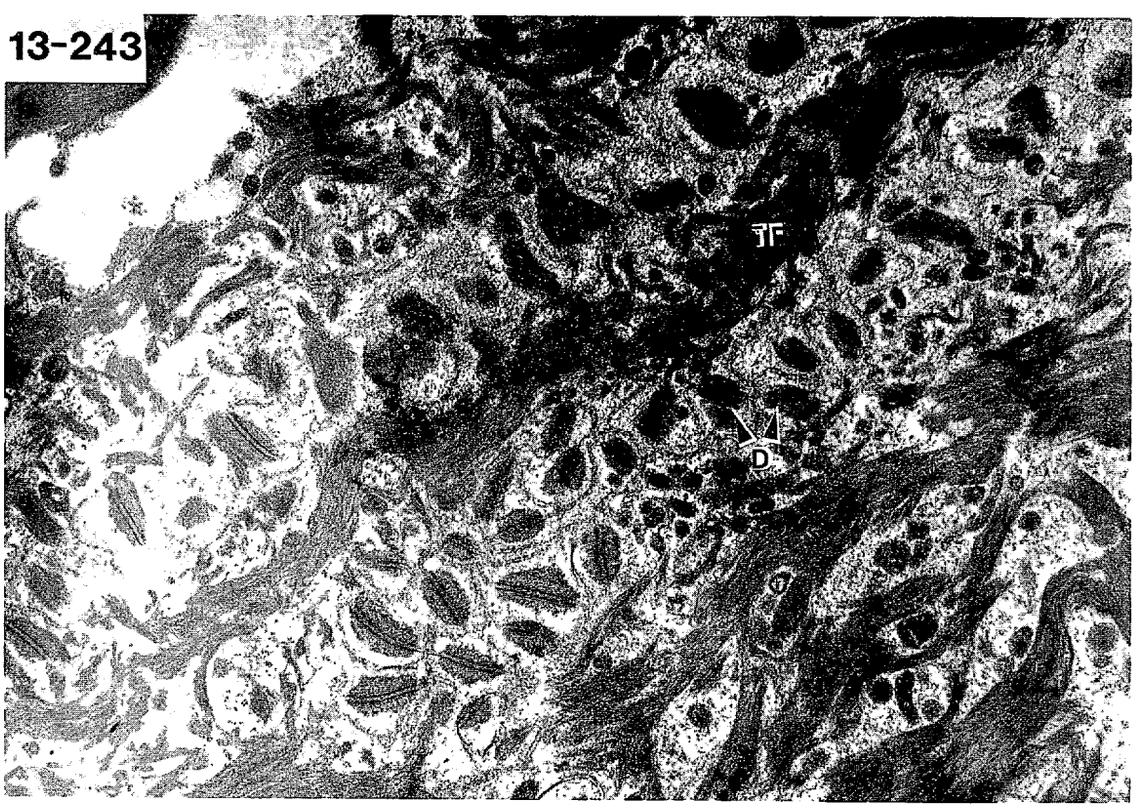
13-243
TF
D

Figure 13-244A. Photomicrograph, shallow depression lesion, 80B8, Tag 84. A vertical section through this type of epidermal lesion shows the presence of the parakeratotic stratum corneum (SC) still covering the lesion surface. The epidermal rods (ER) show clearly in the stratum spinosum (SS) and continue through the corneum (arrow) as in normal skin. The dark blotches are stain artifacts. X. S., H and E, X50.

Figure 13-244B. Higher magnification photomicrograph of the parakeratotic stratum corneum layer reveals bacteria (arrows), but no diatoms. An epidermal rod (ER) shows clearly in the corneum. X.S., H and" E, X130

Figure 13-245A. Photomicrograph, granular depression lesion, 80B8, Tag 87. A vertical section through this type of lesion indicates that the granular appearance grossly is owing to a hypertrophied parakeratotic stratum corneum (SC) which has larger than normal desquamating flakes within the lesion. The epidermal rods (ER) show in the stratum spi nosum (SS) and extend into the lesion area (arrow). X.S., H and E, X50

Figure 13-245B. Higher magnification photomicrograph of the hypertrophied parakeratotic stratum corneum reveals bacteria upon the surface (arrow) and between cells with Stauroneis (S) diatoms also present. Small spherical cells, which are possibly protozoans (P), are also present. X.S., H and E, X330

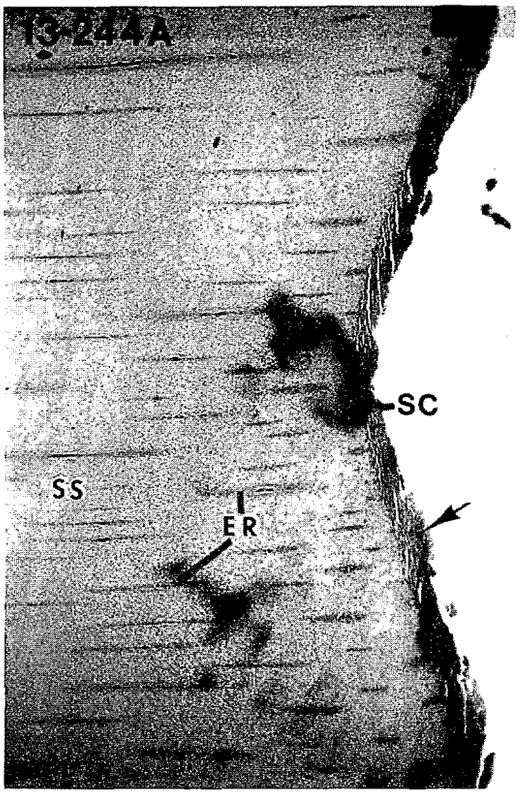
13-244A
SC
SS
ER

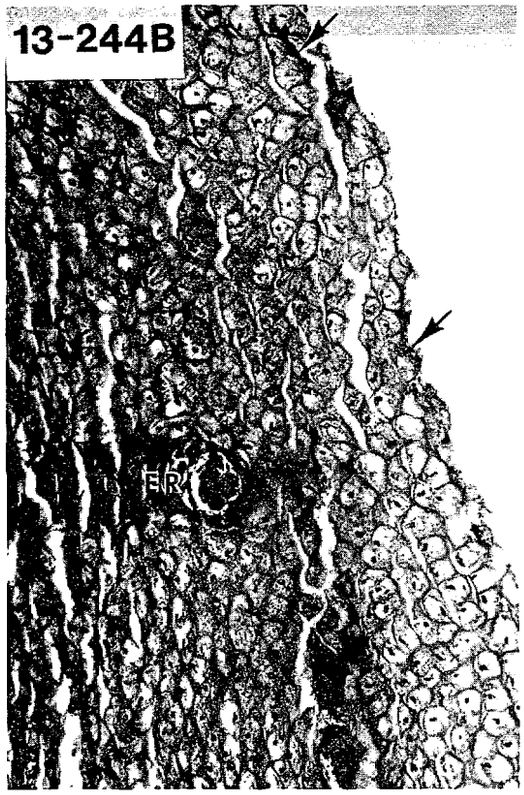
13-244B
ER

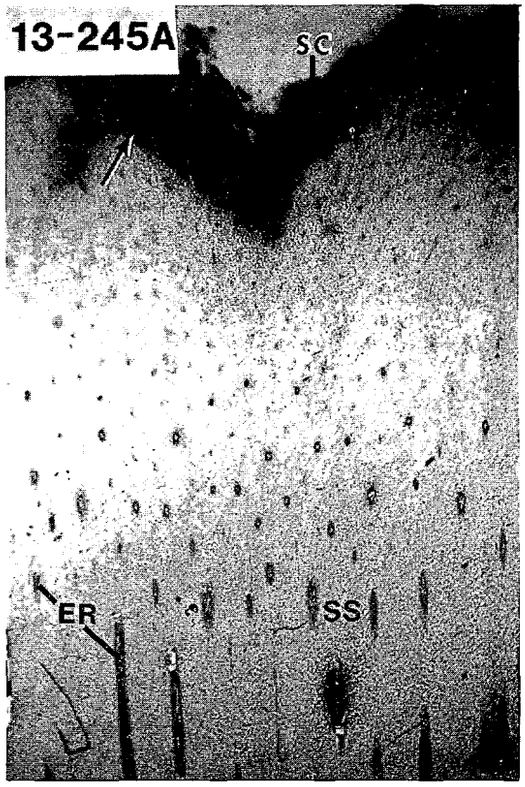
13-245A
SC
ER
SS

13-245B
P
S

Figure 13-246A. Photomicrograph, vertical section of a depression lesion with raised center, 80B8, Tag 85. A vertical section through this type of lesion shows it to have an entirely different configuration. The parakeratotic stratum corneum (SC) is hypertrophied within the lesion, but is missing over the central mass. The central portion (RC) of stratum spinosum cells has sloughed very little and remains firmly attached to the rest of the stratum spinosum cells (arrow). The central mass is separated from the surrounding parakeratotic layer by a moat (arrowhead). See Fig 13-204 for the gross appearance. X.S, H and E, X50

Figure 13-246B. Higher magnification photomicrograph of the raised central mass of exposed stratum spinosum cells shows that its surface and interior are inhabited by numerous bacteria (B) in chain form and clusters. Several large protozoans (P) are in between some cells and on the surface. X.S., H and E, X330

Figure 13-247A. Photomicrograph, vertical section of a depression lesion with raised center, 80B8, Tag 84. A vertical section through a smaller lesion of the raised center (RC) type shows a similar arrangement as the large lesion in Fig 13-246. X.S., H and E, X50

Figure 13-247B. Higher magnification photomicrograph of the raised central mass shows it to be inhabited by chains of bacteria (B) and Stauroneis (S). X. S., H and E, X330

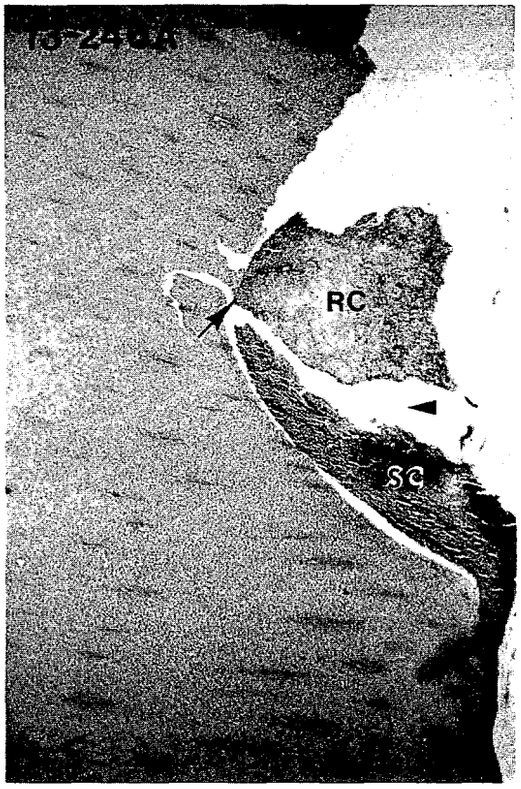
RC
SC

13-246B
P
B
B

13-247A
RC

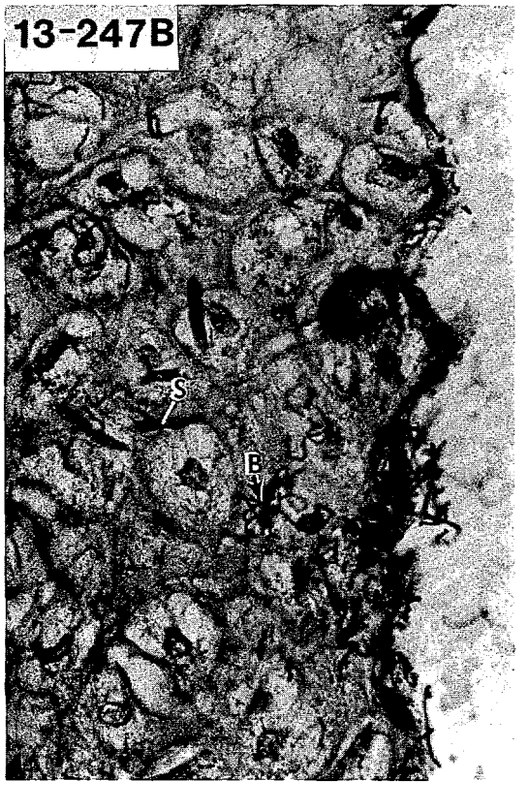
13-247B
S
B

Figure 13-248. Photomicrograph of bowhead lip, 80B8. A sensory papilla (SP) in the epidermal layer (Ep) is seen in longitudinal section with what seem to be numerous nerve fibers and receptors (N). X.S., Verhoeff stain, X40

Figure 13-249A. Photomicrograph of. a frontal section of a tactile hair in the superficial dermis, 80B1. The tactile hair (TH) is seen in the center of the epidermal layer (E) and is surrounded by the heavily keratini zed stratum corneum (SC). Dermal papillae (Dp) are seen at a normal periodicity. The dermal layer (De) is seen surrounding the epidermal layer. The dark perimeter of the epidermis is the stratum basale (arrowheads). F.S., H and E, X40

Figure 13-249B. Higher magnification of the tactile hair in Fig 13-249A. The centrally located tactile hair (TH) is intimately surrounded by the stratum corneum (Se) of the epidermal layer (E). F.S. , H and E, X100

Figure 13-249C. Higher magnification of the junction of the dermal-epidermal 1 ayers. The dark perimeter of the epidermal layer (E) is the stratum basale (arrowheads) which contains mel anocytes (arrows). The dermis (D) consists primarily of collagen fibers (CF). F.S., H and E, X100

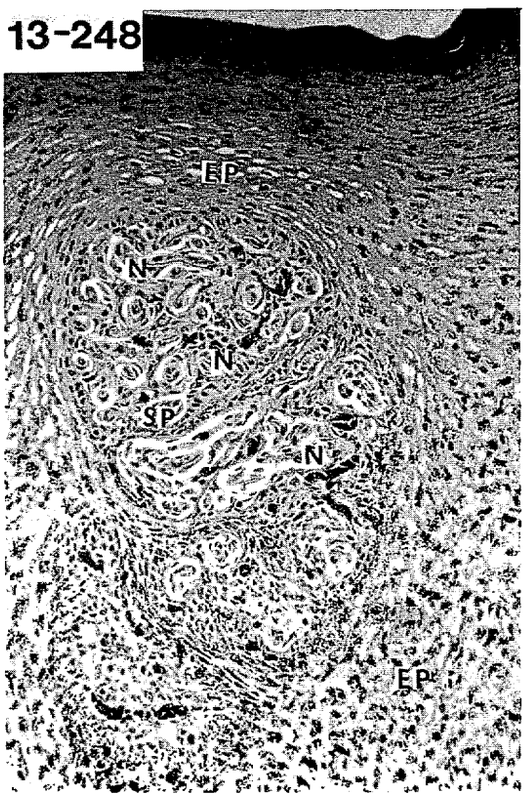
13-248
EP
N
N
SP
N
EP

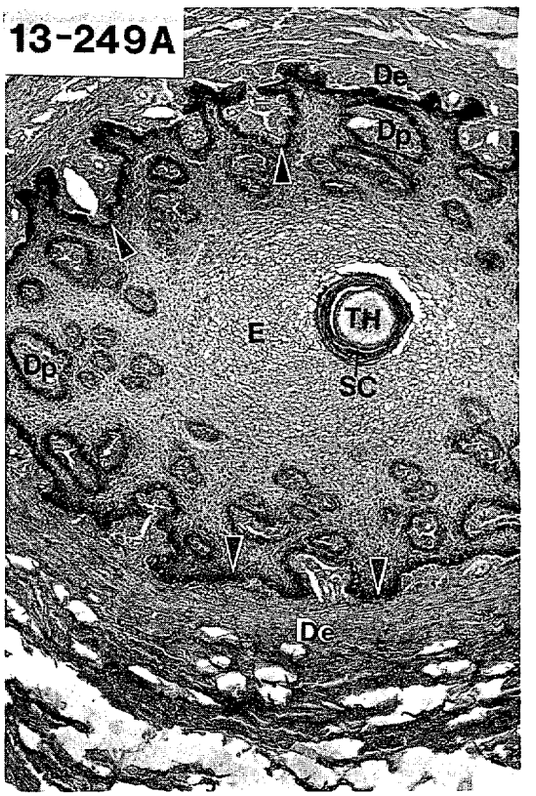
13-249A
De
Dp
E
TH
SC
Dp
De

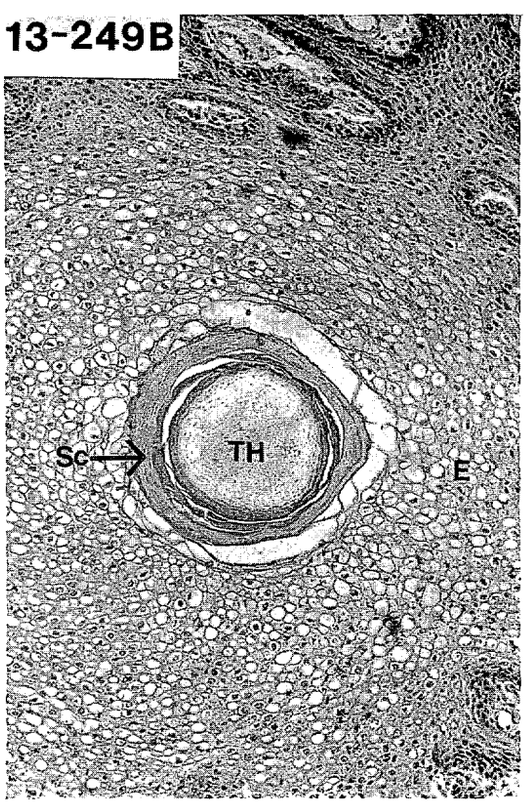
13-249B
Sc
TH
E

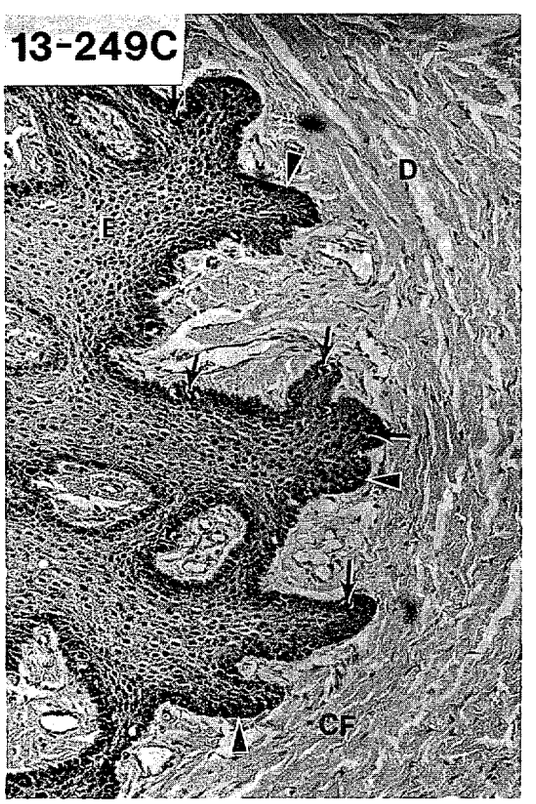
13-249C
D
E
CF

Figure 13-250. Photomicrograph of a tactile hair, 80B1. This section is midway between the rim of the funnel-shaped depression and the deepest part of the depression. Note the decrease in stratum corneum (SC} thickness" as the center of the funnel is approached and its disjuncture-like appearance (arrows). Epidermis (E) Dermis (De). L. S., H and E, X7.1

Figure 13-251A. Photomicrograph of longitudinal section through the hair as it pierces the epidermis. Note the debris and disjuncture-like (arrows) stratum corneum. The hair shaft (S) is seen in the upper one third of the epidermis (E). Note deeper levels of the epidermis sagging into the dermis and the thickening of the dermis (De) forming the dermal sheath (D). L. S., H and E, X7.1

Figure 13-2515. Photomicrograph of a more medial section of the hair follicle. The debris and disjuncture-like stratum corneum (arrows) contain bacteria, diatoms and protozoans. The hair shaft (S) is seen in the epidermis (E). Nerve fibers and receptors (arrowhead) are seen on one side of the dermal sheath (D). L. S., H and E X7,1

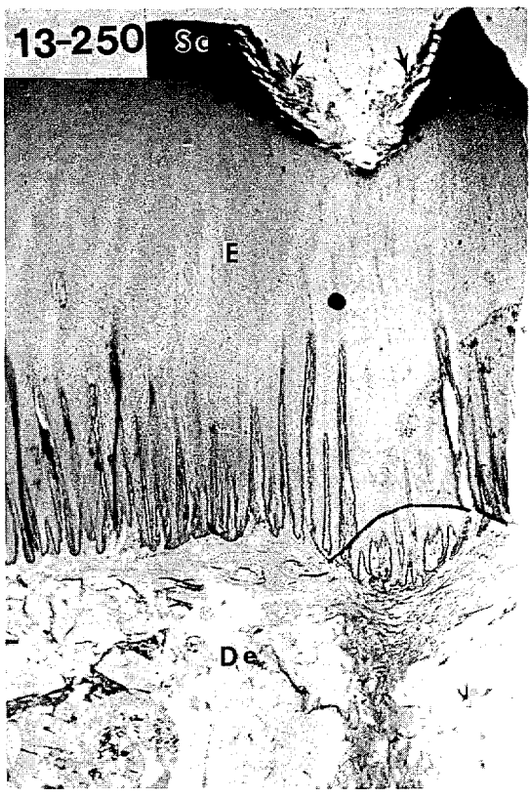
13-250
Sc
E
De

13-251A
E
S
D
De

13-251B
E
S
D
D

Figure 13-252. A montage of photomicrographs of a tactile hair follicle, 80B1 . The hair follicle extends through the epidermis (Ep) and dermis (De) into the hypodermic (H). The hair shaft (S) is seen surrounded by the epidermal sheath (E). Note the dense connective tissue dermal sheath (D) serving as the outer coat of the follicle. Nerve fibers and receptors (arrows) are seen on one side of the follicle in the dermal sheath. Arteries (A) and nerve fibers (N) are seen entering the base (B) of the follicle and a blood sinus (Si) is seen just above the base. L.S., HandE, X7.1

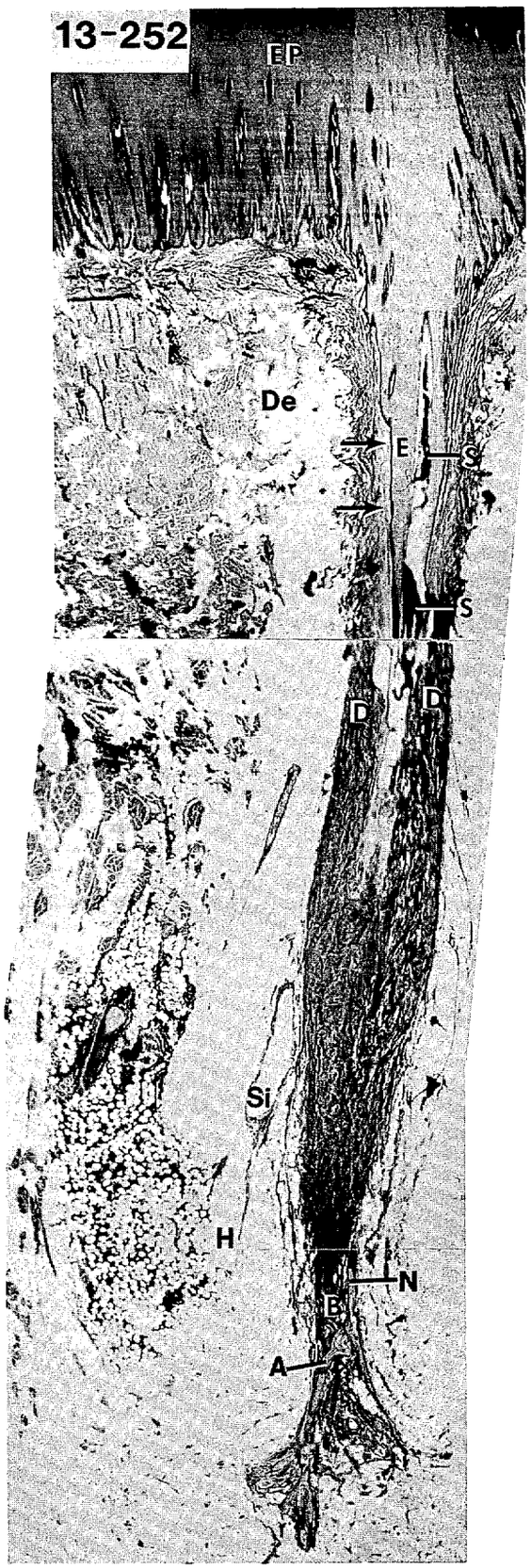
13-252
EP
De
E
S
S
D
D
Si
H
N
B
A

Figure 13-253A. Photomicrograph of dermal sheath nerve fibers and receptors from a tactile hair follicle of 80B1. This is a longitudinal section of the epidermal (E) and dermal (D) sheaths 2.8 - 4.1 mm below the dermal-epidermal junction. Nerve fibers (F) and receptors (arrowheads) are seen in one general area at the side of the dermal sheath. L.S., H and E, x7.1

Figure 13-253B. Photomicrograph of dermal sheath nerve fibers and receptors from a tactile hair follicle of 80B1. This longitudinal section shows that the nerve receptors (arrows) of Fig 13-253Ado not extend deeper in the dermis. Epidermal (E) and dermal (D) sheaths. L.S., H and E, X7.1

Figure 13-253C. Photomicrograph of dermal sheath nerve fibers and receptors from a tactile hair follicle of 80B1. This is a higher magnif i cation of the nerve receptors (arrowheads) and fibers (F) of Figs 13-253A and 13-253B. Epidermal (E) and dermal (D) sheaths. L.S., H and E, X113

Figure 13-253D. Photomicrograph of dermal sheath nerve fibers and receptors from a tactile hair follicle of 80B1. Higher magnification of a nerve receptor. Note the central fiber (arrowhead) and the unsheathing concentric lamellae (L). Dermal sheath (D). L. S., H and E, X284

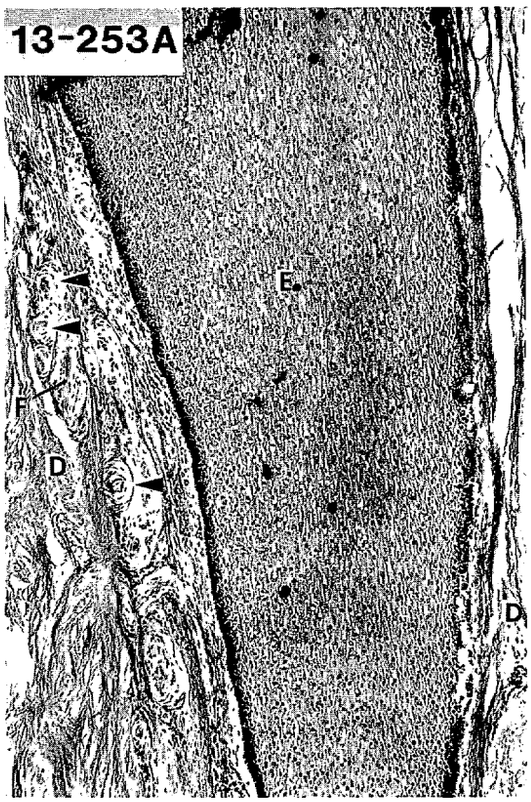
13-253A
E
F
D
D

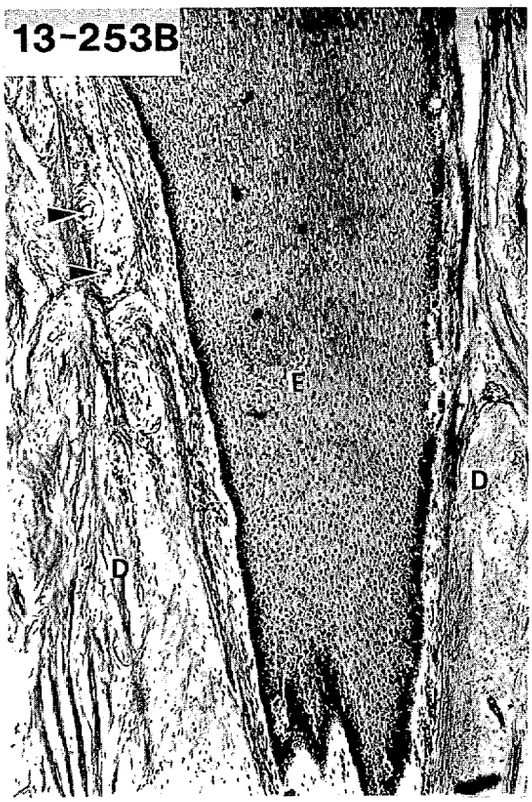
13-253B
E
D
D

13-253C
D
E
F

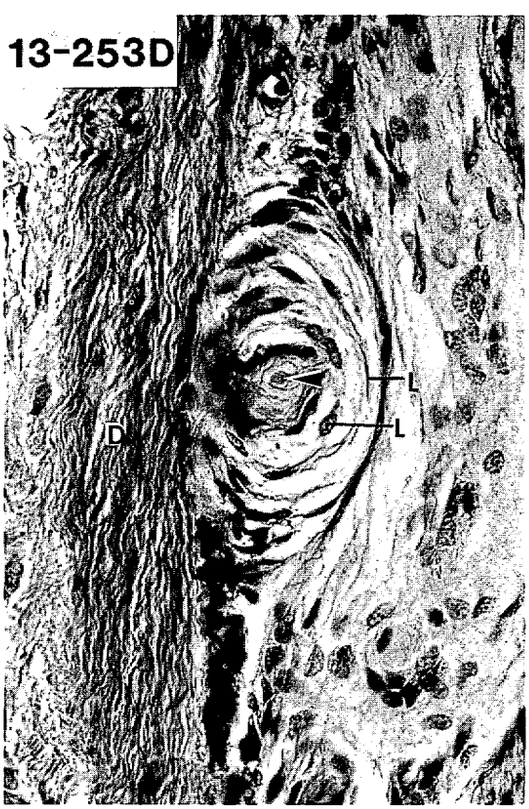
13-253D
L
L
D

Figure 13-254. Photomicrograph of the base of a tactile hair follicle, 80B7. The base of the hair follicle is surrounded by the dermal sheath (D) which has a looser (Lo) inner connective tissue 1 ayer. Artery (A) and nerve (N) trunks are seen entering the area. The hair originates at the bulb (Bu) which rests on the dermal papilla (P). Blood sinuses (S) are seen in the base of the follicle. L.S., Masson's stain, X44

Figure 13-255. Photomicrograph of the base of the tactile hair follicle of 80B7 . This longitudinal section of the hair follicle bulb (Bu) shows the extensive blood sinus (S) network in the lower portion of the dermal sheath (D). Notice the looser (Lo) and denser (De) portions of the dermal sheath. Nerve (N), artery (A). L. S., Masson's stain, X44

Figure 13-256. Photomicrograph, horizontal section of gum, 80B1. Simple baleen hairs (S9) originate around the bases of the connective tissue papillae at the bottom of the figure. Sections through simple baleen hairs further from their origin (SB2), and compound baleen hairs (CB) still further from their points of origin are indicated. The gum (G) surrounding the baleen hairs is modified stratum spinosum. F.S., H and E, X50

Figure 13-257. Photomicrograph, horizontal section of simple baleen hair, 80B1. The loose connective tissue (CT) with capillaries (C) of the papilla extends for only a short distance into the medulla of the constantly growing simple baleen hair. The epidermal cells that form the cortex are keratinized (K). The cells of the surrounding stratum spinosum of the gum (G) become compressed by enlargement of the baleen. X.S., H and E, X330

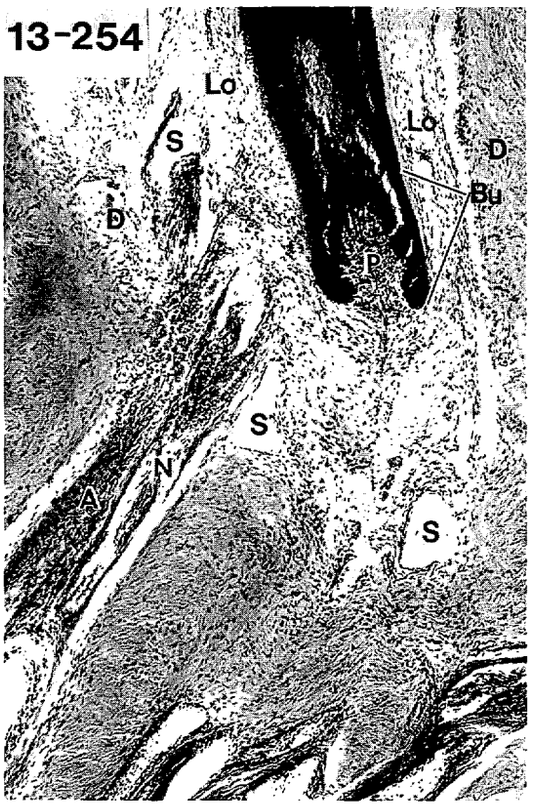
13-254
Lo
S
D
Lo
D
Bu
P
S
N
A
S

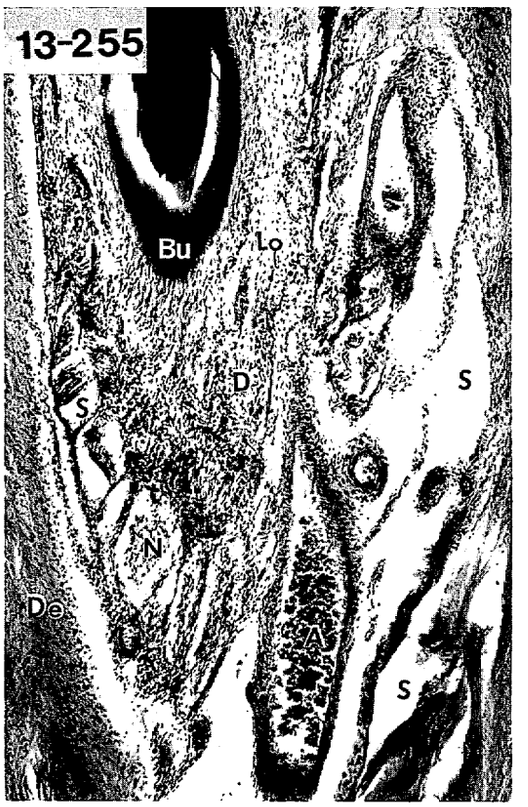
13-255
Bu
Lo
D
S
S
N
De
A
S

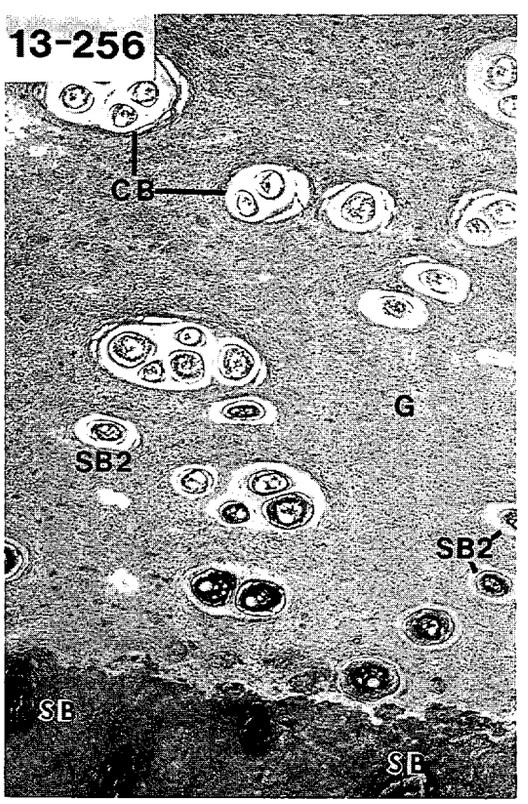
13-256
CB
G
SB2
SB2
SB
SB

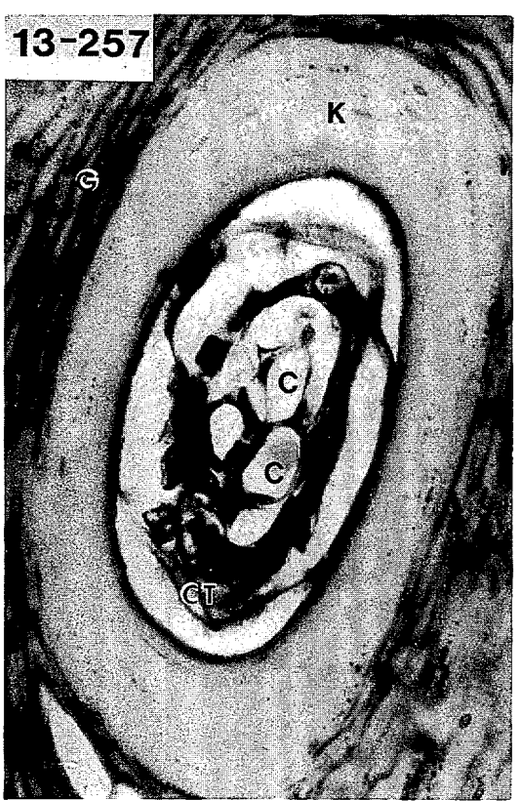
13-257
K
G
C
C
CT

Figure 13-258. Photomicrograph, vertical section of simple baleen hair emerging from gum, 80B1. The medulla (M) is essentially empty at the gum (G) surface with the papilla and blood vessels present only basally (above, out of the photo). The surface cell layers of the gum adhere tightly to the baleen shaft as it emerges (arrows). L.S.; H and E, X120

Figure 13-259. Photomicrograph, horizontal section of compound baleen hair, 80B1 . Compound baleen hairs (CB) originate as a cluster of simple baleen hairs (SE) from a group of connective tissue papillae that are closer together than in the simple baleen hair region. As the originally simple hairs approach the ends of their dermal papillae, the epidermal layers forming keratinized cortex (K) fuse forming a continuous cortex around the group. X.S., H and E, X120

Figure 13-260. Photomicrograph, horizontal section of compound baleen hair, 80B1 . At the ends of the connective tissue papillae and beyond, the now formed compound baleen hair (CB) assumes a more cylindrical form with the addition of more members. X.S., H and E, X330

Figure 13-161. Photomicrograph, vertical section of compound hair emerging from the gum, 80B1. The compound baleen hair (CB) emergence from the gum is similar to that of simple baleen hairs (Fig 13-258) with the surrounding cells of the gum adhering tightly. The multiple medullary cavities (M) are also essentially empty. L.S., H and E, X120.

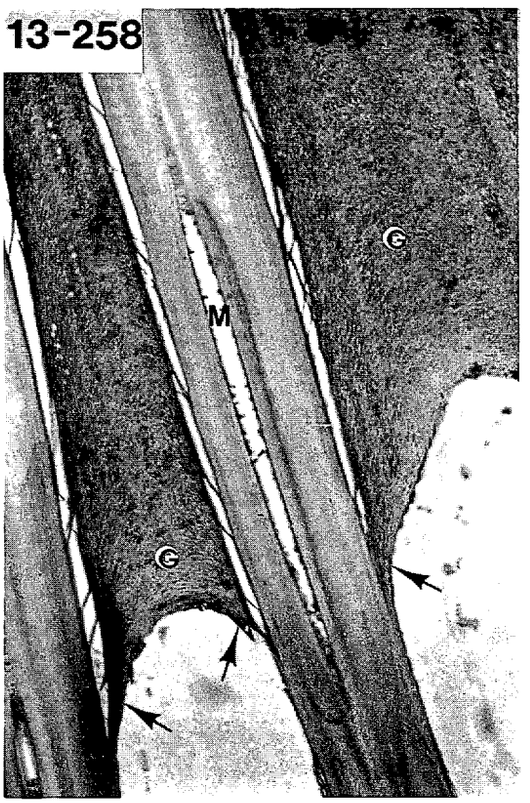
13-258
G
M
G

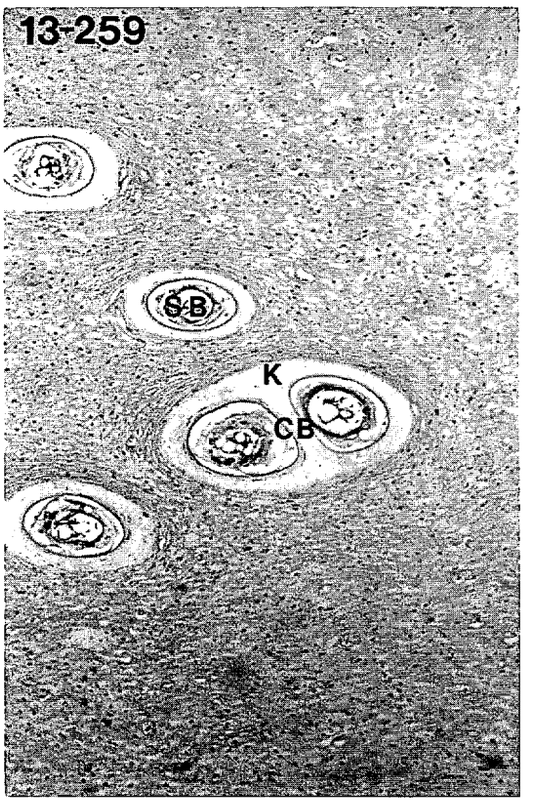
13-259
SB
K
CB

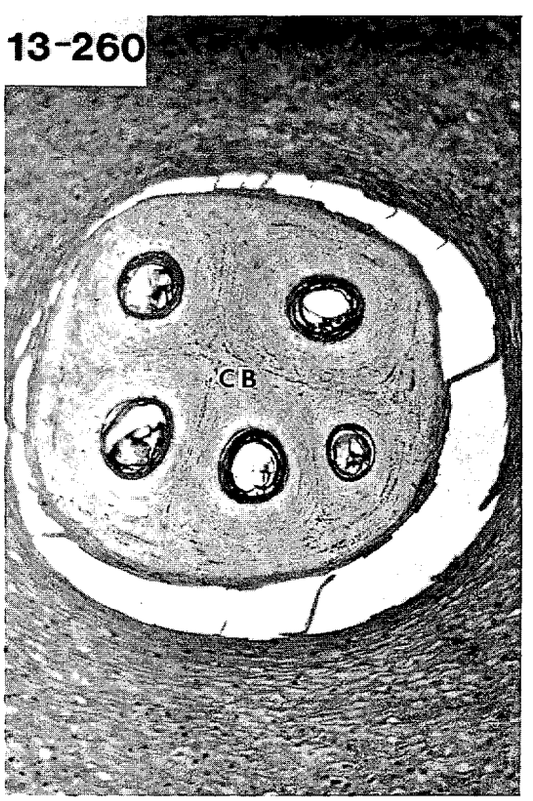
13-260
CB

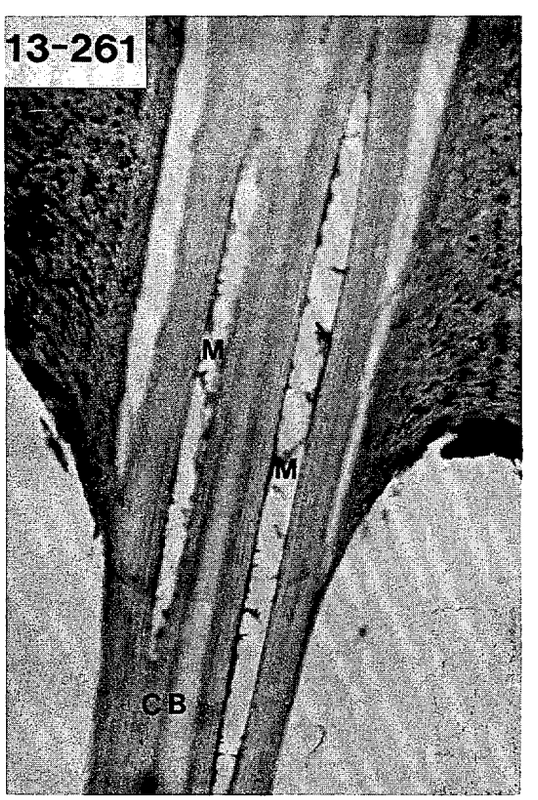
13-261
M
M
CB

Figure 13-262. Photograph of crude oil on a piece of chin skin and vibrissae, 79B2. Preserved skin with two vibrissae was lifted through an oil slick and returned through the slick to the aquarium three times at 3°C simulating a short series of breathing rolls. The crude oil (0) adhered to the skin in small patches which tend to increase in size with each exposure. One vibrissa (arrow) also acquired some oil, but the other (arrowhead) did not. X3

Figure 13-263. Photograph of crude oil on a piece of blowhole skin and vibrissa, 79KK1. The skin around the blowhole was much more dried out and rougher than the other samples tested. After three "rolls", oil (0) adhered to a greater extent than on the smoother chin. The vibrissa acquired two rings of oil (arrows) and a smal 1 droplet (arrowhead) adhered in the funnel-like epidermal depression that surrounds the vibrissa. x7.5

Figure 13-264A. Photograph of a piece of cream colored skin of the chin, 8061, Tag 54. The skin surface appears smooth with only a few very shallow, but smooth, brownish areas (arrows) probably covered with diatoms. The edge of the piece is to the left. Note the scratch artifact (arrowhead). x3

Figure 13-264B. Photograph of the same piece after three simulated breathing rolls through an oil slick. The three brown areas acquired some oil (arrows) with other areas acquiring even more (0). The edge of the piece is to the left with the scratch artifact (arrowhead) for comparison with Fig 13-264A. X3

13-262

13-263

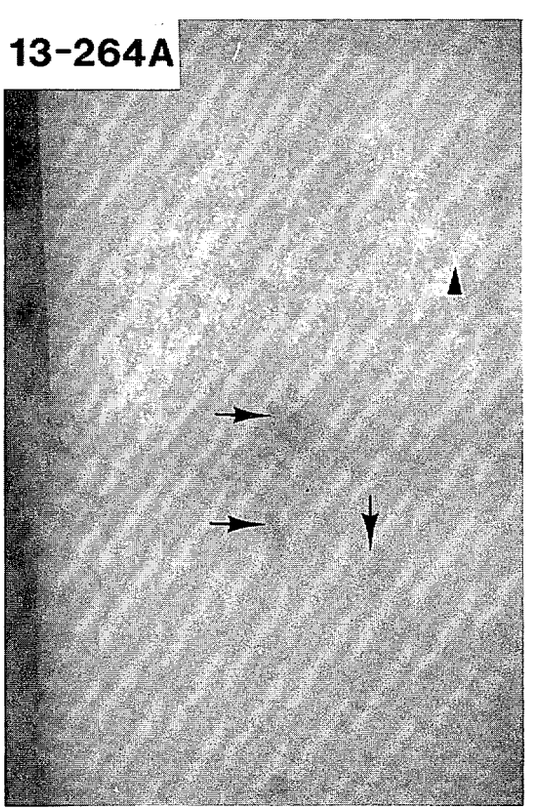
13-264A

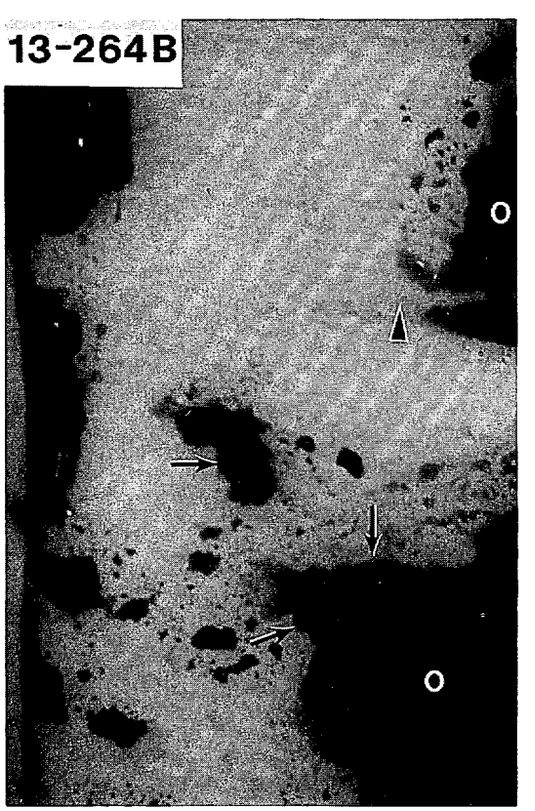
13-264B

Figure 13-265A. Photograph of a piece of the inner upper lip skin with large sensory papillae, 80B7, Tag 12. The epitheliums of this region of the upper lip contains large sensory papillae (SP) about 1 mm in diameter which are covered by only a few layers of cells (see Fig 13-218 for vertical section). The relatively thin epidermis (E) between papillae shows the ends of the darker epidermal rods (arrows)., X3

Figure 13-265B. Photograph of the same piece after three simulated breathing rolls through an oil slick. Most of the sensory papillae became covered by a large oil patch (0) with those not completely covered having at least very small spots of oil (arrows). X3

Figure 13-266A. Photograph of a large depression lesion in cream colored chin skin, 80B8, Tag 30. The crater of the lesion is the largest (2 X 3 cm) that was available for testing. The wall (W) drops almost vertically to the crater floor (F) which is rough and almost as large as the rim diameters. An area much whiter than the rest of the floor region contains two puncture-like depressions (arrows). X3

Figure 13-266B. Photograph of the same lesion after three simulated breathing rolls through an oil slick with the epidermis down. Small patches of oil (0) adhered to the lip of the crater and the surrounding normal epidermis. The pool of water maintained within the crater upon emergence through the slick apparently kept most of the oil out of the lesion with one exception (oC). The puncture depressions (arrows) did remain clear. x3

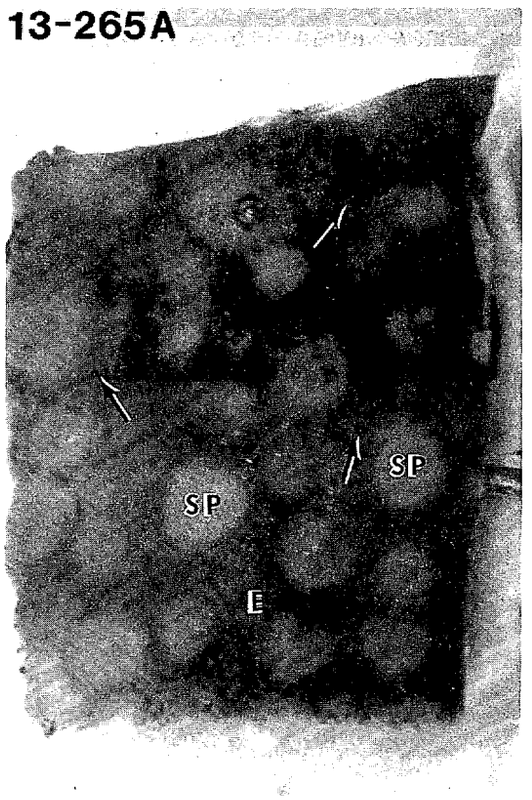
13-265A
SP
SP
E

13-265B
O

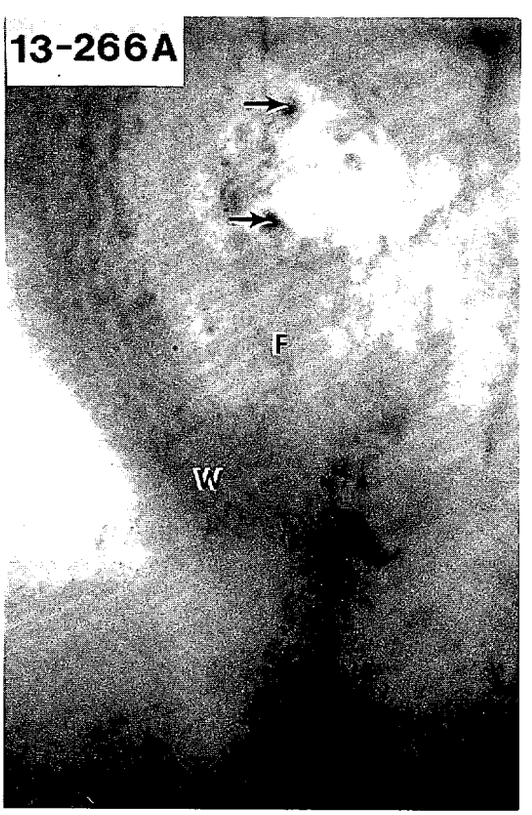
13-266A
F
W

13-266B
OC
O
O

Figure 13-267A. Photograph of an apparent abrasion on the upper lip, 80B7, Tag 22. The abrasion (A) is a very shallow groove. The surrounding epidermis (E) shows the normal appearance of the rosettes (R) of epidermal rods of the normal, lightly pigmented skin surface. The rods are also visible on the cut surface (right). X3

Figure 13-267B. Photograph of the same piece after three simulated breathing rolls through an oil slick with the epidermis down. The abrasion (A) acquired very little oil with more (0) adhering to the surrounding area. X3

Figure 13-268A. Photograph of a piece of upper lip with two lesions, 80B8, Tag 3A. An even granular lesion (EG) and a depression lesion (DL) show on this piece with a definitive diatom film (F) covering the epidermal surface. X3

Figure 13-268B. Photograph of the same piece after three simulated breathing rolls through an oil slick. With the epidermal surface held in its approximate normal position (down, inclined at one end about 200), small oil patches (arrows) adhered to the wall and rim of the depression lesion, the diatom film, and the even granular lesion. X3

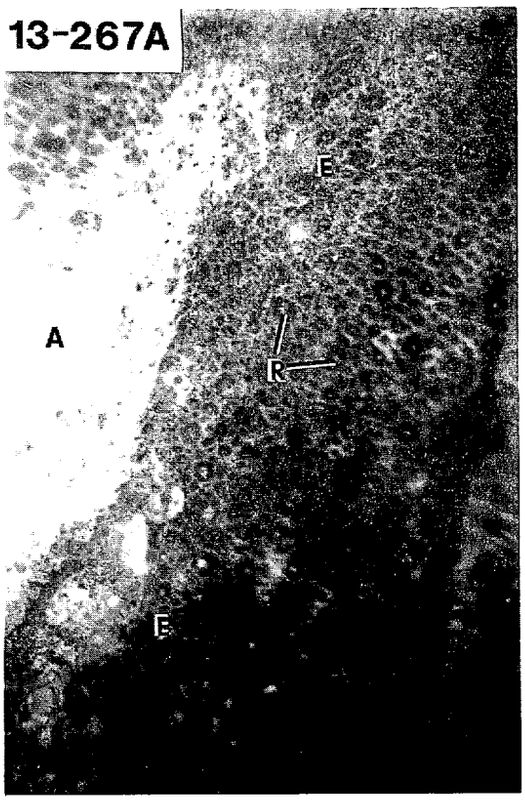
13-267A
E
A
R
E

13-267B
A
O

13-268A
DL
F
EG

13-268B

DISCUSSION

The degree of anatomical description just presented for each organ or system was affected directly (enhanced or retarded) by the number of adequately preserved pieces and intact organs available through RU 180 whose personnel were restricted by several uncontrollable factors.

The completeness of any anatomical study is also a function of time. Even with small animals where everything needed may be readily obtained or recollected, the "complete" story is achieved only after several years of study and, even then, is subject to revision as new techniques are developed which provide information not previously available. The development of transmission and scanning electron microscopy during the last 30 years is. a prime example. The very short time allowed for this project has had a detrimental effect on several aspects of the study. The overall results of the present study are in our judgement a valuable basic description to which our group and others may add during ensuing years.

I. Lung

The lung subgroup was fortunate in receiving entire organs of the respiratory system except for the blowhole (most but not all of one was available), the nasal cavity mucosa (nothing available), and the larynx (the cranial portion of an 8.7 m Ingutuk and the caudal portion of a 10.9 m ordinary bowhead were available, but did not fit together because of size). The trachea and lungs were complete with more than sufficient lung tissues. Preserved chunks of lung were well fixed for light microscopy and gross anatomical study. The special thin slices for electron microscopy did not fix well hampering their study, therefore, formalin fixed slices were utilized to help establish basic morphology.

The respiratory system of the bowhead appeared to have many characteristics which are common in Cetacea. The nasal passages begin at the paired external nares (blowholes). The external nares sit on the dorsalmost area of the skull which was referred to as the "crown" by whalers (Eschricht and Rei nhardt 1866). The nares are reported 337-380 cm (Omura et al 1969) and 480 cm (McVay 1973) caudal to the tip of the snout (lips) in black and Greenland right whales respectively. The external nares of the sperm whale are located near the rostral end of the head (Clarke 1979) which necessitates a longer nasal passage. The bowhead nares were 20 cm in length which falls in the

reported ranges of 8-30 (Omura et al 1969), 27 cm (Omura 1958) and 15-20 (McVay 1973) for right whales. The smaller values were on fetuses.

The bowhead external nares, separated anteriorly by only 3 cm, were closer together than the 10 cm separation of the right whale (Omura, 1958). Caudally they were separated 18 cm which yields a "V" shaped blow (vapor steam) when the whale exhales (Slijper, 1979). The nares were passively closed by the narial sphincter which was located in their rostral and lateral vestibular walls. The sphincter has been referred to as a thick tumid fold of skin (Eschricht and Reinhardt 1866) and melon shaped mass (Albert 1980). We found it to be a thickened "U" shaped structure with the united portion in the rostral wall of the vestibules. It was composed of blubber traversed by skeletal muscle cords which radiated out from the rostral and lateral surfaces of the vestibular walls. They probably inserted on the medial and rostral surfaces of the recessed area of the maxillae which housed this mass of tissue. The sphincter was enclosed by a dense connective tissue capsule which isolated it from the normal hypodermal blubber. The sphincter apparently serves to passively hold the nares closed except during in- or exhalation when contraction of the skeletal muscle cords pull the blubber mass laterally and rostrally opening the vestibular and nasal cavities.

The vestibular and nasal cavities were separated by paired nasal cartilages. The nasal cavities lead into the nasopharynx which is divided from the oropharynx by the soft palate. The caudal portion of the soft palate had a circular muscular opening (palatopharyngeal sphincter) through which the pharyngi communicated similar to what is reported in other cetaceans (Fanning and Harrison 1974).

The rostral protuberance of the mobile larynx was blunter than in most cetaceans. It is apparently inserted into the palatopharyngeal sphincter during respiration, thus forming a sealed respiratory passage from the lungs to the dorsal surface of the cranium.

The laryngeal cartilages seemed similar to those of other mysticetes. The trough shaped cricoid cartilage formed a less rigid structure than the typical ring-shaped mammalian cricoid. This configuration may lend itself to a more effective seal with the arytenoid cartilages. The arytenoids had no vocal cords associated with them, which is typical of cetaceans. They terminated caudally as two separate rods, without the fusion described by Eschricht and Reinhardt (1866) in the Greenland right whale.

The thyroid cartilages had a stout cricothyroid muscle which could also aid in an effective closure of the larynx along with the median pyramidal eminence of the epiglottis cartilage. The laryngeal cavity was a bit different than in other species. It lay between the arytenoid and cricoid cartilages with a caudal diverticulum (laryngeal sac) exiting between the caudalmost tips of the arytenoid and thyroid cartilages. The laryngeal sac is reported to extend from the ventral surface of the laryngeal cavity in other species of Mysticeti, being referred to as the sublaryngeal pouch, tracheal bag, and ventral laryngeal pouch (Benham 1901, Hosokawa 1950). The mucous membrane lined diverticulum with stratified squamous epitheliums was surrounded by a heavy skeletal muscle wall, which served not only as the sac wall, but as the ventral floor of the trachea. The muscle fibers attached primarily to the ventral free tips of the C-shaped tracheal cartilages. However, the rostralmost fibers attached to the caudoventral aspect of the cricoid cartilage, the caudolateral margins of the arytenoids, and the dorsal surface of the tracheal cartilage midline. Because these muscle fibers served as the wall of the laryngeal sac, probably represent the fusion of portions of the classical cricothyroid, transverse arytenoid and cricoarytenoid muscles, and served as the tracheal floor, it is difficult to select an appropriate name. No distinct divisions appeared to separate the muscle into bundles. Therefore, we chose to refer to this muscular mass as the muscle of the laryngeal sac.

The laryngeal cavity inclined dorsocaudally over the caudal ends of the arytenoid cartilages to join the trachea. Apparently, contraction or relaxation of the laryngeal sac muscle alters the lumen of the airway at the laryngotracheal junction. The laryngeal cavity was lined by keratinized stratified squamous epitheliums except at its caudalmost limits where it became nonkeratinized stratified squamous epitheliums.

The trachea consisted of ten C-shaped vascularized hyaline cartilage rings which were open ventrally. Ventrally open C-shaped cartilages are reported also for the Sei whale (Hosokawa 1950). Eschricht and Reinhardt (1866) found the last three tracheal cartil ages to be complete rings in the Greenland right whale. Most reports confirm the presence of at least some closed tracheal rings (Benham 1901, Wislocki 1929) in most whales. The yellow color of the surrounding tissue was indicative of the high elastic fiber content of the perichondrium and surrounding tissue. The trachea was relatively short (19 cm) in length with the horizontal diameter about twice the vertical

diameter. All of the preceding seems to indicate that the trachea could collapse to some extent with increased pressure during dives.

The epitheliums changed at the laryngotracheal junction from stratified squamous to a ciliated, pseudostratified columnar type which overlay a heavy lymphatic infiltration in this area. Lymphatic nodules were found on the laryngeal side of the junction but the trachea had only a diffuse infiltration for a short distance as reported in other cetaceans (Fanning and Harrison 1974, Simpson and Gardner 1972). The midportion of the trachea had mucoserous glands in the elastic lamina propria.

The trachea terminated at the bifurcation into principal bronchi which were nearly the same width as the trachea, possibly aiding in rapid air exchange. No tracheal bronchus was present in the bowhead as is reported for most cetaceans (Benham 1901, Fanning and Harrison 1974, Slijper 1979, Wislocki 1929). The bronchial epitheliums was ciliated, pseudostratified columnar with underlying glands. No lymphatic accumulations were noted in the mucosa, which appeared similar to that reported in other cetaceans (Fanning and Harrison 1974).

The epithelial surface morphology of the bronchi of the bowhead was similar to what is reported in other species (Andrews 1974, Breeze and Wheeldon 1977, Boshier and Hill 1974) with both ciliated and conciliated cells present. The presence of microvilli on the surface of both ciliated and non-ciliated cells is likewise reported in other species (Andrews 1974, Breeze and Wheel don 1977). The significance of the increased number of ciliated cells between the primary bronchus and smaller bronchi seen here is not known. Large individual variations in the degree of bronchial ciliation are reported in other species (Andrews 1974). Our observations, therefore, could simply represent the pattern in one individual and not be generalizable to the species. On the other hand, the decreased ciliation could reflect an epithelial response to the mechanical stresses of the large volume of gas moving over the surface at high velocity. Clarification of the significance of our observations awaits a more complete survey of the epithelial surfaces of airways from the trachea to the respiratory bronchiole from several individuals. The presence of a great deal of debris on the surface of the bronchi probably represents material, such as blood, from the trauma of the hunt and the butchering process. Such material would become entrapped in the mucous sheet and subsequently be retained when the tissue was fixed.

At the ultrastructural level, the overall morphology of the bronchial epitheliums was similar to what has been reported in other species (Breeze and Wheel don 1977). The mucus producing cells containing microvilli were similar to those of other species (Andrews 1974, Breeze and Wheeldon 1977) including other cetaceans (Fanning and Harri son 1974). The complex lateral and basal extension of the columnar cells plus the wide spaces between basal cells with cell junctions, notably desmosomes, between adjacent processes are all reported in other species (Breeze and Wheel don 1977). Since the pseudostratified columnar epitheliums reported here was similar to that seen in other species, it may be possible to use data from other species in assessing potential effects on bowhead bronchial epitheliums. The presence and morphology of submucosal mucous glands beneath the epitheliums of the primary bronchus was similar to what has been reported in other species (Junqueira and Carneiro 1980). Relatively poor preservation of the intracellular components prevented a more detailed examination of the structure of individual cells making up the bronchial epitheliums and its underlying connective tissue.

The lobar bronchi gave off segmental bronchi at obtuse angles similar to the angles reported for the Weddel 1 seal (Boshier and Hil 1 1974). Segmental bronchi of medium size were found throughout the lung parenchyma and also near the surface. This would appear to allow a quick exchange of air in all areas of the lung simultaneously. Segmental bronchi had complete cartilaginous rings which were lined with ciliated, pseudostratified columnar epithelium. The lamina propria contained an abundance of elastic fibers and mucous glands.

As bronchioles became smaller, the pseudostratified columnar epithelium became thinner, the number of ciliated cells increased, and mucous glands were absent. Cartilaginous rings were seen in bronchioles as small as 0.3 mm. A muscularis mucosae (smooth muscle layer) was present in primary bronchioles through the smallest terminal bronchioles. This arrangement was similar to other species (Belanger 1940, Simpson and Gardner 1972, Wislocki and Belanger 1940, Wislocki 1935). Myoelastic sphincters within the bronchioles seen in smaller cetaceans (Goudappel and Slijper 1958, Belanger 1940, Wislocki and Belanger 1940) and to varying degrees in larger cetaceans (Murata 1951) were not present in the bowhead. The manatee and dugong (Wislocki 1935), the harbor propoise and other large whales (Lacoste and Baudrimont 1933, Harrison and Tomlinson 1963) also lack the sphincters in their bronchioles;

Occasional alveoli opened from the distal portion of some terminal bronchioles. At the terminal bronchial ar-respiratory bronchiolar junction, the pseudostratified columnar epitheliums changed to simple squamous epitheliums which nearly surrounded the capillaries. The cartilaginous rings became plaques and the muscularis mucosae terminated at the transition to respiratory bronchioles and was absent throughout the alveolar ducts, alveolar sacs, and alveoli. The walls of the respiratory bronchioles were pierced by openings to individual alveoli and small alveolar sacs so that there was proportionately more area occupied by openings than by wall tissues. Wall structure was similar to that in other cetaceans except that the mucosa and knob-like sphincters around the openings contained elastic fibers only. Muscle and elastic (myoelastic) sphincters are reported in other cetaceans (Boshier and Hill, 1974, Simpson and Gardner 1972).

The alveolar ducts and alveolar sacs had the cetacean characteristic of thin respiratory epitheliums nearly surrounding the capillaries (more completely than in terrestrial mammals). The alveolar epitheliums did not surround the capillaries as extensively, but adhered closely to the capillaries as in the ducts and sacs. The interalveolar septa had not only double respiratory epithelial linings, but double capillary beds as reported in other cetaceans (Wislocki 1935, Goudappel and Slijper 1958, Simpson and Gardner 1972, Harrison and Toml inson 1963, Boshier and Hil 1 1974).

At the alveolar junction with an alveolar duct or alveolar sac, there were no myoelastic sphincters as reported in other cetaceans (Engle 1966, Goudappel and Slijper 1958, Murate 1951, Simpson and Gardner 1972, Wislocki 1935, Wislocki and Belanger 1940). The bowhead sphincters were composed only of elastic fibers as previously reported in other large whales by Simpson and Gardner (1972). These observations are contrary to Wislocki and Belanger (1940) and Goudappel and S1 i jper (1958). Some alveoli and alveolar sacs anastomosed as also reported by Murata (1951). These anastomoses would facilitate the spread of pneumonia, as would the lack of continuous connective tissue septa between lobular units.

The respiratory epitheliums composed of both type I and type II pneumocytes was similar to that observed in other species. (Simpson and Gardner 1972, Fanning and Harrison 1974, Kuhn 1978). The relatively large number of type II cells observed here and their lack of confinement to the intercapil-1 ary spaces is also reported in other Cetacea (Ito et al 1967). A quantitative study of the number and position of type 11 pneumocytes could shed light

on the significance of this observation. The large numbers of type II pneumocytes could reflect an increased requirement for the production of surface active agents, but without quantitation it was not possible to conclude any more than that there was an apparent increase in the numbers of type II pneumocytes relative to other species.

The surfactant (surface active agent) is produced in type 11 pneumocytes (Askin and Khun 1971, Buckingham et al 1966, Kikkawa et al 1975). The multilamellar bodies are thought to be the source of at least part of this material (Williams 1977, Callas 1974, Gill and Reiss 1973). The existence of both multilamellar bodies and tubular myelin lying free in the respiratory spaces is likewise reported in other species (Williams 1977) but has not been reported in other cetaceans. The very dense thin coat on the surface of the plasma membrane of cells of the respiratory epitheliums may represent the phospholipid component of the surfactant. Tannic acid was used as a mordant to enhance the staining of phospholipid containing materials.

Chondrocytes of the cartilage supporting the bronchi were similar in morphology to chondrocytes seen in other species (Junqueira and Carneiro 1980, Rhodin 1975).

At the ultrastructural level no evidence was found for the presence of smooth muscle cells in the elastic knobs associated with alveoli. Fibroblast-like cells were present and contained microfilaments. Their highly irregular, branched cellular processes and lack of organized bundles of microfilaments clearly differentiated them from classical smooth muscle cells (Junqueira and Carnei no 1980, Rhodin 1975). Ultrastructurally the wall of the alveolus was similar to that reported in cetaceans and other species (Fanning and Harrison 1974, Khun 1978).

The presence of mononuclear cells in the connective tissue and capillaries of the lung was not surprising and, in the case of those in capillaries, may represent a source of alveolar macrophages. Few cells were seen, therefore, their significance and indeed their unambiguous identification could 'not be made at this time. The unusual inclusion shown in a type II pneumocyte (Fig 13-90) is unidentified, but may represent an abnormal intracellular release of surfactant by the multilamellar bodies.

II. Kidney

Studies on the cetacean kidney began in 1680 with Tyson (Arvy 1974) . Since then, the number of species studied has increased with 47 spe-

ties having been described in 153 investigations to date. Meek (1918) shows a diagram of the kidney of a 41 cm long bowhead whale (Balaena mysticetus). This is the only mention of the kidney of this species in the literature.

Studies on the kidney of small cetaceans are easier to conduct than on large species. Kidney size varies from 7.8 x 5 cm in the Altantic harbor porpoise (Phocoena phocoena) to 2 m in the fin-backed whale (Balaenoptera physalus) (Arvy 1974). For this reason, the small sized cetacean kidneys are available to investigators whole, while in larger species, the large organ is often only available in pieces. This immediately eliminates direct information about the kidney such as shape, size, weight, general outline and arrangement of hili and sinuses. Small pieces of the organ also fail to allow the study of branching patterns and general architecture of the blood vessels and ureteric system of the entire kidney. To infer these patterns from pieces of kidney is difficult. Injection masses leak through the cut surfaces and do not render a complete filling of the systems injected. The kidney of the bowhead whale is a large one and all the material available for study was in small chunks.

From the specimens available to us, the kidney of the bowhead whale had the basic characteristics of cetacean kidneys. It was highly lobulated with the morphological and functional unit being the individual lobule or renicule. The terminology for these lobules varies among authors; reniculus (Cave and Aumonier 1961, 1962, 1964a, 1964b, 1965, 1967a, 1967b, Arvy 1974) renule (Owen 1868 quoted by Arvy 1974), reniculus and reniculi (Daut 1898 quoted by Arvy 1974). Other authors called the individual units lobulins, lobules or grains. Each renicule corresponds to a unipapillary kidney of terrestrial animals which exhibit lobulated kidneys e.g. the ox and bear. The number of lobules is always small in terrestrial mammals, 12-25 in the ox and 34 in the bear while the number of renicules in cetaceans is rarely less than 100. Even a small cetacean like the Atlantic dolphin (Delphinus delphis) has more than 400 (Arvy 1974). The arrangement of these renicules in the kidney of cetaceans varies being either grouped in clusters or scattered without grouping. In the fin-backed whale and blue whale (Balaenoptera musculus), the renicules are arranged in groups of three, five or six with their cortices or medullae fused (Arvy 1974). In the bowhead whale, the renicules were arranged in clusters of the same numbers with the same possibility of fusion between cortices and medullary tissue; most clusters were, however, without fusions (Figs 13-98, 13-99, 13-100, 13-101, 13-116). The renicules were covered by

a loose connective tissue fascia with its deepest layer adherent to the renicular capsule. The renicular capsule was very thin and fibrous and was not adherent like that of terrestrial animals. It did not send septa into the cortex to subdivide it into lobes. The Atlantic dolphin, Atlantic harbor porpoise and grey porpoise demonstrate the same feature (Arvy 1974). On the other hand, Bouvier (1892) and Anthony (1922) (quoted by Arvy 1974) found that the capsule was adherent on renicules of the bottle-nose whale (Hyperoodon). In addition, the capsule penetrates the renicules in the beaked whale (Mesoplodon) (Arvy 1974) "

Measurements for renicules in the kidney of the bowhead whale ranged from 7.8-14.1 mm at their widest diameter and 7-10.1 mm at their narrowest diameter (Figs 13-114, 13-115). The following are measurements of renicules from different cetaceans. In a young goose-beaked whale (Ziphius) the diameter of the renicules was between 1.3 and 1.8 cm (Scott and Parker 1885). In the Atlantic bottle-nosed dolphin (Turisops truncates,) the greatest renicular size was 11 x 9 mm. In the little piked whale (Balaenoptera acutorostrata), the smallest renicule measured 13.5 x 10 mm and the largest 14.8 mm, and in the pigmy white whale (Caperea marginata) maximum diameter measured 16 mm and the smaller diameter was 9 mm (Cave and Aumonier, 1961, 1964a, 1964b, 1967a, 1967 b). In adult fin-backed whales, the mean renicular diameter varied from 150 mm to 293 mm, while in the blue whale it varied from 199 mm to 390 mm (Ommanney 1932 quoted by Arvy 1974). From this comparison the average renicule size in the bowhead whale was larger than that of the Atlantic bottle-nosed dolphin and the pigmy white whale, about the same as that of little piked whale, but smaller than those of fin-backed and blue whales.

Dissection of renicules revealed that the majority have their own cortex, medulla, papilla and calyx with a small number possessing a cortex or medulla fused with a neighboring renicule (Figs 13-143, 13-144). No renicules were found to be fused together at both cortical and papillary levels. Fused papillae shared one calyx. In some renicules, two calyces communicated with each other and joined one infundibulum. Arvy (1974) reports that in the Ganges dolphin (Platanista gangetica), an odontocete, generally three calyces open into one infundibulum. Anthony (1922) (quoted by Arvy 1974) observed renicules with three papillae in the beaked whale while in fin-backed and blue whales, both mysticetes, renicules in clusters of two or three have both fused cortices and medullae or just fused medullae (Arvy 1974).

One of the outstanding characteristics of cetacean kidneys is the presence of a connective tissue sheet at the corticomedullary junction. This structure was first described by Cave and Aumonier (1961) and subsequently in 18 cetacean species (1962, 1964a, 1964b, 1965, 1967a, 1967 b). Cave and Aumonier (1961) stated that it is a basket-shaped structure that consists of fibrous connective tissue with smooth muscle fibers and named it "sporta perimedullaris musculosa." In their first publication (Cave and Aumonier 1961) they speculated that "the sporta is associated with the maintenance or enhancement of renal function in a group of animals who are devoid of sweat glands, subsist on an excessively saline diet and sustain life at variable (often considerable) depths. " Cave and Aumonier (1961) further state that "The prepapillary 'basket' of muscle and collagen, sporta perimedullaris musculosa, appears to represent a mechanism controlling the outflow of urine from the reniculus... For the muscle of this basket is quantitatively sufficient so to compress or milk the Bellini ducts as to expedite urine-discharge into the renicule calyx, but it seems insufficient (and mechanically ill-disposed) to effect total temporary obstruction of these tubules. The renicular arteries, lying essentially outside the basket, are not subject to compression by basket contraction. It seems, therefore, the basket device cannot influence the production of urine, but can and does, influence the medullary outflow thereof." Simpson and Gardner (1972) in their description of the microscopic anatomy of the cetacean kidney include a photomicrograph of the kidney of a false killer whale. Its legend reads "A prominent band of connective tissue surrounds the renicular pyramid at the corticomedullary junction. This fibrous tissue extends from the ureteric calyx and runs near to but apparently separate from the arcuate vessels. This structure has been called intrarenicular sporta perimedullaris musculosa. Its functional significance is unknown." The tissue demonstrated in the photomicrograph was stained with hematoxylin and eosin and was taken under low magnification of x75. There is no mention of smooth muscle fibers as a component of the sporta. In the text, however, they describe the sporta as a continuous, coarse band of connective tissue containing a few smooth muscle fibers. The sporta perimedullaris of the bowhead was well developed. It was not restricted to the corticomedullary junction and it did not exist only at a level where it was continuous with the wall of the calyx as Cave and Aumonier (1961, 1962, 1964a, 1964b, 1965, 1967a, 1967b) describe it in other cetaceans. In the bowhead the tissue of the sporta started as a thickening of the cortical stroma about 1 mm from the

cortical capsule. Deeper in the cortex it became a denser sheet. of connective tissue with medullary rays penetrating it. At the corticomedullary junction, it formed a ring of dense tissue that contained arcuate vessels (Figs 13-110, 13-119). The presence of arcuate vessels in the sporta at the corticomedullary area was a new and interesting finding in the bowhead not reported in other cetaceans. Cave and Aumonier (1964a, 1964b, 1965, 1967a, 1967b) studied 18 species of cetaceans. In all of them they describe the corticomedullary junction as the site where arteries enter and veins exit. From that point arteries divide and anastomose to form the perimedullary arterial plexus superficial to and at a distance from the perimedullary sporta. The arterial plexus is enmeshed within a perimedullary venous plexus which communicates with subcapsular veins. They further state that any blood vessels in the substance of the sporta are small vessels that supply its tissue components with nourishment. In the bowhead, arteries and veins entered and exited from the renicule at the corticomedullary junction as described for other cetaceans by Cave and Aumonier (1964a, 1964b, 1965, 1967a, 1967b) but after entering the renicule, the arteries were embedded in the sporta forming arcuate vessels. Veins collected blood from subcapsular, cortical interlobular veins, and vasa rectae which entered the substance of the sporta and exited at the corticomedullary junction (Figs 13-110, 13-119D, 13-119E, 13-120, 13-135, 13-137, 13-139, 13-143).

Our histological sections of renicules of the bowhead were stained using hematoxylin and eosin, Mallory's, Masson's and Milligan's techniques. The last three stains differentiate fibrous connective tissue from smooth muscle cells. The contrast between green stained connective tissue and red-purple smooth muscle, especially that achieved with Milligan's stain, facilitated the differentiation between the two tissues. Our findings indicated that the sporta perimedullaris in renicules of the bowhead did not contain smooth muscle fibers as part of its structure. This was also true for the structure of the calyx and infundibulum. Any smooth muscle observed in these structures was part of a blood vessel only.

Microscopically the renicular cortex and medulla had a typical mammalian structure. The size of renal corpuscles ranged from 120 x 100 µm to 170 x 110 µm in the bowhead whale. In the little piked whale they measure between 110 x 55 µm and 115 x 90 µm (Cave and Aumonier 1964a, 1964b). In the pygmy white whale corpuscles measure approximately 200 µm while in the fin-backed whale and white-sided dolphin (Lagenorhynchus) they measure 175 x 100,

13 x 165 or 150 x 150 μm (Cave and Aumonier 1961, 1964a, 1964b). These latter species have larger glomerular sizes than those of the bowhead.

The juxtaglomerular apparatus of the renicular cortex in the bowhead was well developed (Fig 13-125). The macula densa was large and contained as many as 19 cells crowded next to the polar cushion or extraglomerular mesangium. Cowan (1966a, 1966b) describes a large macula densa in the pilot whale (Globicephala melaena). Simpson and Gardner (1972) state that the macula densa of the juxtaglomerular apparatus in the Atlantic bottlenosed porpoise is easily discernible, but the juxtaglomerular cells are no more conspicuous than in healthy humans. An unusual feature of the afferent glomerular arterioles in the bowhead was the modification of the smooth muscle cells in their walls into juxtaglomerular cells which began as these arterioles branched from interlobular cortical arteries far away from the glomerulus (Figs 13-123, 13-124, 13-125). These juxtaglomerular cells were optically clear and did not stain like smooth muscle cells. They were shorter and stouter and showed no evidence of renin granules next to the macula densa even after staining with the periodic acid-Schiff reaction. There was also no evidence of renin granules in the cells of the macula densa. Eichelberger et al (1940), quoted by Sokabe and Ogawa (1974), extracted renin from the kidney of dolphins similar to that of the dog and pig. Melvin and Vander (1967), quoted by Sokabe and Ogawa (1974), found renin in the gray porpoise, Gill's bottle-nosed dolphin (Turisops gilli), false killer whale (Pseudorca crassidens) and pilot whale. They used the indirect or in vitro method of testing for renin where tissue extract is incubated with an angiotensin preparation. Sokabe and Ogawa (1974) state that the juxtaglomerular cells were missing from the walls of afferent arterioles of the Atlantic right whale (Eubalaena glacilis), but macula densa and extraglomerular mesangium were present.

Certain microscopic structures of renal tubules were visible despite poor preservation of the specimens. Tubules were identified both in the cortex and medulla with identifying features pointed out in Figs 13-121, 13-123, 13-140, 13-141, 13-142. The presence of thin segments of Henle's loop deep in the renal papilla (Fig 13-142) indicated long nephrons as compared with short ones which reached only to the outer zone of the medulla. From the physiological point of view, this could mean an increased ability to concentrate urine. This feature is usually observed in animals which require preservation of body water. The human kidney has short and long nephrons with

good ability to concentrate urine. The kidney of the Rhesus monkey. which has primarily short nephrons can concentrate urine to the same extent as the human organ. It may be speculated that the whale's long nephrons are needed to preserve body water and get rid of excessive amounts of salts taken in during feeding. It is not known whether the bowhead, or any other whale, drinks water.

The fine structure of the bowhead renal corpuscle was similar to that reported for other species (Junqueira and Carneiro 1980, Rhodin 1975). The distance across filtration slits (60 rim), however, was slightly larger than the normal range for terrestrial mammals (Chevil le 1976). A diaphragm across the filtration slits, which is commonly observed in other species (Chevil le 1976, Junquei ra and Carnei ro 1980), was not observed here. Both the large filtration slit dimensions and the lack of a diaphragm could be a result of poor preservation. Poor preservation was certainly evident elsewhere in the kidney (Fig 13-133). On the other hand, the presence of microfilaments, microtubules, and well preserved mitochondria in the secondary (foot) processes of the podocytes (Fig 13-131) may indicate adequate preservation of this region. In general, a quantitative investigation on better preserved kidneys should yield more precise information.

It was not possible to make ultrastructural observations on the tubules of the nephron nor on the structures of the medulla. Very poor preservation is clearly evident in Figs 13-133 and 13-134. The very thick basal lamina seen in Figs 13-133 and 13-134 may be completely artifactual or may incorporate materials not normally found in basal laminae. Information on the fine structure of components of the medulla and on the tubules of the nephron must await better preserved specimens.

In the bowhead, an outstanding feature of interrenicular connective tissue was the large, thin walled veins that surrounded calyces, infundibula, ureteral branches and arteries. When filled with blood, they should form a hydrostatic cushion around these structures (Figs 13-102, 13-103, 13-104, 13-105, 13-106, 13-110). These veins have not previously been described in spite of detailed discussions by Cave and Aumonier (1962, 1964a, 1964b, 1965, 1967a, 1967b) of the vascular architecture of kidneys of 18 cetaceans. These veins, when filled with blood, may constitute the bulk of the interrenicular mass with very little loose connective tissue in between. Attempts to fill these veins with an injection mass to study their branching patterns were unsuccessful. The extensive leakage from cut surfaces in spite of attempts to clamp

and ligate visible vessels was the principle reason for this failure. On the other hand, some of the injection mass was carried immediately during the injection procedure into cortical veins and out to tiny subcapsular venules which were evident on the renicular surface (Fig 13-112). This finding was a good indication that cortical veins communicated directly with interrenicular veins. Figure 13-136 is a section of a renicule with this communication demonstrated. This slide also demonstrates that veins leave and arteries enter the renicule at the corticomedullary junction. Cave and Aumonier (1964a, 1964b, 1966, 1967a, 1967b) studied the vascular patterns in renicules of the Pacific dolphin (Delphinus bairdi), gray porpoise (Stenella coeruleo-alba) beluga or white whale (Delphinapterus leucas), slender beaked porpoise (Stenel 1 a attenuata), long beaked porpoise (Stenella longirostris), white sided dolphin (Lagenorhynchus cruciger), humpback dolphin (Sousa plumbea), Atlantic harbor porpoise and sperm whale (Physter catodon). They found that the renicules have peri- and interrenicular plexuses that assist in the drainage of renicular venous system. This was true in all the species except the white sided dolphin and Atlantic harbor porpoise. Our findings in the bowhead demonstrated that this cetacean did not possess a perirenicular venous plexus on the surface of the cortex. The rapid entry of the injection mass was due to direct communication between intrinsic renicular and extrinsic large renal veins and may also mean that venous blood drains rapidly due to an efficient blood filtering system in this whale's kidney. This also explains the relatively large veins that receive venous blood from the renicules. We can speculate that the large interrenicular veins that surround renal calyces, infundibula, ureteral branches, and arteries may have a dual function. They may act as hydrostatic cushions to ensure patency of these structures, and they are large to accommodate the rapid outflow of venous blood as it returns from filtering renicules.

The structure of the urinary bladder of the bowhead was typically mammalian. One interesting feature was the presence of small blood capillaries next to the basal cell layers of the transitional epitheliums. Search of the literature did not reveal any histological studies of cetacean bladders except those reported by Simpson and Gardner (1972). These authors state that bladders of cetaceans and pinnipeds are lined by a nonkeratinized transitional epitheliums about six cells in average thickness. They do not describe a lamina propria or muscularis mucosae but describe the submucosa as being made of parallel lamellae of loose connective tissue. They describe the tunics

muscularis as composed of fascicles of smooth muscle which run in. a generally circular direction and do not show the same thickness or degree of multidirectionality as seen in the human bladder. A photomicrograph of the urinary bladder of the Atlantic bottlenose porpoise illustrated these descriptions. The bladder of the bowhead had a lamina muscularis mucosae and the muscle layers were multidirectional. The urinary bladder of whale 79B1, a8.7 m male Ingutuk variant, had a 3.7 cm thick wall while that of bowhead 80B7, a 10.0 m female ordinary bowhead, measured 6.5 cm. Also the wall of the male bladder consisted of a tunics mucosa with a lamina muscularis mucosae, tunics submucosa, and a tunics muscularis which consisted of loosely attached bundles of smooth muscle fibers. The wall of the female bladder on the other hand, was made of a combined tunics mucosa-submucosa with bundles of smooth muscle fibers scattered randomly among looser vascular connective tissue. The tunics muscularis differed from that of the Ingutuk variant also in consisting of thick, tightly arranged bundles of smooth muscle fiber. These changes would be significant if they were observed in more than one sample of each sex. The difference could be related to animal size, age, sex, or morphological type. To derive more accurate conclusions, more well preserved specimens are needed.

Whole kidneys (right and left) are needed to complete the macroscopic description of this organ. Better preserved materials for light and electron microscopic studies are also essential to provide more accurate descriptions of the microstructure. Maceration techniques require fresh or frozen specimens to isolate and study nephrons in detail. More specimens are needed for vascular and ureteral injections to study their architectural patterns. Fresh material is needed if assays of renin in kidney extracts are to be conducted. Samples of ureters and ureter-bladder junctions are needed to describe these morphological entities. We feel that this work will not be complete without these studies.

III. Brain

Attempts have been made to assess the degree of "encephalization" in various cetaceans (Pilleri 1966b, Pilleri and Gihr 1970). In general, odontocete whales are said to exhibit a higher degree of encephalization than mysticete whales. Pilleri (1966b) ranked the sei whale (Balaenoptera borealis), the humpback whale (Megaptera novaeangliae), and the Southern right whale (Eubalaena australis) in that order from highest to lowest with regard

to this characteristic. He noted that the temporal lobe is increasingly more developed from right whales to sei whales. The lateral (Sylvian) fissure divides the cerebrum of the former into two halves, but that of the latter into a rostral one-third and a caudal two-thirds (Pilleri 1966a). The temporal pole extends increasingly further ventrally from right whale to sei whales and the degree of "operculization" increases in the same order. The olfactory cortex and insula are partially visible from the lateral aspect in right whales but, not in sei whales. As was expected, the brain of the bowhead whale (Balaena mysticetus) resembled that of right whales more than that of the other two whales (Fig 13-154).

Olfactory peduncles have been described on the brains of mysticete whales but the olfactory bulbs have not been recovered from adult whales. The peduncles have been only a few millimeters thick, but do have nerve fibers in them, so olfactory bulbs are presumed to exist in adult mysticete whales (Breathnach 1955, 1960). No olfactory peduncles were identified on the bowhead brains we examined. The brains were removed through the foramen magnum without opening the cranial cavity, so it is very likely that if olfactory peduncles and bulbs did exist, they were detached from the brain during removal from the skull.

In the bottlenose dolphin (Tursiops truncates), a lateral olfactory gyrus can be easily identified between the olfactory tubercle and the rostral rhinal sulcus, even though this species does not have olfactory peduncles (Jacobs et al 1971). In the humpback whales, faint traces of the lateral olfactory gyrus were seen by Pilleri (1966b) but were not observed macroscopically by Breathnach (1955). In the bowhead brains, a lateral olfactory gyrus could not be identified, possibly because of the traumatized condition of this region due to the method of removal.

The olfactory tubercle was large in the bowhead brain as in all other cetacean brains. The seemingly paradoxical situation of the great size of this structure in anosmatic and microsmatic animals (whales) has been discussed (Breathnach 1960, Jacobs et al 1971). Heimer (1978), studying the connections of this area in the rat, argued that it is misnamed and suggested that it be called the "ventral striatum." A consensus seems to be developing that the olfactory tuercle has multiple inputs, one of which is olfactory, and that it should not be considered as merely a part of the olfactory system.

The hippocampus is relatively small in cetaceans (Breathnach 1960, Filimonoff 1965, Morgane and Jacobs 1972, Jacobs et al 1979). Morgane et al

(1980) note that the development of the hippocampus is inversely related to the development of the parietal, occipital, and temporal lobes and the caudolateral thalamus, all of which are highly developed in cetaceans. The temporal part of the hippocampus does not protrude into the lateral ventricle in the bottlenose dolphin, but does in some other dolphins and in the humpback whale (Jacobs et al 1979). These authors state that the archicortex is better developed both quantitatively and qualitatively in the humpback whale than in the bottlenose dolphin. The temporal part of the hippocampus did protrude into the lateral ventricle in the bowhead brain (Fig 13-165) and the subcallosal and supracallosal parts appeared relatively well developed grossly (Figs 13-162, 13-158, and 13-159),

The size of the cetacean hippocampus has been used as an argument both for and against the hippocampus being part of the olfactory system since it is small, but present, in whales (Breathnach 1960). It is now thought to be more closely related to the limbic system with the olfactory input only one of many (Filimonoff 1965). Pilleri (1966b) suggests that the small size of the hippocampus in the humpback whale is the reason for the hedonistic behavior of this species. Morgane and Jacobs (1972) suggest that the small size of the hippocampus in cetaceans is related to specializations that have taken place in an environment that is less demanding in some ways than the terrestrial environments.

The majority of the hippocampal efferent fibers in the fornix in cetaceans join the precommissural fornix to go to the septum rather than joining the postcommissural fornix to go to the mammillary bodies (Morgane and Jacobs 1972). These authors state that the limbic circuit from the hippocampus via the fornix to the mammillary bodies and via the mammillothalamic tract to the rostral thalamus appears to be less highly developed in cetaceans than in primates and carnivores. The mammillary bodies were not grossly identifiable in the bowhead brain, as has also been reported for most cetacean brains, and the rostral thalamic tubercle was not very prominent. One might wonder whether cetaceans would be less able to alter their behavior in response to an altered environment than animals in which these structures are more highly developed. However, captive cetaceans demonstrate a high capacity to learn and be trained (Breathnach 1960).

The thalamus is extensive in cetacean brains (Breathnach 1960, Pilleri 1964, 1966a, 1966b, Morgane and Jacobs 1972). The lateral geniculate body was a definite raised structure in the bowhead thalamus. Most authors

describing the cetacean nervous system state that all of the optic fibers cross in the optic chiasm, but there is some evidence that a small fraction may remain ipsilateral in some cetaceans. Histologically, laminae like those seen in the lateral geniculate nuclei that receive biretinal projections are not seen in the nuclei of bottlenose dolphin (Morgane and Jacobs 1972). It is presumed that the lateral geniculate nucleus projects fibers to the cerebral cortex as in other mammals. An area that histologically resembles visual cortex has been identified on the medial surface of the cerebral hemisphere in bottlenose dolphins (Morgane and Jacobs 1972, Morgane et al 1980). Similar studies have not been done on baleen whale brains.

The interthalamic adhesion (massa intermedia) was not present in the brain of 80B1 or in the transversely sectioned bowhead brains. It is absent also in the sei whales, but is present in the humpback and southern right whales (Pilleri 1964, 1966a, 1966b). Its presence in the latter is somewhat suprising, because this whale is closely related to the bowhead, and its brain appears to be similar to that of the bowhead in other respects. The interthalamic adhesion is large in the bottlenose dolphin but small or absent in human brains. What significance, if any, should be attached to its absence is unknown.

The pineal body was not identified on any of the bowhead brains examined. Most authors question its presence in cetaceans. Pilleri was unable to demonstrate a pineal body in the southern right whale (1964), but says that there is one in the sei whale closely associated with the choroid plexus caudal to the caudal commissure and directly under the splenium of the corpus callosum (1966a).

The adenohypophysis (AH) and the neurohypophysis (NH) are not closely associated distally in the baleen whales described by Pilleri (1966a, 1966b) . In the humpback whale, the NH is totally subdural, while the AH alone is in a dural pocket. In the sei whale, both NH and the AH are in the dural compartment. In the southern right whale an intermediate situation exists. Apparently, the situation in the bowhead whale is more like that in the humpback or southern right whale than in the sei whale, because in 8081 the NH came out with the leptomeninges, but the AH remained in the dura mater in the skull. Pilleri (1966b) described the surface of the NH as smooth in the sei whale, but it didn't appear to be smooth in the bowhead whale (Fig 13-170).

In this report, the regions of the cerebellum have been designated differently than in most descriptions of the cetacean cerebellum. Although

the appearance of the cerebellum of the bowhead was somewhat different from that of the fin whale (B. physalus) described by Jansen (1950), the regions he named could be recognized on the bowhead cerebellum. However, the resemblance of the latter to the cerebellum of domestic terrestrial mammals was marked in spite of the large parafloccular lobules. Jansen's arguments (1950) are based on an embryological study of the fin whale. The early stages look convincing but there is a big gap between the 220 cm stage and the 430 cm stage. It is possible that the ansiform and paramedian lobules expand rapidly during that period and surround the paramedian lobule as is illustrated for the pig cerebel 1 urn between the 80 mm and 140 mm stages (Larsel 1 1970). If true, then the lobules Jansen (1950) labeled Cr. I and Cr. II may be Cr. I, the lobule labeled 1. pm. may be Cr.II, the lobule labeled pfl. d. may be 1. pm., and the lobule labeled pfl. v. may be pfl. d. This would correspond to the labels applied in this report.

The description of the cerebellum in most articles on cetaceans depicts a very small ansiform lobule, whereas this is the largest lobule in terrestrial mammals. The justification for this, that the cetaceans have reduced limbs (Jansen 1950), is not convincing because the somatotopic maps have been located on the rostral lobe and paramedian lobules, not the ansiform lobules. That lobule has been found to receive a projection from the premotor areas of the cerebral cortex, however (Snider and Eldred 1952). It may be assumed that the high degree of digital dexterity in humans is in some way related to the large semilunar (ansiform) lobules, but how is not known. Recent investigations suggest that the cerebellum is involved in preprogramming voluntary movements in monkeys (Brooks et al 1973, Allen and Tsukahara 1974, Thach 1975, Evarts and Tanji 1976, and Strick 1976). The movements have not been complex, just to push or pull a lever, but the contexts in which the movements take place are complex, requiring planning and control of range and velocity. The pathway for cerebella influence on voluntary movements is believed to incorporate the dentate cerebella nucleus and the ventrolateral thalamic nucleus. The identification of the dentate or lateral nucleus of the cerebellum in cetaceans is not clear (Breathnach 1960) and its connections are not known. If they are more similar to those in other mammals than has been supposed, maybe the large ansiform lobule is involved in programming relatively simple but precise movements of the flippers to accomplish intricate maneuvers.

The prominent lobule with the transversely running folia situated next to the vermis was labeled the paramedian lobule because of its appearance and location. The very large lobule ventral to the paramedian and ansiform lobules and separated from them by the parafloccular fissure was labeled the dorsal paraflocculus. A recent paper by Hoddevik and Brodal (1977), using the method of retrograde transport of horseradish peroxidase, has shown that the dorsal paraflocculus receives fibers from the rostral part of the medial accessory olive in the rabbit. A subsequent report by Walberg et al (1979) on the cat demonstrates fibers to the dorsal paraflocculus from the rostral part of the medial accessory olive and also some from the principal olive. Breathnach (1960) commented on the paradox that the rostral part of the medial accessory olive which is large in cetaceans was thought (based on retrograde degeneration) to project in the rabbit and the cat only to the flocculonodular lobe which is small or rudimentary in cetaceans. It is much more satisfying to believe that in cetaceans, as is now known for the rabbit and cat, the rostral part of the large medial accessory olive projects to a dorsal paraflocculus which is also very large. Hoddevik and Brodal (1977) quote Jansen (1969) as saying that both the rostral part of the medial accessory 01 i ve and the dorsal paraflocculus are extremely well developed in the whale and suggesting that the olivary region projects to the dorsal paraflocculus. It has been found also that potentials can be evoked in the dorsal paraflocculus of monkeys and cats by auditory stimuli, but the pathway apparently does not go through the medial accessory olive (Hoddevik ad Brodal 1972). All indications are that the auditory system is very highly developed in cetaceans, and it seems reasonable that a region that receives auditory input, the dorsal paraflocculus, should be well developed in whales. Therefore, it didn't seem unreasonable to label the largest lobule of the cetacean cerebellum the dorsal rather than the ventral paraflocculus.

The ventral paraflocculus was found to receive fibers from the ventral lamella of the principal olive, but not from the medial accessory olive in the rabbit (Hoddevik and Brodal 1977). Some connections from the medial accessory olive were found in the cat by Walberg et al (1979), however. In a few rather poor sections from the brain stem of 8062, the olivary complex in the bowhead looked much like the figures for the porpoise (Phocaena phocaena) given by Breathnach (1960) with a very large medial accessory olive and relatively small principal and dorsal accessory nuclei. If the ventral paraflocculus receives fibers only from the principal olive in whales and the princi-

palolive is small, it seems to follow that the smaller rather than the larger part of the paraflocculuar lobule is the ventral paraflocculus. In other mammals, the dorsal paraflocculus appears to curve around the ansoparamedian lobule to the rostral aspect of the cerebellum and then reflect on itself to become the ventral paraflocculus. These lobules were arranged this way in the bowhead cerebellum (Figs 13-173, 13-174, 13-178, 13-179), so it doesn't seem necessary to invent a new term for the ventromedial part of the parafloccular lobule in cetaceans (accessory paraflocculus).

The flocculus was not identified with certainty on any of the specimens, but it was probably very small as in other baleen whales. Pilleri (1964, 1966b) says that the floccul us of the southern right whale is against the nodule and has little or no peduncle. This may be true also for the bowhead whale, because the pictures of the cerebellum of the southern right whale (1964) greatly resemble those for the bowhead in this report (except for the labels).

The rostral lobe of the bowhead cerebellum was small compared to the caudal lobe and, probably, also compared to the rostral lobe of domestic terrestrial mammals, especially carnivores The folia of the vinculum lingulae, the ala lobuli centralis, and the lobulus quadrangularis extended out equally as far as those of the lobulus simplex of the caudal lobe. This arrangement is not found in the cerebellum of domestic ungulates (Guerra-Pereira 1977) and carnivores and is not described for the cerebellum of other cetaceans. Pictures of the somatotopic map on the monkey rostral lobe show the axial part of the body on the vermis with the tail on the lingula and the 1 imbs on the hemi spheres (Snider and Eldred 1952). Maps of termination zones of Oscarsson's spino-ol ivocerebellar pathways shown in Brodal and Walberg (1977a) and Armstrong (1974) indicate that the limbs are represented in the hemispheric part of the rostral lobe in the cat. Based on these maps, one would expect the lingula to be extensive and the hemispheres (or intermediate zones) to be reduced, but the opposite seemed to be the case in the bowhead cerebellum.

The sagittal section of the vermis was not very successful because of the fragile condition of the caudal part. The primary fissure and the posteri or superior or preansiform fissures were identified with reasonable certainty by matching them up with the surface fissures that limit the obvious lobulus simplex and declive. Pilleri (1964) places the primary fissure more caudally on the cerebellum of the southern right whale, and thus designates

the rostral portion of the ansiform lobule as the lobulus simplex, but this area strongly resembles the area labeled crus I and crus II in most cetacean cerebellum descriptions and it was regarded as crus I here. Many illustrations of sagittal sections of the cerebellum of cetaceans show an intraculminate fissure and two parts to the culmen. The fissure rostral to the primary fissure in Fig 13-182 may be the intraculminate fissure and a less conspicuous fissure previous to that may be the preculminate fissure. Pilleri (1964) places the primary fissure one lobule farther back (as previously mentioned) which would make the lobule labeled declive in Fig 13-182 a part of the culmen (V). This does not seem right for the reasons already stated. The large lobule caudal to the posterior superior fissure in the above figure is thought to be the folium vermis. It lies between the ansiform lobules and is limited caudally by the continuation through the vermis of the wide fissure that forms the caudal limit of the ansiform lobules. The folium vermis (VII A) is supposed to be connected to the ansiform lobules, but that could not be determined. The diagram of the cerebellum of the Amazon dolphin (Inia geofrensis) presented by Gruenberger (1970) shows a folium vermis very similar to the one in Fig 13-182 separated from a similarly shaped tuber vermis by a deep but unlabeled fissure.

The rest of the vermis did not stay together, so the tuber vermis, pyramis, uvula, and nodulus could not be distinguished. The tuber vermis (VII B) and the rostral part of the pyramis (VII A) are supposed to be connected to the paramedian lobule. The portion of the vermis which lies caudal to the deep ansoparamedian fissure was in a position to connect to the paramedian lobule, but such connections could not be identified because of the fragility of the tissue. Diagrams of the cerebellum of other cetaceans vary widely in the caudal part of the vermis. Determining the identity of the classical lobules is probably not of great importance, however, because it appears that the cerebellum is organized functionally more by longitudinal strips than by transverse lobules (Armstrong 1974, Brodal and Walberg 1977a, 1977 b).

The rostral and caudal colliculi of the bowhead midbrain tectum appeared superficially to be about the same size. In domestic ruminants, the rostral colliculi are very large whereas the caudal colliculi are quite small. In domestic carnivores, the rostral and caudal colliculi are about the same size. The rostral colliculi are relatively smaller, but the caudal colliculi are relatively larger than those in ruminants. The rostral colliculi in the bowhead were neither massive as in domestic ruminants nor small as they are in

some cetaceans such as the Ganges river dolphin which has very poor vision (Pilleri and Gihr 1970). The caudal colliculi appeared to be somewhat larger, compared to other brain stem structures, in the bowhead than in the domestic dog, but they were probably not larger than those in some other cetaceans, especially odontocetes. The lateral lemniscus and the brachium of the caudal colliculus were also very prominent. In general, the corpora quadrigemina and associated tracts in the bowhead look very similar to those pictured for other baleen whales by Pilleri (1964, 1966a, 1966b).

The trigeminal nerve is the largest of the cranial nerves in the bowhead, as in other baleen whales. The average width of the trigeminal nerve for three brains was 16 mm. This equals the size given for gray whales by Pilleri and Gihr (1970), which is the largest size given in their table of 18 species. The bowhead whale has a very large head and apparently has sense organs around the mouth which may correlate with a large trigeminal nerve. However, the figure given for the southern right whale is 13 mm.

The trigeminal nerve is larger than the vestibulocochlear nerve in the bowhead as in other baleen whales, but this relationship is reversed in many toothed whales, not so much because the vestibulocochlear nerve is 1 arger, but because the tri geminal nerve is smaller (Pil leri and Gihr 1970). The vestibulocochlear nerve averaged 10.5 mm in three bowhead brains, which is larger than the figures given for all but two of the baleen whales (fin whale and blue whale) and larger than all of the toothed whales except the sperm whale. The figure given for the southern right whale is 7 mm. Although the vestibulocochlear nerve is actually smaller than that in the river dolphins, in relation to the size of the brain it is probably more highly developed in them than in the other cetacean species (Pilleri and Gihr 1970). The above authors note that there are more fibers in the vestibulocochlear nerve of a toothed whale than in an equal-sized vestibulocochlear nerve in a baleen whale.

The ventral cochlear nucleus of the bowhead was large as seen grossly and from some prel imi nary sections from the brain stem of 80B2. Thus, in the bowhead as in other cetaceans, the auditory structures, including the vestibulocochlear nerve, the ventral cochlear nucleus, the trapezoid body, the lateral lemniscus, the caudal colliculus, its brachium, and the medial geniculate body were all well developed:

Breathnach (1955) described the floor of the fourth ventricle in the humpback whale as relatively featureless in contrast to earlier descrip-

tions of the area in other cetaceans. Pilleri (1964) noted that the median sulcus is deep rostrally and caudally and described a hypoglossal trigone and an ala cinerea caudally in the southern right whale. His picture of the fourth ventricle resembles Figs 13-184 and 13-187 with respect to these features.

IV. Skin

A maximum epidermal depth of 24 mm on the bowhead's dorsal body wall is 7 to 8 times thicker than the maximum epidermal thickness of most whales (Giacometti 1967, Nakai and Shida 1948, Simpson and Gardner 1972. Slijper 1979), but corresponds well with the thickness reported by Albert et al (1980) and Durham (1980). The thickness and density produced technical difficulties in obtaining adequate sections for routine histological study. Standard dehydration and embedding techniques proved to be inadequate. This problem was solved by lengthening the progressive dehydration and paraffin infiltration cycle to 48 hrs and by utilizing isopropyl alcohol which hardens tissues less than ethanol.

Several gross samples of skin with some blubber attached were received with the 1-2 mm superficial layer (stratum corneum) of the epidermis partially loosened or missing from a small region. No tissues were received, however, without at least part of the superficial layer firmly attached. The very thick cell layers underlying this superficial layer resembled water soaked epidermis from the chestnut or ergot of a horse. Histological and electron microscopic analysis of the epidermis from the various regions of the bowhead verified that the cellular strata were much thicker, but still similar to the strata reported in other cetaceans (Giacometti 1967, Montagna 1967, Sokolov 1960, Spearman 1972).

The cells of the bowhead epidermis arose from a typical stratum basale which also contained melanocytes in the pigmented body areas. The stratum basale cells were in contact with the basal lamina and formed junctions with it by means of hemidesmosome anchors. The basal cells had numerous interdigitations with adjacent basal cells secured by desmosomes. The majority of the epidermis was composed of a fairly typical stratum spinosum consisting of polyhedral to oval cells. In 24 mm thick epidermis, this layer extended as a continuous mass from the stratum basale to as far as 10 mm beyond the distal ends of the 13 mm long interdigitating dermal papillae. The stratum basale cells capping the distal ends of the dermal papillae gave rise

to a circularly arranged array of spinosal cells which maintained this configuration through the stratum spinosum and stratum corneum. These dense concentrations of cells were best described as epidermal rods which extended toward the surface surrounded by the more typical, larger polyhedral spinosal cells. They definitely were not vestigial hair follicles as surmised by Heckmann et al (1979). All of the spinosal cells gradually became flatter and reduced in volume as they approached the epidermal suface. This process concentrated the keratohyalin granules within their cytoplasm so that the final 12-60 cell layers of the epidermis formed a normal parakeratotic stratum corneum of squamous cells that retained recognizable, but pyknotic, nuclei.

The terminology used in this report was chosen deliberately based on our observations, staining results, and analysis of the literature. The final degree of keratinization and squamous cell flatness is a function of the immediate environment. The stratum corneum of the inner surface of the whale's lower lip was highly keratinized with very flat, typically clear staining cells which were mostly without stainable nuclei. This layer stained red with Masson's, Milligan's, and the Ayoub-Shklar keratin stains and appeared very similar to the stratum corneum of the palms and soles of humans and other primates. This area of the lower lip is not constantly bathed in sea water but is subjected to abrasion during feeding. Based on staining reactions, the cells of the stratum corneum of the generally thicker outer body surface which are constantly bathed in sea water with little abrasion appeared just as heavily keratinized. These cells did not become as flat, however, owing to their apparent higher fluid content and most of the degenerating nuclei took stain which gave the parakeratotic appearance to the stratum.

Montagna (1967) states "In the. skin of aquatic mammals, the very thick stratum corneum is solidly cemented together as if it were parakeratotic, and there is no stratum granulosum, whether the epidermis is glabrous, as it is in whales, or hairy, as in seals." Spearman's (1972, 1973) conclusions are, however, similar to ours, i.e., the stratum corneum of whales consists of moderately flattened cells which retain pyknotic nuclei which is parakeratosis. He also reports that the transition from spinosum to corneum is more gradual than in other mammals which we also observed. A medical dictionary defines parakeratosis as "persistence of the nuclei of the keratinocytes into the stratum corneum (horny layer) of the skin" (Friel 1974). Smith and Jones (1966) also define parakeratosis as follows: "Parakeratosis - The retention

of nuclei in the keratin layer (stratum corneum), usually with diminution or absence of the granular layer (stratum granulosum). This change is more frequent on moist surfaces and is characterized grossly by scaling of flaky, 1 oosely adherent material (dandruff)." See Fig 13-226 through 13-233 to verify that whale skin flakes. In addition to routine histological stains and electron microscopic analysis, histochemical and other tests (Spearman 1972) indicate whale stratum corneum cells contain protein-bound phospholipid, cystine, and cysteine (components of keratin) with an absence of ribonucleic acid (RNA) resembling the normal parakeratotic stratum corneum of the pouch epidermis of kangaroos. The best examples of terrestrial mammal integumentary structures with similar thickness and structure are the ergots and chestnuts of horses or the corresponding structures on animals such as deer. The obvious differences, of course, are the degrees of keratinization and the environments. Preserved bowhead skin that is allowed to dry out grossly resembled ergots and chestnuts very closely. The soaking of ergots and chestnuts after fixation should yield specimens very similar to preserved bowhead skin.

The use of the term stratum externum instead of stratum corneum by some authors (Harrison and Thurley 1974) may be less confusing in terms of location within the epidermis, but ignores the fact of keratinization and the more widespread usage of the term corneum by others (Ling 1974, Montagna 1967, Spearman 1972). The use of stratum intermedium in place of stratum spinosum by Harrison and Thurley (1974) is likewise descriptive, but tends to lose sight of the numerous desmosomes which are present between the cells of this layer and again ignores conventional terminology.

The vibrissae or tactile hairs located on the jaws and behind the blowholes have been reported to possess "sensitive tactility like the whiskers of a cat" in the Sei whale (Nakai and Shida 1948), with definite venous sinuses and nerves present. Fetter and Everitt (1979) report that bowhead vibrissae are identical to the sinus hairs of terrestrial mammals contrary to our findings. We found the bowhead tactile hair follicles to be like those described by Nakai and Shida (1948) although some generalized differences appeared to exist, possibly owing to the much longer follicle length (3-4 cm) and the increased thickness of the surrounding epidermis. These factors may affect the ability of the hair to move and produce stimuli. The deep funnel-like epidermal depression around the hair shaft and the presence of nerve fibers with probable nerve end organs (apparently Herbsti-type) certainly seem to indicate a tactile function in the bowhead.

The occurrence of diatoms on the surface of the parakeratotic stratum corneum of most samples of bowhead skin is not surprising. The Bering Sea which is the bowhead's winter habitat has several species of indigenous diatoms. Notably these are various species of Cocconeis, Stauroneis, and Plumostigma which occur regularly On other whales Of the North pacific (Nemoto 1956) . Various species of Synedra and Gomphonema are also reported as "fortuitous" inhabitants which can occur in the skin film. Primarily Cocconeis species occur on fin, Sei, blue, humpback, and sperm whales (Nemoto et al 1977) . Our preliminary analysis of normal bowhead skin (Table 13-8) showed at least 4 genera of diatoms present on and in various samples. The four are Cocconeis sp, Gomphonema sp, Navicula sp, and Stauroneis sp. One or two bacterial or diatom forms that occur in chains, but are as yet unidentified, also occur in some types of lesions. See RU 1280 also.

A surprisingly large number of morphologically different types of epidermal lesions occurred on the skin samples studied. These were notably: elevated smooth areas, even but granular appearing areas, elevated granular areas, shallow smooth depressions, granular deep depressions, and smooth deep depressions. Histological analysis showed that each morphological type tended to have a somewhat different population of microflora (Table 13-9). Each lesion type was an example of restricted epidermatitis (see RU 780) which affected the stratum corneum and may affect the more superficial layers of the stratum spinosum. At this point, it is not clear whether the various "depressions" actually come about by loss of cells within the central area or are merely the result of retention of squamous cells around the lesion. Such retention would elevate the surrounding rim causing the central area to appear depressed. A third possibility is a combination of the two processes which now seems most likely. Definite conclusions must await further study.

We have followed the terminology proposed by Williamson (1973) when describing baleen even though we are not in total agreement. The use of the term "hair" in reference to baleen structures is, at best, misleading despite the general gross appearance of these structures to the untrained eye. Two distinct types of "hairs" were found in bowheads, simple baleen hairs and compound baleen hairs. Each type developed from the deep stratum basale cells encircling the bases of the long connective tissue papillae that interdigitated with the very thick gingival epitheliums. The tubular structures that resulted were horn tubules very similar in density and structure to horn tubules produced in the horns of cattle and hooves of many animals. A major

difference was that the stratum spinosum cells between the growing horn tubules of baleen did not form intertubular horn as the hooves and horns of terrestrial mammals. The tissue between the baleen horn tubules became only slightly firmer than the thick stratum spinosum of the body skin, possibly permitting the horn tubule to elongate more rapidly, emerge through the gingival surface, and extend down as hair-like structures. The organization of the baleen horn tubules after emergence from the gums was a direct function of the depth of the gingival epitheliums. The greater the depth of the epitheliums the greater the number of horn tubules that became fused forming compound baleen hairs or baleen plates. The shallowness of the gingival plate adjacent to the hard palate yielded individual (simple) baleen hairs. As the stratum spinosum thickened laterally (Fig 13-217), the individual horn tubules became fused into groups emerging as larger, darker, compound baleen hairs. Finally from the thickest (most lateral) part of the gingival plate, laterally elongated fusion groups emerged as the baleen plates. The fringe of filaments (Williamson 1973) on the medial surfaces of the baleen plates was merely the result of the fusion layer holding individual horn tubules together becoming worn which released the distal ends of the horn tubules to hang free increasing the filtering effectiveness of the baleen apparatus.

The dermis of the skin consisted of typical dense irregular connective tissue arranged as: (1) a papillary layer of highly vascularized looser connective tissue that interdigitated with the overlying epidermis and (2) a superficial layer (subpapillary) immediately beneath the papillary layer composed of denser collagenous connective tissue with elastic fibers, medium sized muscular arteries, thin walled veins, venous sinuses, and myelinated nerve fibers. The deeper (reticular) layer of the dermis was essentially nonexistent since it was heavily infiltrated with adipose cells and undistinguishable from the generally very deep hypodermic or blubber (see RU 480). The superficial or subpapillary dermis of the bowhead ranged between 2-4 mm thick when blubber was present. This corresponds to the report of Sokolov (1960) that the dermis of baleen whales is thinner than that of the toothed whales.

Very simple preliminary trials were conducted in an attempt to determine possible interactions between bowhead skin and crude oil. The increased viscosity of Prudhoe Bay raw crude oil cooled slowly to 3°C produced a rather tough elastic film about 4 mm thick in our artificial environment. It resembled in action an equally thick layer of melted paraffin that has

skinned over just before cooling enough to actually solidify. Prudhoe Bay crude oil has a pour point of about -9.5°C (15°F) (Thompson et al 1971) and is an intermediate-gravity, high sulfur, high nitrogen oil containing a high percentage of aromatics. It is brownish-black in color and has a high carbon residue and asphalt content. See Thompson et al (1971) and Roselius and Steffans (1971) for specific characteristics of Prudhoe Bay and other North Slope crude oils.

When formalin fixed skin samples were raised through a nonagitated crude oil slick at 3°C and resubmerged through the oil with limited agitation for 3 cycles simulating short breathing rolls of bowhead whales, the oil stuck to the parakeratotic stratum corneum in varying degrees. Vibrissae of both the blowhole (Fig 13-263) and the chin (Fig 13-262) became partially coated with definite globules of oil remaining on the shafts themselves. The amount of oil adhering to the surrounding skin and epidermal depression appeared to be directly proportional to the degree of "roughness" of the stratum corneum. The chin without vibrissa (Fig 13-264), the upper lip with sensory papillae (Fig 13-265), and outer lip epidermis (Fig 13-267) showed some oil adherence. Lesions, regardless of type, showed oil adhesion in patches, particularly on the roughened raised rim around the lesions (Figs 13-26 and 13-27). The three simulated "breathing rolls" also produced some patchy oil adherence within the lesion depressions. The unmeasured quantities and sizes of the oil patches adhering to the various types of formalin fixed skin samples after the 3 roll actions to simulate 1 short breathing cycle were, at best, merely indicative of the possible adherence to the live skin of an active bowhead. The quantity of adherent oil increased with each immersion and seemed to be related to the "roughness" of the surface of the skin sample. More oil in somewhat larger patches did adhere to those areas of the bowhead skin that were "normally" rough, i.e., the funnel-shaped depressions through which vibrissae emerged, the various types of lesions, and possibly of significance, the areas of the body that were covered by a diatomaceous film that was responsible for the slightly yellowish tint present on the majority of our skin samples.

Apparently as long as a water film was maintained on the preserved bowhead skin surface, little or no crude oil adhered with up to 3 immersions. Once the oil made sufficient contact with the skin to adhere, however, a patch of variable size and shape formed which tended to enlarge with each successive immersion. The reason appears to be that the water film did not remain over

the first oil patch leaving successive oil coats on the patch which coalesced to cover more skin surface with each immersion. Geraci and Smith (1976, 1977) report that crude oil does not adhere to the pelt of ringed seals (possibly owing to interaction with the trapped air layer within the fur with the water film on the surface). They also report, however, that oil did affect the eyelids (relatively hairless) and cornea. Even without adherence, they report there is definite absorption of some oil components and detectable kidney damage after 24 hours of exposure (Geraci and Smith 1976, 1977).

The dermal papillae extended into the generally extremely thick epidermis to within only 5 mm (flipper, fluke), 11 mm (general body), or in the thinnest regions to within 0.1 mm of the outer surface of the parakeratotic stratum corneum. All dermal papillae contained blood capillaries which could absorb and distribute throughout the body any soluble crude oil components taken in through the cells of the stratum corneum. Since some diatoms (Stauroneis, Gomphonema) were normally present within the stratum corneum to a depth of 3-6 cell layers, this might allow oil penetration to that level before entering the cells, thereby reducing the distance for absorption through the cells into the blood stream. Deep epidermal lesions may also provide the potential for oil contact with the dermal papillae and possible absorption. The eyelids, conjunctival, and corneas (see RU 680 also) will provide rapid access of oil components into the body owing to their thinness, particularly if the whales open their eyelids to help locate the surface when rolling through an oil slick.

Absorption such as mentioned above would be contingent on specific environmental conditions that may lead to contact with soluble fractions of oil.

SUMMARY

1. Lung

Tissues from the lungs, airways, and larynx of Balaena mysticetus were examined utilizing a variety of techniques. In the nasal region the orifices of the external nares were apparently regulated by a narial sphincter composed of specialized blubber and skeletal muscle fibers. In addition, the nasal septal cartilages were paired rather than single as has been reported in other cetaceans. In the laryngeal region, the covering of the epiglottis and arytenoids was composed of keratinized stratified squamous epitheliums with connective tissue papillae containing encapsulated nerve end organs, the arytenoid cartilages were not fused caudally, and lymphatic tissue occurred only at the laryngotracheal junction.

In the airways, the tracheal cartilages were C-shaped and open ventrally. This opening was filled by skeletal muscle which also encircled the laryngeal sac. The primary and segmental bronchi branched at obtuse angles as did their accompanying arteries and nerves. The pulmonary veins did not follow this pattern. Mucous glands occurred continuously in the large airways but were seen only between cartilage rings in smaller bronchi and were absent in the bronchioles and below. Myoelastic sphincters were absent but smooth muscle was present in the bronchioles. Hyaline cartilage was found in all bronchi and bronchioles down to the level of the terminal and respiratory bronchioles. The bronchial epitheliums contained cells with only microvilli on their surface as well as cells which contained both cilia and microvilli. The degree of ciliation of the bronchial lining appeared to vary with the bronchial diameter. At the ultrastructural level, the pseudostratified columnar epitheliums of the primary bronchus was similar to what is seen in other cetaceans. Desmosomes were seen between adjacent cells in the basal region and hemidesmosomes were seen between the basal cells and the basal lamina. Plasma cells were also seen beneath the basal lamina. Apparently encapsulated nerve endings were seen in the submucosa of bronchioles only. The respiratory bronchioles were lined by a typical respiratory epitheliums composed of both type I and type II pneumocytes.

In the air exchange system, the respiratory bronchioles, alveolar ducts, alveolar sacs, and alveoli were lined by respiratory epitheliums. Solely elastic laminae and sphincters were found in these walls. The elastic fibers of these structures were of typical ultrastructure being composed of

both amorphous substance and microfibrils. The alveolar walls were typically cetacean with few fibroblasts and relatively little collagen contained in the septa. The type II pneumocytes of the respiratory epitheliums contained typical multilamellar bodies which were also seen free in the air spaces as was the tubulomyelin they produce. Few alveolar macrophages were observed.

Finally, no internal septa occurred in the lung and no external or internal lobulation occurred. The pleura was composed of a thick, highly elastic dense connective tissue with a mesothelial covering.

11. Kidney

The kidney of Balaena mysticetus was studied microscopically, microscopically and to a limited extent under the transmission electron microscope. Poor preservation of specimens limited the studies on the ultrastructural level. A few anatomical differences existed between the kidney of the bowhead and those of other cetaceans. The major difference was the absence of any smooth muscle in the sporta perimedullaris and calyx walls. Another difference was the presence of the arcuate vessels in the substance of the sporta as opposed to their reported location some distance from the sporta in other cetaceans. A unique morphological finding in the bowhead was the presence of large thin-walled veins that fill the spaces between renicules and intimately surround calyces and ureteral branches. Theories of their function are proposed. Long nephrons may indicate good ability to preserve body water. No morphological differences between Ingutuk variants and ordinary bowheads were found.

111. Brain

The cerebral hemispheres of the bowhead brain exhibited deep sulci and convoluted gyri as is characteristic of other cetacean brains. No attempt was made to identify them because no intact brains were available. The temporal lobes of the hemispheres were not as well developed in the bowhead brain as in brains of some other mysticete whales. The corpus callosum was long and thin and its caudal part was deflected ventrally.

No olfactory bulbs, peduncles, or tracts were observed on the bowhead brains, probably because of the method of removal and the resultant trauma to that area. The paleocortex (olfactory lobe) was rather large. As in other cetaceans, the most prominent feature was the large olfactory tubercle, which underlay the head of the corpus striatum. The diagonal area was

wide and the rostral perforated substance covered an extensive area. The amygdalar complex was probably well developed but this area was also traumatized. The stria terminals was wide and easily seen. More of the paleocortex was visible from the lateral aspect than in the humpback and sei whales, as is true in the southern right whale.

The hippocampus was not well developed compared to domestic mamreals, but the temporal part did protrude into the temporal horn of the lateral ventricle, and the sub- and supracallosal parts were easily seen grossly. There was no occipital horn of the lateral ventricle. The rostral commissure was difficult to discern grossly. Most of the fibers of the fornix apparently pass rostral to the rostral commissure into the septal area.

The caudate nucleus is illustrated and some other basal nuclei are shown in cross sections. The dorsal part of the lateral thalamus was very well developed. The medial geniculate body was very large compared to domestic mammals, which is true for other cetaceans. The lateral geniculate body was a definite elevated structure, but was not nearly as large as the medial geniculate body. The stria habenularis was easily identified, but the habenula was not easily seen grossly. The pineal body was not identified. An interthalamic adhesion (massa intermedia) was not present. The mammillary bodies were not identified. The rostral thalamic tubercle was recognizable, but not prominent.

As in other cetaceans, the adenohypophysis and neurohypophysis were not closely associated. The neurohypophysis was shown with the meninges, but the adenohypophysis apparently remained in the skull.

The cerebellum was very large as in other cetaceans. Because of the resemblance of the bowhead cerebellum to that of domestic mammals, the lobules are named differently here than in most descriptions of the cerebellum of cetaceans. The ansiform lobule was regarded as being large, occupying most of the caudal lobe dorsal to the parafloccular fissure as in domestic mammals. The prominent lobule with transversely running folia adjacent to the caudal vermis was regarded as the paramedian lobule. The large caudoventral lobule was regarded as the dorsal paraflocculus. The rostral lobe was relatively smal 1. Its lateral portions were more extensive than in domestic mammals. The flocculonodular lobe was not identified, but is presumed to be small as in other mysticete whales.

The rostral and caudal colliculi of the midbrain tectum appeared superficially to be about the same size. The caudal colliculi were large

compared to domestic mammals, but are probably typical for cetaceans. The lateral lemniscus and brachium of the caudal colliculus were prominent.

The rhombencephalon appeared to be wide and shallow. It curved up around the caudal aspect of the cerebellum. The transverse fibers of the pons formed a massive structure. The trigeminal nerve was the largest cranial nerve and was large compared to that of other cetaceans. It exited through the transverse fibers of the pons. The next largest cranial nerve was the vestibulocochlear (VIII) nerve seen at the lateral border of the well developed trapezoid body which was visible caudal to the transverse pontine fibers. As in other cetaceans, the olives were seen immediately adjacent to the ventral median fissure on the ventral surface of the medulla oblongata. These were the surface representations of the very large medial accessory olivary nuclei . The pyramids coursed around the lateral edges of the olives and decussated caudal to them. The median sulcus in the floor of the fourth ventricle was deep rostrally and caudally. On either side caudally were a pair of ridges which may represent the hypoglossal trigone and the ala cinerea. The fibers of the hypoglossal nerve exited lateral to the pyramids as they coursed around the olives as in other cetaceans.

IV. Skin

Skin samples from a variety of body regions of the bowhead were examined. The epidermis was up to 8 times thicker than that reported in other whales. Regional variations in thickness occurred with the thinnest areas observed occurring on the eyelids. A distinctive parakeratotic stratum corneum and the underlying stratum spinosum extended over the entire body surface varying in thickness in different regions. Several diatom species resided in/on the stratum corneum producing a rougher surface in many areas. In thick areas, epidermal rods resembling those in the ergot and chestnut of horses were seen. In thin epidermal areas of the lips and eyelids large dermal papillae with encapsulated nerve end organs were seen.

Vibrissae, which emerge from the skin only in specific regions, inserted into modified tactile hair follicles with associated nerve nets. Baleen hairs arose as hard keratin tubules from around connective tissue papillae in the gums. Laterally, compound baleen hairs with several medullary centers resulted from the fusion of several tubules. In general, the origin and structure of baleen hairs more closely resembled the origin and structure of horns and hooves in terrestrial mammals than hair.

Severa"l types of epidermal lesions were seen. Each type seemed to be characterized, at least partially, by specific microflora. The degree of epidermal erosion in lesions seemed to also be correlated with the microflora. The significance of the erosion may be misinterpreted because epidermal thickening also occurred at the rim of some lesions resulting in no actual decrease in the distance between the epidermal surface within the lesion and the tips of the dermal papillae.

Crude oil cooled slowly to 3°C (Beaufort Sea summer temperature) formed a film resembling partially solidified paraffin on nonagitated artificial sea water. It adhered in small patches to the epidermal surface and to vibrissae of preserved skin immersed through the film. The amount of adherent oil appeared to be dependent on the number of exposures and the roughness (diatoms, lesions, vibrissae) of the prepared skin surface. The ability of the skin to maintain a tightly associated water film seemed to prevent oil adhesion in certain regions.

ACKNOWLEDGEMENTS

We acknowledge our indebtedness to the tissue collection team (RU 180) for the excellent collection and supply of the multitude of properly identified and tagged specimens in spite of adverse conditions; Dr. R. A. Heckmann of RU 1280 for confirmation of diatom identifications; Dr. K. O. Meyers and Arco Oil and Gas Company for furnishing samples of Prudhoe Bay raw crude oil; Dr. C. W. Titkemeyer, Head, Department of Veterinary Anatomy and Fine Structure and Dr. K. M. Kerr, Assistant Dean for Research for support from our department and the School of Veterinary Medicine of Louisiana State University and A and M College.

Special thanks with deep appreciation for attention to details are extended to our staff: Research Associates-Lee Fogleman, Sherry Gibson, Ross Payne; Veterinary Laboratory Technologists-Linda Cherepow, Pam DuRousseau, Mark LeCoq; Secretaries- Jamie Troxclair, Janice Allen. Thanks are also extended to veterinary' medical student Harry Kleinman for willing and able assistance.

Special thanks. and appreciation are also extended to our families for their patience and understanding and, particularly, to Jean Haldiman and Cindy Henk for helping with the typing and proofing of the manuscript.

REFERENCES

Albert, T. F. 1980. Personal communication.

Albert, T. F., G. Migaki, H. W. Casey and L. M. Philo, 1980. Healed penetrating injury of a bowhead whale. Marine Fisheries Rev. 42:92-36.

Allen, G. I. and N. Tsukahara. 1974. Cerebrocerebellar communication systems. Physiol. Rev. 54:957-1006.

Andrews. P. M. 1974. A scanning electron microscopic study of the extrapulmonary respiratory tract. Am. J. Anat. 139:399-423.

Armstrong, D. M. 1974. Functional significance of connections of the inferior olive. Physiol. Rev. 54:358-417.

Arvy, L. 1974. The kidney, renal parasites and renal secretion in cetaceans. In: Investigation on Cetacea. G. Pilleri (cd.), Vol. 5, pp 231-310. Institute of Brain Anatomy, University of Berne.

Askin, F. B. and C. Kuhn. 1971. The cellular origin of pulmonary surfactant. Lab. Invest. 25:260-268.

Belanger, L. F. 1940. A study of the histological structure of the respiratory portion of the lungs of aquatic mammals. Amer. J. Anat. 67: 437-461.

Benham, W. B. 1901. On the larynx of certain whales (Cogia, Balaenoptera, and Ziphius). Proc. Zool. Sot. (London) 1:278-300.

Boshier, D. P. and P. McN. Hill. 1974. Structural aspects of ventilation and diffusion in the Weddell seal. In: Functional Anatomy of Marine Mammals, R. J. Harrison (cd.), Vol. 2, pp 197-230. Academic Press, New York.

Bouvier, E. L. 1892. Appareil urinaire in observation anatomique sur le hyperoodon rostratus Lilljeborg. Ann. Sci. Nat. Zool. 7(13):360-1.

Breathnach, A. S. 1955. The surface features of the brain of the humpback whale (Megaptera novaeangliae). J. Anat. 89:343-354.

Breathnach, A. S. 1960. The cetacean central nervous system. Biol. Rev. 35:187-230.

Breeze, R. G. and E. B. Wheeldon. 1977. The cells of the pulmonary air-ways. Am. Rev. Respir. Dis. 116:705-777.

Brodal, A. and F. Walberg. 1977a. The olivocerebellar projection in the cat studied with the method of retrograde axonal transport of horseradish peroxidase IV. The projection to the anterior lobe. J. Comp. Neur. 172:85-108.

Brodal, A. and Fe Walberg. 1977b. The olivocerebellar projection in the cat studied with the method of retrograde axonal transport of horseradish peroxidase VI. The projection onto longitudinal zones of the paramedian lobule. J. Comp. Neur. 176:281-294.

Brooks, V. B., I. B. Kozlovskaya, A. Atkin, F. E. Horvath and M. Uno. 1973. Effects of cooling dentate nucleus on tracking-task performance in monkeys. J. Neurophysiol. 36:974-995.

Buckingham, S., H. O. Heinemann, S. C. Sommers and W. F. McNary. 1966. Phospholipid synthesis in the large pulmonary alveolar cell. Amer. J. Path. 48:1027-1041.

Callas, G. 1974. A new fixative technique for the electron microscopic study of pulmonary surfactant. Anat. Rec. 180:457-463.

Carroll, G. M. and J. R. Smithhisler. 1980. Observations of bowhead whales during spring migration. Marine Fisheries Rev. 42:80-85.

Cave, A. J. and F. J. Aumonier. 1961. The visceral histology of the primitive cetacean Caperera (Neobalaena). J. Roy. Micr. Soc. 80(1):25-33.

Cave, A. J. and F. J. Aumonier. 1962. Morphology of the cetacean reniculus. Nature 193(4817):799-800.

Cave, A. J. and F. J. Aumonier. 1964a. Observations on the cetacean reniculus. Proc. Anat. Sot. of Great Britain and Ireland. 98:687.

Cave, A. J. and F. J. Aumonier. 1964b. The reniculus in certain Balaenoptries. J. Roy. Micr. Sot. 83(3):255-264.

Cave, A. J. and F. J. Aumonier. 1965. Further observations on the cetacean reniculus. J. Roy. Micr. Sot. 84(4):539-548.

Cave, A. J. and F. J. Aumonier. 1967a. The reniculus of the sei whale (Bal aenoptera boreal is), J. Nat. Hi stor. 1:575-583.

Cave, A. J. and F. J. Aumonier. 1967b. The reniculus of Turisops truncatus, Stenella longirostris and other cetaceans. J. Roy. Micr. Sot. 86(4):323-342.

Cheville N. F. 1976. Cell Pathology. The Iowa State University Press, Ames, 1A. -

Clarke, M. R. 1979. The head of the sperm whale. Sci. Am. 240(1):128-32, 134, 136-141.

Cowan, D. 1966a. Observations on pilot whale Globicephala melaena: organ weight and growth. Anat. Rec. 155:623-629.

Cowan, D. 1966b. Pathology of the pilot whale Globicephala melaena. Arch. of Path. 82:178-289.

Durham, F. E. 1980. External morphology of bowhead fetuses and calves. Marine Fisheries Rev. 42:74-80.

Engl e, So 1966. The respiratory tissue of the blue whale and the fin whale. Acts. Anat. 65:381-390.

Eschricht, D. F. and J. Reinhardt. 1866. On the Greenland right-whale (Balaena mysticetus, Linn.). In: Recent Memoirs on the Cetacea, W. H. Flower (cd.), Vol. 40, pp 1-150. Ray Society, London.

Evarts, E. V. and J. Tanji. 1976. Reflex and intended responses in motor cortex pyramidal tract neurons of monkeys. J. Neuro-physiol. 39: 1069-1079.

Fanning, J. C. and R. J. Harrison. 1974. The structure of the trachea and lungs of the South Australian Bottlenosed Dolphin. In: Functional Anatomy of Marine Mammals. R. J. Harrison (cd.), Vol. 2, pp 231-252. Academic Press, New York.

Fetter, A. W. and J. I. Everitt. 1979. Tissues structure/function (RU 280a). In: Investigation of the Occurrence and Behavior Patterns of Whales in the Vicinity of the Beaufort Sea Lease Area. J. Kelley and G. Laursen (eds.), pp 331-349. Final Report to the Bureau of Land Management from the Naval Arctic Research 'Laboratory, Barrow, Alaska.

Filimonoff, I. N. 1965. On the so-called rhinencephalon in the dolphin. J. Hirnforsch., 8:1-23.

Friel, J. P. (cd.) 1974. Dorland's Illustrated Medical Dictionary. 25th Ed. W. B. Saunders, Philadelphia.

Geraci, J. R. and T. G. Smith. 1976. Direct and indirect effects of oil on ringed seals, Phoca hispida. J. Fish. Res. Board Can. 33:1976-1984.

Geraci, J. R. and T. G. Smith. 1977. Consequences of oil fouling on marine mammals. In: Marine Environments and Organisms, Vol. 11, pp 400-409. Academic Press, New York.

Giacometti, L. 1967. The skin of the whale (Balaenoptera physalus). Anat. Rec. 159:69-76.

Gill, J. and O. K. Reiss. 1973. Isolation and characterization of lamellar bodies and tubular myelin from rat lung homogenates. J. Cell Biol. 58:152-171.

Goudappel, J. R. and E. J. Slijper. 1958. Microscopic structure of the lungs of the Bottlenose whale. Nature 182:479.

Gruenberger, H. B. 1979. On the cerebral anatomy of the 'Amazon dolphin, Inia geoffrensis. In: Investigations on cetacea. G. Pillleri (cd.), Vol. 2, pp 129-44. Institute of Brain "Anatomy, University of Berne.

Guerra-Pereira, M. L. 1977. Morphology and terminology of the cerebellum of cattle, sheep, and goats. Zbt. Vet. Med. C Anat. Histol. Embryol. 6:1-20.

Harrison, R. J. and K. W. Thurley. i974. Structure of the epidermis in Tursiops, Delphinus, Orcinus and Phocoena. In: Functional Anatomy of Marine Mammals. R. J. Harrison (cd.), Vol. 2,pp 45-72. Academic Press, New York.

Heckmann, R., R. Warnock and L. Jensen. 1979. Tissue structure/function (RU 979)* In: Investigation of the Occurrence and Behavior of Whales in the Vicinity of the Beaufort Sea Lease Area. J. Kelley and G. Laursen (eds.), pp517-538. Final Report to the Bureau of Land Management from the Naval Arctic Research Laboratory, Barrow, Alaska.

Heimer, L. A. 1978. The olfactory cortex and the ventral striatum. In: Limbic Mechanisms. The Continuing Evolution of the Limbic System Concept. K. E. Livingston and O. Horny kiewicz (eds.), pp 95-187. Plenum Press, New York.

Hoddevik, G. H. and A. Brodal. 1977. The olivocerebellar projection studied with the method of retrograde axonal transport of horseradish peroxidase. V. The projections to the flocculonodular lobe and the paraflocculus in the rabbit. J. Comp. Neur. 176:269-280.

Hosokawa, H. 1950. On the cetacean larynx, with special remarks on the laryngeal sate of 'the sei whale and the aretynoepiglottideal tube of the sperm whale. Sci. Rep. Whales Res. Inst. No. 3:23-62.

Ito, T., K. Kobayashi and Y. Takahashi. 1967. Histological studies on the respiratory tissue in a dolphin lung. Arch. Histol. 28:453-470.

Jacobs, M. S., W. L. McFarland and P. J. Morgane. 1979. The anatomy of the brain of the Bottlenose dolphin (Tursiops truncates). Rhinic lobe (Rhinencephalon): The Archicortex. Brain Res. Bull. 4, Suppl 1:1-108.

Jacobs, M. S., P. J. Morgane and W. L. McFarland. 1971. The anatomy of the brain of the Bottlenose dolphin (Tursiops truncates). Rhinic lobe (Rhinencephalon) 1. The Paleocortex. J. Comp. Neur. 141:205-272.

Jansen, J. 1950. The morphogenesis of the cetacean cerebellum. J. Comp. Neur. 93:341-400.

Jansen, J. 1969. On cerebella evolution and organization from the point of view of a morpholist. In: Neurobiology of Cerebella Evolution and Development. R. Llinas (cd.), pp 881-893. Amer. Med. Ass. Education and Research Foundation, Chicago, IL.

Junqueira, L. C. and J. Carneiro. 1980. Basic Histology. 3rd Ed. Lang Medical Publications. Los Altos, CA.

Kenney, R. M. and J. 1. Everitt. 1979. Tissues structure/function (RU 579b). In: Investigation of the Occurrence and Behavior Patterns of Whales in the Vicinity of the Beaufort Sea Lease Area. J. Kelley and G. Laursen (eds.), pp 227-253. Final Report to the Bureau of Land Management from the Naval Arctic Research Laboratory, Barrow, Alaska.

Kikkawa, Y., K. Yoneda, F. Smith, B. Packard and K. Suzuki. 1975. The type II epithelial cells of the lung. II. Chemical composition and phospholipid synthesis. Lab. Invest. 32:295-302.

Kuhn, C. III. 1978. Ultrastructure and cellular function in the distal lung. In: The Lung, W. M. Thuribeck, M. R. Abell (eds.), pp 1-20. The Williams and Wilkins Co., Baltimore, MD.

Lacoste, A. and A. Baudrimont. 1933. Dispositifs D'Adaptation Fonctionnelle A La Plongee Dans L'Apparell Respiratoire Du Marsouin (Phocoena communis, Less.). Arch. Anat. Histol. Embryol. 17:1-46.

Larsen, O. 1970. The Comparative Anatomy and Histology of the Cerebellum from Monotremes through Apes. J. Jansen (cd.). The University of Minnesota Press, Minneapolis.

Ling, J. K. 1974. The integument of marine mammals. In: Functional Anatomy of Marine Mammals. R. J. Harrison (cd.), Vol. 2:pp 1-44. Academic Press, New York.

Luna, L. G. 1968. Manual of Histologic Staining Methods of the Armed Forces Institute of Pathology. 3rd Ed. McGraw-Hill, N.Y.

McFarland, W.L., P.J. Morgane and M.S. Jacobs. 1969. Ventricular System of the Brain of the Dolphin, Tursiops truncatus, with Comparative Anatomical Observations and Relations to Brain Specializations. J. Comp. Neur. 135:275-368.

McVay, S. 1973. Stalking the arctic whale. Am. Sci. 61:24-37.

Meek, A. 1918. The reproductive organs in cetacea. J. of Anat. 52:186-210.

Migaki, G. 1979. Tissues structure/function (RU 579a). In: Investigation of the Occurrence and Behavior Patterns of Whales in the Vicinity of the Beaufort Sea Lease Area. 'J. Kelley and G. Laursen (eds.), pp 213-225. Final Report to the Bureau of Land Management from the Naval Arctic Research Laboratory, Barrow, Alaska.

Montagna, W. 1967. Comparative anatomy and physiology of the skin. Arch. Derm. 96:357-63.

Morgane, P. J. and M. S. Jacobs. 1972. Comparative anatomy of the cetacean nervous system. In: Functional Anatomy of Marine Mammals. R. J. Harrison (cd.), Vol. 1, pp 117-244. Academic Press, New York.

Morgane, P. J., M. S. Jacobs and W. L. McFarland. 1980. The anatomy of the brain of the Bottlenose dolphin (Tursiops truncates). Surface configurations of the telencephalon of the Bottlenose dolphin with comparative anatomical observations in four other cetacean species. Brain Res. Bull. 5, Suppl 3:1-107.

Murata, T. 1951. Histological studies on the respiratory portions of the lungs of cetacea. Sci Rep. Whales Res. Inst. No. 6:35-47.

Nakai and Shida. 1948. Sinus hair of the Sei whale (Balaenoptera borealis). Sci. Rep. Whale Res. Inst. No. 1:41-47.

Nemoto, T. 1956. On the diatoms of the skin film of whales in the Northern Pacific. Sci. Rep. Whales Res. Inst. No. 11:99-132.

Nemoto, T., R. L. Brownell and T. Ishimaru. 1977. Cocconeis diatom on the skin of Franciscan. Sci. Rep. Whales Res. Inst. No. 29:101-105.

Ommanney, F. D. 1932. The vascular networks (rete mirabilia) of the fin whale (Balaenoptera physalus). Discovery Rep.' 5:363.

Omura, H. 1958. North Pacific right whale. Sci. Rep. Whales Res. Inst. No. 13:1-52.

Omura, H., S. Ohsumi, T. Nemoto, K. Nasu and T. Kasuya. 1969. Black right whales in the North Pacific. Sci. Rep. Whales Res. Inst. No. 21: 1-78.

Pilleri, G. 1964. Morphologic des gehirnes des southern right whale (Eubalena austral is, Desmoul ins). Acts. Zool. 46:245-272.

Pilleri, G. 1966a. Morphologic des gehirnes des seiwals (Balaenoptera borealis, Lesson). J. F. Hirnforsch. 8:221-267.

Pilleri, G. 1966b. Morphologic des gehirnes des buckelwals, Megaptera novaeangliae. J. F. Hirnforsch. 8:437-491.

Pilleri, G. and M. Gihr. 1970. The central nervous system of the mysticete and odontocete whales. In: Investigations on Cetacea. G. Pilleri (cd.), Vol. 2, pp 89-128. Institute of Brain Anatomy, University of Berne.

Reynolds, E. S. 1963. The use of lead citrate at high pH as an electron opaque stain in electron microscopy. J. Cell Biol. 17:208-212.

Rhodin, J. A. G. 1975. An Atlas of Histology. Oxford University Press, New York.

Ridgway, S. H. (cd.). 1972. Mammals of the Sea Biology and Medicine. Charles C. Thomas Co., Springfield, IL.

Roselius, R. R. and J. H. Steffens. 1971. North slope oils score high with hydroprocessing. The Oil and Gas Journal, May 17, 1971, pp 124-131.

Schaller, O., R. E. Habel and J. Frewin (eds.). 1973. Nomina Anatomica Veterinarian, 2nd Ed. World Assoc. Vet. Anatomists, Vienna.

Scott, J. H. and T. J. Parker. 1885. On a specimen of Ziphius recently obstained near Duonedin. Trans. Zool. Sot. London. 12:24-248.

Simionescu, N. and M. Simionescu. 1976. Galloylglucoses of low molecular weight as mordant in electron microscopy. I. Procedure and evidence for mordanting effect. J. Cell Biol. 70:608-621.

Simpson, J. G. and M. B. Gardner. 1972. Comparative microscopic anatomy of selected marine mammals. In: Mammals of the Sea Biology and Meditine. S. H. Ridgway (cd.), pp 298-418. Charles C. Thomas. Springfield, Il.

Slijper, E. S. 1979. Whales, 2nd Ed. Cornell University Press, Ithaca, N.Y.

Smith, H. A. and T. C. Jones. 1966. Veterinary Pathology, 3rd Ed. Lea and Febiger, Philadelphia.

Snider, R. S. and E. Eldred. 1952. Cerebrocerebellar relationships. J. Neurophysiol. 15:27-40.

Sokabe, H. and M. Ogawa. 1974. Comparative studies of the juxtaglomerular apparatus. Int. Rev. Cytol. 37:271-372.

Sokolov. W. 1960. Some similarities and dissimilarities in the structure of the skin among members of the suborders Odontoceti and Mysticeti (Cetacea). Nature 185(4715) :745-747.

Spearman, R. I. 1972. The epidermal stratum corneum of the whale. J. Anat. 113(3):373-81.

Spearman, R.I. 1973. The Integument, A Textbook of Skin Biology. Cambridge University Press, London.

Strick, P. L. 1976. Activity of ventrolateral thalamic neurons during arm movement. J. Neurophysiol. 39:1032-1043.

Thach, W. T. 1975. Timing of activity on cerebella dentate nucleus and cerebral motor cortex during prompt volitional movement. Brain Res. 88:233-241.

Thompson, C. J., H. J. Coleman, J. E. Dooley and D. E. Hirsch 1971. Bumines analysis shows characteristics of Prudhoe Bay crude. The Oil and Gas Journal Oct. 25, 1971, pp 112-120.

Walberg, F., N. Kotchabhakdi and G. H. Hoddevik. 1979. The olivo-cerebellar projections to the flocculus and paraflocculus in the cat compared to those of the rabbit. A study using horseradish peroxidase as a tracer. Brain Res. 161:389-398.

Watson, M. L. 1958. Staining of tissue sections for electron microscopy with heavy metals. J. Biophys. Biochem. Cytol. 4:475-478.

Williams, M. C. 1977. Conversion of lamellar body membranes into tubular myelin in alveoli of fetal rat lungs. J. Cell Biol. 72:260-277.

Williamson, G. R. 1973. Counting and measuring baleen and ventral grooves of whales. Sci. Rep. Whales Res. Inst. No. 25:279-292.

Wislocki, G. B. 1929. On the structure of the lungs of the porpoise (Tursiops truncates).' Amer. J. Anat. 44:47-77.

Wislocki, G. B. 1935. The lungs of the manatee (Trichecthus latirostris) compared with those of other aquatic mammals. Biol. Bull. 68:385-396.

Wislocki, G. B. and L. F. Belanger. 1940. The lungs of the larger Cetacea compared to those of smaller species. Biol. Bull. 78:289-297.